

N°: 40670

BI-NATIONALLY SUPERVISED DOCTORAL THESIS

For acquiring a degree of
Doctor of Philosophy

UNIVERSITE LILLE 1 - SCIENCES ET TECHNOLOGIES
Ecole doctorale Sciences Pour l'Ingénieur Université Lille Nord-de-France

UNIVERSITY OF BELGRADE

DISCIPLINE: Mechanics, energetics, materials

Candidate
Stojanka PETRUŠIĆ

Macro and micro forms of thermosensitive hydrogels
intended for controlled drug release applications

Defense date: November 29, 2011

Jury members

Prof. D. ADOLPHE	<i>Jury president</i>
Prof. I. VROMAN	<i>Reporter</i>
Prof. J. RANOGAJEC	<i>Reporter</i>
Prof. V. KONČAR	<i>Ph.D. supervisor</i>
Prof. P. JOVANČIĆ	<i>Ph.D. co-supervisor</i>
Dr. M. LEWANDOWSKI	<i>Examiner</i>
Prof. B. BUGARSKI	<i>Examiner</i>
Prof. B. PILIĆ	<i>Examiner</i>
Dr. S. GIRAUD	<i>Invited member</i>

Mojim roditeljima

PREFACE

This thesis has been based on convention on double Ph.D. program between Lille University of Science and Technology (Université Lille 1 – Sciences et Technologies - Ecole Doctorale Sciences Pour l'Ingénieur Université Lille Nord-de-France) in France and the University of Belgrade in Serbia. This is the first example of bi-nationally supervised doctoral thesis between these two universities.

The realization of the thesis was provided by the project ARCUS (Action en Région de Coopération Universitaire et Scientifique) entitled «*Nord – Pas de Calais / Bulgarie – PECO*» and granted by the French Ministry of Foreign Affairs and the Region Nord-Pas De Calais. The aim of the ARCUS project has been development of mutual research cooperation among the region Nord-Pas de Calais in France and east European countries, by favoring primarily conductance of the doctoral theses in the form of bi-national supervision. The financial support for research within this thesis has been also provided by the projects number 142075 and III46010, granted by the Ministry of Science of Republic of Serbia.

During the past three and a half years, research presented in this report was done interchangeably in France and in Serbia, each time in duration of six months. The main laboratory exploited for research in France was GEMTEX, at ENSAIT, Roubaix, whereas in Serbia experimental work was performed in laboratories at the Faculty of Technology and Metallurgy, University of Belgrade, Belgrade.

ACKNOWLEDGEMENTS

I wish to sincerely acknowledge and thank all those who helped me conduct this project and contributed to its completion.

Foremost, I am genuinely thankful to my leading supervisors, Prof. Vladan Končar and Prof. Petar Jovančić, for their priceless support, in practical and moral ways, and their excellent guidance through this French-Serbian research journey and even beyond. They are the most credited for me getting the privilege to be involved in and complete this bi-national project.

I am deeply thankful to Prof. Isabelle Vroman and Prof. Jonjaua Ranogajec for accepting to be reporters for this thesis and giving me the privilege of participating in the jury. I would like to equally thank Prof. Dominique Adolphe and Prof. Branka Pilić who honoured me by accepting to be members of the jury.

My co-supervisors in France, Dr. Maryline Lewandowski and Dr. Stéphane Giraud deserve my sincere gratitude for their highly-valued assistance and advice, for giving me motivation in difficult moments and support in all aspects. I would like to thank my co-supervisor in Serbia, Prof. Branko Bugarski, for believing in me and giving useful advice during the work on the project. My special gratitude goes to Prof. Jasna Đonlagić from the Faculty of Technology and Metallurgy at the University of Belgrade for her help in the last part of my experimental work, for her endless patience and precious advice.

This report would not be in the given form if there was not support from people at various institutions who have provided me their equipment and services for certain experimental analyses. Those are: Prof. Maja Radetić from the Faculty of Technology and Metallurgy, University of Belgrade, Belgrade, Dr. Claude Dufour and Christophe Boyal from iEMN, Lille, Dr. Mirjana Dimirijević from the Institute for Biological Research «Siniša Stanković», Belgrade, Dr. Aleksandar Marinković from the Faculty of Technology and Metallurgy, University of Belgrade, Belgrade, Dr. Smilja Marković from the Institute of Technical Sciences of the Serbian Academy of Sciences and Arts, Belgrade, and Prof. Vlatka Vajs from the Faculty of Chemistry, University of Belgrade, Belgrade. My deep gratitude goes to the technicians at GEMTEX and all staff of ENSAIT for their kindness and help.

I am especially grateful to all my office mates, lab mates and colleagues at GEMTEX in ENSAIT and at the Faculty of Technology and Metallurgy in Belgrade, for their company, support and precious moments of joy we have spent together, at and away from work.

I want to express my honest gratitude to the family of Prof. Vladan Končar, who has given me much-needed support during my stays in France.

Finally, my parents, my brother and my grandmother (Božana, Miroslav, Boško and Danica) deserve my special acknowledgement for their belief, encouragement and love they have given me during the work on this project that was truly inspiring and unique experience.

TABLE OF CONTENT

PREFACE	iii
ACKNOWLEDGEMENTS	iv
TABLE OF CONTENT.....	v
GLOSSARY.....	ix
GENERAL INTRODUCTION	2
Chapter I : STATE OF THE ART	5
I.1 Hydrogels	6
I.1.1 Definition and properties of hydrogels.....	6
I.1.2 Preparation of hydrogels.....	6
I.1.3 Swelling properties.....	7
I.1.4 Classification of hydrogels.....	8
I.1.5 Thermosensitive hydrogels	11
I.2 Poly(<i>N</i> -isopropylacrylamide)-based hydrogels	13
I.2.1 Properties of linear polymer	13
I.2.2 Phase separation in PNIPAAm solutions.....	13
I.2.3 Properties of PNIPAAm-based hydrogels.....	15
I.3 Calcium alginate	16
I.3.1 Alginate	17
I.3.2 Mechanism of formation of calcium alginate	17
I.3.3 Properties of calcium alginate.....	18
I.4 Interpenetrating polymer networks	20
I.4.1 Definition and properties	20
I.4.2 IPN hydrogels based on PNIPAAm	21
I.4.2.1 <i>Miscellaneous IPN hydrogels</i>	21
I.4.2.2 <i>IPN hydrogels with alginate</i>	22
I.5 Hydrogels as controlled drug release systems.....	24
I.5.1 Mechanisms of drug release from hydrogels.....	25
I.5.2 Parameters influencing drug release from hydrogel	27
I.5.3 Transdermal drug delivery	28
I.5.4 Local anesthetics	29
I.5.4.1 <i>Procaine hydrochloride</i>	30
I.5.4.2 <i>Release of procaine hydrochloride from hydrogels</i>	31
I.5.5 PNIPAAm-based hydrogels as drug release systems	32
I.5.6 PNIPAAm/CA hydrogels as drug release systems	34
I.6 Hydrogel-based functional textiles.....	37
I.6.1 Smart textiles	37
I.6.2 PNIPAAm-based functional textiles	38
I.7 Conclusion	41

Chapter II : MATERIALS AND METHODS	42
II.1 Chemicals	43
II.1.1 <i>N</i> -isopropylacrylamide	43
II.1.2 <i>N,N'</i> -methylenebis(acrylamide)	43
II.1.3 Ammonium persulfate	44
II.1.4 <i>N,N,N',N'</i> -tetramethylethylenediamine.....	44
II.1.5 Sodium alginate.....	44
II.1.6 Polyoxyethylene (20) sorbitan monooleate.....	45
II.1.7 Maleic anhydride.....	45
II.1.8 Procaine hydrochloride	45
II.2 Methods of hydrogel preparation	46
II.2.1 Theory.....	46
II.2.1.1 <i>Free-radical polymerization</i>	46
II.2.1.1.1 Polymerization in solution.....	46
II.2.1.1.2 Inverse suspension polymerization.....	48
II.2.1.2 <i>Ionic crosslinking</i>	49
II.2.1.2.1 Electrostatic extrusion.....	50
II.2.2 Experimental	52
II.2.2.1 <i>Thermosensitive hydrogel films</i>	52
II.2.2.2 <i>Thermosensitive hydrogel microbeads obtained by inverse suspension polymerization</i>	54
II.2.2.3 <i>Formation of thermosensitive hydrogel microbeads using electrostatic extrusion</i>	56
II.2.2.3.1 Synthesis of linear PNIPAAm.....	56
II.2.2.3.2 Process of electrostatic extrusion	57
II.3 Methods of hydrogel characterization	58
II.3.1 Fourier Transform Infrared Spectroscopy.....	58
II.3.2 Differential Scanning Calorimetry	58
II.3.3 Dynamic Mechanical Analysis	59
II.3.4 Gravimetry.....	60
II.3.4.1 <i>Swelling behavior of hydrogel films</i>	60
II.3.4.2 <i>Swelling behavior of hydrogel microbeads</i>	61
II.3.5 Scanning Electron Microscopy	62
II.3.5.1 <i>Freeze-drying</i>	62
II.3.6 Optical Microscopy and Image Analysis.....	63
II.3.6.1 <i>Optical microscopy</i>	63
II.3.6.2 <i>Image analysis</i>	63
II.3.7 Laser diffraction	64
II.4 Methods of characterization of polymer solutions.....	65
II.4.1 Viscosimetry	65
II.4.2 Surface tension measurements	66
II.5 Methods of drug loading and release	66
II.5.1 Hydrogel microbeads obtained by electrostatic extrusion.....	66
II.5.1.1 <i>Drug loading</i>	66
II.5.1.2 <i>Drug release using dissolution test</i>	67
II.5.2 Hydrogel microbeads obtained by inverse suspension polymerization	67

II.5.2.1	Drug loading.....	67
II.5.2.2	Drug release using Franz diffusion cell.....	67
II.5.2.3	High Performance Liquid Chromatography.....	69
Chapter III	: SYNTHESIS AND CHARACTERIZATION OF THERMOSENSITIVE	
	HYDROGEL FILMS.....	70
III.1	Synthesis.....	71
III.2	Chemical structure	72
III.3	Thermal characteristics	74
III.3.1	Volume phase transition temperature	74
III.3.2	Glass transition temperature	77
III.4	Swelling behavior	79
III.4.1	Equilibrium swelling ratio of hydrogels.....	79
III.4.2	Swelling kinetics	83
III.4.3	Deswelling kinetics	84
III.4.4	Reswelling kinetics	85
III.5	Morphology.....	87
III.6	Mechanical properties.....	90
III.7	Conclusions.....	92
Chapter IV	: APPLICATION OF ELECTROSTATIC EXTRUSION IN PREPARATION	
	OF THERMOSENSITIVE HYDROGEL MICROBEADS.....	94
IV.1	Preparation of hydrogel microbeads by electrostatic extrusion.....	95
IV.1.1	Pure CA hydrogel microbeads.....	95
IV.1.2	Thermosensitive semi-IPN hydrogel microbeads	103
IV.1.2.1	<i>Influence of PNIPAAm concentration in extruded solution</i>	103
IV.1.2.2	<i>Influence of surfactant</i>	106
IV.1.2.3	<i>Influence of the operating parameters</i>	108
IV.2	Characterization of semi-IPN hydrogel microbeads prepared by electrostatic extrusion.....	119
IV.2.1	Chemical Structure	119
IV.2.2	Thermal Characteristics.....	121
IV.2.3	Swelling Behavior	122
IV.2.4	Morphology.....	123
IV.3	CONCLUSIONS	123
Chapter V	: SYNTHESIS AND CHARACTERIZATION OF THERMOSENSITIVE	
	HYDROGEL MICROBEADS OBTAINED BY INVERSE SUSPENSION	
	POLYMERIZATION	125
V.1	Synthesis.....	126
V.2	Chemical structure	127
V.3	Optical microscopy	129
V.3.1	Influence of concentration of emulsifier and the oil-to-aqueous phase ratio.....	130
V.3.2	The influence of PNIPAAm crosslinking degree	131

V.3.3	The influence of the presence of MA.....	133
V.3.4	Influence of presence of linear and crosslinked alginate	134
V.4	Size and size distribution	135
V.4.1	Influence of concentration of emulsifier and the oil-to-aqueous phase ratio.....	136
V.4.2	The influence of PNIPAAm crosslinking degree	139
V.4.3	The influence of the presence of MA.....	139
V.4.4	Influence of the presence of linear and crosslinked alginate	140
V.5	Thermal characteristics	142
V.6	Swelling behavior	146
V.6.1	Equilibrium swelling ratio.....	146
V.6.2	Response of dried microbeads to water presence	149
V.7	Morphology	151
V.8	CONCLUSIONS	156
Chapter VI : CONTROLLED DRUG RELEASE FROM THERMOSENSITIVE		
 HYDROGEL MICROBEADS		
		157
VI.1	Thermosensitive hydrogel microbeads obtained by electrostatic extrusion.....	158
VI.1.1	Drug loading	158
VI.1.2	Drug release using dissolution test	160
VI.2	Thermosensitive hydrogel microbeads obtained by inverse suspension polymerization.....	161
VI.2.1	Drug loading	161
VI.2.2	Drug release using Franz diffusion cell.....	163
VI.2.3	Drug release mechanism.....	166
VI.3	CONCLUSIONS	168
GENERAL CONCLUSIONS		170
REFERENCES		174
APPENDIX		187
LIST OF PUBLICATIONS		198
ABSTRACT.....		199

GLOSSARY

Chemical compounds and entities

NIPAAm	<i>N</i> -isopropylacrylamide
PNIPAAm	poly(<i>N</i> -isopropylacrylamide)
MBAAm	<i>N,N'</i> -methylenebis(acrylamide)
TEMED	<i>N,N,N',N'</i> -tetramethylethylenediamine
APS	ammonium persulfate
SA (Alg ₂ Na; ALG)	sodium alginate
CA	calcium alginate
MA	maleic anhydride
PAAm	polyacrylamide
BSA	bovine serum albumin
Procaine HCl	procaine hydrochloride
PVP	polyvinylpyrrolidone
AA	acrylic acid
IA	itaconic acid
EDTA	ethylenediaminetetraacetic acid
PEG	poly(ethylene glycol)
PET	poly(ethylene terephthalate)
PP	polypropylene
PES	polyester
Tween 80	polyoxyethylene (20) sorbitan monooleate
Tween 20	polyoxyethylene (20) sorbitan monolaurate
Brij 35	polyoxyethylene (35) lauryl ether
AC	acetate cellulose
G	guluronate residue in alginate
M	mannuronate residue in alginate

Physico-chemical dimensions and relative symbols

De	Deborah's number
τ	characteristic relaxation time (s)
θ	characteristic diffusion time (s)
L	characteristic length of the controlled release device (m)
D_{wp}	water diffusion coefficient ($m^2 s^{-1}$)
T	temperature ($^{\circ}C$)
T_g	glass transition temperature
t	time (min)
pH	potential of hydrogen, measure of the concentration of hydrogen ions
pK_a	acid dissociation constant (K_a) at logarithmic scale
HLB	hydrophilic-lipophilic balance
ΔH	enthalpy change during the volume phase transition ($J g^{-1}$)
g	needle gauge
F_g	gravitational force (N)

F_e	electrostatic force (N)
F_γ	surface tension force (N)
γ	surface tension (N m^{-1})
r	radius (m)
ρ	density (kg m^{-3})
q	electric charge (C)
E	electric field strength (N C^{-1})
r_0	inner radius of a needle
G'	storage modulus (Pa)
G''	loss modulus (Pa)
D	volume-weighted mean diameter (m)
δ	size dispersal coefficient
M_t	absolute cumulative amount of drug released at time t (kg)
M_∞	absolute cumulative amount of drug released at infinite time (kg)
k	rate constant in Peppas equation
n	release exponent in Peppas equation
R^2	correlation coefficient
W_t	weight of the swollen hydrogel at predetermined time interval
W_s	weight of the equilibrium swollen hydrogel
W_d	weight of the dried gel (xerogel)
wt %	weight fraction of a substance
w/v %	weight per volume fraction of a substance
vol %	volume fraction of a substance

General chemical terms and specific terms in characterization of hydrogels

IUPAC	international union of pure and applied chemistry
IPN	interpenetrating polymer network
LA	local anaesthetic
PE	polyelectrolyte
LBL	layer-by-layer
CST	critical solution temperature
LCST	lower critical solution temperature
UCST	upper critical solution temperature
VPTT	volume phase transition temperature
T_{onset}	onset temperature of the volume phase transition
SR	swelling ratio
ESR	equilibrium swelling ratio
EWC	equilibrium water content

Techniques of instrumental analysis

FTIR	fourier transform infrared spectroscopy
DSC	differential scanning calorimetry
DMA	dynamic mechanical analysis
SEM	scanning electron microscopy
ESEM	environmental scanning electron microscopy

GENERAL INTRODUCTION

GENERAL INTRODUCTION

Polymer science is continuously developing, permanently resulting in new materials with interesting and unique properties. Among these, hydrogels play a special role and arouse a considerable interest in scientific public even 50 years after development of the first synthetic hydrogel (crosslinked poly(2-hydroxyethyl methacrylate)) by Wichterle and Lim [1]. It is interesting to note that hydrogels were the first biomaterials designed for use in the human body [2]. Advances in polymer science have brought new approaches in hydrogel design which have resulted in their novel, attractive properties and hence, their expanded use. Today, application of hydrogels extends to a myriad of fields, from agriculture [3] to medicine [4].

These crosslinked polymeric structures are able to absorb large amounts of biological fluid while keeping their three-dimensionality. General properties of hydrogels such as soft and rubbery consistency and flexibility in size and shape qualify them as desirable materials in transdermal delivery of drugs. Among them, thermosensitive hydrogels take special attention due to the ability to respond to changes in temperature of surrounding medium by absorbing or expelling water from their structure. This change of hydrogel volume triggered by temperature could be efficiently applied in the field of controlled drug release. Textile materials appear to be attractive and promising supports for hydrogels intended for that purpose. However, application of various forms of thermosensitive hydrogels on textile materials has not been extensively studied. Reports on systems of thermosensitive hydrogel/textile are mainly based on simultaneous formation of hydrogel layer and its grafting on textile support [5, 6]. There are a few studies on thermosensitive hydrogel nanobeads applied on cotton, intended for textile functional finishing [7, 8]. The separation of hydrogel nanobeads from the liquid medium requires additional efforts and obstacles in their characterization. Also, concerns have been raised about potential undesirable effects of possible penetration of nanobeads through human skin. Since transdermal application of hydrogel/textile systems implies direct and efficient contact of hydrogels with skin, micron-sized hydrogel beads of diameters close to average fiber diameter could be regarded as applicable forms in a design of such systems.

Aiming at the realization of a thermosensitive hydrogel-based system for the controlled drug release via transdermal route, this project focuses on synthesis and characterization of hydrogels based on the most applicable thermosensitive polymer poly(*N*-isopropylacrylamide) (PNIPAAm). Mutual advantages but also shortcomings of the pure PNIPAAm hydrogels inspired many researchers to modify them to obtain materials with new or improved functionalities. An imperative has been put on the improvement of mechanical properties [9-11], adjustment of the volume phase transitions [12, 13], pore structure [14, 15], alteration of the swelling behavior [16, 17], etc.

The combination of PNIPAAm, as a synthetic polymer, and alginate, as a natural polymer, was expected to result in hydrogels with improved properties with regard to the pure PNIPAAm hydrogels in various aspects. This could be achieved by the formation of interpenetrating polymer networks (IPNs) whose properties could be controlled more easily than those of the individual components. Also, the characteristics of individual components

could be maintained in the resulting structure. PNIPAAm and alginate could be combined to form semi-IPNs if one component is crosslinked and the other one linear, and to form full-IPNs when both components are crosslinked. Alginate was chosen as an adequate interpenetrant in hydrogel structures beside the PNIPAAm due to its biocompatibility and ability to form ionotropic hydrogel by crosslinking with calcium ions in mild conditions. Calcium alginate (CA) hydrogel has been widely used in release of physiologically active agents primarily because of its simple preparation procedure, morphological and mechanical properties [18, 19].

The main part of this thesis therefore refers to the synthesis and characterization of thermosensitive hydrogels based on PNIPAAm and alginate. Potential biomedical usage of these hydrogels in transdermal delivery is justified by the fact that both, PNIPAAm and alginate are biocompatible materials [20]. The thermosensitive hydrogels will be developed in the form of films and in the form of microbeads. Results of drug release studies from the selected hydrogel microbeads will show the possibility of adjusting the release profiles by temperature changes and thus the potential application of these microbeads as controlled drug release matrices.

The thesis will be divided into six main chapters. After a state of the art on the subject presented in Chapter I, the materials, preparation methods and characterization techniques are reviewed in Chapter II.

The PNIPAAm-based hydrogels in the form of films are described in Chapter III. The accent is put on advantageous properties of hydrogels with full-IPN structure, composed of crosslinked PNIPAAm and CA, over pure PNIPAAm hydrogels. The influence of the crosslinking degree of PNIPAAm and alginate content on thermal, swelling, mechanical, and morphological properties of hydrogels is investigated in detail.

Chapter IV includes study on electrostatic extrusion for the production of thermosensitive hydrogels in the form of microbeads. The main part of this chapter refers to investigating the influence of operating parameters on microbeads size and shape. The aim in application of this technique is to produce thermosensitive hydrogel microbeads of around 20 μm in diameter and close-to-spherical shape by adjusting values of applied voltage, electrodes distance, flow rate and choosing adequate needle size.

Another approach in preparation of thermosensitive hydrogel microbeads is elaborated in Chapter V. Pure PNIPAAm microbeads, PNIPAAm/maleic anhydride copolymer microbeads, semi-IPN PNIPAAm/sodium alginate microbeads, and full-IPN PNIPAAm/CA microbeads are studied thoroughly. Influence of the addition of hydrophilic copolymer and linear and crosslinked interpenetrant will be investigated using various methods of characterization.

Finally, Chapter VI encompasses the application of selected hydrogel microbeads in the controlled drug release. The studies are conducted using Franz diffusion cell as a standard for testing of transdermal pharmaceutical formulations. Different drug release profiles at temperatures below and above the volume phase transition temperature (VPTT) of hydrogels serve as a promising point of reference in the future research with the field of

hydrogel microbeads application on a textile material and formation of intelligent medical patch.

Contribution of this thesis lies in detailed characterization of macro and micro forms of thermosensitive hydrogels based on PNIPAAm that are necessary to conduct prior to design of a hydrogel/textile systems intended for transdermal application. The results elaborated hereby constitute a valuable starting point in the development of an intelligent textile patch with a property to release a drug at a rate controlled simply by the patch temperature, i.e. by heating and cooling the patch.

Chapter I : STATE OF THE ART

I.1 Hydrogels

I.1.1 Definition and properties of hydrogels

Hydrogels are defined as three-dimensional polymeric networks capable of swelling in water or biological fluid while maintaining their shape [21]. In other words, hydrogels represent water-swollen, cross-linked polymeric structures (Figure I.1) [22].



Figure I.1. Simplified general structure of hydrogel network

Hydrogels can absorb from 10 % up to thousands of times their dry weight in water [4, 23]. The ability of hydrogels to absorb water arises from hydrophilic functional groups (such as –OH, –CONH–, –CONH₂, –COOH, and –SO₃H) attached to the polymer backbone. On the other hand, their resistance to dissolution is provided by the crosslinks between the network chains [24]. A presence of chemical or physical crosslinks provides a network structure and a physical integrity to the system. This is demonstrated through the specific water-insoluble behavior of hydrogels when they are in an aqueous medium. During the swelling, the polymer chains separate to an extent determined by the properties of the solvent in which the hydrogel has been placed and the extension of polymer chains [21]. In the swollen state, there are little interactions among the chains, whereas in a dehydrated or deswelled state, the polymer chains of hydrogel network are in close proximity.

What distinguish hydrogels from other polymeric materials are unique properties like soft and rubbery consistency, low interfacial tension with water, and a considerable percentage of water in their structure [25]. Hydrogels are generally biocompatible materials, which is a direct result of their high water content, and compositional and mechanical resemblance to the native extracellular matrix. Apart from the biocompatibility, the water content in the hydrogels also affects other properties like permeability, mechanical and surface properties [26].

I.1.2 Preparation of hydrogels

The properties of hydrogel network are closely related to the conditions under which the hydrogels are synthesized. Formation of hydrogel network, governed by desired characteristics for a given applications, still poses some problems to scientists since a number of network properties are inversely coupled [27]. There are various techniques and procedures used for the preparation of hydrogels. The most common synthetic route is free-

radical cross-linking copolymerization of acrylamide-based monomers with a divinyl monomer (cross-linker) in aqueous solutions [24].

There are two general approaches in hydrogel synthesis:

1. copolymerization/crosslinking reaction between one or more abundant monomers and one multifunctional monomer, which acts as a crosslinking agent, and
2. crosslinking of linear polymers or a combination of monomer and linear polymeric chains [28].

The first method implies initiation of polymerization reaction by a chemical initiator. The polymerization reaction can be carried out in bulk, in solution, or in suspension. In solution co-polymerization/crosslinking reactions, monomers are mixed with the crosslinking agent and the polymerization is initiated thermally, by UV-light, or by redox initiator system. Suspension polymerization results in formation of spherical hydrogel microbeads, with the size range of 1 μm to 1mm [26]. Dispersion of monomer solution in the non-solvent that results in fine droplets is done in the presence of stabilizer. The polymerization is initiated by thermal decomposition of free radicals. In the second approach, two methods of polymer crosslinking are possible: chemical and physical crosslinking. Chemical crosslinking includes radical polymerization, chemical reaction of complementary groups, high energy irradiation and enzyme usage [29]. Radiation reactions utilize electron beams, γ -rays, X-rays, or ultraviolet light to excite a polymer and produce a crosslinked structure. When crosslinking is provided by use of chemical compounds, there should be in the system should be at least one difunctional, cross-linking agent, which reacts with the functional groups in polymer chains, usually linking two longer molecular chains. Some of the commonly used crosslinking agents include *N,N'*-methylene bisacrylamide, divinyl benzene, and ethylene glycol dimethacrylate [26]. Physical or ionic crosslinking is a simple and mild procedure. In contrast to covalent crosslinking, no auxiliary molecules such as catalysts are required and use of toxic crosslinking agents is avoided.

1.1.3 Swelling properties

One of the most significant properties of hydrogel networks is their swelling behavior, which may be described using various approaches [30]. Polymer networks are characterized by highly nonideal thermodynamic behavior in electrolyte solutions. Hence, there are no precise theories which can predict their exact behavior. Flory-Rehner theory and its modifications are still widely used for describing the swelling behavior of hydrogels [31]. This theory regards gels as neutral, tetrafunctionally crosslinked networks with polymer chains exhibiting a Gaussian distribution. However, it was proved that a Gaussian distribution fails for chain lengths of less than about 100 monomers [32]. Swelling of a three-dimensional polymer network, i.e. absorption of a liquid the network is placed in contact with happens for the same reason that the solvent mixes spontaneously with an analogous linear polymer to form an ordinary polymer solution [33]. During the absorption of the solvent, the chains between network junctions are required to assume elongated configurations. This induces an opposing force (equivalent to the elastic retractive force in rubber) to develop. Process of swelling is followed by an increase in this force and a decrease in the diluting force. Eventually, equation of these two forces denotes a state of equilibrium. The elastic reaction of the network structure may be interpreted as pressure acting on the solution, or swollen gel. In the equilibrium state this pressure is sufficient to increase the chemical potential of

the solvent in the solution to equal that of the excess solvent surrounding the swollen gel [33].

Many dynamic swelling models are based on Fick's law of diffusion [30]. In numerous systems that do not exhibit much swelling, where the relaxation time of the polymer is much shorter than the characteristic diffusion time for solvent transport, standard Fickian diffusion is observed. However, water diffusion in hydrogels often deviates from the predictions of Fick's law, leading to anomalous or non-Fickian diffusional behavior. The deviation from Fickian behavior has been associated with the finite rate at which the polymer structure rearranges, to accommodate water molecules, and has been observed for many hydrophilic polymer systems [26].

One of the important parameters affecting the swelling behavior of hydrogels is their degree of crosslinking. Highly crosslinked hydrogels have a tighter, more compact structure and swell less in comparison with loosely crosslinked hydrogels. Furthermore, the chemical structure of hydrogel forming-polymers also dictates the swelling properties of hydrogels. The presence of hydrophilic groups on polymer chains of hydrogel network increases swelling degree in water comparing to the systems containing hydrophobic groups. Hydrophobic groups aggregate leading to collapse of the hydrogel structure in the presence of water, thus minimizing their exposure to water molecules [34].

I.1.4 Classification of hydrogels

Classification of hydrogels can be done based on several criteria. Table I.1 gives the summary of classification from different sources [23, 28]. The most elemental classification of hydrogels is according to the origin of the materials constituting a hydrogel. A variety of synthetic and naturally derived materials may be used to form hydrogels. Synthetic hydrogels are convenient for many biomedical applications because it is possible to control their properties in a reproducible manner. On the other hand, advantages of natural materials lie in their availability and suitability for *in vivo* use. Popular synthetic materials, particularly in the field of biomedicine, include poly(ethylene oxide), poly(vinyl alcohol), poly(acrylic acid), poly(propylene fumarate-co-ethylene glycol), and polypeptides. The most widely used naturally derived polymers are alginate, chitosan, agarose, collagen, fibrin, gelatin, and hyaluronic acid [35].

Among an array of hydrogel types given in Table I.1, it is important to emphasize the difference between chemical and physical hydrogels, as well as to explain the properties of stimuli-sensitive hydrogels that are the subject of the work presented in this report. Chemical hydrogels, also called "permanent", are covalently crosslinked polymer networks. The presence of functional groups like $-OH$, $-COOH$, $-NH_2$ on the polymer chain, can be used to prepare hydrogels by forming covalent linkages between the polymer chains and complementary reactivity, such as amine-carboxylic acid, isocyanate- $-OH/NH_2$ or by Schiff base formation [26]. Chemical hydrogels are mainly inhomogeneous, usually due to the presence of regions of low water swelling and high crosslinking density. Sometimes phase separation in these hydrogels can occur, creating water-filled "voids" or "macropores" [4]. As opposed to chemical, physical or "reversible" hydrogels are characterized by the presence of molecular entanglements and/or secondary forces including ionic, H-bonding or

hydrophobic forces. All these interactions are reversible, and can be disrupted by changes in the physical conditions or the application of stress. Inhomogeneties in physical hydrogel originate from the clusters of molecular entanglements, hydrophobically- or ionically-associated domains, or free chain ends or chain loops. Both chemical and physical hydrogels may appear in various physical forms such as: solid molded forms, pressed powder matrices, microparticles, coatings, membranes or sheets, encapsulated solids and liquids [4].

Table I.1. Classification of hydrogels

Criterion	Hydrogel type
Origin of constituting materials	Natural
	Synthetic
	Hybrid
Type of crosslinks in the network	Chemical
	Physical
Method of preparation	Homopolymer
	Copolymer
	Multipolymer
	Interpenetrating polymeric hydrogels
Nature of side groups	Neutral
	Anionic
	Cationic
	Ampholytic
Mechanical and structural characteristics	Affine networks
	Phantom networks
Physical structure of the networks	Amorphous
	Semicrystalline
	Hydrogen-bonded structures
Response to environmental stimuli	Conventional
	Stimuli-sensitive

Difference between conventional and stimuli-sensitive hydrogels arises from the “intelligence” of constituting polymers. Intelligent or smart polymers have the ability to respond to small changes in physiological or biological environment. They form systems in which slight changes in thermodynamic parameters (pressure, temperature, concentration, solvent, etc.) cause considerable variations in the physicochemical properties of the macromolecules (solubility, structure, shape, size) and their solutions (stability) [27]. Inducing the phase transition depends on the appropriate balance of hydrophobicity and hydrophilicity in the molecular structure of the polymer. Stimuli-sensitive hydrogels usually contain a hydrophobic domain and may or may not be charged [23]. In comparison with these, conventional hydrogels are not sensitive to changes in the environment. They are usually uncharged.

These “smart” polymers constitute stimuli-sensitive hydrogels (as smart polymer systems), exhibit volume changes, i.e. shrinking and swelling, in response to small changes in the environment. According to Galaev [27], “these microscopic changes, which are triggered by small changes in the microenvironment, are apparent at the macroscopic level as precipitate formation in solutions of smart polymers, as changes in wettability of the surface to which a smart polymer is grafted, or as dramatic shrinking/swelling of a hydrogel”. Figure 1.2 gives elementary physical and chemical environmental stimuli that might cause volume phase transition of these smart hydrogels.

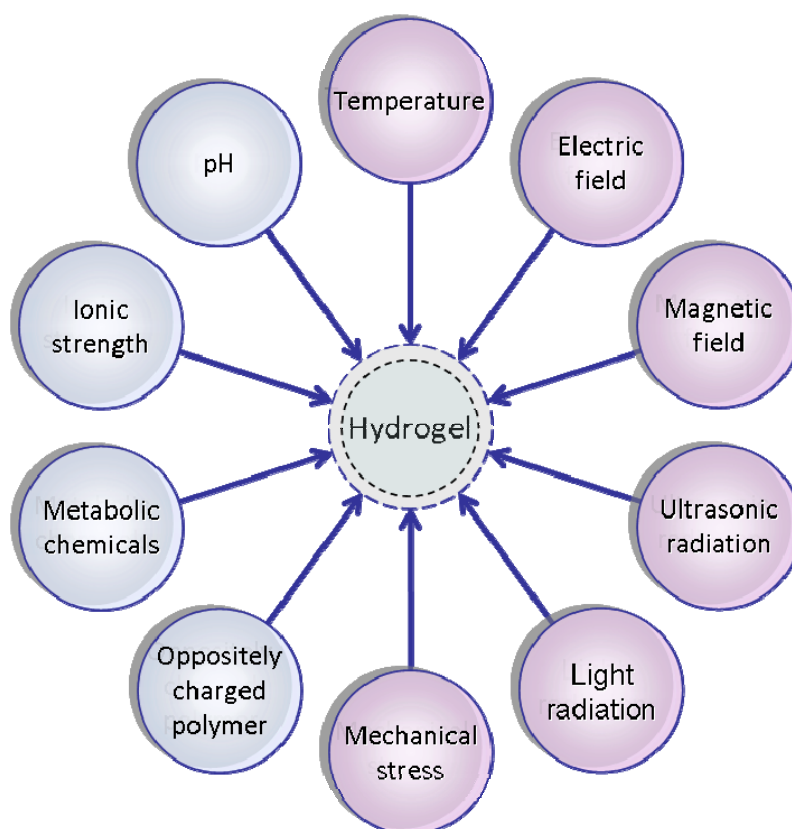


Figure 1.2. Environmental stimuli inducing changes in swelling behavior of stimuli-sensitive hydrogels (adapted from [36])

In 1968, it was predicted that the net repulsion between a polymer network and a poor solvent (intramolecular condensation) can cause a phase transition and a change in the swelling degree [37]. Ten years later, Tanaka observed and explained the collapse of polymer network in polyacrylamide gels [38]. The existence of a critical endpoint when the segment length of the polymer reaches a certain value was confirmed theoretically and experimentally. From this discovery of “volume phase transition” phenomena further on, hydrogels took the important role in research of functional materials. Sensitivity of “smart” polymers which form hydrogels determines the sensitivity of the whole network. Temperature, pH, and electric field (signal) are probably the most exploited stimuli for control of swelling behavior of smart hydrogels. Table 1.2 displays several representative polymers that respond to these three types of stimuli, and are able to form stimuli-sensitive hydrogels.

Table 1.2. Examples of stimuli-sensitive polymers constituting smart hydrogels [39-45]

Thermosensitive polymers	pH-sensitive polymers	Electric signal-sensitive polymers
Poly(<i>N</i> -isopropylacrylamide)	Poly(acrylic acid)	Poly(2-acrylamido-2-methylpropane sulfonic acid-co-n-butylmethacrylate)
Poly(acrylamide-co-butyl methacrylate)	Poly(methacrylic acid)	Poly(2-acrylamido-2-methylpropanesulfonic acid)
Poly(<i>N,N</i> -diethylacrylamide)	Poly(dimethylaminoethyl methacrylate)	Poly(acrylamide-grafted-xanthan gum)
Poly(ethylene oxide) - poly(propylene oxide) block copolymers	Poly(<i>N,N'</i> -diethylaminoethyl methacrylate)	Poly(acrylic acid)/poly vinylsulfonic acid
Poly(ethylene glycol)-poly(lactic-co-glycolic acid)-poly(ethylene glycol)	Poly(vinylacetaldiethylaminoacetate)	Poly(vinyl alcohol)
Xyloglucan	Chitosan	Agarose

Tanaka et al. showed that ionization of the polymer network plays an essential role in the volume phase transition of hydrogels [46]. This was demonstrated with the aid of Flory-Huggins theory, i.e. formula for the osmotic pressure of an ionic hydrogel [33]. Stimuli-sensitive hydrogels sense a stimulus as a signal and show volume change which may occur continuously over a range of stimulus level or discontinuously at a critical stimulus level. This depends on a design of the hydrogel matrices [24, 47]. Stimuli-sensitive hydrogels are able to sense an external stimulus, evaluate it and take an action. In other words, they possess sensor, processor and actuator functions [48].

1.1.5 Thermosensitive hydrogels

Stimuli-sensitive hydrogels represent a class of hydrogels that exhibit considerable changes in their swelling behavior, and hence, network structure, permeability or mechanical strength, in response to slight changes in their environment. Among them, thermosensitive hydrogels have found the broadest application, due to the fact that temperature is an operational parameter that can be easily controlled. In addition, this type of hydrogels does not require any chemical stimulus beside temperature to respond.

The volume phase transition of thermosensitive hydrogels is known to result from the interactions between the thermosensitive polymer chains in hydrogel network and solvent molecules at shrunken and at swollen states. Thermosensitive polymers exhibit a critical solution temperature (CST), behavior where phase separation is induced by surpassing a certain temperature. Lower critical solution temperature (LCST) is characteristic for polymers that become insoluble in a solvent as the temperature rises above the critical value. On the

other hand, thermosensitive polymers that undergo the phase transition with decrease in temperature possess upper critical solution temperature (UCST). Analogous to the CST of thermosensitive polymers, thermosensitive hydrogels are characterized by the volume phase transition temperature (VPTT).

Depending on the type of polymer(s) constituting the hydrogel, response of thermosensitive hydrogels to temperature changes can be positive (corresponding to swelling process with increase in temperature), negative (corresponding to shrinking process with increase in temperature), and reversible (that swell and then shrink with rise in temperature). Accordingly, the thermosensitive hydrogels can be classified into three categories:

1. thermo-shrinking type of hydrogel (temperature-positive response) (Figure 1.3),
2. thermo-swelling type of hydrogel (temperature-negative response), and
3. “convexo” type of hydrogel (shrinking-swelling-shrinking behavior with temperature decrease [49]).

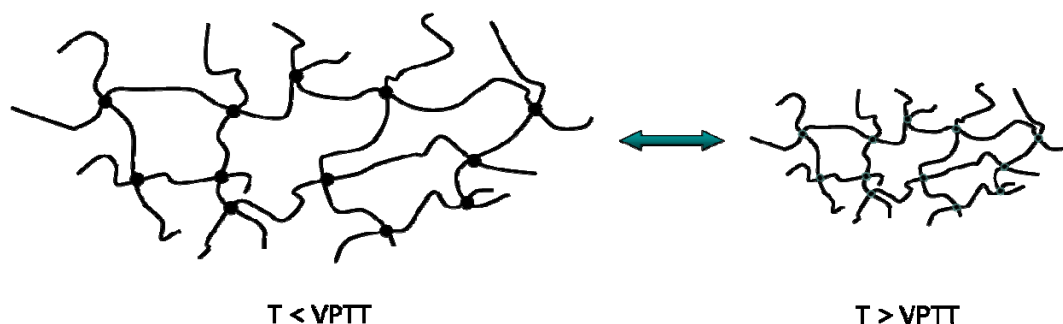


Figure 1.3. General structure of thermo-shrinking type of hydrogel before and after the volume phase transition

Thermo-shrinking type of hydrogel is made of polymer chains with moderately hydrophobic groups or contains a mixture of hydrophilic and hydrophobic segments. At lower temperatures, hydrogen bonding between hydrophilic segments of the polymer chain and water molecules dominates. As the temperature rises, hydrophobic interactions among hydrophobic segments become strengthened while hydrogen bonding becomes weaker. The net result is shrinking of the hydrogels due to inter-polymer chain association through hydrophobic interactions [39]. So called hydrophobic effect represents the phenomenon of the entropy increase due to water–water associations, which are the governing interactions in the system and results in volume phase transition of the hydrogel at high temperatures [40]. In addition, the phenomena of thermo-shrinking type phase transition can be explained through the hydrophobic hydration and hydrophobic interactions that take place when hydrophobic solutes are introduced in water [50]. During the hydrophobic hydration, which is exothermic and entropically unstable process, the water molecules concentrate around the hydrophobic solutes. A rise in temperature causes the reduction in the total number of water molecules structured around the hydrophobic solutes and thus promotes the hydrophobic interaction. Since hydrophobic interaction is endothermic and entropically stable, it is favored by temperature increase [51].

Thermo-shrinking type of hydrogel is, in comparison with the thermo-swelling type of hydrogel, more interesting for the drug release application. This is because in thermo-

swelling systems a drug loading needs to be performed at relatively high temperature, which may damage some unstable drug molecules and change the drug formulation.

I.2 Poly(*N*-isopropylacrylamide)-based hydrogels

I.2.1 Properties of linear polymer

Poly(*N*-isopropylacrylamide) (PNIPAAm) belongs to the group of “smart” or “intelligent” polymers because it responds to temperature changes by exhibiting phase separation. PNIPAAm is soluble in a solvent at low temperatures, but becomes insoluble as the temperature rises above the critical value [52]. This temperature is known as the lower critical solution temperature (LCST), but it is also called precipitation threshold since it represents the extreme temperature at which the phase separation can occur at all [53]. It corresponds to the minimum in the “temperature–composition” phase diagram (Figure I.4). The first thermally sensitive acrylamide derivative polymers have been reported by Heskins et al. through the elaboration of PNIPAAm synthesis via radical polymerization method [54].

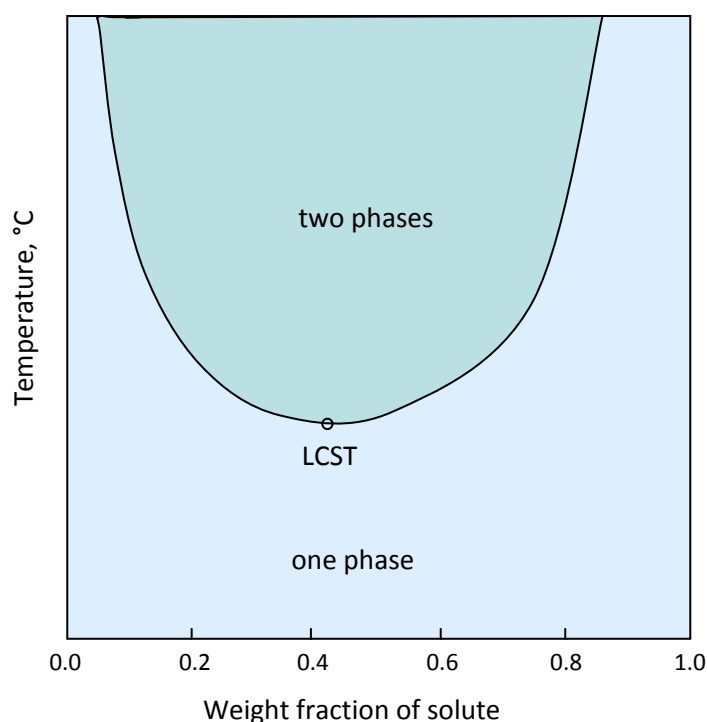


Figure I.4. “Temperature–composition” phase diagram of a system with thermosensitive polymer having LCST (adapted from [52])

I.2.2 Phase separation in PNIPAAm solutions

An aqueous solution of pure PNIPAAm exhibits the phase separation upon heating above 31°C [55], usually around 32°C [56]. Dynamic and static light scattering measurements of diluted PNIPAAm solution indicated that specific dimensional change of the polymer chains corresponds to coil-to-globule transition, when the temperature of the solution reaches a critical value [57]. When examining the thermosensitivity of PNIPAAm, its structure should

be firstly considered. The phase separation of PNIPAAm can be explained as a result of the breakdown of the delicate hydrophilic/hydrophobic balance within a polymer network, due to the presence of both hydrophilic amide groups and hydrophobic isopropyl groups in its side chains (Figure I.5) [58].

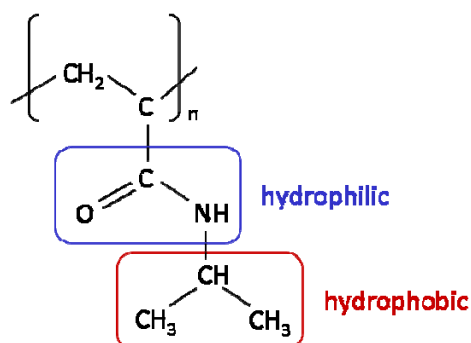


Figure I.5. Poly(N-isopropylacrylamide) structure with highlighted hydrophilic/hydrophobic groups

There are various opinions on whether “hydrophobic effect” [59] and/or “hydrogen bonds” [60] are major determinants of the coil-to-globule transition in PNIPAAm solution. Certain authors attribute the chain collapse to changes in both hydrogen bonding and hydrophobic interactions phenomena [61, 62]. They argue that hydrogen bonds formed around the polymer coil between the water molecules and the N-H and C=O groups break when the temperature of solution of a linear PNIPAAm chains is approaching the phase separation temperature. This phenomenon induces the collapse of the polymer molecules from hydrated random coils configuration into packed hydrophobic globules. Isopropyl groups of PNIPAAm are distributed on the surface of newly formed globular particles and thus hydrophobic interactions among them occur [57]. As a result of this phenomenon and weakening and breakage of hydrogen bonds, the aggregation of individual chain molecules and the subsequent precipitation of the polymer out of solution take place [53].

More than 20 years ago Fujishige et al. were tracing the phase separation of 1 wt % PNIPAAm solution [57]. Their results indicated that the phase separation of linear PNIPAAm is sensitive, reversible, and reproducible to the thermal stimulation. Apart from these properties, PNIPAAm is widely used in an array of fields also because of its LCST, which is close to human body temperature [27, 63]. This convenient LCST gives advantage to PNIPAAm in comparison with other thermosensitive polymers particularly in the controlled drug delivery applications (Table I.3).

Applications of linear PNIPAAm in biotechnology and biomedicine are of great importance. PNIPAAm-grafted dishes for cell culturing are convenient for stimulation of cell adhesion and detachment through temperature changes [64, 65]. PNIPAAm aids cell adherence above its LCST, whereas below this temperature it binds water thus pushing the cells away. This fully reversible phase-transition behavior of PNIPAAm has been utilized by conjugating it, for instance, to protein kinase A, which responds to an intracellular signal [66], or to enzyme trypsin [67]. Generally, PNIPAAm homopolymer is rarely used due to the simple structure, and quite frequently its monomer NIPAAm is copolymerized to give systems with higher functionality and required properties [68]. In addition, NIPAAm monomer can be grafted

onto the polymer substrates by electron beam, irradiation or UV-initiated graft polymerization to achieve special modification of the polymer surfaces intended for pervaporation of liquid mixtures or separation membranes [64].

Table I.3. List of thermosensitive polymers with different LCST

Thermosensitive polymer	LCST, °C	Literature source
Poly(<i>N</i> -ethylacrylamide)	73	[69]
Poly(2-ethyl-2-oxazoline)	65	[70]
Poly(<i>N</i> -ethylmethacrylamide)	50,58	[71],[72]
Poly(<i>N</i> -acryloylpyrrolidine)	56	[71]
Hydroxypropyl cellulose	41	[73]
Poly(methyl vinyl ether)	34	[74]
Poly(<i>N</i> -isopropylacrylamide)	32	[56]
Poly(<i>N</i> -vinylcaprolactam)	26	[73]
Poly (<i>N</i> -acryloyl piperidine)	5.5	[71]

I.2.3 Properties of PNIPAAm-based hydrogels

When PNIPAAm is crosslinked or is combined in linear form with other crosslinked polymers, it gives thermosensitive hydrogel of thermo-shrinking type. Hydrogels based on PNIPAAm respond to temperature changes by shrinking/swelling and possess a volume phase transition temperature (VPTT). The temperature-induced collapse transition of the hydrogels is analogous to the phase separation of polymer solutions with a LCST [61]. In other words, the volume phase transition of hydrogels is a macroscopic manifestation of the coil-to-globule transition of individual linear chains [75]. Hydrogels based on PNIPAAm shrink with increase in temperature above their VPTT and swell below it, due to phenomena previously explained in general for thermo-shrinking type of hydrogels (section I.1.5 of this chapter). In simple terms, hydrogel swells to the limit of its crosslinks below VPTT, and collapses above VPTT to form a dense polymer-rich phase. The kinetics of hydrogel swelling and collapse are determined mostly by the rate of water diffusion in the hydrogel, but also by the heat transfer rate to the hydrogel [76].

In spite of the widespread opinion that PNIPAAm hydrogels are hydrophobic in water above their VPTT [77, 78], recent indications deny this characterization [79]. Measurements of the contact angle on PNIPAAm hydrogel immersed in water gave values of around zero, below and above VPTT as well. However, the surface of the same hydrogels appeared to be hydrophobic above the VPTT, when in contact with air, out of an aqueous environment. This is reasonable result since the PNIPAAm surface rearranges depending on the energy of the opposing phase both below and above VPTT. The isopropyl groups concentrate near air and other hydrophobic phases, whereas PNIPAAm presents hydrophilic domains to water (Figure I.6).

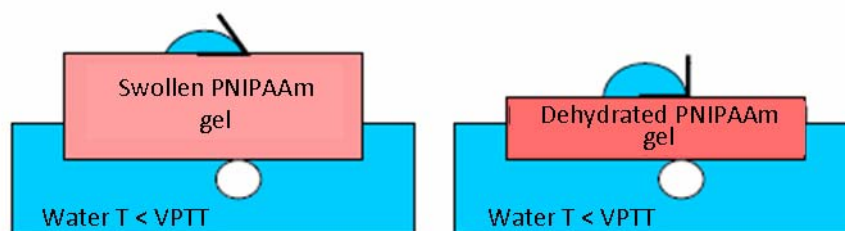


Figure 1.6. Advancing contact angles on PNIPAAm hydrogels are high whereas receding angles are ~ 0 [79]

VPTT of PNIPAAm hydrogels is reported to be in the range 31–35°C [56, 64]. This critical temperature can be varied by changing chemical structure on incorporating components of different hydrophilicity/hydrophobicity [68, 80, 81]. Enhancing hydrophilic character could strengthen hydrogen bonds in the final network and thus cause an increase in VPTT, since higher energy is needed for their breakage. As opposed to this, addition of more hydrophobic components can give PNIPAAm-based hydrogels that exhibit volume phase transition at lower temperatures in comparison with the pure PNIPAAm hydrogels. Also, changes of hydrophilic/hydrophobic balance in these hydrogels have an impact on their swelling abilities [47].

What is also interesting in PNIPAAm hydrogel is its response to a pressure increase. It is experimentally verified that this hydrogel swells more as pressure increases (at a constant temperature), as a result of minimizing the free energy of the hydrogel-water system by increasing the hydrogel-water interactions [82]. Higher pressures reduce the overall free volume of the system, increasing the mixing of the solvent and polymer, which allows an expanded hydrogel phase to exist at higher pressures [76].

PNIPAAm-based hydrogels have found broad application in biomedicine and biotechnology. They play important role in cell-sheet engineering, as micro-sized valves in the flow control [48], in separation processes [76], as sensors [24, 83], controlled drug release [84–86], etc. Application of PNIPAAm-based hydrogels is limited because of their poor mechanical properties [10, 48]. These disadvantages can be overcome by applying various approaches [9], among which the formation of interpenetrating polymer networks (IPNs) with different components appeared to be efficient [10, 87, 88].

1.3 Calcium alginate

Calcium alginate (CA) represents a physical “ionotropic” hydrogel that has been widely used in immobilization of physiologically active agents and drug release applications [89–91]. The reasons for this are primarily its biocompatibility and particularly mild conditions of preparation. The preparation procedures do not require the use of solvents that may influence the activity of protein. CA is generally formed by ionic crosslinking of sodium alginate in the presence of two-valent calcium ions.

1.3.1 Alginate

Alginate (algin, alginic acid) is a linear polysaccharide present in the cell walls of brown algae. It is commercially available as sodium salt – sodium alginate (SA). It appears as biodegradable copolymer linear copolymer of (1-4)-linked β -D-mannuronate (M) and its C-5 epimer α -L-guluronate (G) residues, covalently linked together in different sequences or blocks (Figure 1.7). The orientation of the carboxyl group on the C-5 carbon of the pyranose ring is above the plane of the ring in the M unit and below the plane in the G unit.

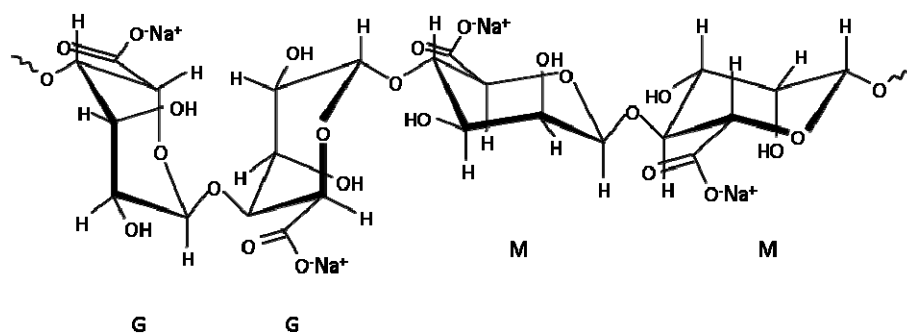


Figure 1.7. Structural unit of alginate chain

Alginates¹ may be organized as homopolymeric G blocks, homopolymeric M blocks, and heteropolymeric GM blocks [92]. Also, the combinations of all these structures may be present in a single alginate molecule. Due to the fact that alginates do not have any regular repeating unit, they may form many different three-dimensional structures.

Alginates in the form of sodium, calcium, potassium and ammonium salts are abundantly used in food industry, usually as additives for viscosifying, stabilizing, emulsifying, and gelling aqueous solution [93]. In addition to food industry, alginates are applied in pharmaceutical formulations [94], in stomatology [94], water treatment [95], textile and paper industry [96], etc.

1.3.2 Mechanism of formation of calcium alginate

One of the most important physical features of alginates is their ion-binding ability, which is the basis for their gelling properties. Affinity of alginates toward earth alkaline metal ions increases in the order $\text{Mg}^{2+} \ll \text{Ca}^{2+} < \text{Sr}^{2+} < \text{Ba}^{2+}$. It was found that the selectivity for alkaline earth metals and transition elements increased considerably with increasing content of α -L-guluronate residues in the chains, whereas M blocks and alternating blocks were almost without selectivity [92, 93]. This difference in affinity towards different ions indicated that the ion-binding is influenced by some kind of chelation apart from nonspecific electrostatic binding only. This property was explained by the so-called “egg-box” model based on the linkage conformations of the guluronate residues [97]. According to the “egg-box” model, calcium ions first bind only to G residues, until saturation is achieved, or rather, until all places on G residues available for bonding are filled. Afterwards, by further adding of

¹ Term “alginate” is used for denotation of alginate salts, mainly sodium alginate, in addition to its primary reference for alginic acid.

calcium ions, M units start to bind them as well [97]. G blocks chelate Ca^{2+} ions in an egg-box-like structure which results in stronger gels, whereas M-rich alginates bind Ca^{2+} ions less strongly and thus form more flexible gels (13) [98]. G blocks are dominantly responsible for ion-binding ability of alginates, since they form a “buckled” chain conformation that binds Ca^{2+} ions [92]. In other words, when two or more polyuronate chains interlink, they create cavities (as those in the “egg-box”) for disposal of Ca^{2+} ions, which is able to fit into these structures (Figure I.8).

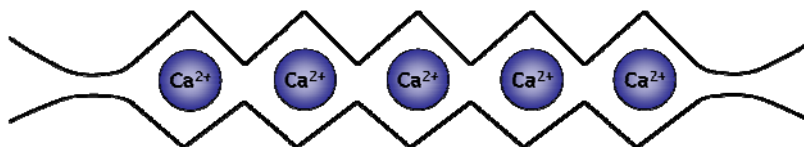


Figure I.8. Simplified scheme of placing calcium ions into G-blocks of alginate according to “egg-box” model (adapted from [97])

Nuclear magnetic resonance studies [99] of lanthanide complexes of related compounds suggested a possible binding site for Ca^{2+} ions in a single alginate chain as shown in Figure I.9 [99, 100].

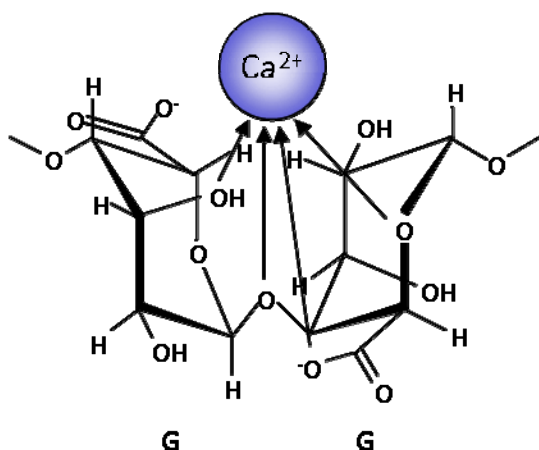
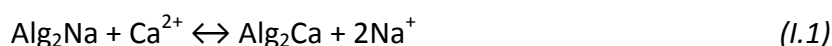


Figure I.9. Formation of the calcium alginate structure according to the “egg-box” model

The simple “egg-box” model of CA structure from 1973 is still regarded as principally correct. It contributes to the understanding of the characteristic chelate-type ion binding properties of alginates [93]. The model can be extended to be three-dimensional. The structure of the guluronate chains gives distances between carboxylate and hydroxyl groups which allow a high degree of coordination of the calcium [96]. Process of CA formation (i.e. process of gelling) from sodium alginate (Alg_2Na) could be simply presented through the following monovalent–divalent ion-exchange equilibrium:



1.3.3 Properties of calcium alginate

Properties of CA are function of the number and strength of the crosslinks and on the stiffness and length of the chains between these junction points. According to what was previously stated, alginate hydrogels that are formed from polymer rich in G residues will

feature enhanced mechanical rigidity, i.e. improved ionic binding is characteristic of alginates rich in G residues [101]. On the contrary, those originating from M-rich polymer will be characterized by softness and elasticity [102]. Alginates from different seaweeds can have differing ratios of mannuronic acid to guluronic acid in their structures and different proportions of M, G and MG blocks. Apart from the source (algal species) of the alginate, the mechanical strength of CA depends also on the concentration of alginate, its degree of polymerization and the calcium concentration [96].

The greatest popularity of Ca^{2+} as divalent ion for gel formation lies in low price of its salts, their availability and non-toxicity [96]. The structure of CA based on ionic bonds can be heat-treated without melting [103]. CA is stable in the range of temperatures from 0 to 100°C [96]. However, this hydrogel could be destabilized in the solution with high concentration of sodium, potassium, magnesium ions or in the presence of phosphate, citrate, and lactate ions that have high affinity for calcium ions [104]. Alginates form strong complexes with chitosan, polypeptides such as poly-L-lysine, and synthetic polymers such as polyethylamine. These cationic complexes make hydrogels stable even in the presence of calcium chelators [105].

Another important characteristic of CA (and other alginate hydrogels) is their pH-sensitivity. CA network contains polymer chains composed of guluronate and mannuronate residues that bear carboxylate groups. Values of pK_a for mannuronic and guluronic acid monomers are reported as 3.38 and 3.65, respectively [106]. At a pH below the pK_a of the G/M residues, carboxylic groups are in nonionic, protonated form. Upon immersion of the hydrogel in media with higher pH, the carboxylic groups are ionized. Under these conditions, the electrostatic repulsion between anionic groups within the hydrogel causes it to swell. If the swollen hydrogel is then placed in an acidic environment, it will collapse because of the protonation of ionic groups. Hence, the volume changes of the hydrogel are most often due to changes in the ionic charge within the hydrogel. This ability of CA is of great significance in studies of controlled drug release via oral route during which a drug-loaded hydrogel comes in contact with media of different pH [90, 107]. However, in transdermal delivery of a drug, this property of CA is not of great relevance, and hence it was not studied during the realization of this thesis.

The most popular forms of CA hydrogels are beads of both macro and micro sizes, due to their high specific surface area and large inner volumes [108]. Extrusion-dripping methods are the most exploited in the production of CA beads and are based on extrusion of the solution of sodium alginate into solution of divalent salt (usually calcium chloride, CaCl_2) [109-111]. Apart from this, CA beads could be formed by dripping CaCl_2 into SA solution to form the inner side of the membrane, and then dipping the partially gelled capsules in a CaCl_2 solution to finish the gelation from outside [108, 112]. Acceleration of the beads formation and significant decrease of the droplets size in comparison with simple dripping method may be achieved by applying electrical potential to polymer solutions passing through a needle [113, 114]. Spray technique known as electrostatic extrusion or electrostatic droplet generation has been used for the formation of micro-sized CA beads [115-120].

CA has been applied in immobilization of enzymes and living cells [121, 122]. By immobilization of biocatalysts in these hydrogels, the production time is shortened, costs of production are reduced, and continuity of the system is achieved. Hence, CA hydrogels are present in different sectors such as food industry, pharmaceutical industry, or medicine [92, 123]. One of the main advantages of alginate hydrogels is the fact that they are made of natural polymer, which boost its use as a scaffold material as well [124]. CA hydrogels have been widely used as drug carriers primarily due to their biocompatibility, good morphological and mechanical properties [19].

I.4 Interpenetrating polymer networks

I.4.1 Definition and properties

A group of multicomponent polymeric materials encompasses polymer blends, composites, or combinations of both [125]. Several structures can be classified under polymer blends, defined as any finely divided combinations of two or more polymers: the block, graft, star, starblock, and AB-cross-linked copolymers (conterminously grafted copolymers), and interpenetrating polymer networks (IPNs). In addition, there is a class of polymer blends characterized by the absence of chemical bonding between the various polymers making up the blend [125].

The importance of interpenetrating polymer networks (IPNs) lies in the unique possibility to combine cross-linked polymers. According to IUPAC, an IPN is a polymer comprising two or more networks which are at least partially interlaced on a molecular scale but not covalently bonded to each other and cannot be separated unless chemical bonds are broken [126].

Classification of IPNs “by chemistry” includes two types:

- a) sequential (the second network is formed after completion of polymerization of the first monomer), and
- b) simultaneous (the networks are created at the same time during two independent reactions) [127].

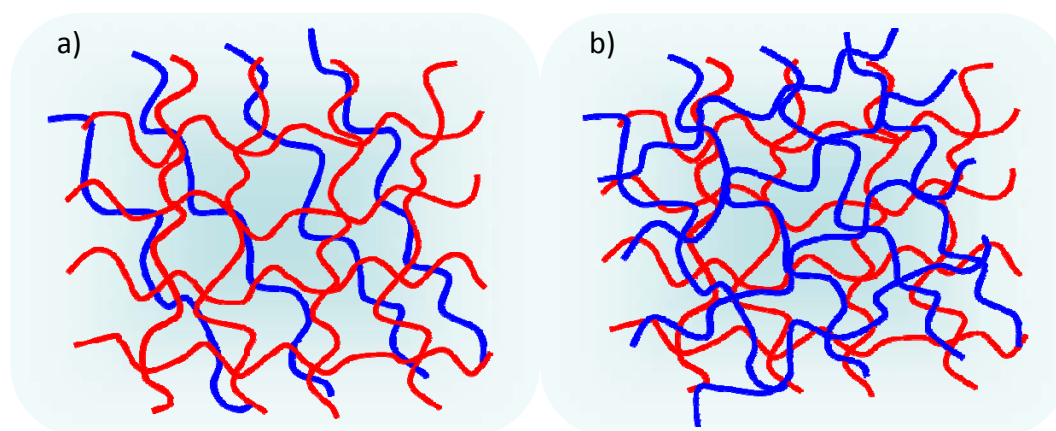


Figure I.10. Scheme of semi-IPN (a) and full-IPN (b) structures

IPNs can be formed either in the presence of a crosslinker to produce a fully interpenetrating polymer network (full-IPN) or in the absence of a crosslinking mechanism to generate a network of embedded linear polymers entrapped within the original hydrogel (semi-IPN) [128], as schematically displayed in Figure I.10. Beside these two structures, there are homo-IPNs (as a subgroup of full-IPNs, where the same polymer is used in both networks), latex IPNs (formed by emulsion polymerization), and thermoplastic IPNs (which are moldable and made of at least one block copolymer) [127].

A strong reason for the application of IPNs is also the absence of phase separation. When an IPN hydrogel is physically formed from two polymers at a given temperature, a physical phase separation between two polymers would be almost impossible because of the infinite zero viscosity of the gel. IPN hydrogels may have more favorable mechanical properties due to the physical entanglements as compared with individual crosslinked networks [129]. The main advantage of IPNs comparing to conventional hydrogels lies in the fact that stiffer and tougher hydrogel matrices could be produced, with more widely controllable physical properties, and more efficient drug loading [128].

I.4.2 IPN hydrogels based on PNIPAAm

Up to date, many different components were combined with PNIPAAm to form semi- or full-IPN hydrogels [9, 130, 131]. The preparation of IPN hydrogels based on PNIPAAm has been conducted with different aims: increasing the response rate to temperature, enhancing the water uptake capabilities, improving the mechanical properties, adjusting the VPTT, etc.

I.4.2.1 Miscellaneous IPN hydrogels

Very interesting work is reported by Zhang et al. who synthesized IPN hydrogels from two PNIPAAm networks in order to overcome the drawbacks of a normal PNIPAAm hydrogel [10]. Due to the incorporation of the second network component, the mechanical properties of these IPNs (with unchanged VPTT) were significantly improved with regard to conventional hydrogel. In addition, it was demonstrated that the initial burst and subsequent sustained release rates from the IPN PNIPAAm hydrogels could be successfully slowed down when comparing to the corresponding normal PNIPAAm hydrogels. This was explained by the higher mass per unit volume, more intermolecular interactions, and the slower release of bovine serum albumin (BSA) release at 37°C than at 22°C by contracting of PNIPAAm structure due to the volume phase transition.

Guilherme et al. investigated the water uptake and permeability properties of thermosensitive membranes from poly(acrylamide) (PAAm) networks with entangled PNIPAAm chains [131, 132]. They concluded that the presence of PNIPAAm not only increases the concentration of polymer chains compared to PAAm hydrogels but also decreases the average mesh size, resulting in a reduction of the Orange II dye permeability. However, the greater shrinking of PNIPAAm in PAAm/PNIPAAm hydrogels is avoided in the presence of PAAm network. Depending on the hydrophilicity/hydrophobicity of permeating molecules across the hydrogel membrane, the solubility of the permeant could be higher or smaller and controllable by temperature changes.

1.4.2.2 IPN hydrogels with alginate

An early study referring to combination of PNIPAAm and alginate to design thermosensitive hydrogels was based on preparation of semi-IPN structures [133]. These hydrogels were composed of linear PNIPAAm chains and CA as a crosslinked component. The researchers investigated the permeability of Orange II dye through the prepared thermosensitive hydrogel membranes at different temperatures. It was proposed that above the VPTT of hydrogels the CA networks mechanically support the collapsed PNIPAAm chains, but the system became more hydrophobic and the permeability of orange II is minimized.

The IPN hydrogels based on full-IPNs of CA and PNIPAAm intended for use as scaffolds for adherent cells growth and detachment (and as separation membranes) were prepared by Guilherme et al. [134]. This work was one of the first dealing with formation of CA network inside PNIPAAm network by reaction of SA with Ca^{2+} ions. The full-IPN hydrogels developed in this work showed decrease in pore sizes at temperature above their VPTT, causing the slower diffusion of the Orange II dye through the hydrogel membrane. The same authors reported the full-IPN hydrogels of PNIPAAm and CA that possess better mechanical properties in comparison with those of individual networks [135]. The combination of CA with crosslinked PNIPAAm results in hydrogel with a more regular structure when compared to the structure of each of its components (Figure I.11). Also, the compressive stress of these full-IPN hydrogels is dependent on the content of CA and PNIPAAm at temperatures below VPTT, but that at temperatures above VPTT, it depends only on PNIPAAm network.

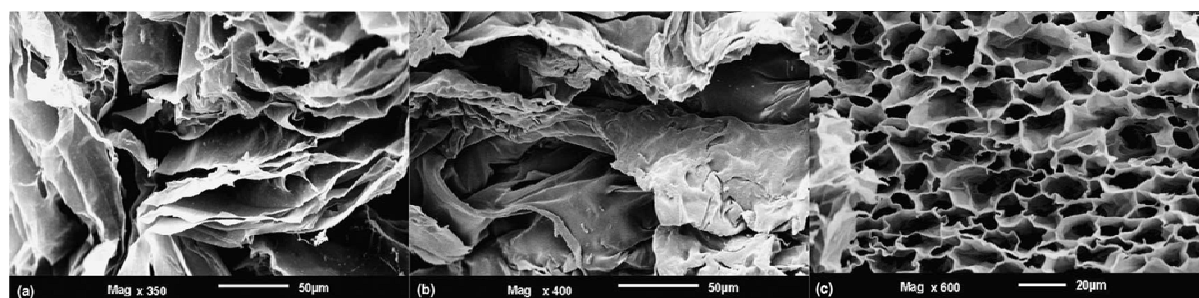


Figure I.11. SEM micrographs of: pure CA (a), PNIPAAm (b), and PNIPAAm/CA IPN hydrogel (c) (after swelling at 25 °C) [135]

To obtain biocompatible thermosensitive hydrogels that exhibit VPTT close to 37°C and good gel consistency, Muniz et al. associated crosslinked PNIPAAm with CA to form full-IPN hydrogel [13]. The heating of the IPN hydrogels up to VPTT region drastically increases the solubility of hydrophilic Orange II dye in the polymer networks. Above VPTT, hydrophobic interactions in hydrogel become dominant and Orange II interacts more with the surrounding water molecules rather than the IPN hydrogel. It is shown that the hydrogel compaction and VPTT values increase with increase in PNIPAAm and CA contents.

Zhang et al. have prepared semi-IPN hydrogels by introducing linear alginate (sodium alginate, SA) into the crosslinked PNIPAAm hydrogel network with the aim to obtain hydrogels with high deswelling rates in response to both, pH and temperature changes [136]. These hydrogels exhibited the porous structure within the hydrogels in the presence of the ionized SA during the polymerization process of NIPAAm and this phenomenon

caused higher deswelling rates than pure PNIPAAm hydrogels (Figure I.12). The hydrogels developed in this work have potential application as temperature-sensitive actuators and chemical valves.

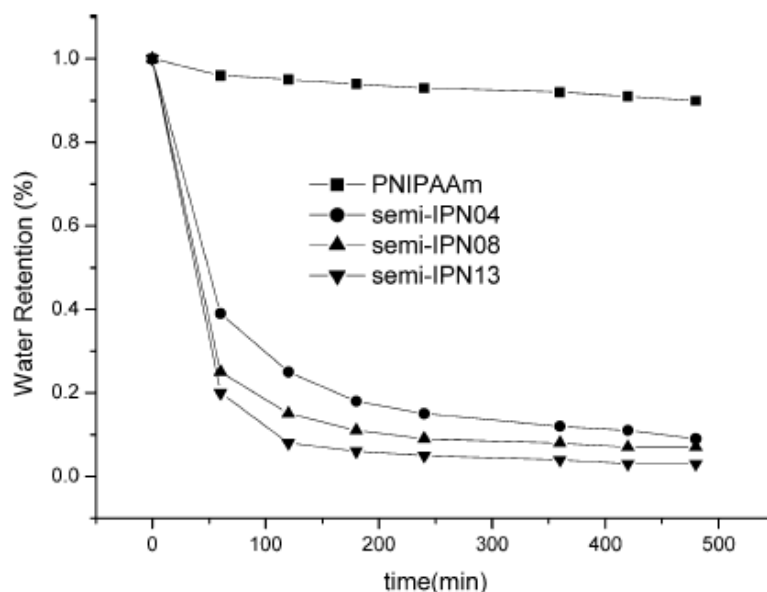


Figure I.12. Deswelling kinetics of the semi-IPN hydrogels at 45°C (pH 6.8) [136]

With the aim to improve the response rate of PNIPAAm hydrogels to temperature changes, Hernández and Mijangos [137] synthesized cylindrically-shaped hydrogels with semi-IPN structure of alginate and crosslinked PNIPAAm incorporating iron oxide nanoparticles. They combined these two components due to higher porosity and more homogeneous pore structure of semi-IPN hydrogels than pure PNIPAAm hydrogel. Obtained hydrogels featured faster deswelling rate at 37°C and higher porosity than pure PNIPAAm hydrogel. This qualifies them as efficient systems for hyperthermia treatment of cancer, which consists of raising the temperature of tumor-loaded tissue to 40-43°C by means of an alternating magnetic field.

Dumitriu et al. prepared a novel covalently crosslinked PNIPAAm/alginate “mixed-IPN” hydrogels [138]. Although ionic crosslinking of alginate is the most widely spread procedure for the formation of alginate hydrogel, covalent crosslinking could be also applied. In this system, alginate was covalently bonded to PNIPAAm chains through MBAAm units, which also crosslinked PNIPAAm chains. The obtained hydrogels showed rapid response to temperature changes and enhanced swelling capacity with increase in alginate content. This qualifies them as promising pulsatile drug delivery devices.

Kim et al. synthesized hydrogels composed of thermosensitive PNIPAAm grafted on the surface or bulk of the macroporous pH-sensitive CA. These hydrogels exhibited fast response to changes in pH and temperature and showed suitable mechanical strength without collapsing during repeatable shrinkage and expansion changes, as opposed to conventional porous hydrogels. Hence, they are qualified as a rapid pH/thermosensitive drug release system, or as biomimetic actuators in biomedical fields [139].

1.5 Hydrogels as controlled drug release systems

The main function of systems that release drugs in a controlled manner is maintenance of a desired blood plasma level of a drug for longer periods, without reaching a toxic level or dropping below the minimum effective level (Figure 1.13). In addition, control of a drug release implies prediction and reproducibility of release rates over a longer period of time. It provides better patient compliance by eliminating frequent drug dosing [127].

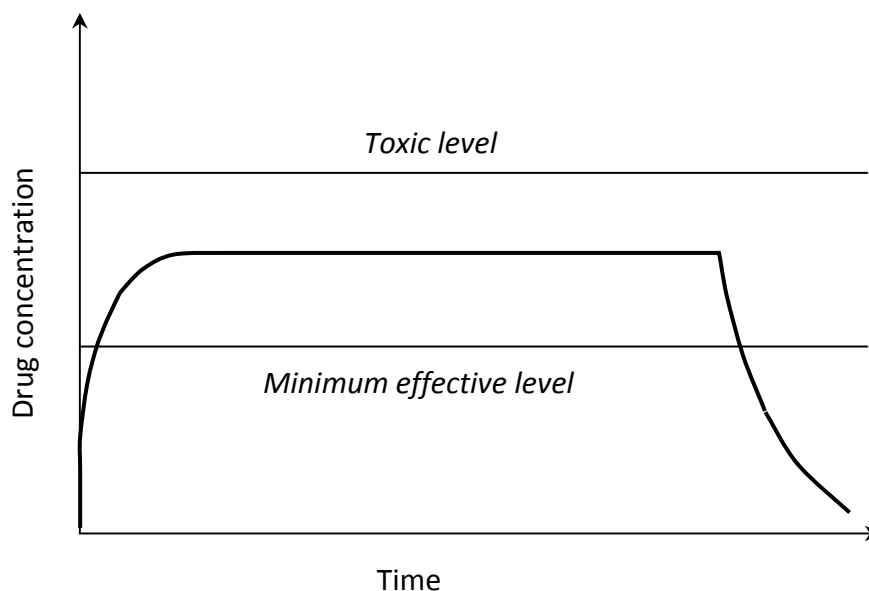


Figure 1.13. Drug levels in the blood with controlled-delivery dosing [140]

In spite of rather large number of corresponding pharmaceutical products, there are only several distinct mechanisms for controlled drug release (Table 1.4). General classification of controlled release mechanisms encompasses chemical and physical mechanisms. The chemical mechanisms are based on breakage of covalent bonds between drug molecules and a release vehicle, such as polymer chains, by either chemical or enzymatic degradation. Hence, it implies modification of a drug molecule, as opposed to physical mechanism, which relies on diffusion of drug through polymer matrix, dissolution/degradation of polymer matrix, osmotic pressure, or use of ion exchange [141]. Hence, physical mechanisms are predominant in comparison with the chemical ones.

Table I.4. Classification of controlled release systems [142]

Type of system	Rate controlling mechanism
Diffusion controlled	
Reservoir devices	Diffusion through membrane
Monolithic devices	Diffusion through bulk polymer
Water penetration controlled	
Osmotic systems	Osmotic transport of water through semipermeable membrane
Swelling systems	Water penetration into glassy polymer
Chemically controlled	
Monolithic systems	Either pure polymer erosion (surface erosion) or combination of erosion and diffusion (bulk erosion)
Pendant chain systems	Combination of hydrolysis of pendant group and diffusion from bulk polymer
Regulated systems	
Magnetic or ultrasound	External application of magnetic field or ultrasound to device
Chemical	Use of competitive desorption or enzyme-substrate reaction; rate control is built into device

I.5.1 Mechanisms of drug release from hydrogels

Among various biomedical applications of hydrogels [40, 143], drug release systems represent a particularly interesting target field. The main reason for that is the possibility of controlling and modifying the drug release profiles [26, 144]. The ability of molecules of different sizes to diffuse into (drug loading), and out (drug release) of hydrogels, permits their use in drug release. The most convenient classification of drug release mechanisms, describing the drug release from hydrogel-based delivery systems, includes four mechanisms:

- diffusion-controlled,
- chemically-controlled,
- swelling-controlled, and
- modulated release [127].

Since hydrogels feature high permeability for water soluble active substances, the most common mechanism of drug release from the hydrogel system is diffusion. Actually, ordinary diffusion takes place in each of these mechanisms to a certain degree. An active agent can diffuse through the pores in the polymer matrix, or by passing between the polymer chains. In pure diffusion-controlled release system, there is no change induced in the polymer itself, i.e. swelling or degradation does not occur. In matrix diffusion-controlled systems the drug can be either dissolved or dispersed throughout the network of the hydrogels, while reservoir diffusion-controlled systems drug makes a core that is separated from the external environment by a polymer membrane [145].

Chemically-controlled release is governed by reactions that occur within hydrogel systems. There are erodible and pendant chain systems referring to this mechanism. In erodible systems, the drug release rate is controlled by degradation or dissolution of the polymer. In pendant chain systems, cleavage of polymer chains between the polymer network and a drug occurs via hydrolytic or enzymatic degradation [145].

Swelling-controlled release is characteristic for the system in which diffusion of a drug is faster than hydrogel swelling. In general, this mechanism refers to dry hydrogel loaded with a drug when it comes in contact with water or other biological fluid. The polymer matrix begins to swell and two phases can be observed, the inner glassy and the swollen rubbery phase.

Release of a drug from stimuli-sensitive hydrogels belongs to modulated drug release. However, certain scientists categorize it in swelling-controlled drug release systems [146]. Stimuli-sensitive hydrogels possess the ability to change their swelling behavior as a result of changes in the environment. This directly impacts the diffusion of the drug out of the matrix, contributing to the control over drug release [27].

Several possible ways of drug release from hydrogel-based drug delivery systems, are given in Figure I.14, in the form of more comprehensible, simplified schemes.

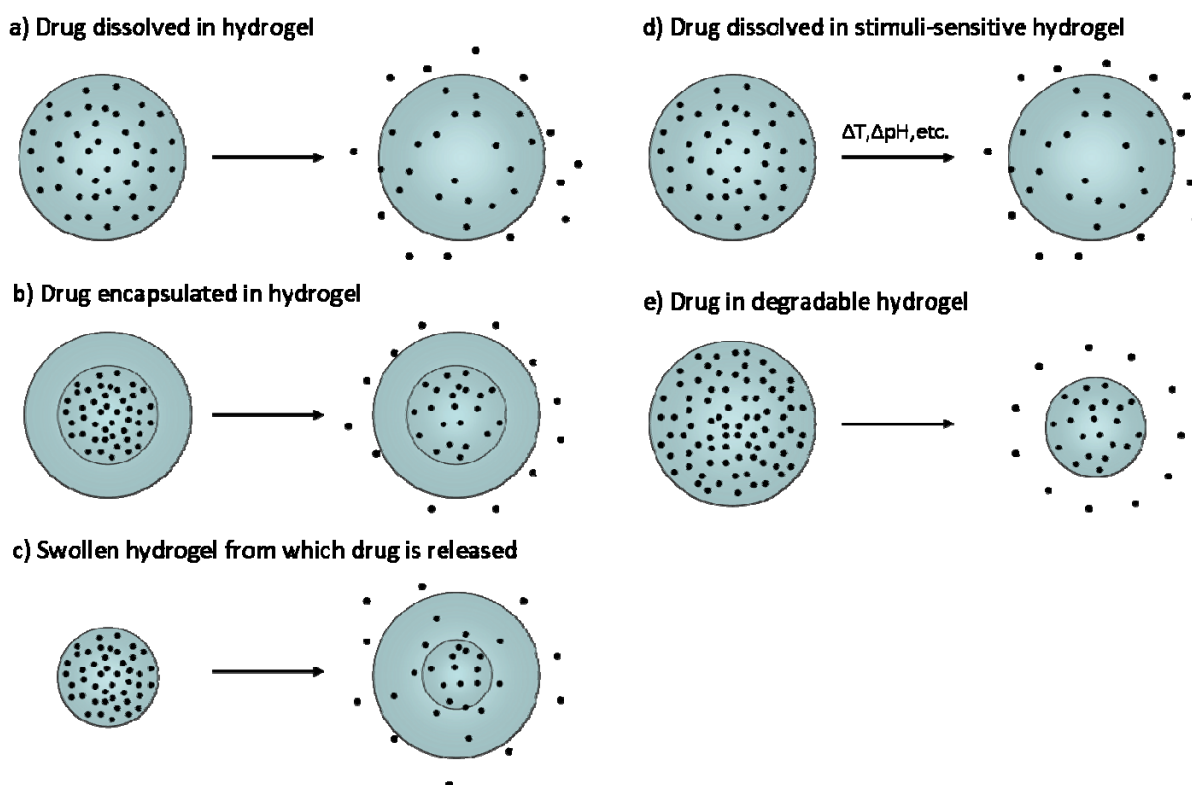


Figure I.14. Examples of mechanisms of drug release from hydrogels: diffusion-controlled (a,b), swelling-controlled (c), modulated release (d) and chemically-controlled (e)(adapted from [41])

1.5.2 Parameters influencing drug release from hydrogel

Factors like polymer composition, water content, crosslinking density, and crystallinity, can be used to control drug release rate and drug release mechanism from hydrogels. The size and shape of drug molecule, its degree of hydrophilicity/hydrophobicity are also of importance regarding its permeation through hydrogel matrix [23]. In addition, significant role in drug permeation have its net charge, groups of the polymer chains making a hydrogel, as well as the availability of free water molecules to hydrate and dissolve the solute molecules. Important factors are also the addition of partition enhancers to the solution, temperature, pH, ionic strength, and possible drying method [4].

The adsorption and diffusion of drug molecules through the hydrogel are the function of the volume fraction of water in hydrogel. The character of water in hydrogel is of considerable significance, since it can determine the overall permeation of active substance in and out of the gel. Primary bound water comprises of the water molecules entering the matrix of a dry hydrogel which hydrate the most polar, hydrophilic groups. As the polar groups are hydrated, the network swells, and exposes hydrophobic groups, which also interact with water molecules, leading to secondary bound water. After the polar and hydrophobic sites have interacted with bound water molecules, the network will imbibe additional water. The continued swelling is due to osmotic forces. These forces are in opposition with the elastic retraction forces of the network (due to the covalent or physical crosslinks) [23]. Thus, the hydrogel reaches an equilibrium swelling level. The additional swelling is caused by water that is imbibed after the ionic, polar and hydrophobic groups become saturated with bound water, and it is called free water or bulk water. This type of water is assumed to fill the space between the network chains, and/or the centre of larger pores, macropores or voids [4].

The main factors that control the pore volume fraction of hydrogel, the pore sizes and their interconnections are the compositions of the polymer chains and the crosslinking density. What is crucial in designing a hydrogel network for controlled release of a drug is matching the polymer composition and crosslinking density with the particular size and composition of the drug molecule to be delivered [4]. Two basic approaches for control of drug diffusion out of the hydrogel are modification of its bulk structure and surface-specific modifications [128]. If an agent is a sensitive therapeutic drug, hydrogel should be designed in a way to maintain its integrity. This can be achieved by controlling degree of crosslinking, crystallinity, or complexation [34].

In spite of many advantageous properties, hydrogels have several limitations. The low tensile strength of many hydrogels limits their use in certain applications and can result in the premature dissolution or rupture of the hydrogels in the targeted local site. Also, the quantity and homogeneity of drug loaded into hydrogels may be limited, particularly in the case of hydrophobic drugs. The high water content and large pore sizes of most hydrogels often result in relatively rapid drug release, over a few hours to a few days. The ease of application can also be problematic [128].

However, design of adequate hydrogel matrices for drug loading and release demands modification of properties that are often inversely coupled. Swelling capacity, mechanical

properties, regular porous structure and rate of response to temperature changes could be regarded as the most important parameters in engineering of thermosensitive hydrogels.

1.5.3 Transdermal drug delivery

Benefits of transdermal route in drug delivery encompass the easiness of interruption of drug delivery by simply removing the transdermal device, and avoidance of undesired early drug metabolism. Furthermore, the blood level peaks and troughs produced by oral dosage forms are in this way eliminated.

The major limitation of transdermal drug delivery is the intrinsic barrier property of the skin. Many drugs have difficulties in permeation through human skin. There are chemicals that have ability to improve diffusion through the skin, through different mechanisms. Some of these excipients are: ethanol, isopropyl palmitate, lauryl alcohol, glyceryl monolaurate, oleic acid, propylene glycol, etc [147]. Many of these compounds are regularly used in transdermal devices such as those given in Table I.5. Also, supersaturation of a drug can improve the flux through the skin. Efficient physical method for increasing the skin permeation is iontophoresis (low voltage electrical current drives charged drugs through the skin), electroporation (short electrical pulses of high voltage create transient aqueous pores in the skin) and sonophoresis (low frequency ultrasonic energy disrupts the stratum corneum) [147].

Table I.5. Examples of transdermal patches [147, 148]

Active agent	Brand name
Fentanyl	Duragesic®
Nitroglycerin	Nitrodisc®
	Nitrol®
	NTS®
Estradiol	Estraderm®
	Climara®
	Vivelle®
Testosterone	Androderm®
Scopolamine	Transderm-Scop®
Clonidine	CatapresTTS®
Nicotine	Nicotrol®, Nicoderm CQ®

Apart from their ability to easily penetrate the skin barrier, certain classes of drugs are not appropriate for transdermal applications due to other properties as well. This primarily refers to chemotherapeutic and cytotoxic agents, drugs with doses greater than 50 mg, drugs that are unstable in acid pH, and drugs with narrow therapeutic margins. Drug candidates for transdermal delivery should have molecular weight around 200 to 500 Da according to Doh et al. [149].

Hydrogel-based drug delivery devices can be used for oral, rectal, ocular, transdermal and subcutaneous application [145]. Advantage of using hydrogels in transdermal delivery lies in their relative deformability that enables them to conform to the surface they are applied to [128]. Furthermore, swollen hydrogels can provide better feeling for the skin in comparison with conventional ointments and patches, due to their high water content. Some of hydrogel-based systems intended for transdermal delivery of various physiologically active agents are given in Table I.6. It is important to emphasize conspicuous role of formulations based on hydrogels for use in occlusive enhancement of topical therapies of psoriasis [150].

Table I.6. Hydrogel-based transdermal delivery systems

Hydrogel-forming polymers	Active agent	Source
Poly(2-hydroxyethyl methacrylate)	Nitroglycerin	[151]
Copolymer of bovine serum albumin and poly(ethylene glycol)	Theophylline, acetaminophen, cortisone, etc.	[152]
Block copolymers of lactic acid oligomers and polyethylene glycol	Urokinase, tissue plasminogen activator	[153]
Polyacrylamide	Gonadotropin releasing hormone	[154]
Sodium polyacrylate and carboxymethylcellulose	Triclosan	[155]

1.5.4 Local anesthetics

A pharmacologically active substance that could be delivered through the skin may belong to the group of therapeutic drugs, vaccines, or cosmetic substances. Local anesthetics (LAs) belong to the class of pharmacologically active compounds used to eliminate pain.

Principle of LA action is based on cutting the signal of nerve impulses in nerve cell membranes through the shutting of voltage-gated Na^+ channels. Clinical LAs belong to one of the two classes: amino esters (Figure I.15-a) and amino amide (Figure I.15-b). Ester-based LAs are hydrolyzed and inactivated by plasma esterase, primarily plasma cholinesterase. Amide-based LAs are degraded by hepatic endoplasmic reticulum, leading to a slower removal from the body and higher concentration in the plasma [156].

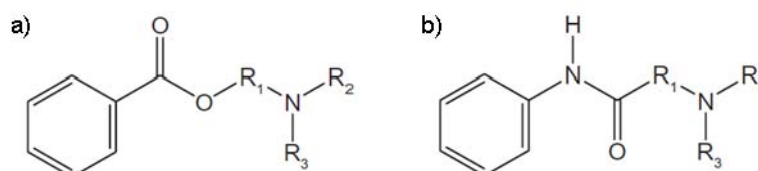


Figure I.15. General chemical structures of LAs amino ester (a) and amino amide (b)

The use of LA could be limited by relatively short therapeutic action and systemic toxicity related to high drug plasma concentration as a result of fast systemic uptake [156]. Improvement of regional administration of LAs could be achieved by incorporating them into

an adequate carrier. Thus, control of drug release rate could be achieved. With the aim to control delivery of LAs and thus ensure their prolonged effect and reduced toxicity, the encapsulation of the LA molecules is required. Many LAs are delivered by oral or injection route, and hence the studies referring to controlled release (delivery) of LA are in general referring to nanoscale systems [156-158]. It is important to note that hydrogels figure as one of most popular types of LA drug carriers [156].

1.5.4.1 Procaine hydrochloride

Procaine hydrochloride (procaine HCl) is a synthetic drug that belongs to the therapeutic family of LAs (Figure I.16). Its structure of amino ester resembles natural compounds actively participating in nerve impulse transmission. It is believed that the cationic form of the drug, which seems to be the active principle, joins the Na^+ channels on the nerve membrane, thus blocking the initiation and transmission of nerve impulses [159]. The result of this is a reversible loss of sensation. Microencapsulation of procaine HCl may reduce undesirable effects due to its short duration of action causing cardiac and neurological toxicity, accompanied sometimes by allergic reactions.

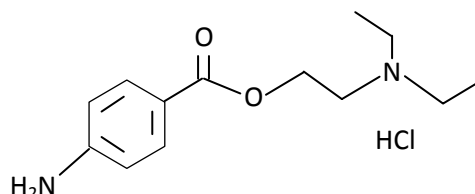
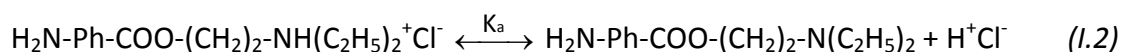


Figure I.16. Structural formula of procaine HCl

Procaine HCl, or 2-diethylaminoethyl p-aminobenzoate hydrochloride, may suffer hydrolysis in aqueous media. Its cationic form is in equilibrium with its nonionized form, as follows [160]:



Where K_a is the equilibrium constant. A certain study has demonstrated that in aqueous solution of procaine HCl with the concentration from 0.6×10^{-5} M to 11.1×10^{-5} M the ester is not hydrolyzed and the above given equilibrium is almost totally shifted toward the ionized form of the drug, with a negligible contribution of the nonionized form [159].

Table I.7 summarizes the main properties of procaine HCl. Instrumental methods such as spectrophotometry, high-performance liquid chromatography, gas chromatography, chemiluminescence, fluorometry, ultraviolet-visible spectrophotometry and electrochemistry, have been used for determining the concentration of procaine HCl in drug release studies [160].

Table I.7. Properties of procaine HCl [161]

Molecular formula	$C_{13}H_{20}N_2O_2 \cdot HCl$
Molecular weight	272.77
Melting point	154-158°C
Water solubility	soluble
pK _a [160]	9.3

1.5.4.2 Release of procaine hydrochloride from hydrogels

Procaine HCl has been used in the studies of drug release from hydrogels that were mainly of sub-micron sizes. Tan et al. developed hydrogel-based system aimed at intracorporeal controlled release of procaine HCl [162]. They synthesized pH-responsive hydrogel nanobeads consisting of methacrylic acid-ethyl acrylate crosslinked with di-allyl phthalate. The drug release was higher at nanogels with lower crosslinking density. Furthermore, the release is promoted at higher pH when nanogels are in swollen state and of high porosity (Figure I.17). This study proved that the drug could be released from the carrier in different regions of the physiological environment.

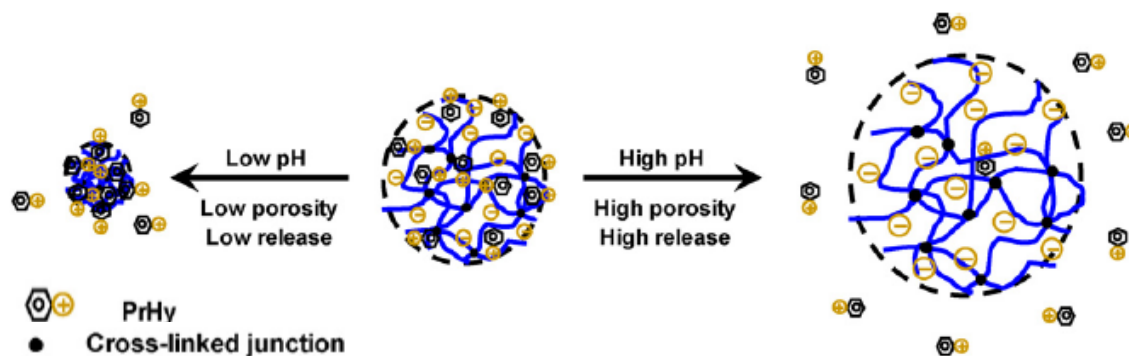


Figure I.17. Schematic display of procaine HCl release from pH-responsive nanogel under different pH [162]

Tan et al. investigated the release of procaine HCl from methacrylic acid-ethyl acrylate nanogels that were modified using layer by layer (LBL) technique [163]. This technique makes use of electrostatic attractions between oppositely charged polyelectrolytes (PE) to construct layers with controllable thickness at nanometer length scale onto planar or curved surfaces. The examined nanogels were intended for enteral administration and LBL coating was applied to alleviate the undesirable initial burst release. (LBL coating included alternating layers of poly(allylamine hydrochloride) (cationic) and poly (sodium 4-styrenesulfonate) (anionic) polyelectrolytes). The bare nanogels without coating possessed a hydrodynamic radius of 47 nm, and with the addition of the fifth layer, the radius approached 56 nm. Nanogels with more PE layers swelled the least, resulting in a corresponding lower diffusion of procaine HCl.

Thermosensitive bulk hydrogels based on PNIPAAm and poly(vinylpyrrolidone) (PVP) intended for oral delivery of procaine HCl were investigated by Greever et al. [146]. These

hydrogels were prepared by free-radical polymerization using ultraviolet light and had VPTT near human body temperature ($\sim 38^\circ\text{C}$). Dried samples loaded with procaine HCl at 1 wt % were employed in drug release studies as a function of temperature. It was observed that the drug was released at a slower rate at temperatures above VPPT (Figure I.18). Drug release is delayed for the period of time required for hydration of the matrices, and since the hydrophobic interactions become more dominant above VPTT, the rate of water sorption is considerably slowed and thus the drug release time.

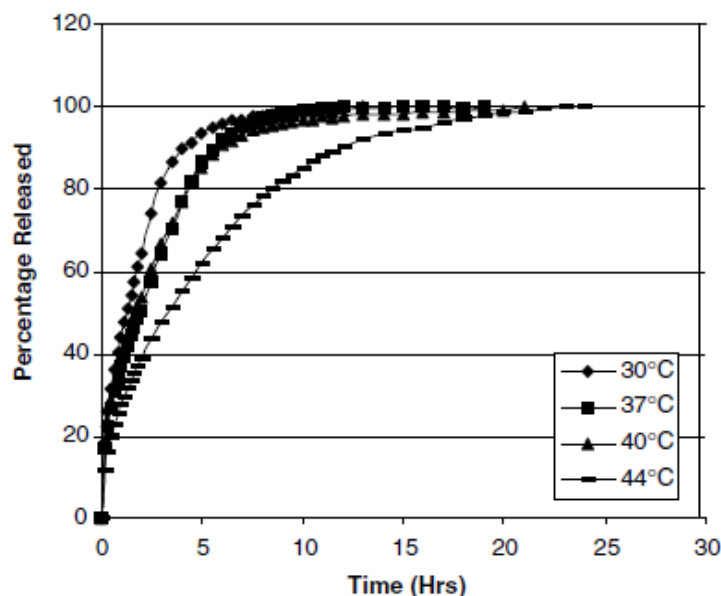


Figure I.18. Effect of temperature on the release rate of procaine HCl from chemically crosslinked PNIPAAm/PVP hydrogels in distilled water [146]

I.5.5 PNIPAAm-based hydrogels as drug release systems

Pure PNIPAAm hydrogels in the form of disks of 15 mm in diameter were examined for the use in pulsatile drug delivery systems using a range of model probe molecules with different solubility, size and chemical nature [164]. It was demonstrated that the hydrogel swelling rate was decreased by the presence of hydrophobic drugs and may be increased by the osmotic influence of hydrophilic drug molecules. The shrinking of hydrogels with increase in temperature resulted in a drug pulse. Wu et al. reported the study of the interactions between proteins (bovine serum albumin and insulin) and pure PNIPAAm hydrogels (in the form of slabs) and their influence on protein loading and release kinetics [165]. The presence of proteins in hydrogel matrix led to increase in VPTT. The release of proteins above VPTT of hydrogels the release was retarded due to the formation of skin layer.

Dually responsive PNIPAAm-co-acrylic acid (AA) hydrogel nanobeads with cage-like structure have been prepared by Gu et al. [166]. They applied SiO_2 emulsion copolymerization method resulting in hollow spheres of diameters between 300 to 370 nm at 25°C . The hydrogel spheres were used for controlled release of hydrophilic drug isoniazid and were aimed for the oral delivery route. Cavity structure of spheres brought a more profound volume transition than a solid PNIPAAm/AA sphere, as well as higher drug loading capacity. Also, the

drug was encapsulated in both, shell and cavities and its release was governed by dissociation of the drug-matrix interactions.

One of the methods for synthesis of micro-sized PNIPAAm hydrogels is inverse suspension polymerization. Certain studies dealing with this system resulted in PNIPAAm microbeads from around 60 μm up to 400 μm in diameter, depending on the amount of the crosslinker in reaction mixture or the addition of comonomer [62, 167]. The characterization of these microbeads implied their potential use in drug delivery.

A study of drug release from PNIPAAm-based hydrogel microbeads was conducted by Taşdelen et al., who also applied method of inverse suspension polymerization for microbeads synthesis [168]. The polymerization reactions were performed without addition of emulsifier and resulting microbeads had diameters in the range from 180 to 250 μm . Lidocaine hydrochloride and viagra were incorporated into the pure PNIPAAm microbeads (Figure I.19) and PNIPAAm microbeads modified with itaconic acid (IA) by irradiation induced grafting. P(NIPAAm/IA).

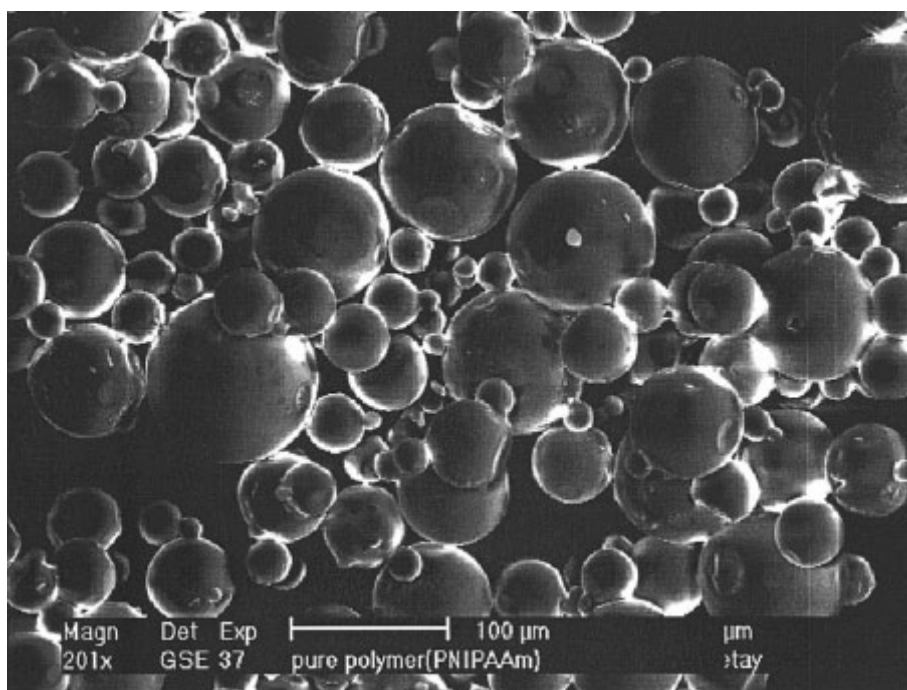


Figure I.19. ESEM micrograph of pure PNIPAAm microspheres [168]

The P(NIPAAm/IA) microbeads featured improved drug loading capacity, possessed pH-sensitivity enabled but kept thermosensitivity that affected the drug release profiles (Figure I.20). This qualified the modified microbeads for the local therapeutic application of cationic drugs under controlled pH and temperature conditions.

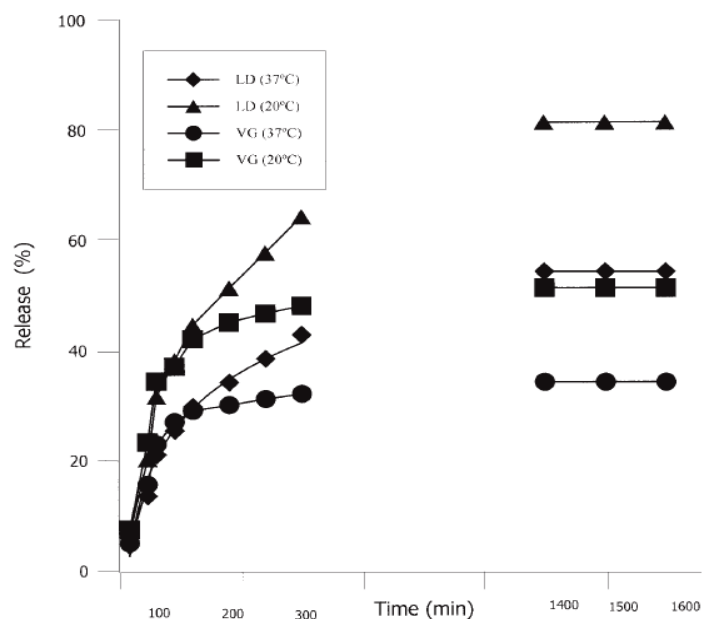


Figure 1.20. Release percentage of nonspecific adsorbed lidocaine (LD) and viagra (VG) from P(NIPAAm/IA) microspheres in phosphate-buffered solution of pH 7.4 at two different temperatures (20 and 37°C)

I.5.6 PNIPAAm/CA hydrogels as drug release systems

Temperature-dependent release of bovine serum albumin (BSA) from full-IPN bulk hydrogels of PNIPAAm and CA was reported by de Moura et al. [169]. The authors prepared the IPN hydrogels in the form of 3mm-thick films by free-radical polymerization/crosslinking reaction of NIPAAm followed by crosslinking of alginate with Ca^{2+} ions. The transport of BSA from these bulk thermosensitive hydrogel was governed by the diffusion and chain relaxation. The importance of the chain relaxation in the BSA release increased with the PNIPAAm and/or alginate content in the hydrogel. The chain relaxation was almost exclusive mechanism of drug release from the hydrogels at 37°C, above VPTT of PNIPAAm. The rate of BSA release from hydrogels was inversely proportional to both amount of PNIPAAm and temperature. In addition, the full-IPN hydrogels showed improved mechanical properties in comparison with the pure PNIPAAm hydrogel.

There are many studies on PNIPAAm/CA hydrogels in the form of beads above 1 mm in diameter that will be referred to as macrobeads. The principle of the macrobeads formation is based on the extrusion-dripping of adequate polymer solution into solution with Ca^{2+} ions where crosslinking of alginate occur.

Shi et al. synthesized hydrogel macrobeads with semi-IPN structure of linear PNIPAAm and CA and used them for the release studies of indomethacin [170]. The hydrogel macrobeads were prepared by dispersion of indomethacin and PNIPAAm (previously synthesized) in an alginate aqueous solution, and subsequent dropping of the mixture into a solution of calcium salt where gelling occurred. Furthermore, analogous biomineralized macrobeads were prepared using calcium phosphate associated with alginate/chitosan outer membrane. In addition to thermosensitivity of synthesized macrobeads, their pH-sensitivity contributed to the enhanced release of the drug at higher pH as a result of higher swelling ratio, and at

higher temperature (Figure I.21), due to the squeezing effect. This study is of interest for hydrogels application in oral drug delivery.

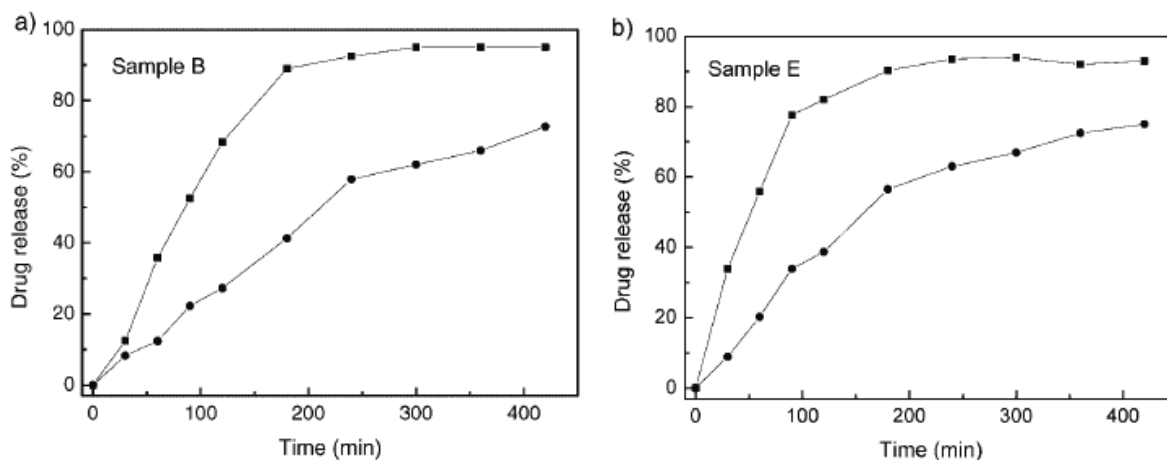


Figure I.21. Temperature-dependent release profiles at pH 7.4 for sample B based on PNIPAAm/alginate weight ratio 1:6 (a) and sample E based on PNIPAAm/alginate weight ratio 1:1.3 (b), measured at 25°C (●) and 37°C (■) [170]

An interesting approach in modifying the drug release profiles from semi-IPN hydrogels of linear PNIPAAm and CA was also proposed by Shi et al. [171]. They prepared drug-loaded hydrogel macrobeads with biomineralized polysaccharide coating (based on phosphate and chitosan) using the same principle as in previously described study [170]. It was shown that the mineralized polysaccharide membrane could prevent the permeability of encapsulated drug (indomethacin) and reduce the drug-release rate effectively when the temperature was below VPTT of hydrogels.

A work reported by Kim et al. encompassed study of the preparation of thermosensitive hydrogel macrobeads from the graft copolymer of alginate and PNIPAAm [19]. The solution of this copolymer with dissolved model drug (blue dextran) was dropped into calcium chloride solution and the drug release studies were performed using the prepared hydrogel macrobeads. A distinctive feature of these macrobeads is higher drug release rate at temperature above VPTT of the hydrogel in comparison to temperature below it. This is explained by the presence of PNIPAAm side chains that act as a thermosensitive valve for the pores of the macrobeads.

Khorram et al. synthesized hollow hydrogel macrobeads (Figure I.22) with full-IPN structure of PNIPAAm and CA [172]. The solution of monomer (NIPAAm), crosslinker (MBAAm), catalyst (TEMED) and SA was added to the solution of calcium chloride and initiator (TEMED) where the polymerization was carried out (in nitrogen atmosphere). The IPN beads were eventually chelated in EDTA/phosphate solution and dried. The authors studied the influence of the drug loading method on encapsulation. Prepared macrobeads had a diameter of around 3 mm in dried state and were used for loading of diltiazem hydrochloride and acetaminophen. Injection of the drug into the hollow macrobead enhanced loading efficiency of drug with low aqueous solubility, while no advantage exists compared to the soaking method for highly soluble drugs.

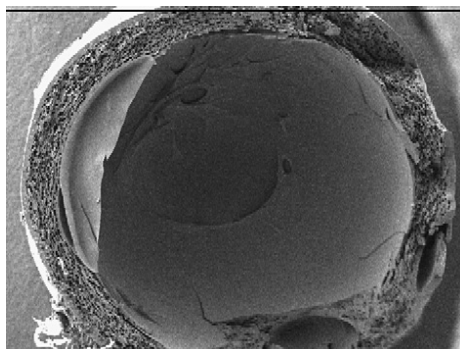


Figure I.22. SEM of hollow beads of chelated PNIPAAm [172]

Novel CA macrocapsules with aqueous core and thermosensitive membrane of PNIPAAm were reported by Wang et al. [108]. They employed co-extrusion minifluidic approach, as presented in Figure I.23. The outer solution was SA solution blended with previously prepared and freeze-dried PNIPAAm nanobeads (using precipitation polymerization). The core was made of aqueous solutions of poly(ethylene glycol) (PEG) of different molecular weights and vitamin B12.

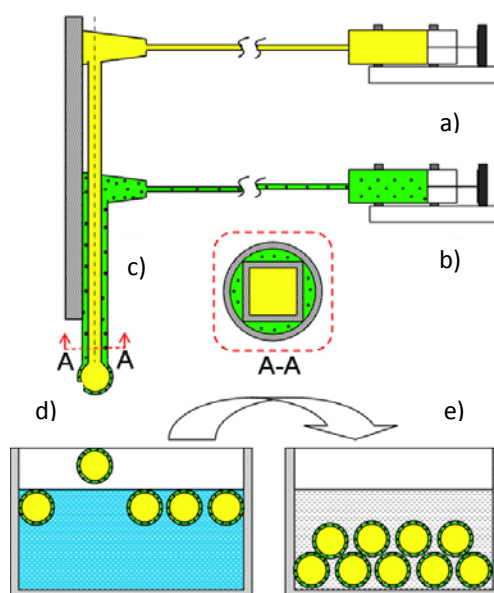


Figure I.23. Schematic illustration of the apparatus and process for preparation of CA capsules with aqueous core and alginate membrane. Constant flow pump for core solution (a); constant flow pump for SA solution (b); co-extrusion minifluidic device (c); container of CaCl₂ solution (d); container for CA capsule storage (e) [108]

The hydrogel macrocapsules in this work showed retarded release of model drug at temperature below their VPTT due to the closure of “gates” in CA capsule membranes by swollen PNIPAAm nanobeads. The opposite is observed at higher temperature (40°C) (Figure I.24).

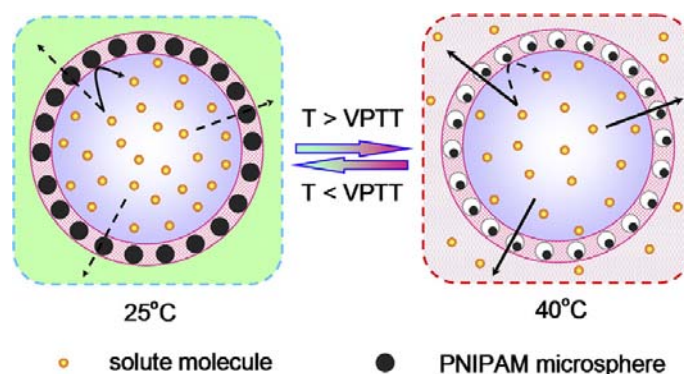


Figure I.24. Schematic illustration of the thermo-responsive characteristic of CA capsule with aqueous core and thermo-responsive membrane [108]

Fabrication of thermosensitive microcapsules (and ultrathin multilayer films) could be also achieved by layer-by-layer (LBL) assembly of charged polyelectrolytes. Wang et al. synthesized microcapsules by LBL assembling the PNIPAAm and alginate onto manganese carbonate and melamine formaldehyde cores, and subsequently removing the templates [20]. In addition, they examined release profile of recrystallized taxol coated with multilayer films of PNIPAAm and alginate ((PNIPAAm/ALG)₁₂). The results showed that the drug release rate is almost equal at 25°C and 37°C (Figure I.25). This was explained by the fact that compact structure of PNIPAAm at high temperature (above VPTT) reduced the permeability of the multilayer films and counteracted the effect of increasing release rate.

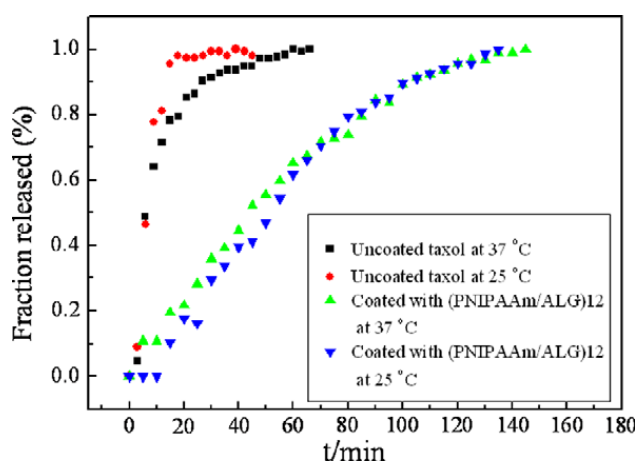


Figure I.25. Release profile of coated and uncoated recrystallized taxol with multilayer films of (PNIPAAm/ALG)₁₂ at 25°C and 37°C [20]

I.6 Hydrogel-based functional textiles

I.6.1 Smart textiles

The original and main function of textile materials has always been clothing. Clothing items improve the quality of people's life, providing them protection and comfort. Recent decades are marked with a progress in manufacturing of textile materials that feature additional properties apart from esthetic and decorative. These materials have been known as

technical textiles [173]. This definition of technical textiles sometimes refers to functional textiles. One of the increasingly exploited and developing type of textiles, which can be classified under the technical textiles, are smart textiles. These materials are regarded as “smart” because they are capable of sensing changes in environmental conditions or body functions and responding to these changes [174].

Major medical applications of smart textiles encompass textile sensors for different monitoring purposes and transdermal drug delivery systems [175]. The latter application implies added biofunctionality to these special types of textile materials. The use of textile materials to support and release a drug is ancient, as found for example in the application of an ointment to a fabric for covering a wound [174]. However, design of textile-based transdermal drug delivery vehicles is a complex process. It implies fulfillment of requests such as concerning optimal release properties and bioavailability of the drug [175]. As discussed in the section 1.5.3, transdermal drug delivery has multiple advantages over the other routes.

Development of textiles based on stimuli-sensitive linear polymers or stimuli-sensitive hydrogels belongs to the field of smart textiles. Application of thermosensitive hydrogels and other types of smart hydrogels onto textile substrates has been increasingly exploited in last two decades, which is testified through several reviews [176-178]. Among the ultimate aims of extensively growing interest in this area is development of efficient and controllable drug release systems, whether in tissue engineering, as degradable implants, or in transdermal delivery, which encompass an array of potentially promising medical applications.

Environmentally friendly activation of textile materials enhances adhesion capabilities and binding efficiency toward hydrogel formulations [176]. Plasma treatment generates different plasma constituents like electrons, ions, free radicals, meta-stables and UV photons that contributed the introduction of reactive groups and free radicals onto the surface [179]. Thus, interactions with polymer solutions or hydrogels are improved usually through hydrogen bonds, Van der Waals forces or dipolar interactions [180].

Taking into consideration a contact of the “intelligent”, hydrogel-based textile system with a skin, a cotton fabric appeared to be good choice, due to its unique physical and aesthetic properties combined with its natural origin and biodegradability. Knitted cloths have high porosity (among textile materials), providing high capacity of a medicine (in the case of medical bandages) [181] and better substrate for application of various polymeric materials, such as hydrogels. On the other hand, nonwovens are particularly popular in the production of medical and surgical textiles. The reasons for this are properties of nonwovens such as high porosity, short production cycles, higher flexibility and versatility, and lower production costs [173].

1.6.2 PNIPAAm-based functional textiles

Adding thermosensitivity to textile materials could be done achieved using polymer solutions having this property. The aims of developing thermosensitive textiles could be various, from achieving better thermal isolation necessary for divers [182], over wound

management [183] to the drug delivery [155]. Among these, controlled drug release systems are one of the most intriguing and demanding to design.

Applications of linear PNIPAAm on textile materials are far more studied than applications of PNIPAAm-based hydrogels. One of the most common methods of hydrogel attachment to the textile substrate surface is coating [178]. In a considerable number of studies dealing with the application of linear PNIPAAm to textiles, researchers mainly focused on grafting reactions. For instance, cotton cellulose fabric was used as a textile substrate for grafting of linear PNIPAAm by Jianqin et al [184]. They used pre-irradiation process in air by ^{60}Co - γ ray, followed by immersion of the treated fabric in a grafting solution (aqueous NIPAAm solution). The main active particles initiating reaction were the trapped radicals located in the interphase between the crystal and amorphous regions of cotton cellulose. Measured LCST was 35.4°C that is close to that of pure PNIPAAm. Research group of Gupta et al. [185] applied a similar principle of preparation to obtain thermosensitive textile material. They have achieved graft copolymerization of monomers NIPAAm and acrylic acid on polyester fabric in two steps. First, the radiation activation (by ^{60}Co - γ source) of polyester backbone was performed. This was followed by grafting of the monomer mixture on the activated surface was accomplished. Obtained system was proven to be potentially applicable as thermosensitive textile patch, which provides enhanced transdermal release of a drug (antibiotic tetracycline hydrochloride) at temperature above its relatively high LCST (around 37°C). Above given examples are based on pre-irradiation grafting of NIPAAm solutions on textile substrate. Beside pre-irradiation method, direct radiation is also appropriate and efficient in preparation of thermosensitive textiles [186, 187].

Apart from irradiation processes, chemical grafting of NIPAAm in different systems on textile materials was a topic of research interest as well. For instance, free-radical graft copolymerization of NIPAAm and vinyl-capped polyurethane anionmer was achieved on nonwoven fabric (70 % cellulose fiber, 30 % polyester), initiated by ammonium persulfate [188]. The authors labeled their system as hydrogel-grafted fabric that exhibit a type of elasticity and a high degree of swelling. The grafted nonwoven fabric was characterized by pH- and temperature sensitivity (VPTT around 33°C), potentially applicable as smart wound dressing and skin care cosmetic materials. Possible modification in the grafting process of PNIPAAm hydrogel on a textile surface is in the presence of ammonium cerium nitrate, having a function to initiate the grafting reaction on the cellulose fabric surface [6]. Treated fabric possessed thermosensitivity that qualifies it for use as wound dressing material and drug release device.

Another possible method of preparation of grafted thermosensitive hydrogel onto nonwoven fabric is a photo-induced graft polymerization. Chen et al [189] grafted pure PNIPAAm hydrogel on a polyethylene terephthalate (PET) film and a polypropylene (PP) nonwoven fabric surface (Figure I.26). The bonding between PNIPAAm hydrogel and PET film (as well as PP surface) was enhanced by argon (Ar^*) plasma treatment of the nonwoven, probably due to peroxy groups on the polymer surface formed by Ar^* plasma. The experimental procedure involved placement of plasma treated fabrics in feed mixture containing NIPAAm, crosslinker MBAAm, initiator APS, and a catalyst TEMED, followed by irradiation using a high-pressure mercury lamp.

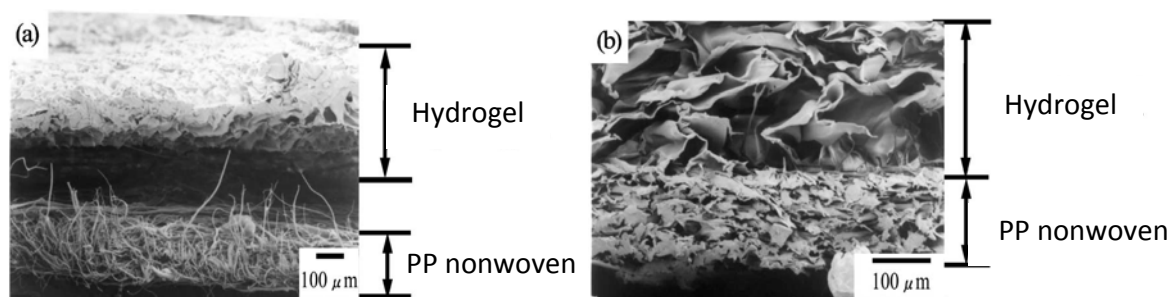


Figure I.26. SEM of freeze-dried PNIPAAm hydrogel onto: a) PP nonwoven and b) Ar* plasma-treated PP nonwoven (UV-graft + APS +TEMED+ MBAAm) [189]

According to several reports, grafting of PNIPAAm-based hydrogels on textile materials is enhanced by the presence of hydrophilic monomers with free carboxylic groups that easily react with modified surface of a textile substrate. For instance, the controlled substrate surface modification by introduction of new chemical groups could be effectively done by the low temperature plasma technique [190]. Maleic anhydride (MA) as a hydrophilic comonomer was employed in the preparation of PNIPAAm-based copolymer hydrogels with improved swelling capacities [191-194]. Therefore, MA is regarded as proper component for development of thermosensitive hydrogels based on PNIPAAm and intended for formation of smart textiles for controlled drug release applications.

Above given examples of studies on hydrogel-based textile structures refer to the formation of hydrogel films on the textile surface. However, the studies dealing with hydrogel nano- or microbeads are quite poor. One such study was done by Kulkarni et al. who prepared hydrogel nanobeads of PNIPAAm and chitosan copolymer by surfactant-free emulsion method [7]. This research encompassed functional finishing of cotton fabric with the pH and thermosensitive hydrogel nanobeads of around 200 nm in diameter (Figure I.27). The hydrogel nanobeads were covalently bonded to cotton fabric using polycarboxylic acid as crosslinking agent, which was followed by the simple pad-dry-cure application method. The water uptake of the functionalized fabric was controlled by pH and temperature.

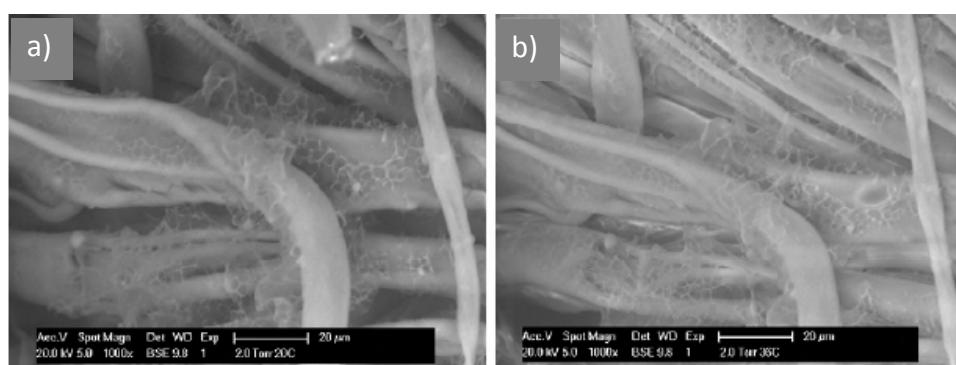


Figure I.27. ESEM images of cotton with incorporated hydrogel nanoparticles at 20°C (a) and 36°C (b) [7]

Coating of textiles with suitable polymeric materials for drug depot and release is a demanding and challenging task for chemical and textile engineers. The theoretical possibilities for design of smart clothes for controlled transdermal drug delivery are

numerous. Whether the drug to be released is a hormone (corticoids for patients suffering from neurodermitis or insulin for diabetes patients), an antiseptic substance or a local anesthetic, the crucial step in creation of the textile-based drug release system is an adequate design of polymeric materials in which the drug will be encapsulated. Among a myriad of novel multifunctional polymeric materials, thermosensitive hydrogels are good candidates in the mentioned application.

I.7 Conclusion

This literature review has shown an interest of using thermosensitive hydrogels as drug release system whose properties could be easily controlled via thermal stimulus. The choice of PNIPAAm, combined with alginate, seems to be an adequate one in view of the biomedical application intended. For these hydrogels, both macro form (patch) and micro forms (microbeads, nanobeads) can be found in drug release applications, though few studies can be found concerning their application on textiles. Considering this textile end-use, the first form, hydrogel film, usually implies simultaneous processes (hydrogel formation and grafting on textile material) that would industrially be interesting. On the other hand, there are many advantages of micro forms of thermosensitive hydrogels over macro forms like faster response to temperature changes and higher drug loading capacity. The applicability of both physical forms on a textile material is therefore worth consideration and their properties will hence be studied in this thesis.

Chapter II : MATERIALS AND METHODS

II.1 Chemicals

Chemicals employed for the preparation of thermosensitive hydrogels of all structures and physical forms presented in this report were:

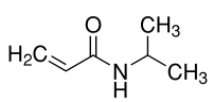
- *N*-isopropylacrylamide,
- *N,N'*-methylenebis(acrylamide),
- *N,N,N',N'*-tetramethylethylenediamine,
- Ammonium persulfate,
- Sodium alginate salt,
- Calcium chloride,
- Paraffin oil,
- Polyoxyethylene (20) sorbitan monooleate (Tween 80),
- Maleic anhydride, and
- Procaine hydrochloride.

Apart from these chemicals, solvents *n*-hexane and acetone were also used. General information on the relevant chemicals used in synthesis of all types of hydrogels is presented in the following sections.

II.1.1 *N*-isopropylacrylamide

Monomer *N*-isopropylacrylamide, NIPAAm (Table II.1) was employed in the synthesis of all analyzed hydrogels, giving them thermosensitivity via its polymerization to PNIPAAm.

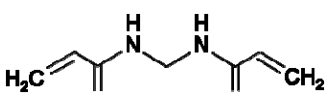
Table II.1. Properties of NIPAAm (Sigma-Aldrich)

Chemical formula	Appearance	Molecular weight	Assay, %	Melting point, °C
	White to light yellow crystalline powder	113.16	97	60-63

II.1.2 *N,N'*-methylenebis(acrylamide)

N,N'-methylenebis(acrylamide), MBAAm (Table II.2) was used as a crosslinking agent for PNIPAAm in the preparation of thermosensitive hydrogel films by solution polymerization and thermosensitive hydrogel microbeads by inverse suspension polymerization.

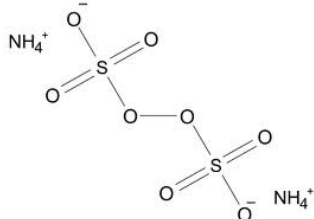
Table II.2. Properties of MBAAm (Sigma-Aldrich)

Chemical formula	Appearance	Molecular weight	Assay, %	Melting point, °C
	White, crystalline powder	154.17	99	>300

II.1.3 Ammonium persulfate

Ammonium persulfate, APS (Table II.3) was used as an oxidizing agent with *N,N,N',N'*-tetramethylethylenediamine to catalyze the polymerization of NIPAAm.

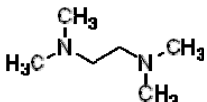
Table II.3. Properties of APS (Panreac)

Linear formula	Appearance	Molecular weight	Assay, %	Melting point, °C
	White, crystalline substance	228.20	98	120

II.1.4 *N,N,N',N'*-tetramethylethylenediamine

N,N,N',N'-tetramethylethylenediamine, TEMED (Table II.4) was used with APS to catalyze the polymerization of NIPAAm.

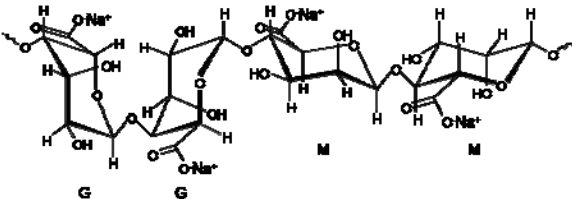
Table II.4. Properties of TEMED (Sigma-Aldrich)

Structural formula	Appearance	Molecular weight	Assay, %	Boiling point, °C	Density, g cm ⁻³ (20 °C)
	Yellow liquid	116.20	99	120-122	0.775

II.1.5 Sodium alginate

Sodium alginate, SA (Table II.5) was used in the preparation of PNIPAAm-based thermosensitive hydrogels with full-IPN and semi-IPN structures in different physical forms, and for preparation of pure CA hydrogel beads using electrostatic extrusion.

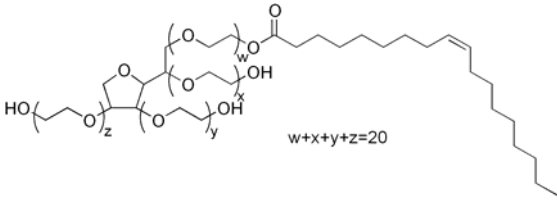
Table II.5. Properties of SA (Sigma-Aldrich)

Structural formula of unit	Appearance	Viscosity, cP (2 %, 25 °C)
	Cream colored powder	~250

II.1.6 Polyoxyethylene (20) sorbitan monooleate

Polyoxyethylene (20) sorbitan monooleate, Tween 80 (Table II.6) is nonionic emulsifier used in synthesis of hydrogel microbeads by inverse suspension polymerization using paraffin oil as a continuous phase.


Table II.6. Properties of Tween 80 (Riedel-de Haen)

Structural formula of unit	Appearance	Molecular weight	Density, g cm ⁻³	HLB
	Yellow viscous liquid	1310	1.06-1.09	15

II.1.7 Maleic anhydride

Maleic anhydride, MA or furan-2,5-dione (Table II.7) was used in the synthesis of PNIPAAm/MA copolymer hydrogel microbeads by inverse suspension polymerization.

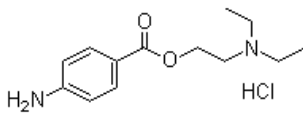
Table II.7. Properties of MA (Duga holding a.d.)

Structural formula	Appearance	Molecular weight	Assay, %	Melting point, °C
	white solid	98.06	99.5	52.8

II.1.8 Procaine hydrochloride

Procaine hydrochloride, procaine HCl (Table II.8) was selected as a model drug for release studies from thermosensitive hydrogel microbeads. Its properties are already described in detail the section I.5.3.1.2 of the Chapter II.

Table II.8. Properties of procaine HCl (Fisher Scientific)

Structural formula	Appearance	Molecular weight	Assay, %	Melting point, °C
	white solid	272.77	99	154-158°C

II.2 Methods of hydrogel preparation

The basic principles underlying the formation of thermosensitive hydrogel films and thermosensitive hydrogel microbeads using two approaches will be presented in the following sections.

II.2.1 Theory

II.2.1.1 Free-radical polymerization

Among the methods used for preparation of thermosensitive polymers, the most popular method is conventional free-radical polymerization (FRP) [195]. FRP proceeds via a chain mechanism, which basically consists of four different types of reactions involving free radicals. The generation of free radicals can be done by UV-light or by a redox initiator system. The most commonly used methods for free-radical polymerization are bulk polymerization, polymerization in solution, suspension polymerization, and emulsion polymerization.

II.2.1.1.1 Polymerization in solution

In this work, full-IPN PNIPAAm-based hydrogels in the form of films were prepared by solution copolymerization/crosslinking. Polymerization of NIPAAm can be performed in an organic solution, or in aqueous media using redox initiator system [61]. This is possible due to solubility of monomer NIPAAm in organic solvents such as toluene, dimethyl sulfoxide, but also in water. The shortcomings in use of organic solvents are understandable from the ecological and health point of view given that the final application of the polymers/hydrogels is in biomedical field. We opted for the most common redox system for polymerization of NIPAAm in an aqueous media. It consist of ammonium persulfate (APS) as an initiator and *N,N',N₀,N₀'*-tetramethylethylenediamine (TEMED) as a catalyst. Scheme of free-radical generation using redox system persulfate-TEMED is given in Figure II.1.

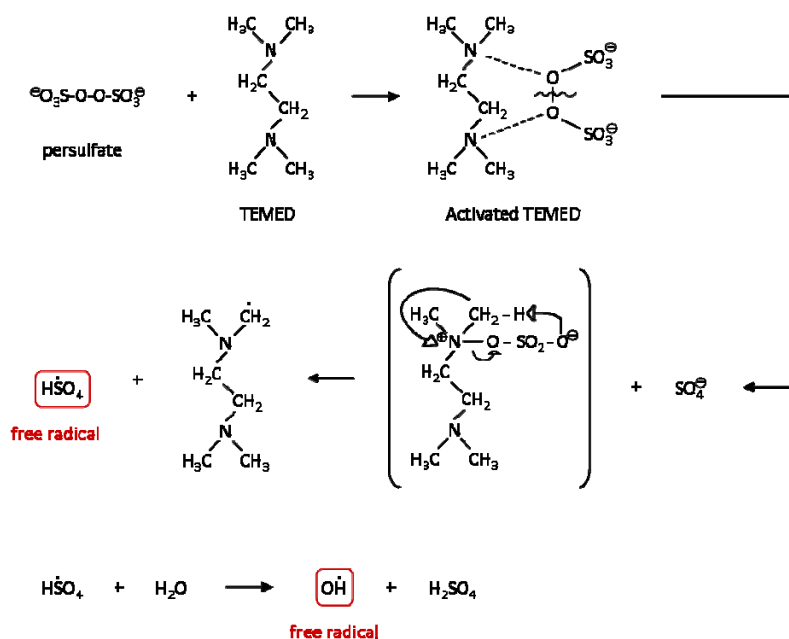


Figure II.1. Generation of free-radicals in the most common redox system for polymerization of NIPAAm

Free radicals that are able to initiate the polymerization of NIPAAm are persulfate and hydroxyl radicals that are very sensitive to oxygen presence. In general, FRP is inhibited or retarded by the presence of oxygen since it is highly reactive toward propagating polymer radicals, forming peroxides and hydroperoxides, which are unable to propagate the polymerization [196]. Hence, the reaction is carried out under an inert atmosphere, usually of nitrogen. General reaction synthesis of linear PNIPAAm by free-radicals is given in Figure II.2.

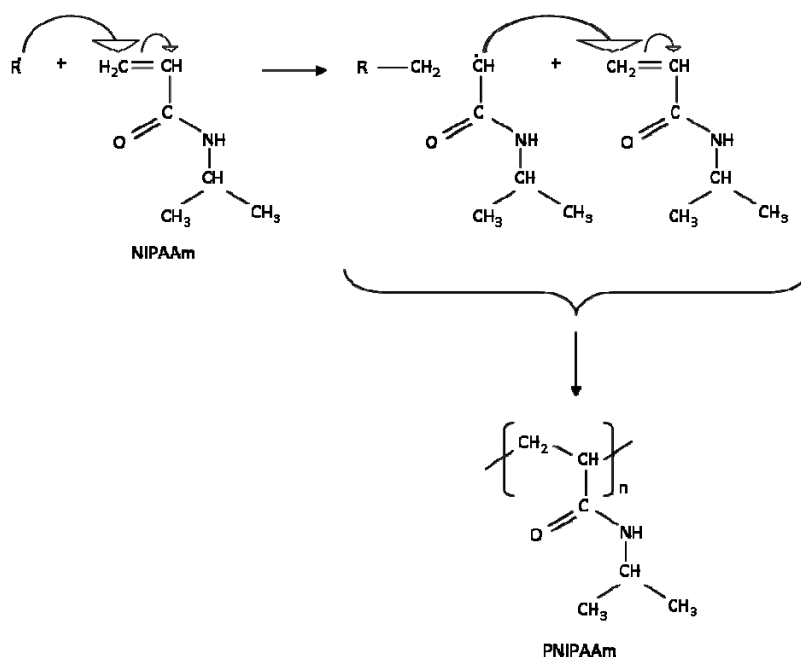


Figure II.2. Reaction of free-radical polymerization of NIPAAm

For the formation of a polymer 3D network, i.e. PNIPAAm hydrogel, a crosslinker is added in the initial reaction solution. In our aqueous system it was difunctional crosslinker *N,N'*-methylene bisacrylamide (MBAAm). Thus, a simultaneous copolymerization–crosslinking reaction between one monomer and crosslinker is achieved. Figure II.3 displays the structure of such a PNIPAAm hydrogel, i.e. PNIPAAm crosslinked with MBAAm.

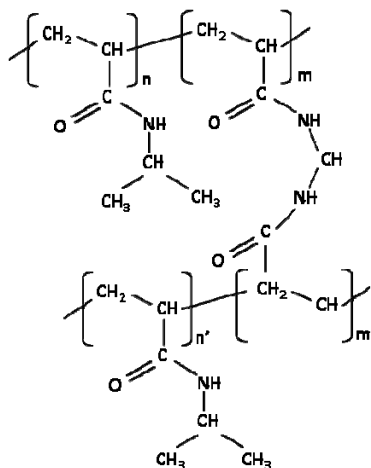


Figure II.3. Structure of PNIPAAm crosslinked with MBAAm (adapted from [197])

II.2.1.1.2 Inverse suspension polymerization

Heterogeneous (or particle forming) free-radical initiated chain polymerization in general includes suspension, emulsion, dispersion, and precipitation polymerization. In suspension polymerization, monomer phase is suspended in a continuous liquid phase in the form of micro droplets. This is done by means of a stirrer and an adequate droplet stabilizer. Polymerization occurs inside the drops and usually proceeds via a mechanism similar to that found in bulk free-radical polymerization, depending on the absence or presence of a monomer diluent in the monomer droplets [198]. The products of the polymerization are corresponding polymer microbeads, of approximately same size as the monomer microdroplets. In suspension polymerization water-insoluble monomers are suspended in water. In inverse suspension polymerization, solutions of the monomer and initiator are suspended in an oil phase. The size of droplets depends, in addition to reactor design, on stirring speed, volume ratio of water to monomer, concentration, and type of emulsifier and viscosities of both phases [199]. The stability of dispersed droplets is enhanced by addition of emulsifiers. The small amounts of emulsifier hinder coalescence and agglomeration and break-up the droplets during polymerization.

Polyacrylamide and water soluble acrylates are well known examples of polymers produced by inverse suspension polymerization. Regarding the formation of 3D polymer networks (i.e. hydrogels), acrylamide is usually copolymerized with bisacrylamide, using the most popular system of initiator and catalyst, persulfate-TEMED. Hence, reactions displayed in the previous section (II.2.1.1.1) are applicable in this case, in the formation of PNIPAAm hydrogel microbeads. Emulsifiers used in acrylamide inverse suspension polymerization include

sorbitan esters [200], polyoxyethylene-polyoxypropylene block co-polymers [167], various amphiphilic oligomers such as Span and Tween [198], etc.

II.2.1.2 Ionic crosslinking

Sodium alginate (SA) as sodium salt of linear polysaccharide was used in the preparation of the following hydrogel types:

- thermosensitive hydrogel films with full-IPN structure (crosslinked PNIPAAm/CA),
- thermosensitive hydrogel microbeads with semi-IPN structure formed using electrostatic extrusion (linear PNIPAAm/CA),
- CA hydrogel beads formed using electrostatic extrusion,
- thermosensitive hydrogel microbeads with semi-IPN structure obtained by inverse suspension polymerization (crosslinked PNIPAAm/SA), and
- thermosensitive hydrogel microbeads with full-IPN structure obtained by inverse suspension polymerization (crosslinked PNIPAAm/CA).

In the last step of certain preparation procedures (a, b, c, and e), alginate was crosslinked by means of ionic interactions in the solution of calcium salt. During the crosslinking of alginate in aqueous solution, which is composed of guluronate and mannuronate residues, sodium ions are replaced with calcium ions. The structure of guluronate residues accommodating calcium ions in formed network is displayed in Figure II.4.

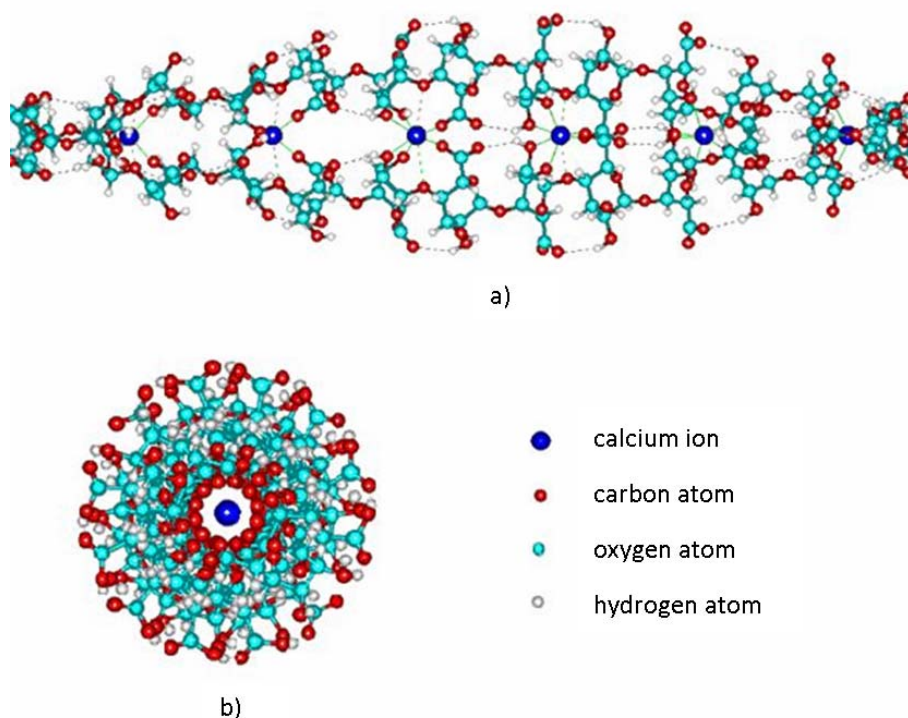


Figure II.4. Helix of Ca-poly- α -L-guluronate: view along the axis with a display of hydrogen bonds and binding places of calcium (a) and view perpendicular to the axis (b) [201]

II.2.1.2.1 Electrostatic extrusion

A technique of electrostatic extrusion was applied with the aim of producing thermosensitive hydrogel microbeads having a structure of semi-IPNs, composed of PNIPAAm as linear component CA as crosslinked component.

This spray technique has overcome the drawbacks of the simple dropping method, with regard to the reduction of the beads size as well as the higher rate of beads formation. Electrostatic extrusion is based on the extrusion of a polymer solution through a needle in the presence of an electric field, established between the needle tip and a collecting solution which reacts with the droplets to form hydrogel microbeads. Electrostatic forces contribute to the disruption of the liquid filament at the needle tip by forming a charged stream of small droplets [114, 202]. Collecting solution is also known as hardening since gelation of the extruded droplets occurs in it. In the case of alginate, calcium ions are responsible for the crosslinking, i.e. gelling of the forming beads. There are three main system geometries into which electric field can be applied to liquid extrusion, as shown in Figure II.5.

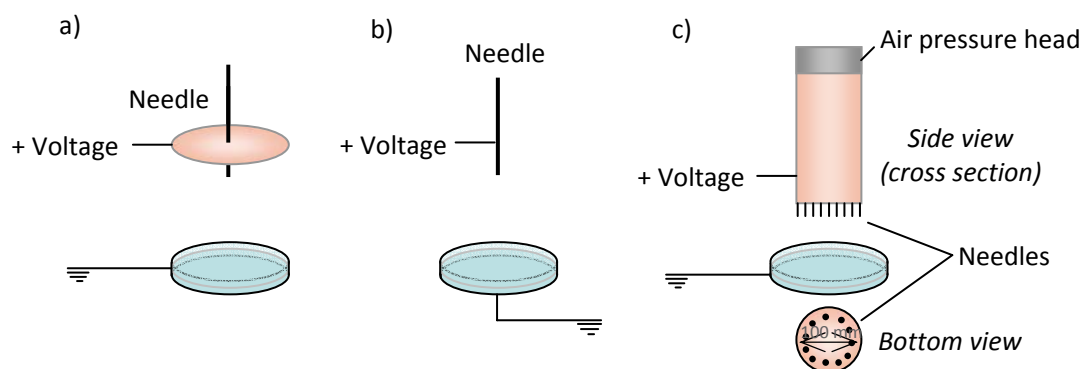


Figure II.5. Different geometries of the electrostatic extrusion process: parallel-plate setup with plate charged positively (a), positively charged needle setup (b), and multi-needle parallel-plate device (c) (adapted from [118])

Electrostatic force depends on geometry of a system and since it is relatively small, reduction of droplet diameters is mainly caused by the decrease in surface tension and voltage. However, its effect on the extrusion is expected to increase considerably near the critical electrical potential [118]. When taking into consideration a negatively single needle configuration with positively charged plate, i.e. the collecting solution, it can be easily concluded that resulting droplets will be of significantly larger size because of the reduced diffusional mobility of negatively charged functional groups of polyelectrolyte (in our case of alginate) in comparison with the counterions (Na^+ ions). Therefore, due to the lower surface density of a droplet in the second configuration, the surface tension value increases and hence, the droplets of greater size are formed [114]. In the case of sodium alginate solution, it is proved that the most efficient configuration for microbeads production is a system with positively charged needle [114, 116, 203]. As opposed to the geometry of parallel plates, in this system a significantly smaller surface (needle tip) is available, having as a consequence higher surface charge at the same value of applied voltage, and hence, formation of much smaller droplets. Furthermore, due to the mutual charge repulsion resulting in an outwardly

directed force, the surface tension, acting against the gravitational force, is decreased, and droplets of smaller diameter, in comparison with the absence of electric field, are formed.

The main components of the setup for electrostatic extrusion in this study were: a syringe pump that forces a polymer solution through a plastic syringe with a needle, a high voltage power supply, and a solution of a salt of multivalent cation in which a gelling of droplets occurs (Figure II.6).

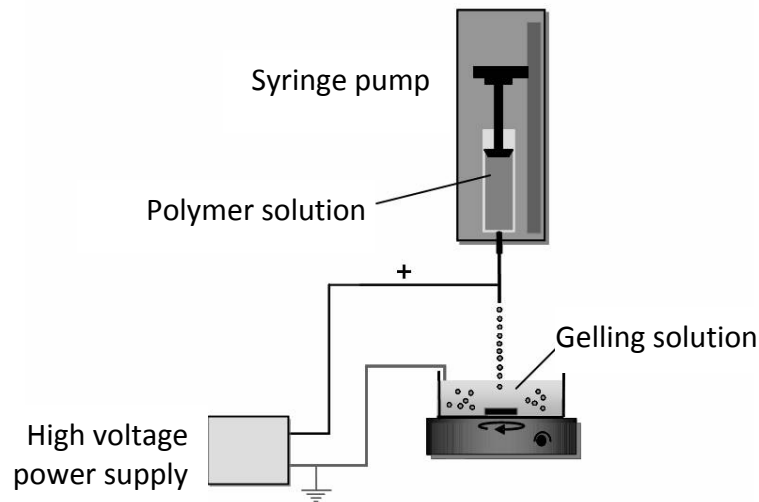


Figure II.6. Setup for the electrostatic extrusion (adapted from [116])

When positive pole is applied on a needle tip, it induces charge separation, and, in the case of sodium alginate solution, the concentration of small positive sodium ions on a surface of a droplet. The mass of a formed droplet at the moment of its detachment from the needle tip is determined by the balance among three forces: gravitational, electrostatic and surface tension [114]:

$$F_g + F_e = F_\gamma \quad (II.1)$$

$$\frac{4}{3} r^3 \rho g + qE = 2\pi r_0 \gamma(U) \quad (II.2)$$

Where r is the droplet radius, ρ the density of extruded solution, q the charge on a droplet, E the strength of the electric field, r_0 the inner radius of a needle, and γ is the surface tension of the polymer solution. The moment of detachment of a droplet from a needle tip is determined by the acquirement of the state of the lowest energy (corresponding to the formation of many small drops rather than the large one). Rayleigh [204] proved that the disruption occurs when the charge, q , on a droplet of radius, r , is given by:

$$q \geq 8\pi(\epsilon_0 \gamma r^3)^{0.5} \quad (II.3)$$

Where ϵ_0 is the permittivity of air ($\epsilon_0=8.85 \times 10^{-12} \text{ C}^2 \text{ N}^{-1} \text{ m}^{-2}$). Surface tension drops down when the applied voltage is increased and theoretically becomes zero when the voltage reaches a certain critical value that corresponds to the diameter of a formed drop. The process of electrostatic extrusion is a complex function of a number of parameters that

influence beads size and shape. In the case of pure CA beads, it is proved that the final diameters can be varied by changing applied voltage, needle diameter, the distances from the needle tip to the surface of the gelling solution (electrodes distance), or by modifying the properties of polymer solution [114, 205]. There are several extrusion modes that depend on the strength of electric field such as dripping mode, pulsating mode, stable jet mode, and unstable jet mode [206]. In comparison with other extrusion techniques, electrostatic droplet generation can give much smaller particles [113].

II.2.2 Experimental

II.2.2.1 Thermosensitive hydrogel films

Two types of hydrogel films were prepared: pure crosslinked PNIPAAm and full-IPNs based on crosslinked PNIPAAm and calcium alginate (CA). The synthesis implied the copolymerization/crosslinking in solution of NIPAAm based on free-radical polymerization mechanism. In the case of full-IPN films, (sodium) alginate was crosslinked in the presence of two-valent calcium ions by means of ionic interactions. Hence in the preparation of full-IPN hydrogel films, in addition to free-radical polymerization in solution than encompassed copolymerization/crosslinking reactions (synthesis of PNIPAAm network), ionic crosslinking was conducted (synthesis of crosslinked alginate, CA).

In the following procedure description, all quantities in wt % are based on the amount of monomer (NIPAAm) employed. NIPAAm was purified prior to use by recrystallization from *n*-hexane. Initially, an aqueous solution of 5 wt % NIPAAm monomer and crosslinker MBAAm (2 and 3 wt %) was prepared and purged with nitrogen, while kept on a magnetic stirrer in an ice-water bath. The synthesis of IPNs based on PNIPAAm and CA was performed in the same manner, with a difference in the first step, which implied dissolution of predetermined amount of sodium alginate in distilled water prior to adding NIPAAm and MBAAm. In all cases, after completion of deoxygenation in duration of 40 min, the solution was quickly transferred in a desiccator where vacuum was established for 20 min. Afterwards, the solution was removed from vacuum and under the stream of nitrogen an initiator APS (1 wt %) in the form of freshly prepared 10 w/v % aqueous solution and a catalyst TEMED (1 wt %) were added. After a short homogenization on a stirrer (around 20 s), solution was injected with a syringe in a glass mould, composed of two glass plates separated by a 1.5mm-thick gasket. The moulds were stored at 4°C for 24 h. Afterwards, in the case of pure PNIPAAm, the films were removed from the moulds and placed in distilled water. Concerning the IPN-hydrogel films, instead of water, the moulds were placed into 1.5 w/v % aqueous solution of CaCl₂, after removing gaskets, for 24 h. Then the films were removed from the glass plates and placed into a fresh CaCl₂ solution for 24 h more. The basic steps in preparation of IPN-hydrogel films are displayed in Figure II.7.

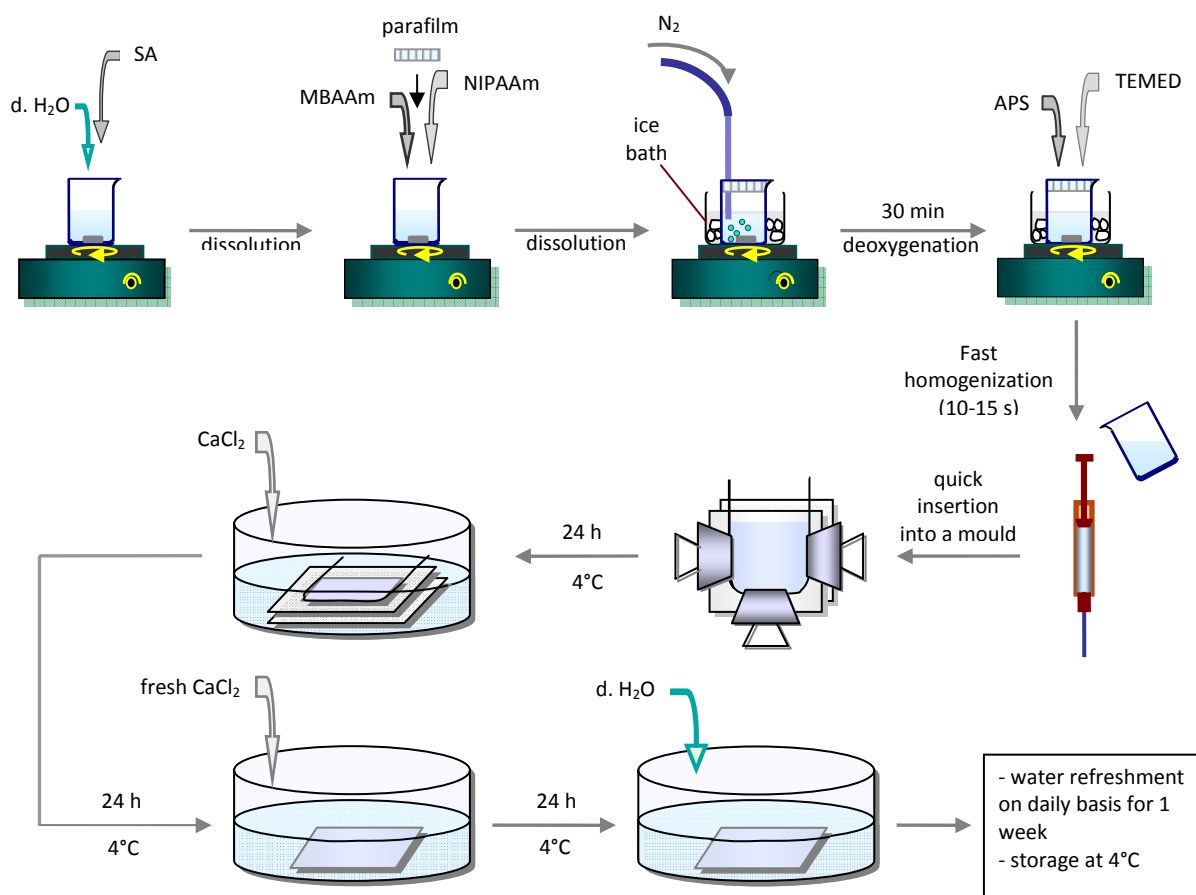


Figure II.7. Steps in synthesis of full-IPN hydrogel films

Finally, all synthesized hydrogel films were kept in fresh distilled water with daily refreshment for a week, with the purpose of purification and removal of excess reagents. Eight different hydrogel films were prepared: 2 pure PNIPAAm films (P-0-5-2 and P-0-5-3) and 6 IPN films based on PNIPAAm and calcium alginate (IPN-1-5-2, IPN-2-5-2, IPN-3-5-2, IPN-1-5-3, IPN-2-5-3 and IPN-3-5-3). Letters P and IPN in the name codes describe pure PNIPAAm network and interpenetrating polymer network respectively. The first number stands for the weight fraction of SA, the middle one defines the weight fraction of the monomer NIPAAm and the last one represents the weight fraction of the crosslinker MBAAm based on the weight of NIPAAm, all referring to the composition of the initial reaction solutions. Absolute amounts of chemicals and their concentration employed in preparation of these hydrogel films are given in Table II.9.

Table II.9. Composition of feed solutions in the synthesis of hydrogel films

Sample	SA, g	NIPAAm, g (mmol)	MBAAm, g (mmol)	APS (10w/v%), μ l (mmol)	TEMED, μ l (mmol)
P-0-5-2	0	1.25 (11.05)	0.0252 (0.165)	125 (0.055)	16.3 (0.110)
IPN-1-5-2	0.2399	1.25 (11.05)	0.0252 (0.165)	125 (0.055)	16.3 (0.110)
IPN-2-5-2	0.4847	1.25 (11.05)	0.0252 (0.165)	125 (0.055)	16.3 (0.110)
IPN-3-5-2	0.7350	1.25 (11.05)	0.0252 (0.165)	125 (0.055)	16.3 (0.110)
P-0-5-3	0	1.25 (11.05)	0.0378 (0.248)	125 (0.055)	16.3(0.110)
IPN-1-5-3	0.2399	1.25 (11.05)	0.0378 (0.248)	125 (0.055)	16.3 (0.110)
IPN-2-5-3	0.4847	1.25 (11.05)	0.0378 (0.248)	125 (0.055)	16.3 (0.110)
IPN-3-5-3	0.7350	1.25 (11.05)	0.0378 (0.248)	125 (0.055)	16.3 (0.110)

II.2.2.2 Thermosensitive hydrogel microbeads obtained by inverse suspension polymerization

Inverse suspension polymerization was applied as one of the methods for syntheses of thermosensitive hydrogel microbeads based on PNIPAAm. The first type of hydrogel microbeads was synthesized without addition of emulsifier, for comparison purposes. In all other syntheses a nonionic emulsifier Tween 80 was used.

The procedure of synthesis of pure PNIPAAm microbeads is further explained in detail. Polymerization was carried out in a 500-ml round bottom reactor equipped with a stirrer, reflux condenser, sampling port, and inlet for nitrogen supply (Figure II.8). The stirrer blade was kept at a constant distance of 0.5 cm from the bottom of the reactor.

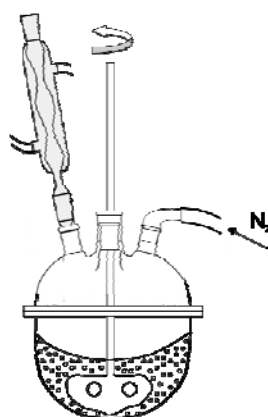


Figure II.8. Setup used in synthesis of hydrogel microbeads by inverse suspension polymerization

The reactor was maintained at 25°C in a water bath throughout the whole procedure. Initially, paraffin oil and emulsifier Tween 80 were introduced into reactor, and stirred at a rate 280 min⁻¹ in an atmosphere of nitrogen during 45 min. Simultaneously, monomer

NIPAAm, crosslinker MBAAm and initiator APS were added to water, previously deoxygenated by nitrogen bubbling for 20 min. Bubbling was continued for the following 20 min, after the addition of chemicals. Afterwards, the aqueous solution was poured into reactor, and 1 min later, catalyst TEMED was added. The mixture was kept under nitrogen until polymerization was finished, 3 h after TEMED addition.

In the preparation of PNIPAAm/MA copolymer hydrogel microbeads, comonomer MA was added to aqueous phase along with NIPAAm, MBAAm, and APS. The syntheses of the semi-IPN PNIPAAm/SA and full-IPN PNIPAAm/CA microbeads encompassed initial dilution of SA in water, followed by addition of NIPAAm, MBAAm, and APS. All further steps were as previously explained for the pure PNIPAAm hydrogel microbeads. The last step in the preparation of full-IPN microbeads encompassed the incubation of purified microbeads in CaCl₂ solution (1.5 w/v %) to achieve alginate crosslinking by calcium ions. Table II.10 gives compositions of the feed mixtures in synthesis of various types of hydrogel microbeads by inverse suspension polymerization.

Table II.10. Composition of oil and aqueous phase in the synthesis of hydrogel microbeads by inverse suspension polymerization

Sample	Paraffin oil, ml	Tween 80, ml (mmol)	MBAAm, g (mmol)	SA, g	MA, g (mmol)
M-50/1 (10/1)-E 0	200	0	0.054 (0.350)	0	0
M-50/1 (10/1)-E 1	200	2.00 (1.64)	0.054 (0.350)	0	0
M-50/1 (5/1)-E 0.5	100	0.50 (0.410)	0.054 (0.350)	0	0
M-25/1	100	1.00 (0.821)	0.109 (0.710)	0	0
M-50/1	100	1.00 (0.821)	0.054 (0.350)	0	0
M-75/1	100	1.00 (0.821)	0.036 (0.234)	0	0
M-100/1	100	1.00 (0.821)	0.027 (0.175)	0	0
M-25/1-MA 2.5	100	1.00 (0.821)	0.109 (0.710)	0	0.044 (0.444)
M-25/1-MA 5	100	1.00 (0.821)	0.109 (0.710)	0	0.087 (0.887)
M-25/1-MA 10	100	1.00 (0.821)	0.109 (0.710)	0	0.174 (1.77)
M-25/1-SA 0.5	100	1.00 (0.821)	0.109 (0.710)	0.100	0
M-25/1-SA 1	100	1.00 (0.821)	0.109 (0.710)	0.200	0
M-25/1-SA 2	100	1.00 (0.821)	0.109 (0.710)	0.400	0
M-25/1-CA 0.5	100	1.00 (0.821)	0.109 (0.710)	0.100	0
M-25/1-CA 1	100	1.00 (0.821)	0.109 (0.710)	0.200	0

* The components whose amount in all syntheses were kept constant were: NIPAAm -2.000 g (17.7 mmol), APS - 0.04 g (0.175 mmol), TEMED - 0.120 ml (0.810 mmol), and distilled water – 20 ml.

After the completion of synthesis, hydrogel microbeads were separated from the oil phase by multiple washing in a mixture of acetone and water (1:1), and finally with pure water. The first step in purification of microbeads included the addition of 40 ml of water into the reactor and gentle stirring followed by centrifugation of the mixture for 35 min at a rate of

2000 rpm. After careful removal of the oil phase with emulsifier at interface of phases, the main part of aqueous phase was pipetted off. The next step was re-suspending of microbeads into 100 ml more water and performing another cycle of centrifugation under the same condition. After centrifuging and removal of oil and aqueous phases, the microbeads were transferred into a 100 ml mixture of acetone and water (1:1) and washing steps in this mixture, including centrifugation, were repeated 3 times (30 min at 2000 rpm). Hydrogel microbeads were then stored in a beaker with 100 ml of water. The following day, the microbeads were re-suspended in fresh water. After 24 h, another set of washing was performed. After the removal of water, 50 ml of acetone was added and the suspension was placed in ultrasonic bath two times for 5 min. Then, one centrifugation cycle was conducted (30 min at 200 rpm), sedimented microbeads were suspended in fresh 100 ml mixture of acetone and water (4:1) and again centrifuged under the same conditions. Finally, the microbeads were stored in water with periodical refreshment of aqueous medium once a day for the following 3 weeks. At the end of these purification steps, oil, emulsifier, monomer and other unreacted chemicals were considered removed and hydrogel microbeads purified.

II.2.2.3 Formation of thermosensitive hydrogel microbeads using electrostatic extrusion

Solutions aimed at electrostatic extrusion were prepared from previously synthesized PNIPAAm (in purified, solid form) and sodium alginate. The principle of linear PNIPAAm synthesis based on polymerization in solution was previously explained in the section II.2.1.1.1. Microbeads obtained in this manner had a structure of semi-IPNs.

II.2.2.3.1 Synthesis of linear PNIPAAm

Preparation of linear PNIPAAm was performed according to the similar procedure employed for the first part of the synthesis of hydrogel films, but without a crosslinker. A 5 wt % solution of NIPAAm in distilled water was mixed with a 2 wt% amount of initiator APS. After stirring and deoxygenation with nitrogen for 30 min, the catalyst TEMED was added to the solution (2 wt %). Weight percentages of APS and TEMED are relative to the monomer weight used. After 24 h storage in a refrigerator, PNIPAAm solution was purified by interchangeable precipitation in hot distilled water and dissolution in cold distilled water, according to the procedure found in [171]. Purified PNIPAAm was then dried in air for 24 h, followed by 48 h drying in vacuum oven at 50 °C. Finally, polymer solutions containing PNIPAAm and sodium alginate were prepared for the extrusion in an electric field. Figure II.9 represents the steps in preparation of pure PNIPAAm in solid form.

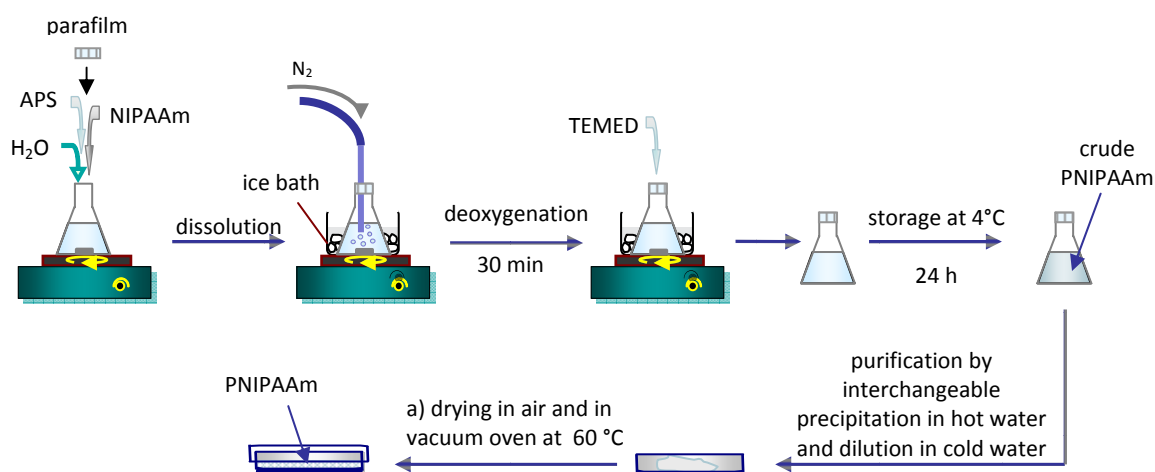


Figure II.9. Experimental steps in synthesis of linear PNIPAAm

II.2.2.3.2 Process of electrostatic extrusion

The setup displayed in Figure II.10 was used for the formation of pure CA microbeads and semi-IPN hydrogel microbeads (composed of linear PNIPAAm and CA). The configuration encompassed: vertically positioned syringe pump (Model R99-E, Razel, Scientific Instruments), plastic syringe with a stainless steel needle, a high voltage power supply unit (Model 30R, Bertan Associates Inc.) with a maximum current of 0.4 mA and variable voltage of 0 to 30 kV, and a collecting solution in a Petri dish (CaCl₂).



Figure II.10. Laboratory setup for the electrostatic extrusion

Extrusion of the polymer solution in an electric field is a complex process where size and shape of the obtained microbeads are function of different parameters. Hence, to more clearly understand this process, different operational parameters have been varied in a set of experiments, primarily implying change of: applied voltage, distance between the needle tip and a surface of the collecting solution (electrodes distance), flow rate of the extruded solution and solution composition. The study of these different parameters also aimed at establishing the optimal conditions for the formation of thermosensitive hydrogel microbeads of required micro sizes and close-to-spherical shape.

Polymer solutions with different ratios of PNIPAAm (synthesized as previously described in the section II.2.1.1) and SA were prepared. Optimization of microbeads production also encompassed variation of formulation parameters, i.e. concentration of PNIPAAm and SA in the extruded solution. The concentration of collecting CaCl_2 solution was always kept constant at 1.5 w/v %. After each extrusion run, a collecting solution with forming CA beads was kept on a magnetic stirrer for the following 30 min to allow uniform gelling to be completed, prior to further manipulation with the beads.

II.3 Methods of hydrogel characterization

II.3.1 Fourier Transform Infrared Spectroscopy

Fourier transform infrared spectroscopy (FTIR) was used to analyze the chemical structure of hydrogel films and hydrogel microbeads, i.e. to investigate the success of polymerization and crosslinking that should result in formation of full- and semi-IPNs. FTIR is important spectroscopic technique for structural elucidation and compound identification and it measures the absorption or transmittance of the light at each different wavelength. A molecule absorbs the IR radiation when a frequency of specific vibration of its atom is equal to the frequency of the IR radiation.

The preparation of the hydrogel samples for the FTIR analysis included initial drying in a vacuum oven at 60°C until reaching constant weight. Dried gels (xerogels) were then grinded into fine powder, mixed, further grinded with potassium bromide and pressed into pellets. For each type of xerogel, powder sample was mixed and grinded with potassium bromide (at sample concentration of 1.5 wt %) in a mortar and pressed in a pellet using a laboratory press. FTIR spectra were recorded at room temperature in transmission mode using a BOMEM spectrometer (Hartmann & Braun), in the range 4000 – 600 cm^{-1} and with a resolution of 4 cm^{-1} .

II.3.2 Differential Scanning Calorimetry

Differential scanning calorimetry (DSC) was employed to characterize the thermosensitivity of hydrogel films and hydrogel microbeads, as well as their thermal stability on a molecular level. DSC instrument monitors the changes in thermal energy that occur as a sample is heated, cooled or held isothermally, together with the temperature at which these changes

occur [207]. Thus, the information about the possible transitions in the materials could be obtained.

Thermosensitivity of hydrogel films and hydrogel microbeads that were obtained by inverse suspension polymerization were analyzed through a heating-cooling-heating cycle using a Q1000 DSC (TA Instruments). Three consecutive temperature ramps were applied at a heating rate of $3^{\circ}\text{C min}^{-1}$, in the range from 15 to 50°C , and under a nitrogen flow of 50 ml min^{-1} . For determination of VPTT of microbeads prepared by electrostatic extrusion by 2920 modulated DSC (TA Instruments), a temperature ramp from 20 to 50°C was applied, at a same heating rate of $3^{\circ}\text{C min}^{-1}$, and under a nitrogen flow of 50 ml min^{-1} . All runs were conducted in hermetically sealed aluminum pans, with distilled water used as a reference material. Calibration was performed using a high purity indium as standard. Temperature of the endothermic maximum was referred to as VPTT [208]. In all analyses, the scans were performed in triplicates.

For determination of the T_g using 2920 Modulated DSC (TA Instruments), the samples were prepared by drying under vacuum until reaching a constant weight. Each sample was placed in hermetically sealed aluminum pan, while the reference pan was empty. The scanning procedure involved initial heating from 20 to 200°C at a rate of $20^{\circ}\text{C min}^{-1}$ for the removal of any thermal history and residual moisture. Immediately afterwards the samples were exposed to cooling down to 10°C at a rate of $10^{\circ}\text{C min}^{-1}$, and this was followed by reheating from 10 to 200°C at a rate of $20^{\circ}\text{C min}^{-1}$. The scans were conducted under a nitrogen flow of 50 ml min^{-1} and calibration was performed using high purity indium as standard. The T_g was determined as the inflection point of the endothermic drift in the second heating curve of thermogram.

II.3.3 Dynamic Mechanical Analysis

Dynamic mechanical analysis (DMA) was used to investigate the viscoelastic properties of the hydrogel films at temperatures below and above VPTT. The measurement principle consists in applying a sinusoidal strain and the resulting stress is measured. The nature of applied forces can be compression, stretching, shearing or torsion [209]. The obtained results can be expressed as values of storage modulus, stiffness and damping values of the treated material [210].

The mechanical viscoelastic properties of hydrogel films were investigated in compression mode using a Dynamic Mechanical Analyzer Q800 (TA Instruments) in a compression mode. Behavior of the hydrogel in a frequency sweep mode was measured. Finally, a scan in temperature (temperature sweep) was applied with a purpose of comparing the storage and loss modulus of hydrogel samples before and after the phase change temperature. Dimensions of the samples used are selected according to the mode of measurement, i.e. disk-shaped samples had a diameter of 13 mm (thickness of 1.5 mm).

Initial tests of strain sweep to determine the linear viscoelastic region have permitted us to choose an amplitude of $10\ \mu\text{m}$, a value close to the one used in the analysis of dextran methacrylate hydrogels [211]. Due to the high water content of the hydrogels, a thin water layer between the hydrogel surface and the geometry acted as a lubricant [212]. To

overcome this problem, a thin spunbond nonwoven fabric was placed on both, upper and lower surfaces of disk-shaped hydrogel samples. Table II.11 summarizes the parameters adjusted for the mechanical testing of hydrogel films.

Table II.11. Operational parameters set in compression tests of hydrogel disks

Mode	Multi-frequency strain
Test	Isothermal / Frequency sweep
Amplitude	10 μm
Preload force	0.5 N
Isothermal temperature	30 $^{\circ}\text{C}$ / 40 $^{\circ}\text{C}$
Frequency	0.1-100 Hz

II.3.4 Gravimetry

Gravimetric measurements were used for the study of swelling behavior of both, macro forms (films) and micro forms (microbeads) of thermosensitive hydrogels. All measurements were done using analytical laboratory scale.

II.3.4.1 Swelling behavior of hydrogel films

Swelling behavior of hydrogels films was studied through the dependence of the equilibrium swelling ratios on temperature, kinetics of swelling from the dried state, kinetics of deswelling, and kinetics of reswelling. The hydrogel samples were punched from the films in the form of disks and further used in the gravimetric measurements of the swelling characteristics in distilled water.

Equilibrium swelling ratio (ESR) of hydrogels over a range of temperatures (from 25 $^{\circ}\text{C}$ to 50 $^{\circ}\text{C}$) was obtained after the incubation of hydrogels in thermostated water, until they reached equilibrium swollen state. ESR was calculated according to the following formula:

$$ESR = \frac{W_s - W_d}{W_d} \quad (II.4)$$

Where W_s represents the weight of equilibrium swollen hydrogel disk at a given temperature and W_d , the weight of the dried gel (xerogel). The weight of the swollen hydrogel was measured after blotting the excess surface water with wet filter paper. The weight of the xerogels was obtained after drying the samples under vacuum at 60 $^{\circ}\text{C}$ until reaching constant weight.

Swelling kinetics was investigated when completely dried samples were immersed in thermostated water at 25 $^{\circ}\text{C}$ and their weight was measured at predetermined time intervals. For the study of deswelling kinetics, the hydrogels were allowed to swell to equilibrium in water at 25 $^{\circ}\text{C}$, then transferred into thermostated water at 40 $^{\circ}\text{C}$, and periodically weighed. Reswelling kinetics of hydrogels was obtained by immersing preweighed equilibrium swollen hydrogels at 40 $^{\circ}\text{C}$ in thermostated water at 25 $^{\circ}\text{C}$, and

weighing them at predetermined time intervals. Swelling, deswelling, and reswelling kinetics of hydrogels were interpreted through the change of swelling ratio (SR) over a time scale, using the following equation:

$$SR = \frac{W_t - W_d}{W_d} \quad (II.5)$$

where W_t is the weight of hydrogel at predetermined time interval. The values of ESR and SR were calculated as the average of 3 measurements.

II.3.4.2 Swelling behavior of hydrogel microbeads

ESR of hydrogel microbeads obtained using electrostatic extrusion and by inverse suspension polymerization was determined in different manner than of hydrogel films due to their micrometer sizes. The microbeads were incubated in dialysis membranes (tubings) closed on both ends. The used membranes were Spectra/Por® 4 regenerated cellulose membranes (Spectrum Laboratories Inc.). These membranes carry no fixed charge and have molecular weight cutoff (MWCO) 12-14000, flat width 25 mm, diameter 16 mm, and volume-to-length ratio 2 ml cm⁻¹. The pieces of 6 cm in length were cut and soaked in distilled water at room temperature for 1 h to remove the preservative (glycerin). Then, the membranes were rinsed thoroughly in distilled water and dried in an oven at 60°C for 2 h, followed by vacuum drying at 60°C for 3 h. For each type of hydrogel microbeads, 5 membranes were prepared. One hundred milligrams of filtered microbeads with carefully removed excess water were weighed into the dry piece of membrane whose both ends were sealed with Spectra/Por® weighted closures of 35 mm in width (Figure II.11).



Figure II.11. Spectra/Por® dialysis tubing and closures [213]

Prepared microbeads in sealed membranes were kept in water at 25°C in a thermostat. The weighing was done after 24 h incubation. Prior to each weighing and after the removal of closures, the membranes were blotted with filter paper. Finally, the membranes containing microbeads were dried until constant weight. First, they were dried in an oven at 60°C for 2 h, and then in vacuum oven at the same temperature for 3 h.

II.3.5 Scanning Electron Microscopy

Scanning electron microscopy (SEM) was applied for studying the hydrogel morphology. SEM is a powerful microscopy technique that uses electrons to form an image and reveals information about sample morphology, chemical composition, crystalline structure and orientation of the materials making up the sample.

It is particularly important to adequately prepare the sample for SEM, taking into consideration vacuum conditions and electrons used in the analysis. This implies complete removal of water that would vaporize in vacuum and covering the non-conductive sample with a thin layer of conductive material. The latter is done in a sputter-coater, where metal target positioned above the sample is bombarded with ionized atoms of a heavy gas (usually argon) produced in an electric field, in a low vacuum environment. As a result, metal atoms ejected from the target deposit on the surface of the specimen making it conductive [214].

The morphology of the freeze-dried hydrogel disks and microbeads was analyzed using a JEOL 5800 SEM (JEOL). Prior to SEM observation, freeze-dried hydrogel disks were carefully fractured in liquid nitrogen and fixed on the sample holder using colloidal carbon paint. In the case of microbeads, certain amount of powder was carefully deposited on carbon double-sided tape adhered on the sample holder. Afterwards, the cross section of each sample was coated with Ag-Pt-Pd alloy by sputtering for 30 s. The scanning was performed at an accelerating voltage of 10 kV and at magnifications ranging from x75 to x2500.

II.3.5.1 Freeze-drying

Procedure of freeze-drying or lyophilization was applied as a pretreatment for hydrogel samples intended for SEM analysis. During this procedure, water is controllably removed from the specimen structure. Hence, it is responsible for maintaining hydrogel pore structure that exists in hydrated state, as opposed to regular air drying when the network structure simply collapses.

The freeze-drying is carried out via three main phases: freezing, primary drying, and secondary drying. During freezing of the sample all fluids take solid state, either crystalline, amorphous, or glass. Primary drying or sublimation is performed under vacuum and at higher temperatures in order to induce ice sublimation. The secondary drying or desorption phase is the last stage of freeze-drying treatment when bound water is extracted. This phase is carried out at a higher vacuum than primary drying and at above-zero temperatures.

The aim of the SEM analysis of hydrogel films and microbeads was to obtain information about the pore structure of hydrogels in the swollen state below and above their VPTT. Concerning hydrogel films, the disk-shaped samples of 10 mm in diameter were incubated in distilled water at 25°C and at 40°C for 48 h, before a treatment in a freeze-dryer GAMMA 1-16 LSC (Martin Christ) for 48 h. Each disk was placed in a small cosmetic container with 2 ml of water and covered with perforated parafilm. Freeze-drying process included freezing at -30°C followed by primary vacuum drying at -23°C and secondary vacuum drying at 20°C. Hydrogel microbeads obtained by inverse suspension polymerization were freeze-dried in another device, using a different procedure. A small cosmetic container was filled with 0.1 g

of equilibrium swollen microbeads at 25°C. After addition of 1 ml of water, each container was covered with perforated parafilm. The treatment was conducted in a freeze-dryer ALPHA 2-4 LD plus (Martin Christ). Freeze-drying was conducted at -70°C and 80 mbar and lasted for 4h. Dried samples were kept in the same containers sealed with lids and additional layer of parafilm and stored in a desiccator.

II.3.6 Optical Microscopy and Image Analysis

II.3.6.1 Optical microscopy

Hydrogel microbeads obtained by electrostatic extrusion (semi-IPN structure) were observed under optical microscope Axioskop (Zeiss) in transmission mode and equipped with a camera IVC 800 I2S. Hydrogel microbeads synthesized by inverse suspension polymerization were recorded under another optical microscope Ergaval (Carl Zeiss-Jena) equipped with TP-1001C Topica CCD camera (Krüss). A drop of the microbeads suspension was deposited on a microscopic slide and covered with a cover slip prior to observation. The magnifications ranging from x10 to x40 were used. In the case of microbeads whose diameter was approaching or entering the millimeter range, a digital camera (Fuji, Finepix F455) was used for generation of microbeads images instead. Determination of the microbeads size and shape was done using adequate image analysis software.

II.3.6.2 Image analysis

Image analysis was employed to determine the size and size distribution of hydrogel microbeads obtained by electrostatic extrusion and by inverse suspension polymerization. In addition, study of the pore size of freeze-dried hydrogel films and microbeads was conducted with help of image analysis.

Software Image-Pro Plus 6.0 (Media Cybernetics) was used on images obtained from optical microscope for characterization of hydrogel microbeads produced by electrostatic extrusion. Examination of microbeads under a microscope provides a two-dimensional image. A mean diameter defined by this software is as an average of the diameters measured at 2 degree intervals. In addition to calculation of size and size distribution, degrees of roundness were also determined. Used formula for roundness within Image Pro Plus v. 4.0 software was $(\text{perimeter}^2) (4*\pi*\text{area})^{-1}$, with 1.0 indicating a perfect circle and larger values indicating oblong and non-circular forms.

Another software, ImageJ 1.44g was applied for determination of mean diameters of hydrogel microbeads obtained by inverse suspension polymerization.

In addition to images from optical microscope, image analysis was also used on SEM micrographs, for closer study of hydrogels morphology. The average pore size and pore size distribution of hydrogels films and hydrogel microbeads (obtained by inverse suspension polymerization) were determined using a software SmartTiff Image Viewer V1.0.0.10 (Carl Zeiss SMT, Ltd.).

II.3.7 Laser diffraction

A technique of laser diffraction or static laser light scattering was employed for the determination of the mean diameter and size distribution of hydrogel microbeads obtained by inverse suspension polymerization. This technique is more valid, precise and reliable than image analysis based on optical microscopy images.

Laser diffraction is one of the most used particle sizing techniques. It has a wide dynamic range, from 0.2 to 2000 microns and is very fast and reliable. Laser diffraction analyzers measure particles sizes based on their interaction with light. The particles that pass through a focused laser beam scatter light at an angle that is directly related to their size. Large particles therefore scatter light at narrow angles with high intensity, whereas small particles scatter at wider angles but with low intensity. The angular intensity of the scattered light is then measured by a series of photosensitive detectors (Figure II.12).

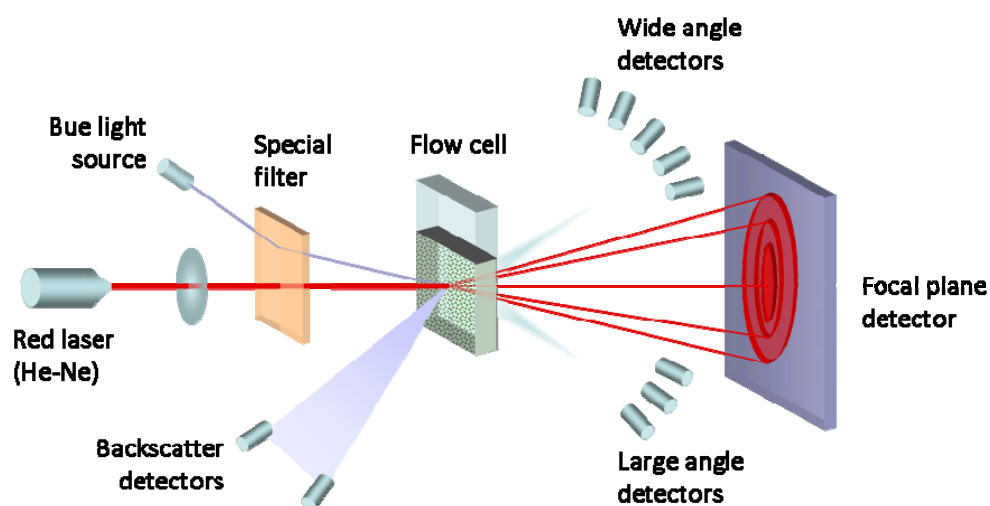


Figure II.12. Scheme of light diffraction measurement in Mastersizer 2000, Malvern Instruments (adapted from [215])

Particle size distribution is calculated by comparing obtained scattering pattern with an appropriate optical model. Mie theory, based on Maxwell's electromagnetic field equations, accurately predicts scattering intensities for all particles, small or large, transparent or opaque. It is important to have information about the optical properties of the particles and the surrounding medium (the refractive index difference). Within this theory, Fraunhofer approximation is relevant for larger particles since it assumes that particles measured are opaque and scatter light at narrow angles [216].

The measurements of microbeads size and size distribution were conducted using Mastersizer 2000 equipped with micro unit Hydro μ (Malvern Instruments). This micro unit enabled use of small sample quantity and ultrasonic treatment required for adequate dispersion of the sample and disruption of possible aggregates of hydrogel microbeads obtained by inverse suspension polymerization. Index of refraction was adjusted at 1.51 [217]. After the dosing of suspension (hydrogel microbeads in water) into a flow cell, the ultrasound in duration of 3 min was applied to disrupt any microbead aggregates that were

possibly present. This was followed by a scanning step and resulted in size distribution histograms. As representative mean diameter, volume moment mean or De Brouckere mean diameter $D[4,3]$ is automatically calculated since laser diffraction measurements produce an initial distribution around volume terms. This mean represents, in analogy to the moment of inertia in mechanics, the center of gravity of volume distribution [218]. Accordingly, surface area has d^3 dependence and volume d^4 dependence, where d is size of a particle (Equation II.6). $D[4,3]$ or equivalent volume mean is identical to the weight equivalent mean if density is constant.

$$D[4,3] = \frac{\sum d^4}{\sum d^3} \quad (II.6)$$

II.4 Methods of characterization of polymer solutions

II.4.1 Viscosimetry

Selected polymer solutions intended for electrostatic extrusion were submitted to determination of dynamic viscosity. For this purpose, a rotational viscosimeter with concentric measuring system (Rheomat RM108E/R, Mettler) was used. This system uses a motor driven bob that rotates within a fixed cylinder, providing a defined geometry (Figure II.13). The shear resistance of the sample in the gap allows for the measurement of motor torque (shear stress) [219]. Viscosity is obtained as ratio of the detected shear stress and previously set shear rate.

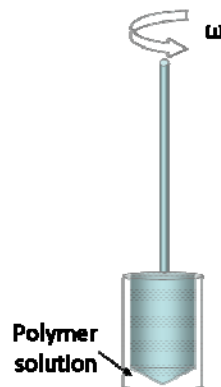


Figure II.13. Concentric measuring system for determination of dynamic viscosity by rotational viscosimeter

II.4.2 Surface tension measurements

Various polymer solutions intended for electrostatic extrusion were further characterized by the measurement of their surface tension. Applied Wilhelmy plate method, is based on interaction of a thin platinum plate with the surface of the solution being tested (Figure II.14). The container with the solution is raised until the contact between its surface and the plate is achieved. The downward force due to wetting is measured by a tensionmeter. Resulting surface tension (mN m^{-1}) is the force divided by the perimeter of the plate. The tensionmeter used was a Prolabo TD 2000. Prior to each measurement, the plate was cleaned in the flame.

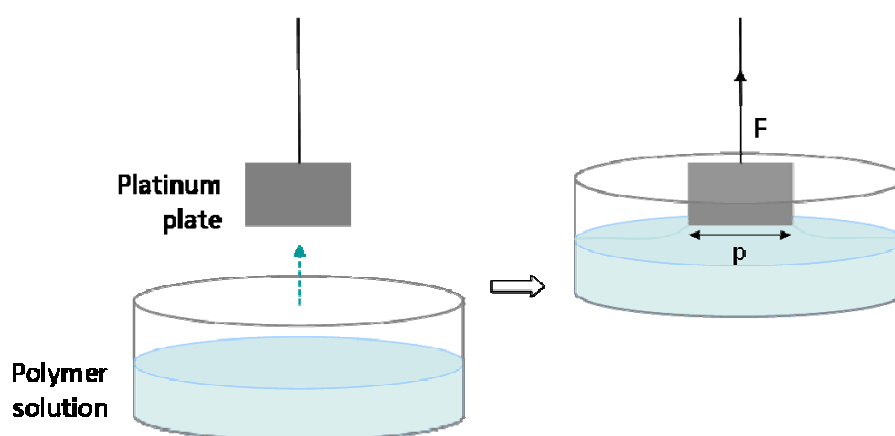


Figure II.14. Measurement of the surface tension using Wilhelmy plate

II.5 Methods of drug loading and release

II.5.1 Hydrogel microbeads obtained by electrostatic extrusion

II.5.1.1 Drug loading

The drug release experiments were performed using procaine hydrochloride (procaine HCl) as a model drug. Procaine HCl was loaded into selected hydrogel microbeads by sorption from concentrated solution (1 mg ml^{-1}). The weight ratio of the swollen beads and the drug solution was 1:10. The incubation was done in a beaker placed on a magnetic stirrer for 24 h at room temperature. Afterwards, swollen drug-loaded hydrogel beads were removed from the loading solution and kept for 5 min in pure distilled water while stirring. Finally, the beads were filtered, carefully controlling the removal of excess surface water and used in drug release tests.

To quantify the total amount of the drug entrapped in the microbead sample, 0.8 g of drug-loaded hydrogel beads were placed in 4 ml of sodium citrate solution (1 mol dm^{-3}) for 24 h. The role of the citrate ion is to chelate the calcium ion, thus destroying the hydrogel network to release the drug. Drug concentration was determined using a UV spectrophotometer (UV3100 spectrophotometer, MAPADA). The absorption spectrum of procaine HCl in sodium

citrate was initially recorded and maximum absorption was detected at 291 nm. A calibration curve was determined with 5 different concentrations of procaine HCl in sodium citrate.

II.5.1.2 Drug release using dissolution test

Drug release experiments were conducted at two temperatures, above (40°C) and below (25°C) the VPTT of the microbeads. To control the drug release at different time intervals, 2 series of 0.8 g samples of drug-loaded microbeads were prepared. Each sample was weighed and placed in a beaker with 4 ml of distilled water, covered with parafilm and kept in a water bath with a shaker at 25°C for the first series, and at 40°C for the second one.

At predetermined time intervals, a beaker was removed from the shaker, the suspension was filtered and drug concentration was determined spectrophotometrically, as described in the previous section for drug loading. Absorbance was recorded at maximum of 291 nm and was correlated with concentration using previously determined calibration curve of procaine HCl solutions in water. The spectrophotometrical analysis was carried out on a UV3100 spectrophotometer MAPADA. Drug release profiles were presented as a fraction of drug released in ratio to initially loaded amount of drug, i.e. as cumulative percentage drug release in time.

II.5.2 Hydrogel microbeads obtained by inverse suspension polymerization

II.5.2.1 Drug loading

Procaine HCl was loaded into the microbeads by simple sorption from concentrated solution (10 mg ml⁻¹). Dried microbeads (150 mg) were incubated in procaine HCl solution (30 ml) for 20 h at room temperature. Afterwards, the solution was removed from the swollen drug-loaded microbeads that were dried until constant weight for use in drug release studies. The amount of entrapped drug was determined by analyzing the solutions prior and after the loading period using HPLC-UV system that will be further described in the following section.

II.5.2.2 Drug release using Franz diffusion cell

Franz diffusion cell was employed for investigation of drug release profiles from hydrogel microbeads obtained by inverse suspension polymerization. The most popular application of Franz diffusion cell is in the development of transdermal pharmaceutical formulations. It is mainly applied for determination of diffusion coefficient from porous solid or semi-solid materials and suspensions using skin-like membranes.

There are different types of Franz diffusion cells depending on the joint type between the two chambers, absence or presence of jacket, glass type, receptor and donor volumes, etc. [220]. The Franz diffusion cell used in this report had jacketed both donor and receptor chamber (Figure II.15). The reason for controlling the temperature of the donor chamber is application of hydrogels as drug delivery matrices that are sensitive to temperature changes. Thus, by controlling the temperature of donor chamber the drug release rate is controlled.

The solution in acceptor chamber is stirred and always kept at the same temperature, usually 37°C, since it corresponds to temperature of the human body. The concentration change is tracked in receptor chamber by continual sampling during the experiment through the sampling port. The drug release studies were conducted using distilled water as a receptor fluid and as a medium in microbeads suspensions in donor chamber. The receptor chamber with capacity 5.65 ml was always maintained at constant temperature of 37°C by circulating thermostated water from the water bath via peristaltic pump to the jacket of the chamber. Acetate cellulose (AC) membrane (0.45 μm mesh size, Fisher Scientific) was used as semi-permeable membrane to mimic a human skin. Surface of area available for drug diffusion was 0.687 cm^2 . Prior to each drug release experiment, AC membrane that was equilibrated at 37°C in distilled water for 1 h.

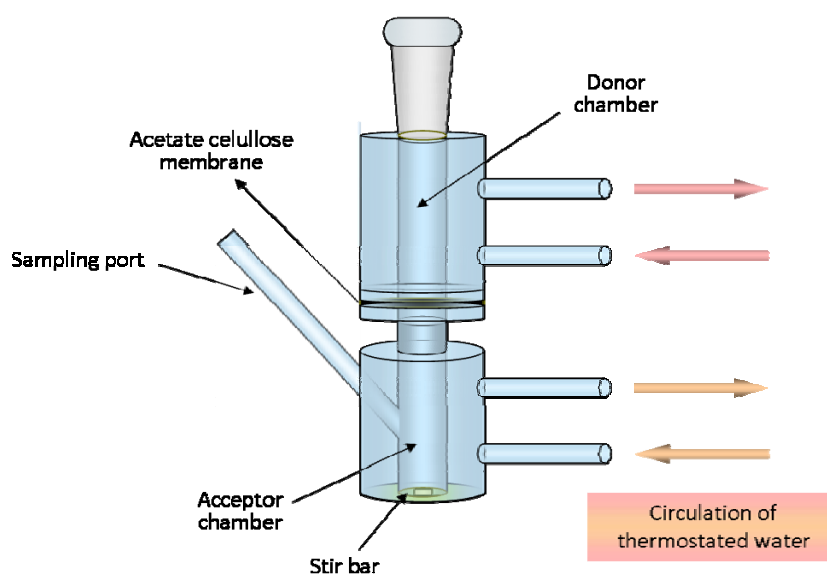


Figure II.15. Vertical Franz diffusion cell with jacketed donor and acceptor chambers

Two series of drug release studies were performed: when donor chamber was thermostated at 25°C and at 37°C. In this way the difference in cooling/heating the potential hydrogel microbeads-based patch was simulated. After filling the receptor chamber with thermostated water at 37°C and membrane equilibration, the cell was assembled and 10 mg of drug-loaded dried microbeads were carefully added to donor chamber. Then, 0.5 ml of fresh distilled water was added to donor chamber to hydrate dried microbeads and serve as a medium of donor suspension. Temperature of the added distilled water was 25°C or 37°C, depending on the temperature of water circulating through the jacket of this chamber). The sampling from receptor chamber was performed through long sampling port, using Teflon tubing as the extension of the needle mounted on a 1 ml graduated syringe. The aliquots of 0.5 ml were periodically withdrawn, after 5, 10, 15, 20, 25, 30, 40, 50, 60, 90, 120, 150, 180, 210, and 240 min. Withdrawn aliquots were replaced with the same volume (0.2 ml) of fresh distilled water (thermostated at 37°C) at each sampling.

II.5.2.3 High Performance Liquid Chromatography

High Performance Liquid Chromatography (HPLC) was applied for detection of procaine HCl concentration in drug release studies using Franz diffusion cell. HPLC is one of the most used analytical methods for the separation of the components of the mixture and very reliable method in quantification of drugs. The advantage of HPLC over UV spectrophotometry is in its higher specificity, sensitivity and applicability in formulations with low dose of a drug [221]. In general, chromatography is a separation process in which the components of a mixture are separated on an adsorbent column in a flowing system [222]. One phase of a system is stationary (adsorbent material), while the other is mobile and passes through the chromatographic bed. In HPLC the mobile phase is liquid and it is mechanically pumped through a column that contains the stationary phase [223]. A detector placed at the exit from the column and connected with a recorder allows obtaining a chromatogram [222]. Each component of the elution is identified by its retention time (the time at which elution from column occurs). The data derived for the chromatogram are usually generated through a refractive index detector, which measures the concentration of substance in the elution at a given point in time [223]. The area under the curve and the height of the peak for a specific compound is a function of the concentration of that component in the original solution.

Content of the procaine HCl in obtained samples was determined using a HPLC-UV system (Surveyor HPLC system, Thermo Fisher Scientific, Waltham, USA). Separation was accomplished using a Zorbax Eclipse® XDB-C18 column of dimensions 4.6 mm x 75 mm x 3.5 µm (Agilent Technologies, Santa Clara, USA). A forecolumn (dimensions 4.6 mm x 12.5 mm x 5 µm) from the same manufacturer was set in front of the column. The mobile phase was a mixture of methanol (A) and deionized water (B) at ratio 75%A:25%B. The elution parameters were a flow rate of 0.8 ml min⁻¹ and an injection volume 10 µl. UV spectrum of procaine HCl was obtained by Surveyor PDA detector. It contained two maxima at wavelengths 220 and 290 nm. Absorption maximum at 290 nm was used for quantitative determination of procaine HCl.

**Chapter III : SYNTHESIS AND CHARACTERIZATION OF
THERMOSENSITIVE HYDROGEL FILMS**

A research on thermosensitive hydrogels intended for application on textile materials and drug release purposes have started with synthesis and characterization of macro forms of hydrogels. The literature review on hydrogel/textile systems [184, 185, 188, 189] showed that grafted layers of hydrogels are most extensively investigated forms and hence we have chosen to initially study hydrogel films, supposing the possibility of using previously activated textile material (e.g. by plasma treatment) as a support at one side of a mould in which the reaction mixture for the formation of hydrogels will be poured into. Hence, thermosensitive hydrogel films of pure PNIPAAm and with full-IPN structure of crosslinked PNIPAAm and CA will be described in this Chapter.

III.1 Synthesis

Thermosensitive hydrogels in the form of films were synthesized by free-radical polymerization in solution at 4°C. Among eight hydrogel types, two were pure PNIPAAm hydrogel (pure PNIPAAm), whereas the other six had a structure of interpenetrating PNIPAAm network and CA network (full-IPN). The concentrations of monomer (NIPAAm), initiator (APS), catalyst (TEMED), and solution for crosslinking of alginate (CaCl_2) were kept constant throughout all syntheses. The fraction of crosslinker for PNIPAAm (MBAAm) was 2.0 and 3.0 wt %, with respect to monomer (NIPAAm), whereas sodium alginate (SA) concentration in reaction mixture was 1.0, 2.0, and 3.0 wt %.

Hydrogel films (~80x80x1.5 mm) were prepared using a glass mold, as displayed in Figure III.1. During and after the purification procedure described in the section II.2.2.1 of Chapter II, the hydrogels were stored in refrigerator.



Figure III.1. A glass mold used for the preparation of thermosensitive hydrogel films

What is relevant to mention is the complete transparency of pure P-0-5-2, P-0-5-3, IPN-1-5-2 and IPN-1-5-3 hydrogels. This can be attributed to low polymerization temperature (4°C), since it is known that synthesis temperature affects the optical clarity and the heterogeneity of the microstructure of PNIPAAm hydrogels [224, 225]. Due to low temperature, formation

of clusters during synthesis of hydrogel network was avoided and hence, no final opacity appeared. Although polymerization/crosslinking at lower temperatures leads to more regular hydrogel structure, it is proven that degree of swelling of such hydrogels is lower than of hydrogels prepared at higher temperatures. This indicates a decrease in crosslinking efficiency with rise in preparation temperature [226]. Figure III.2 presents all eight types of hydrogels punched from equilibrium swollen films at 4°C using a metal cylinder of 10 mm in inner diameter. The full-IPN hydrogels with higher fraction of alginate featured a slightly opaque appearance, as a result of the dominant influence of alginate network.

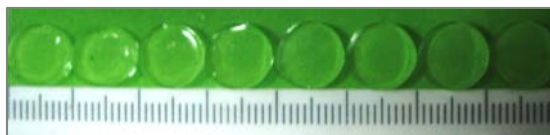


Figure III.2. Equilibrium swollen hydrogels disks at 4°C: P-0-5-2, P-0-5-3, IPN-1-5-2, IPN-1-5-3, IPN-2-5-2, IPN-2-5-3, IPN-3-5-2, and IPN-3-5-3 (in order from left to right)

III.2 Chemical structure

The results of FTIR analysis of thermosensitive hydrogel films with higher crosslinking degree of PNIPAAm (3 wt % MBAAm) are presented in Figure III.3. The spectra of all full-IPN hydrogels are similar. The samples of pure CA, based on 3 wt % alginate (CA-3) were also analyzed and presented for comparison. The spectra of hydrogels with lower crosslinking degree of PNIPAAm are given in the Appendix since they provide equivalent information as spectra given in Figure III.3.

In the spectra of P-0-5-3, IPN-1-5-3, IPN-2-5-3, IPN-3-5-3, characteristic absorptions of PNIPAAm are observed: the amide I band at 1653 cm^{-1} (C=O stretching) and amide II band at 1543 cm^{-1} (N-H bending) of the amide group [227]. The bands at 1388 cm^{-1} and 1367 cm^{-1} are assigned to C-H vibrations of isopropyl group of PNIPAAm [228]. Another characteristic absorption band of PNIPAAm, clearly seen in the spectra of all IPN samples, appears around 2974 cm^{-1} and is attributed to the C-H stretching vibration of -CH- bridges of PNIPAAm network [227]. Thus, the successful polymerization of NIPAAm was verified. This is supported by the fact that characteristic peaks of this monomer are not present in the corresponding spectra, primarily implying the bands at 1617 cm^{-1} (C=C), at 1409 cm^{-1} (CH₂=), as reported elsewhere [229].

The characteristic asymmetric stretching vibration of COO- groups in CA network is manifested through the peak 1635 cm^{-1} [19, 230]. In the spectra of IPNs, this peak is hidden by a broad amide II band of PNIPAAm at 1653 cm^{-1} , as noted earlier. The absorbance at 1082 cm^{-1} and 1090 cm^{-1} in the spectra of CA and IPNs, respectively, is a result of C-O-C stretching of the pyranose ring in mannuronate (M) and guluronate (G) residues [231]. The band at around 1028 cm^{-1} in spectra of CA and IPNs is assigned to O-H bending vibrations [231], as well as to C-O stretching of alginate structural units.

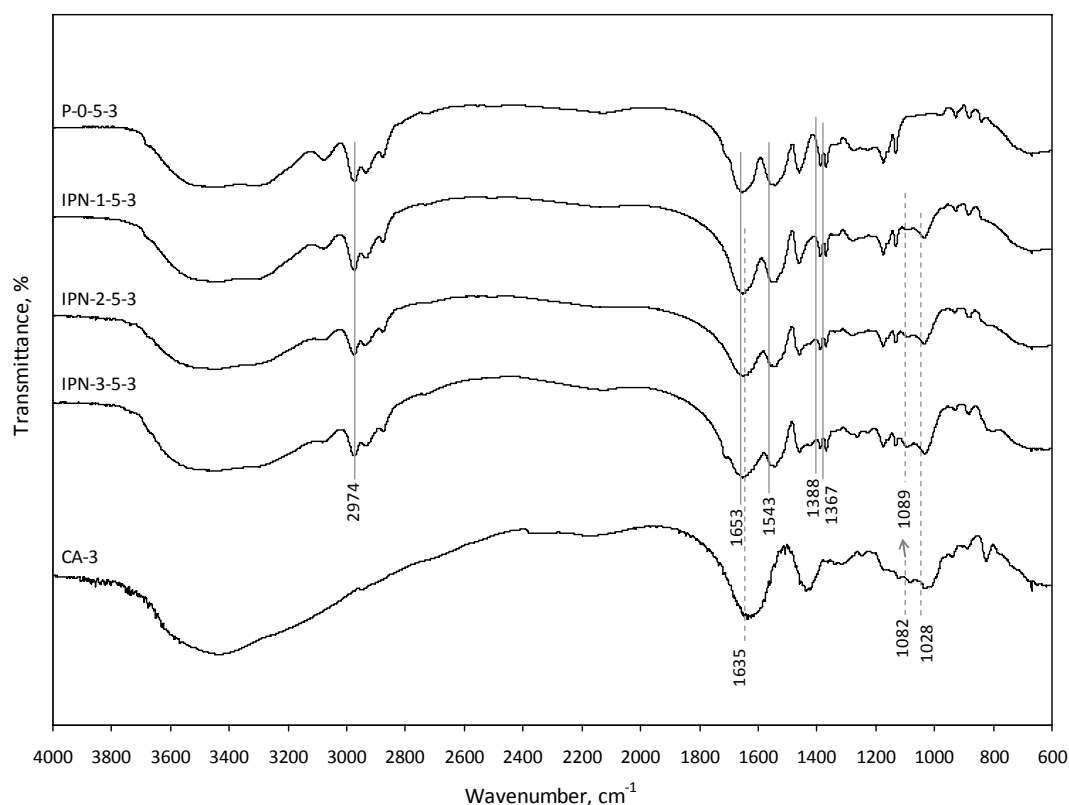


Figure III.3. FTIR spectra of hydrogels with 3 wt % MBAAm (characteristic peaks of PNIPAAm chains indicated by full lines and those of CA network by dotted lines)

In all analyzed spectra a broad peak between 3600 and 3200 cm^{-1} is present due to O-H stretching vibrations, primarily as a sign of moisture absorption. Concerning CA and IPNs, this broad peak arises from hydroxyl groups in G and M residues of alginate chain, indicating the formation of intermolecular hydrogen bonding [232]. Furthermore, in the case of P-0-5-3 and IPNs, there is contribution of N-H stretching of the repeating units of NIPAAm in the same range [227]. Hence, FTIR analysis confirmed the presence of both polymer networks, crosslinked PNIPAAm and CA, in IPN samples.

Figure III.4 presents a reaction scheme for the formation full-IPN hydrogels. It shows polymerization/crosslinking of NIPAAm (in the presence of SA), the subsequent step of crosslinking of alginate by calcium ions according to the egg-box model [97] and the probable full-IPN structure.

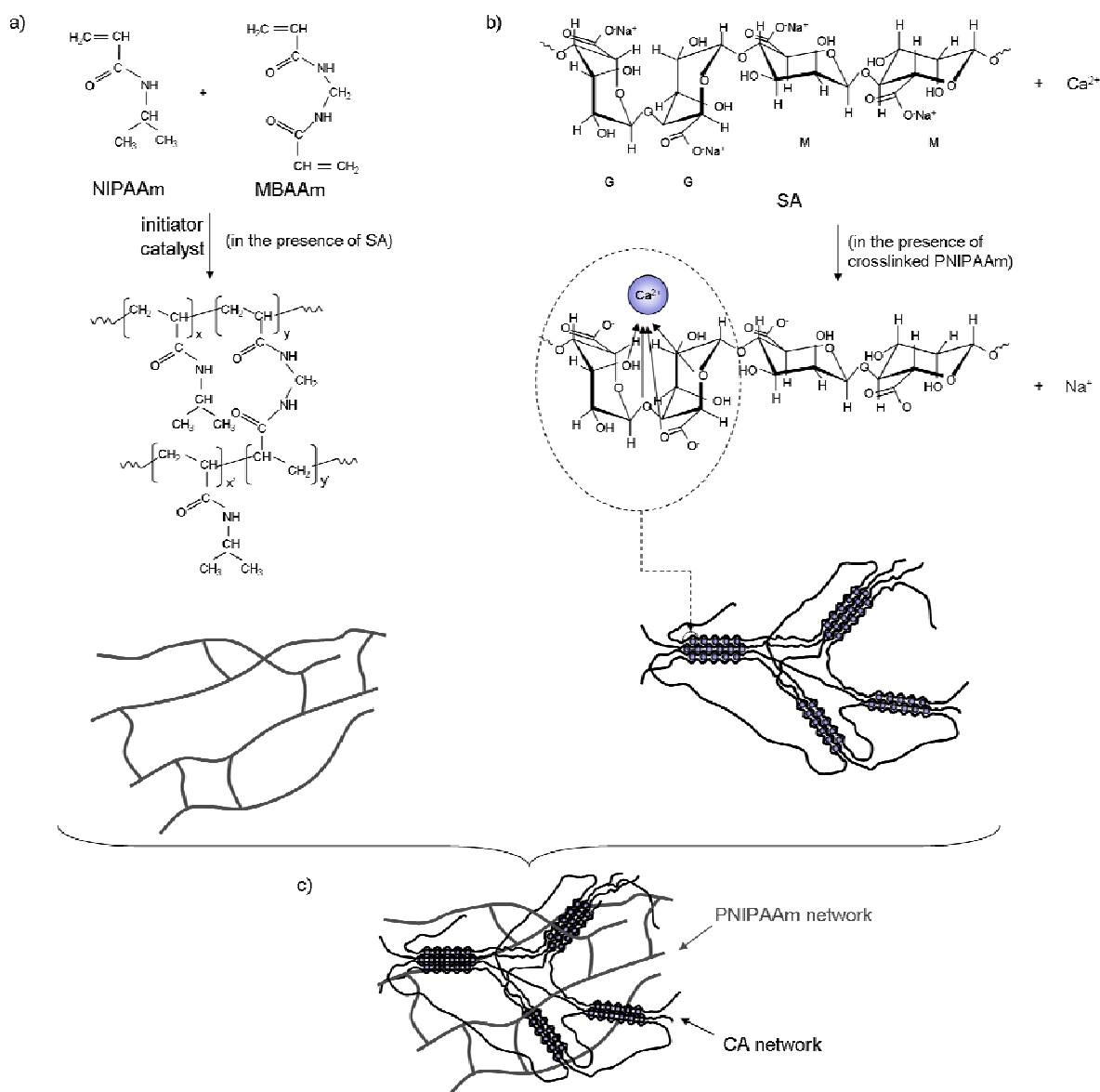


Figure III.4. Formation of the IPN hydrogel structure: copolymerization/crosslinking of NIPAAm (adapted from [197]) (a), crosslinking of alginate (b), and resulting PNIPAAm/CA full-IPN structure (c)

III.3 Thermal characteristics

III.3.1 Volume phase transition temperature

Thermosensitivity of hydrogel films were analyzed through heating-cooling-heating cycle in the range from 15 to 50°C. Three consecutive temperature ramps were applied to examine the reversibility of the volume phase transition. The results obtained by this analysis are given in Table III.1 and include, beside VPPT, onset temperature of the volume phase transition (T_{onset}), and enthalpy change during the volume phase transition (ΔH).

Table III.1. Results of DSC heating-cooling-heating cycle of hydrogel films

Sample	Heating I			Cooling			Heating II		
	T _{onset} * (°C)	VPTT* (°C)	ΔH** (J g ⁻¹)	T _{onset} (°C)	VPTT (°C)	ΔH (J g ⁻¹)	T _{onset} (°C)	VPTT (°C)	ΔH (J g ⁻¹)
P-0-5-2	33.8	34.9	1.10	34.0	33.3	1.15	33.8	34.9	1.18
P-0-5-3	34.0	35.0	1.06	34.2	33.5	1.05	33.8	34.9	1.06
IPN-1-5-2	33.8	35.0	1.03	33.6	31.5	1.01	33.6	34.6	1.04
IPN-1-5-3	33.8	35.1	1.01	33.8	31.7	1.00	33.5	34.8	1.04
IPN-2-5-2	34.0	35.4	0.97	33.6	31.5	1.01	33.4	34.9	1.00
IPN-2-5-3	34.0	35.7	1.01	34.1	31.8	1.02	33.2	34.8	1.01
IPN-3-5-2	34.1	35.5	1.07	34.0	32.3	1.01	33.5	34.8	0.94
IPN-3-5-3	33.9	35.6	1.01	34.3	32.1	1.01	33.2	34.9	1.00

*Standard deviations for T_{onset} and VPTT values were ±0.2°C.

** Standard deviation for ΔH values was ±0.12 J g⁻¹.

VPTT values of P-0-5-2 and P-0-5-3 are slightly higher than the characteristic value generally obtained for chemically crosslinked pure PNIPAAm hydrogels (around 33°C) [212, 233]. This is understandable taking into consideration low preparation temperature of hydrogels that affects the increase in VPPT [226].

In comparison with pure PNIPAAm hydrogels, formation of the full-IPN structures based on 1 wt % alginate has not resulted in change of VPTT, whereas full-IPN hydrogels with higher amount of alginate have slightly higher VPTT. Incorporation of CA network was expected to give prominent rise to VPTT values of the final structures, due to greater number of hydrophilic groups of alginate chains. However, similar VPTT values of pure PNIPAAm hydrogels and full-IPN hydrogels mean that the presence of alginate chains in full-IPN hydrogels does not provide enough interactions to considerably influence the hydrophilic/hydrophobic balance of PNIPAAm chains. This could be explained by the formation of a complex between the carboxylate groups of alginate and the amide groups of PNIPAAm, which is responsible for the lower than expected hydrophilicity of the full-IPNs than expected in comparison with alginate fraction [234]. Furthermore, the number of hydroxyl groups in alginate chains that rises with increase in alginate fraction could not induce proportional increase in number of hydrogen bonds between them and water molecules due to tighter network structure that could not accommodate great amounts of water. Additional reason for negligible differences in VPTT of analyzed hydrogels might lie in relatively high monomer concentration for the preparation of hydrogels. Similar study of PNIPAAm hydrogel networks interpenetrated with CA networks showed that, only at low initial NIPAAm monomer concentration (2.5 wt %), the phase transition is favored at higher temperatures due to easier motion of PNIPAAm chains [13]. This requires greater energy for driving hydrophilic–hydrophobic transition, and hence it should result in higher VPTT. Also, DSC analysis indicated that the structure of each network forming the full-IPNs is retained during the synthesis since the incorporation of CA does not cause any significant deviation from VPTT of pure PNIPAAm network [235]. Graphic representation of the volume phase

transition during the first heating step is given in Figure III.5, and it demonstrates similarity of DSC thermograms of all analyzed hydrogels.

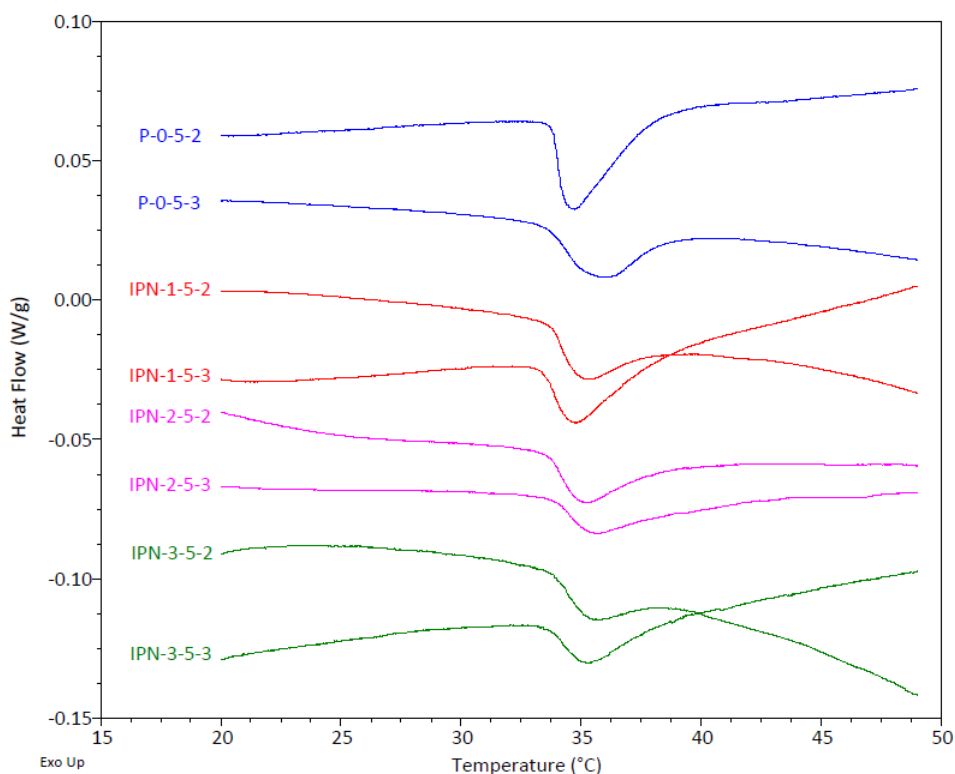


Figure III.5. DSC thermogram of the first heating step of all hydrogels

The obtained results show that analogous hydrogels with the same crosslinking degree of PNIPAAm display the same VPTT value. Hence, increasing crosslinker (MBAAm) concentration from 2 to 3 wt % in the feed solution (i.e. decreasing molar ratio of NIPAAm and MBAAm from 68.1 to 45.4) does not influence VPTT of the hydrogels. This is in accordance with literature data stating that crosslinking degree of PNIPAAm does not affect the [59]. The onset temperatures that indicate the initiation of the phase transition process are very similar in all cases.

What is also noticeable from DSC results (Table III.1) is that cooling cycle results in lower VPTT in comparison with both heating cycles. This hysteresis is typical for first order type phase transitions [236, 237]. Upon cooling, water expelled from gels during heating was re-absorbed, hydrogen bonds with water were re-established and the network expands. The process is delayed, i.e. a hysteresis in heating-cooling cycle appears due to the formation of some additional hydrogen bonds between the $>C=O$ and $H-N<$ groups of PNIPAAm chains only in the collapsed state, which is confirmed by laser light scattering and FTIR analysis of PNIPAAm aqueous solution [238]. Thus, established interchain hydrogen bonds act as “the crosslinking” points among different chains resulting in hysteresis.

In all cases, phase transition enthalpy values of the full-IPN hydrogels upon cooling were the same as those upon heating steps. This indicates that almost same amount of hydrogen bonds was created during cooling process with respect to the previous and the following process of heating. Furthermore, ΔH values during heating steps obtained for the full-IPN

hydrogels are similar to ΔH values of pure PNIPAAm hydrogels. It is known that during thermal induced volume phase transition, the structured water molecules around the hydrophobic isopropyl groups of PNIPAAm are released [239]. This means that water molecules around hydrophilic part of PNIPAAm and alginate chains might not be influenced considerably [236]. It can be concluded that the amount of water around the isopropyl groups is not affected by the hydrophilic chains of alginate and as a result enthalpy changes associated with the volume phase transition are similar for all analyzed hydrogels. The IPN hydrogels composed of PNIPAAm and poly(sodium acrylate) reported by Chen and Hsieh exhibited very close enthalpy changes during phase transition to that of pure PNIPAAm hydrogels [240].

Complete DSC thermographs (heating-cooling-heating cycle) of all hydrogel types showed that the volume phase transition is a reversible process, according to almost identical shape and position of endothermic peaks in the first and the second heating step of the thermal cycle. This is clearly seen from the complete thermogram of the hydrogel P-0-5-2 displayed in Figure III.6 (other individual thermograms are given in the Appendix).

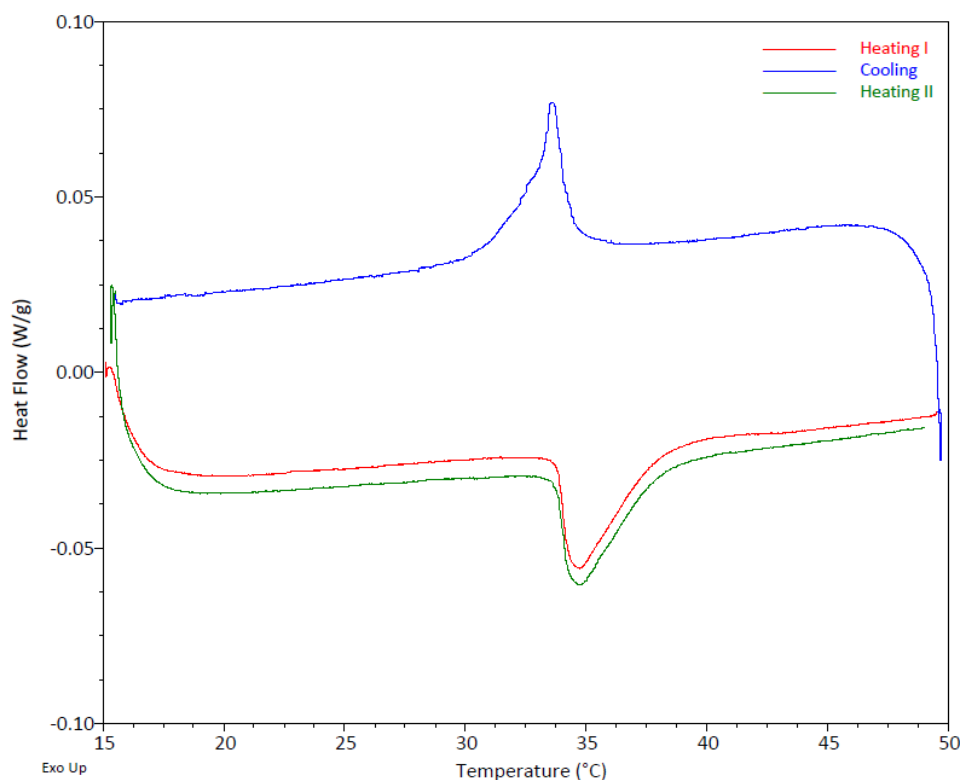


Figure III.6. DSC thermogram of heating-cooling-heating steps of hydrogel P-0-5-2

III.3.2 Glass transition temperature

Results of glass transition analysis by DSC are given in the form of thermograms in Figure III.7. Literature values of the glass transition temperature of linear PNIPAAm range between 85 and 130°C [241]. With regard to crosslinked PNIPAAm, the results obtained by Zhang et al. [10] indicate a T_g of 131.4°C for the PNIPAAm hydrogel based on 6.7 wt % monomer

solution with 2 wt % crosslinker MBAAm (based on monomer), which is close to our results for both P-0-5-2 and P-0-5-3.

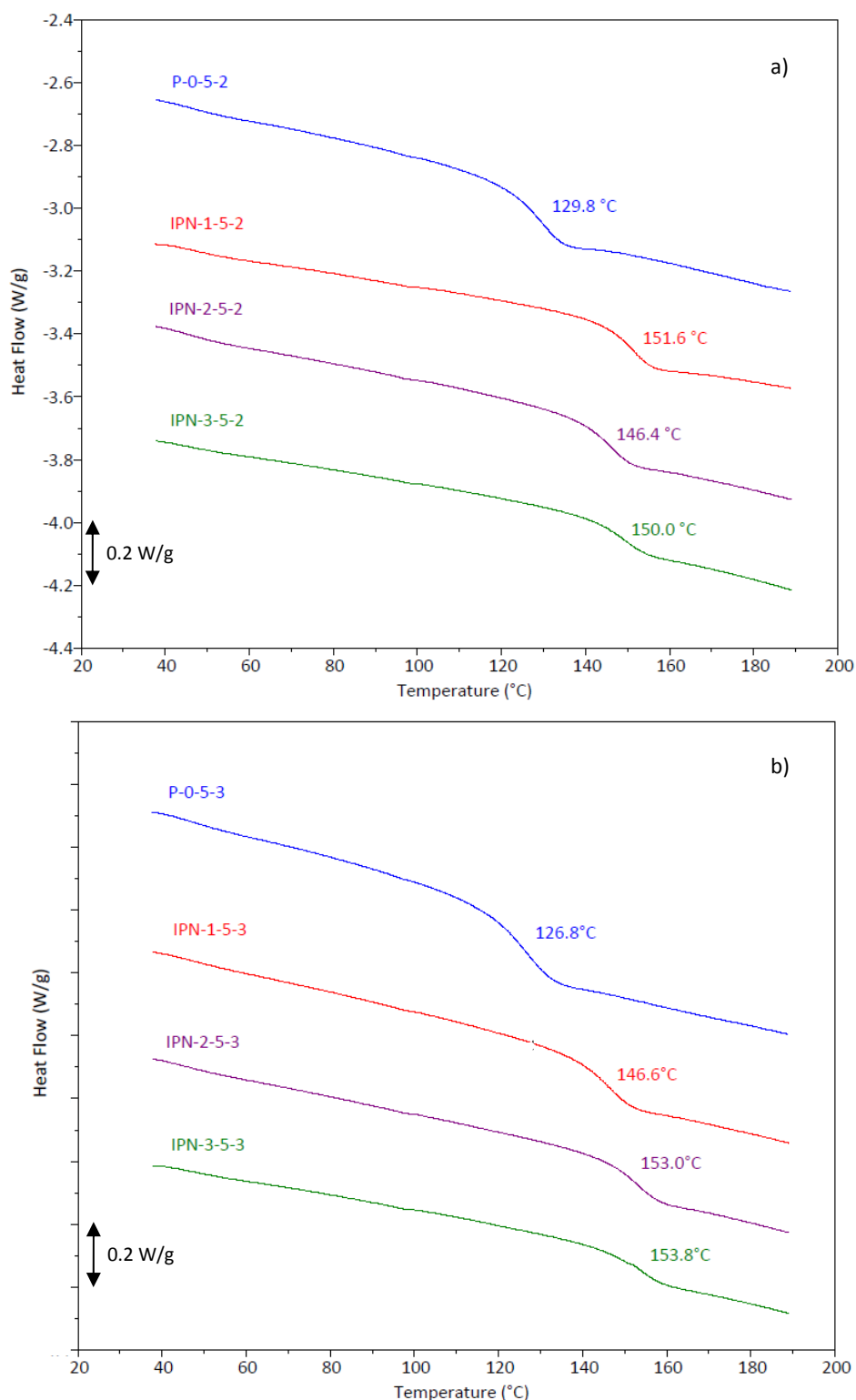


Figure III.7. DSC thermograms for determination of T_g values of hydrogels with lower (a) and higher (b) crosslinking degree of PNIPAAm

In the case of pure PNIPAAm crosslinked by gamma radiation, noticeably higher values of the T_g were reported [242], e.g. a T_g of 149°C was obtained for a PNIPAAm hydrogel based on 10

wt % monomer solution and irradiated at 70 kGy with a 60-Co source, signifying stronger network in comparison with a chemically crosslinked PNIPAAm. However, T_g of chemically crosslinked PNIPAAm hydrogel could be increased by the presence of interpenetrants [10]. Our study shows that the CA network considerably contributes to the improved stability of the full-IPNs, in contrast to pure chemically crosslinked PNIPAAm hydrogel. An increase in fraction of the second network (CA) results in the increase in T_g values, owing to hindering of the chain mobility. This is clearly showed in Figure III.8 where uprising trend of T_g values is noted for hydrogels with both crosslinking degrees of PNIPAAm. A value of T_g of IPN-1-5-2 is not clearly understood since it is unexpectedly higher with respect to T_g of IPN-2-5-2 and IPN-3-5-2.

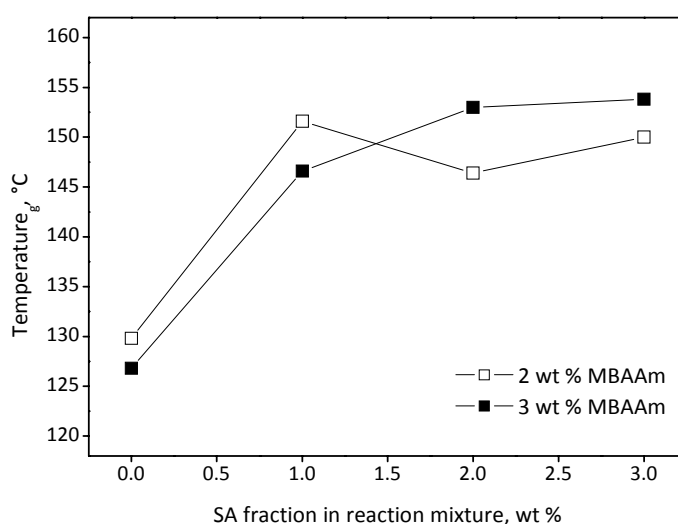


Figure III.8. Influence of the SA weight fraction on the glass transition temperature of hydrogel films

The full-IPN hydrogels are characterized by strong interactions among polymer chains, since a temperature above 153°C in the case of IPN-2-5-3 and IPN-3-5-3 is necessary to promote the chain mobility (Figure III.7b). This T_g value can be compared to the T_g of 149.7°C obtained for hydrogels composed of two interpenetrating networks of PNIPAAm [10]. Therefore, CA network leads to the improvement in strength of the interactions on a molecular level when it is combined with PNIPAAm to form full-IPN.

III.4 Swelling behavior

III.4.1 Equilibrium swelling ratio of hydrogels

Thermosensitivity of synthesized hydrogels was expressed through the values of equilibrium swelling ratio (ESR) over the range of temperatures from 25°C up to 50°C. The swelling profiles in Figure III.9 indicate that the ESR of the IPN samples at lower temperatures (<31°C) is decreasing with increase in alginate concentration due to reduced mobility of PNIPAAm chains in these more compact hydrogel networks. Also, there is a noticeable difference in the ESR at 25°C between the samples with different crosslinking degree of PNIPAAm. Higher

concentration of crosslinks in PNIPAAm network of IPN-1-5-3 resulted in around 18 % lower ESR, in comparison with IPN-1-5-2. The ESR value of pure PNIPAAm hydrogels (22.5 and 19.8 for P-0-5-2 and P-0-5-3, respectively) is lower than those of full-IPN hydrogels based on 1 wt % alginate (24.5 and 21.3 for IPN-1-5-2 and IPN-1-5-3, respectively), which indicates the ability of the latter hydrogels to accommodate more water. This was confirmed by SEM analysis and calculation of the average pore size of the samples at 25°C (see Figure III.17). More developed porous structure of IPN-1-5-x than P-0-5-x (x=2,3) provided higher water swelling capacity. The analogous conclusion could be deduced for the relation of the ESR and the average pore size at 40°C.

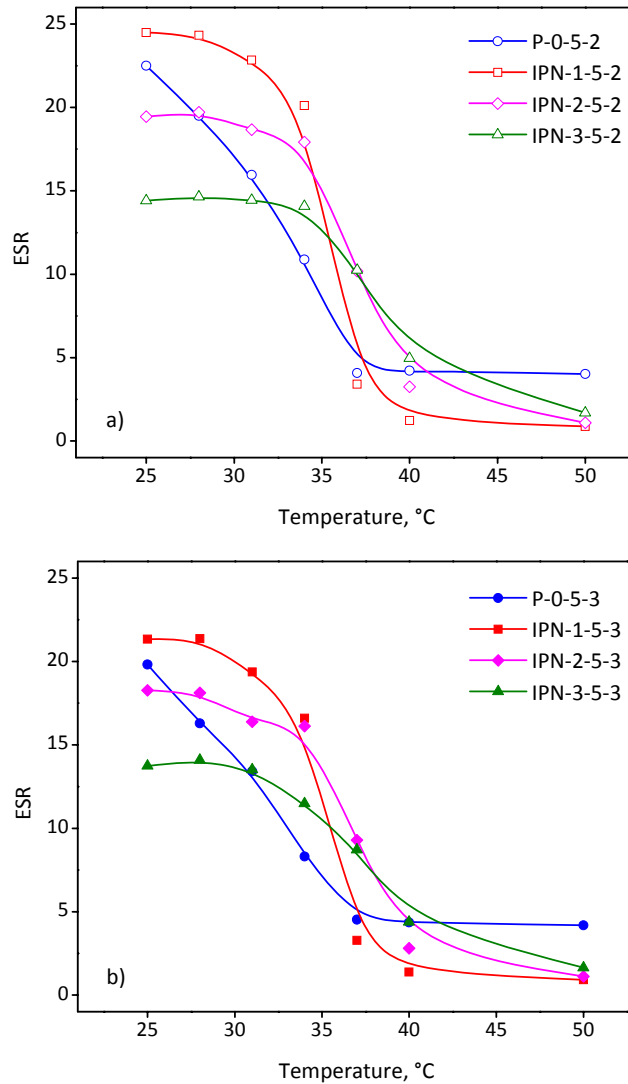


Figure III.9. Equilibrium swelling ratio of hydrogels with lower (a) and higher (b) crosslinking degree of PNIPAAm as a function of temperature

The difference in ESR at lower temperatures (25, 28°C) between two hydrogels with higher fraction of alginate (IPN-3-5-2 and IPN-3-5-3) is only slightly pronounced due to predominant influence of CA network. It probably masks the differences arising from different crosslinking degree of the other network (PNIPAAm) in full-IPNs. The concentration of crosslinker MBAAm in hydrogels with the same amount of alginate affects neither the general shape of the curve, nor VPTT values that could be determined from the inflection point of each

swelling curve. It is estimated that VPTT increases depending on the presence and moiety of CA in full-IPN hydrogels. VPTT values of full-IPN hydrogels based on 2 and 3 wt % of alginate are close to 37°C, which is not in good agreement with the DSC results, since the different methods of measurement can give small changes in this temperature [243].

Obtained swelling profiles confirm well known property of pure PNIPAAm hydrogels to have weaker response to temperature variations, as a result of the formation of a skin layer [244, 245]. The formation of dense, polymer-rich phase due to the collapse of polymer chains results in the opacity of a hydrogel, as shown in Figure III.10.

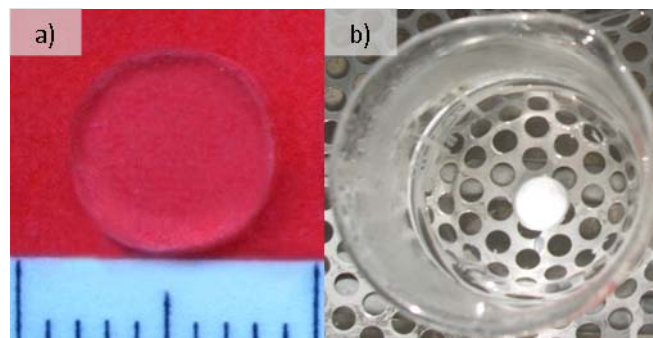


Figure III.10 P-0-5-2 hydrogel in swollen state after removal from aqueous medium at 25°C (a) and in shrunken state in aqueous medium at 40°C (b)

A dense skin layer is formed and it hinders the diffusion of water molecules out of the gel during the deswelling process at higher temperatures ($>VPTT$). Addition of alginate, as hydrophilic component, primarily due to hydroxyl groups, reduces hydrophobic aggregation in the surface layer of hydrogel and formation of the skin layer. It reflects in higher rate of decrease of ESR with the increase in the temperature of IPN hydrogels. The sharpest volume phase transition is exhibited by hydrogel IPN-1-5-2, whose ESR rapidly decreases once the VPTT (34.5°C) is exceeded and drops from 20.1 down to 1.2 between 34°C and 40°C, respectively (Figure III.9a). Hydrogels with higher fraction of alginate have slower response rate than IPN-1-5-2 and IPN-1-5-3. This could be explained by stronger interactions (hydrogen bonds) between hydrogen of hydroxyl groups of alginate and nitrogen of amide groups of PNIPAAm, due to more compact and denser full-IPN structures, and hence, weaker influence on the reduction of hydrophobic aggregation in surface layer.

An increase in alginate content in the full-IPN hydrogels leads to the reduced mobility of PNIPAAm chains in these networks and consequently weaker water uptake ability, as was also the case in similar systems [133]. It is shown that different concentration of alginate in the feed mixture influences swelling properties of IPN hydrogels. Degree of PNIPAAm crosslinking impacts ESR at lower temperatures. This is confirmed by SEM analysis, and presented through the values of the average pore size at 25°C and 40°C (see Figure III.17). After exhibiting phase transition, well above their VPTT (at 50°C), the full-IPN hydrogels show relatively similar swelling ESR values, which indicates the transition of their network into a similar tightly compact structure.

For better understanding of the swelling abilities of the hydrogels at temperatures below and above VPTT, the values of equilibrium water content of hydrogels at 25°C and 40°C are calculated. The ESR of hydrogels is directly related to their equilibrium water content (EWC):

$$EWC = \frac{W_s - W_d}{W_s} = \frac{ESR}{ESR + 1} \quad (III.1)$$

EWC of our full-IPN hydrogels at 25°C ranges from 93.2 wt % (IPN-3-5-3) up to 96.1 wt % (IPN-1-5-2) (Table III.2). These data suggest high capacity and ability of the hydrogels to release important amounts of immobilized drug in response to temperature and good diffusive properties [152]. Furthermore, IPN-1-5-2 loses more than 40 % of water from its structure when it is equilibrated at 40°C. This efficient loss of water from the network qualifies the full-IPN hydrogel based on 1 wt % alginate as promising matrices for controlled drug release.

Table III.2. Equilibrium water content of hydrogels at 25°C and 40°C

Hydrogel	t=25°C	t=40°C
P-0-5-2	95.7%	80.8%
P-0-5-3	95.1%	81.3%
IPN-1-5-2	96.1%	55.0%
IPN-1-5-3	95.5%	57.9%
IPN-2-5-2	95.1%	76.4%
IPN-2-5-3	94.8%	73.7%
IPN-3-5-2	93.5%	83.2%
IPN-3-5-3	93.2%	81.4%

Incubation of hydrogels at temperatures above their VPTT results in obvious reduction in dimensions. As displayed in Figure III.11, the strongest difference in diameter at equilibrium state at 25 and 40°C are shown by IPN-1-5-2 and IPN-1-5-3 disks. This is in accordance with the values of their water content at higher temperature that are smaller by almost two-fold than at 25°C (Table III.2).

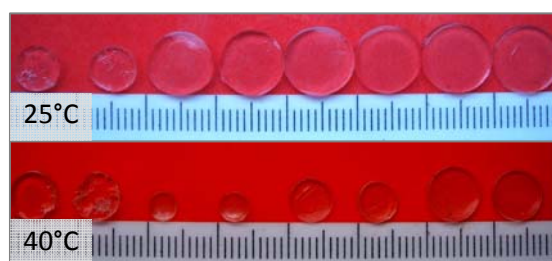


Figure III.11. Equilibrium swollen hydrogel disks at 25°C (a) and 40°C (b) in order (from left to right): P-0-5-2, P-0-5-3, IPN-1-5-2, IPN-1-5-3, IPN-2-5-2, IPN-2-5-3, IPN-3-5-2, and IPN-3-5-3

One of the main factors governing the permeation of a drug through a thermosensitive hydrogels is the hydration of polymer chains that depends on a temperature causing swelling change and hence water content within the polymer network [246, 247]. Sato et al. showed that the solubility of solute through the hydrogel increases with hydrogel hydration [248].

III.4.2 Swelling kinetics

When dried pure PNIPAAm and full-IPN gels are immersed in water at 25°C, they all show similar swelling trend (Figure III.12). The rates of swelling are high during the first hour and then gradually decrease until the equilibrium swelling is reached. The difference between the osmotic pressure in bulk water and in the swelling samples is the highest at the beginning of the process and it decreases with time.

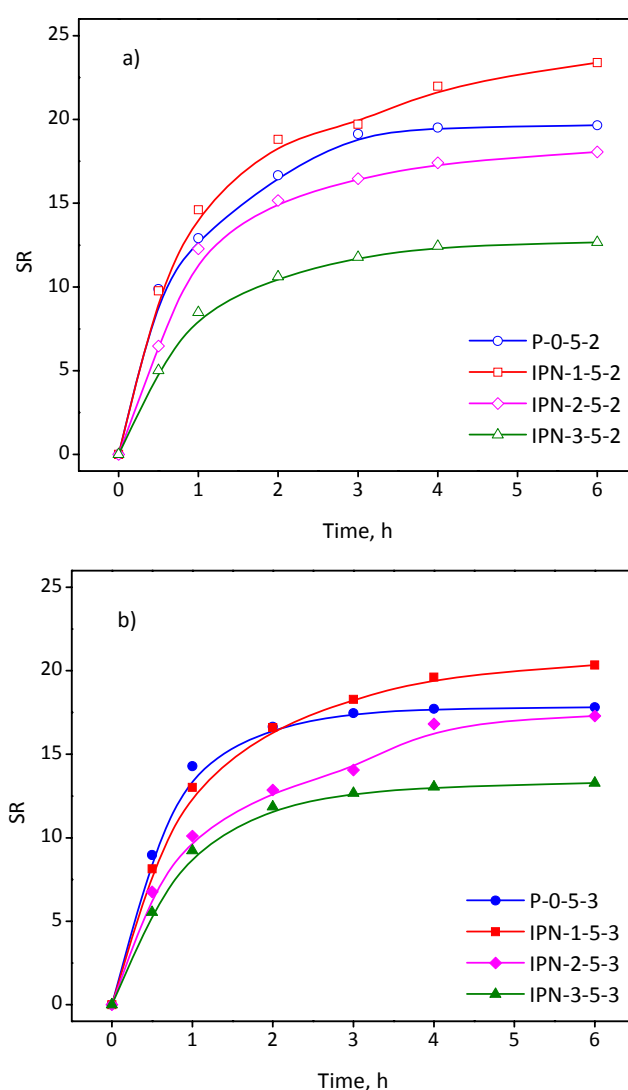


Figure III.12. Swelling kinetics of dried hydrogels with lower (a) and higher (b) crosslinking degree of PNIPAAm at 25 °C

The first hour of swelling was characterized by high water uptake rate that is governed by diffusion of water molecules into the dry sample. This is followed by the relaxation of the

hydrated polymer chains and finally expansion of the hydrogel network [249]. Therefore, all given profiles are marked by slow second phase of swelling. After the initial 30 min of swelling, the highest increase in SR in comparison with the equilibrium value (ESR) is obtained for pure PNIPAAm hydrogels (45 %), followed by IPN-1-5-2 (41%), reaching SR close to 10. These samples have the least compact dried structure with the lowest polymer chain per unit volume, which enables easier water penetration into the gel. Increased presence of alginate network induced slower swelling process so that SR of IPN-2-5-2 and IPN-3-5-2 equaled 15.1 and 10.6 respectively, in comparison with 16.7 obtained for P-0-5-2 after the second hour of swelling. Measurements of the swelling kinetics up to 48 h indicated that the equilibrium swelling time is slightly shortened when the fraction of alginate in the full-IPNs is raised, due to the increased content of hydrophilic segments that favors the absorption of water. The impact of crosslinking degree of PNIPAAm is negligible for the full-IPN samples with high alginate concentration and it is the most pronounced for the full-IPN based on 1 wt % alginate.

III.4.3 Deswelling kinetics

The kinetics of water loss from hydrogels at high temperature, displayed in Figure III.13, clearly indicates rather slow shrinking rate of pure PNIPAAm hydrogels in comparison with the other samples. In general, formation of IPN structures considerably enhanced the deswelling rate of the hydrogels. SR of P-0-5-2 and P-0-5-3 decreased to around 9 and 19 % (respectively) after 2 h of deswelling at 40°C, comparing to the initial state at 25°C. As opposed to them, full-IPN hydrogels based on 1 and 2 wt % alginate showed considerably higher deswelling ability within the same period. Decrease in SR was more than 80 % in 2 h for IPN-1-5-2 and IPN-1-5-3. As already noted, the incorporation of CA network weakens the hydrophobic interactions among isopropyl groups of PNIPAAm in the surface layer. Thus, the formation of a dense skin layer (which blocks the outflux of entrapped water from the hydrogel network) is weakened, leading to a higher deswelling rate of full-IPNs. Rapidly structured skin phase of P-0-5-2 and P-0-5-3 does not allow the water molecules inside these hydrogels to be easily squeezed out. Hence, they feature minimal decrease in SR after the initial 30 min. Furthermore, pure PNIPAAm hydrogels reach equilibrium at 40°C after 48 h, whereas full-IPN hydrogels needs only around 4 h. The given deswelling profiles near equilibrium state correspond to the pore structure of hydrogels at 40°C, i.e. their average pore size that decrease in the order P-0-5-x>IPN-3-5-x>IPN-2-5-x>IPN-1-5-x (see Figure III.17).

When comparing deswelling behavior of the full-IPN hydrogels with different fraction of alginate network, it is observed that increased concentration of alginate chains slows down the shrinking process. According to the obtained results, after the first 30 min of deswelling process, swelling ratio of IPN-1-5-3 equals 4.6, while that of IPN-2-5-3 is almost doubled (Figure III.13b). This lower response rate might be caused by more compact and denser structure of IPNs with higher content of CA due to the additional crosslinking of alginate chains by calcium ions. As a consequence, mobility of PNIPAAm chains in these networks is reduced, and it affects a decrease in the intensity of hydrophobic interactions among isopropyl groups. Hence, the release of entrapped water is the most retarded for hydrogels based on the highest fraction of alginate in comparison with other full-IPN hydrogels, in spite of strong prevention of skin layer formation. Obtained deswelling curves indicate that the

difference in the crosslinking density of PNIPAAm network in full-IPNs is too low to have a substantial impact on deswelling kinetics of analogous hydrogels.

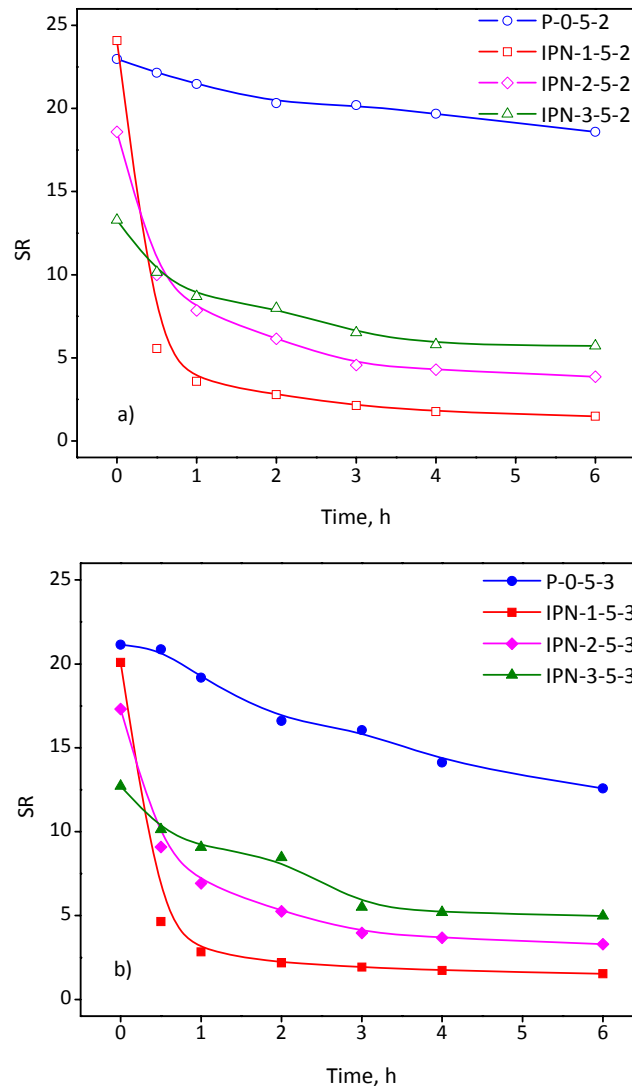


Figure III.13. Deswelling kinetics of hydrogels with lower (a) and higher (b) crosslinking degree of PNIPAAm at 40°C

III.4.4 Reswelling kinetics

Reswelling kinetics of the full-IPN hydrogels was studied in water at 25°C, after they reached equilibrium state at 40°C (Figure III.14). Reswelling profiles of P-0-5-2 and P-0-5-3 hydrogels are not given since it was difficult to manipulate them due to their fragile structure. In the first period of incubation, all analyzed hydrogels have similar trend of reswelling. What is noticeable after 1 h is weaker water uptake ability of hydrogels with higher crosslinking density of PNIPAAm and the same alginate concentration (Figure III.14b). At that time, IPN-1-5-2 has around 26 % higher SR than IPN-1-5-3. Stronger hydrophobic interactions within hydrogel with higher crosslinking degree of PNIPAAm influence the resistance against the influx of water, but only in the first period of reswelling. This is in accordance with the results of other authors who reported that increase in concentration of the crosslinker

MBAAm decreases the rate of swelling of the PNIPAAm hydrogels, found in the case of a crosslinker below 5 wt % [15].

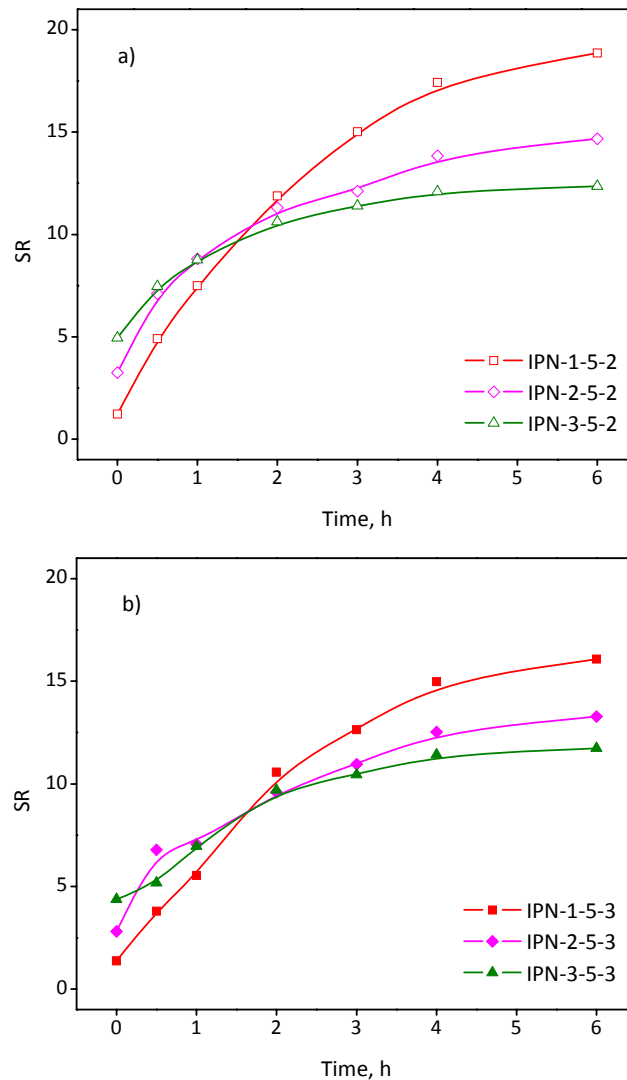


Figure III.14. Reswelling kinetics of hydrogels with lower (a) and higher (b) crosslinking degree of PNIPAAm at 25°C

The full-IPN hydrogels with lower fraction of alginate feature looser networks enabling increased mobility of polymer chains during rehydration. This leads to a better exposure of hydrophilic segments of polymer chains to water and its easier penetration into the matrix, i.e. rate of water uptake. Hence, after the first hour of reswelling, IPN-1-5-x showed around 80 % increase in water uptake in comparison with initial equilibrium state at 40°C, whereas this increase was around 60 % and 40 % for IPN-2-5-x and IPN-3-5-x, respectively (x=2,3). IPN hydrogels based on 1 wt % alginate kept the highest rate of water uptake over other IPN hydrogels until the end of the observed period. After the second hour of reswelling all hydrogels exhibited slowing of water uptake rate, governed by the expansion of polymer chains into the solvent that is more restricted in denser hydrogel matrices [250]. Hydrogels reached equilibrium swollen state after almost 30 h of incubation at 25°C, although the greatest part of swelling capacity is demonstrated after the initial 6 h of reswelling.

III.5 Morphology

The pore structure of hydrogels was examined by SEM. Figure III.15 and Figure III.16 show the SEM micrographs below and above VPTT of the hydrogels. Freeze-drying procedure could be regarded as successful and hydrogel structured preserved since disk-shaped samples retained their dimensions after the treatment. The dependence of the interior morphology on hydrogel composition and their thermosensitivity could be clearly seen.

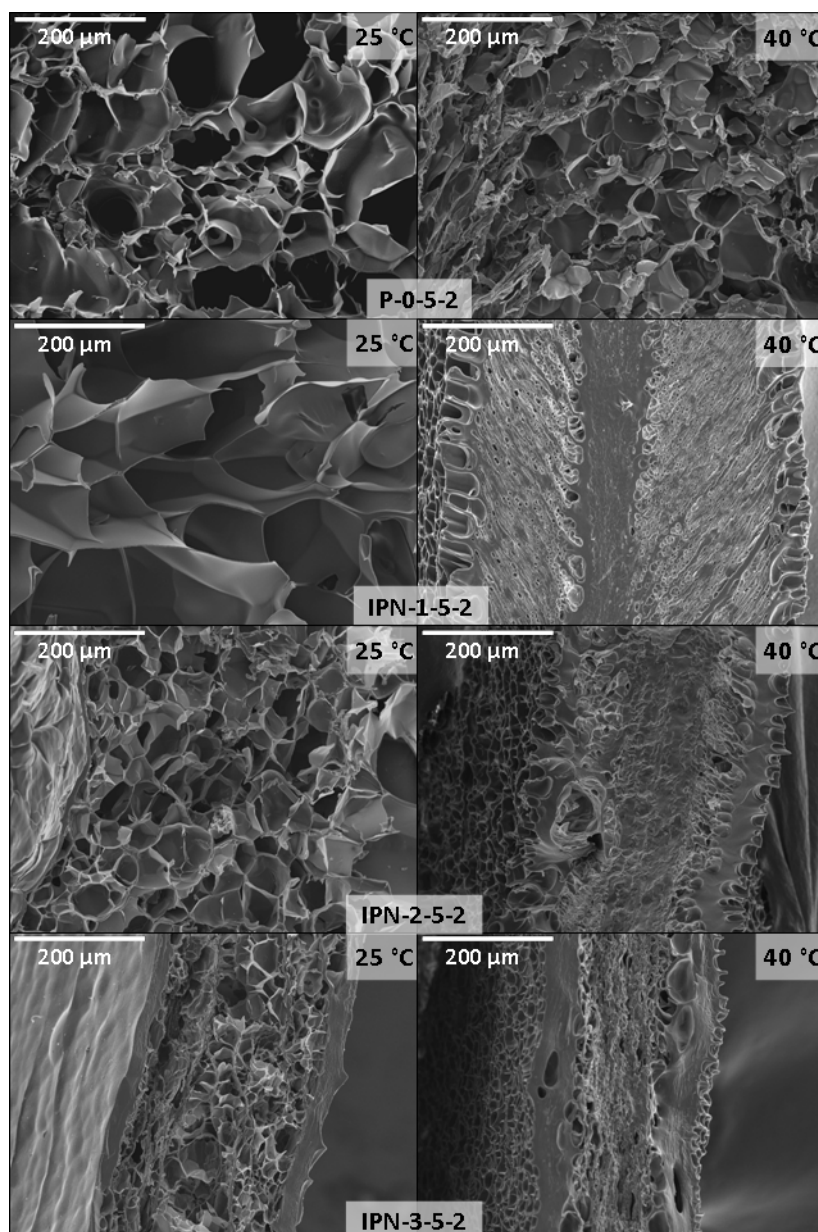


Figure III.15. SEM micrographs of hydrogel films with lower crosslinking degree of PNIPAAm: comparison of interior morphology below and above VPTT

At room temperature, full-IPN hydrogels with the lowest fraction of alginate feature the most porous structure, even more porous than corresponding pure PNIPAAm hydrogels. High porosity of these full-IPN samples can be partly explained by the preparation procedure. The initial phase of hydrogel synthesis encompassed 24 h polymerization and

crosslinking of PNIPAAm in the presence of SA. During this period, electrostatic repulsions among carboxylate groups of alginate chains contribute to the expansion of forming network [136]. This is the case with the samples with the lowest concentration of alginate. In contrast, the structures of the full-IPN samples based on 2 and 3 wt % alginate are more compact than pure PNIPAAm, due to the over dominant influence of crosslinking of alginate with calcium ions in the last step in their preparation. Hence, these hydrogels feature smaller average pore sizes than pure PNIPAAm hydrogels at 25°C (see Figure III.17). This was reflected through the values of ESR at lower temperatures (below VPTT) as well as the results of swelling kinetics (see Figure III.11 and Figure III.12).

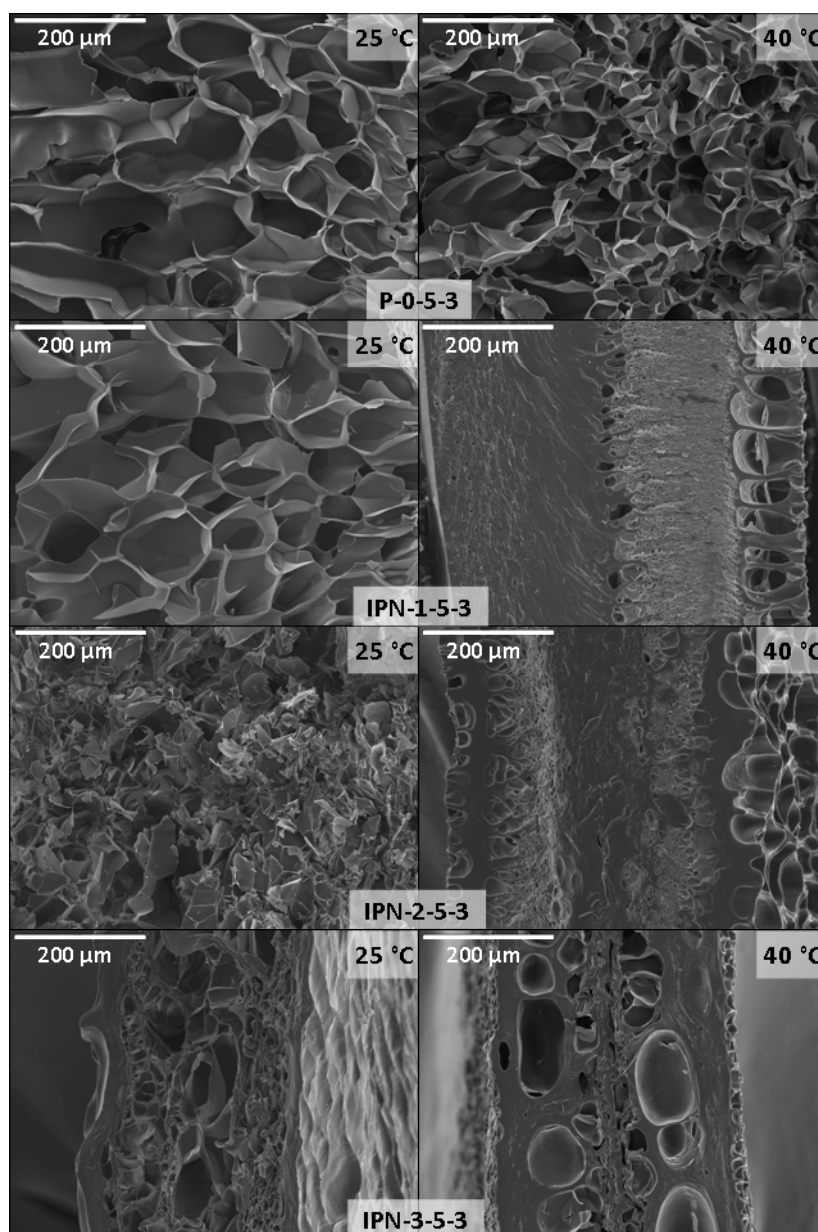


Figure III.16. SEM micrographs of hydrogel films with higher crosslinking degree of PNIPAAm: comparison of interior morphology below and above VPTT

According to the SEM micrographs, the full-IPN matrices become denser and exhibit more emphasized non-uniformity at room temperature with rise in alginate content. It is also clear that the structures of hydrogels become more compact and far less porous after the

incubation at 40°C. This can be ascribed to the strong hydrophobic interactions among hydrophobic segments of PNIPAAm, which prevail above VPTT. As a result, the collapse of the polymer chains and restructuring of the hydrogel matrix occurs. Furthermore, it is reported elsewhere that probable formation of the complex between carboxylate groups of CA and amide groups of PNIPAAm is favored at temperatures higher than the VPTT [134]. The reason for this can be found in the orientation of apolar isopropyl groups towards the surface of the pores, thus decreasing the interaction with water molecules. According to literature data, pure CA hydrogels feature irregular and elongated structure and looser than pure PNIPAAm hydrogel [135]. However, combination of these two networks resulted in more regular structure, emphasizing one of the numerous advantages of full-IPNs in the field of hydrogels [251].

The pore sizes of hydrogels, equilibrium swollen below (25°C) and above (40°C) their VPTT are presented in Figure III.17. Existence of smaller pores in the structure of the full-IPN hydrogels based on higher alginate content is understandable due to the higher possibility of the intermolecular association for formation of junction points [252]. The most pronounced influence of PNIPAAm crosslinking density is noticed for the full-IPN hydrogels based on 1 and 2 wt % alginate. High standard deviations of pore sizes, as a measure of heterogeneous interior morphology might be the result of steric hindrances caused by higher concentration of alginate chains in the system during free-radical polymerization process of NIPAAm [253]. In addition, inhomogeneous distribution of PNIPAAm cross-links throughout the hydrogel sample could be induced by this micro phase separation. Since crosslinker MBAAM has two vinyl groups, its molecules are incorporated into the growing polymer chains faster than NIPAAm molecules. Hence, network regions formed earlier are more crosslinked than those formed later [254].

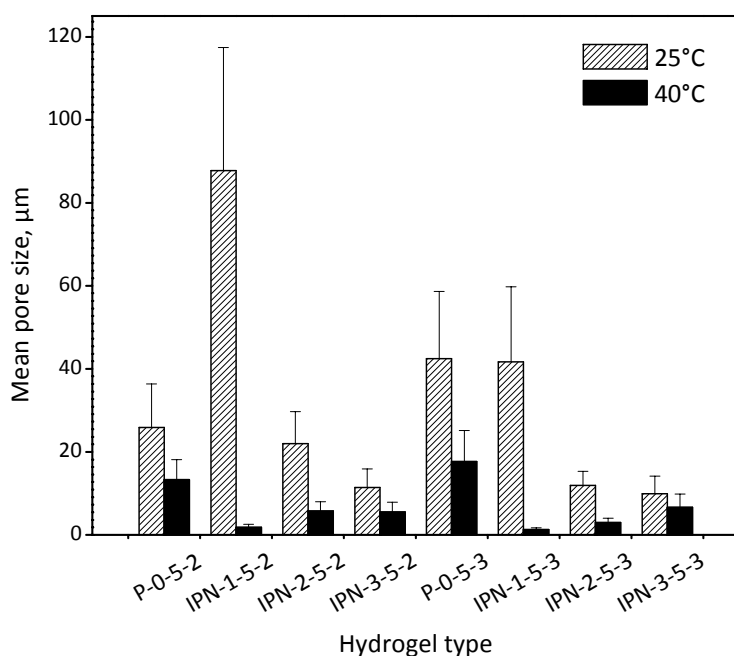


Figure III.17. Pore size values of hydrogels below and above VPTT

The pore size values and SEM micrographs are in accordance with the swelling abilities of hydrogels. The higher the average pore size of the network the higher will be the swelling

ratio (see Figure III.9). At temperatures above VPTT, pure PNIPAAm hydrogels have the largest pores, which is in accordance with the results of deswelling kinetics. As previously mentioned, the strongest collapse of polymer chains when temperature is raised from 25°C up to 40°C (deswelling) is observed in the case of IPN-1-5-2, corresponding to over 97%-decrease in the average pore size (from around 87 μm down to 2 μm).

Taking into account these results, the full-IPN hydrogels developed in this work could be regarded as supermacroporous or macroporous since they are characterized by pores of micron-sizes [255]. High values of pore sizes could be ascribed to the impact of low preparation temperature of hydrogels, causing water to remain in the gel phase throughout the polymerization and thus the formation of expanded polymer network [256]. Taking into consideration the impact of hydrogel pore structure on diffusive characteristic and overall swelling behavior, that hydrogels IPN-1-5-2 (Figure III.15) and IPN-1-5-3 (Figure III.16) are the most desirable as matrices for drug loading and release application [257].

III.6 Mechanical properties

The DMA curves for different full-IPN hydrogels are presented in Figure III.18-Figure III.20. The pure PNIPAAm hydrogels have not been analyzed because they were too fragile for adequate manipulation, indicating their mechanically weak structure.

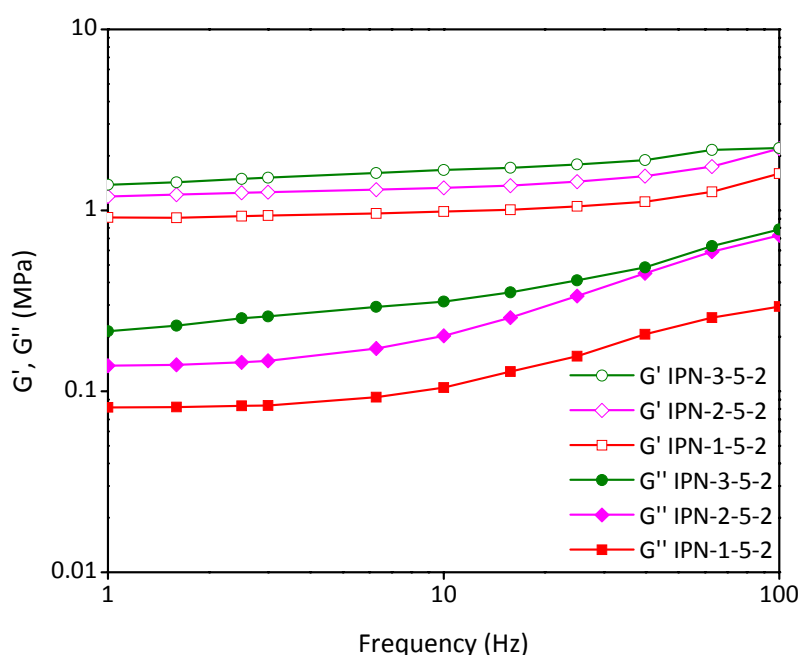


Figure III.18. DMA results for the full-IPN hydrogel films below VPTT (30°C): influence of alginate content

Figure III.18 shows the loss and storage moduli as a function of frequency for hydrogel films at 30°C. The storage modulus (G') accounts for an elastic “solid-like” behavior, while the loss modulus (G'') is in relation with viscous properties. In all cases, G' is higher than G'' , indicating that elastic response prevail in all tested hydrogels. Moreover, an improvement in

mechanical properties is observed when the alginate content rises, as a result of the increase in overall crosslinking density of hydrogels. This means that an increase in values of the compression moduli corresponds to the weaker swelling capacity of hydrogels. The loss or viscous moduli are considerably smaller than the storage or elastic moduli, which is general characteristic of hydrogels and solid-like materials [258, 259]. Obtained values of storage moduli of analyzed hydrogels are considerably higher than those of nanocomposite PNIPAAm hydrogels with incorporated hydrophobic polysiloxane nanoparticles tested in the same DMA mode [212]. Also, our DMA analysis showed that formation of full-IPN of PNIPAAm and CA results in mechanically much stronger hydrogels than PNIPAAm-based IPN hydrogels incorporating 3-methacryloxypropyl- trimethoxy silane, reported by Zhang et al [260]. These hydrogels, when exposed to dynamic strain and frequency sweep tests in the range from 0.1 to 100 rad s^{-1} , featured storage modulus below 1 kPa.

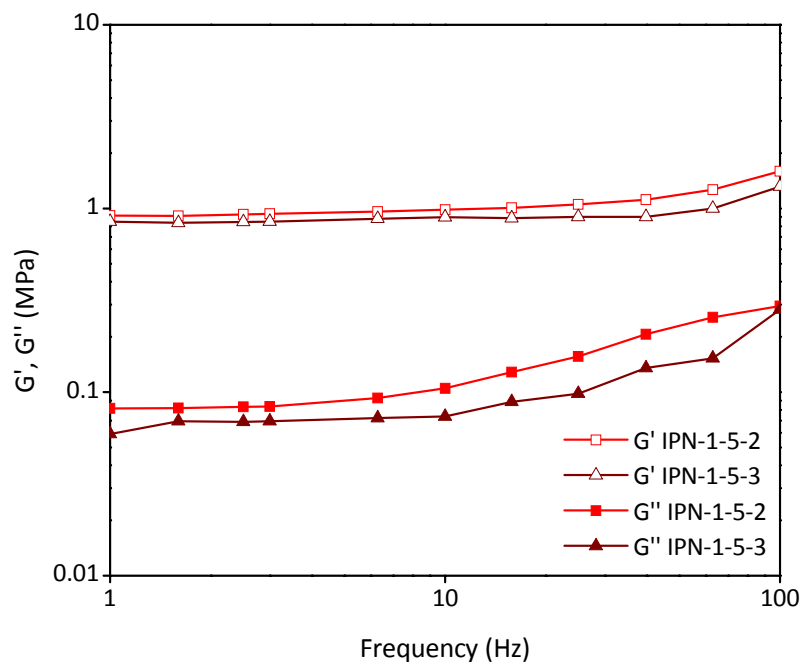


Figure III.19. DMA results for the full-IPN hydrogel films below VPTT (30°C): influence of crosslinking degree of PNIPAAm

According to Figure III.19, an increase in the crosslinking degree of PNIPAAm slightly decreases loss and storage moduli of hydrogels. This confirms that the difference in molar ratio of NIPAAm and MBAAm of 68.1 and 45.4 (in IPN-1-5-2 and IPN-1-5-3, respectively) does not influence the mechanical properties of resulting networks. These results might be also considered as a consequence of the network imperfections. In comparison, the increased concentration of alginate observed above, has more emphasized impact on the improvement of dynamic compressive properties (Figure III.18). Analogically, it contributes to a decrease in swelling capacities, as shown earlier (see Figure III.9). These phenomena are in agreement with the theory of rubber elasticity which could be applied on hydrogels [261].

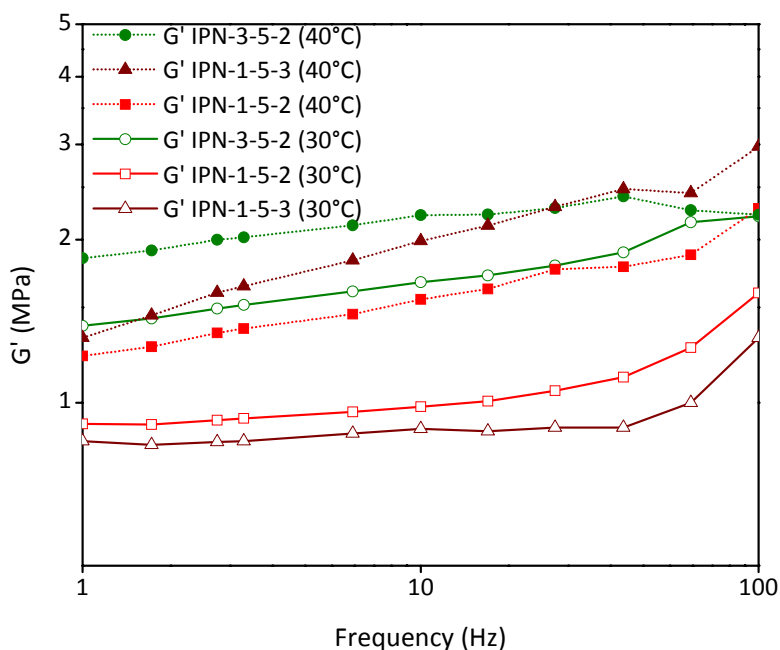


Figure III.20. Comparison of DMA results for the full-IPN hydrogel films below and above VPTT

Another set of experiments was done at 40°C. The G' results are compared to those obtained at 30°C for three full-IPN samples (Figure III.20). Around VPTT (~35°C), analyzed thermosensitive hydrogels undergo a change in hydrophilic/hydrophobic balance that leads to the volume phase transition process. According to the results, a large increase in elastic modulus is observed for all hydrogel samples when operational temperature was 40°C, primarily due to the collapse of polymer chains. Thus, more compact and tight network structure is formed, contributing to the improved mechanical properties to 3D polymer network. Relative increase in G' is the highest for sample IPN-1-5-3, and the lowest for IPN-3-5-2. This is in relation with the results of pore size values obtained by analysis of SEM micrographs and referring to equilibrium states of hydrogels at 25°C and 40°C (Figure III.17).

III.7 Conclusions

Synthesized thermosensitive hydrogel films aimed at transdermal delivery of a drug in a controlled manner have been characterized in detail. Thermal, swelling, mechanical and morphological properties demonstrated the advantages of full-IPN hydrogels composed of crosslinked PNIPAAm and CA over pure PNIPAAm hydrogels. The presence of alginate network in IPN hydrogels has considerable influence on VPTT values. CA considerably contributes to the improved strength of the interactions on a molecular level of the full-IPNs, as indicated by T_g values. The swelling studies showed that increase in alginate content significantly lowers the equilibrium swelling ratios of the full-IPN hydrogels, in particular at temperatures below VPTT. However, full-IPN hydrogels based on 1 wt % of alginate show better swelling capacity than pure PNIPAAm hydrogels at temperatures below VPTT. They also have the most rapid response to temperature increase from 25°C up to 40°C in

comparison with other studied hydrogels. The pure PNIPAAm hydrogels exhibit the lowest rate of deswelling due to the formation of dense skin layer. Different crosslinking densities of PNIPAAm have slight impact on the swelling behavior of analogous full-IPN hydrogels. Higher alginate content contributes to the improved mechanical properties of full-IPN hydrogels. The same effect is observed when the temperature is increased above VPTT, resulting from the formation of tighter network structures. The full-IPN hydrogels based on 1 wt % of alginate feature more porous network comparing to pure PNIPAAm hydrogels at 23°C. The full-IPN hydrogels with 1 wt % of alginate also exhibit the greatest changes in pore size values in response to temperature increase. In comparison with pure PNIPAAm, these hydrogels feature better mechanical properties, greater pore sizes and improved swelling behavior, i.e. response to temperature changes.

The presented results qualify thermosensitive full-IPN hydrogel films based on PNIPAAm and CA as potential matrices intended for a controlled release of a drug. Performed syntheses and characterizations of hydrogels provide a good base for additional study on their combination with heating textiles as a part of drug delivery system for transdermal applications.

**Chapter IV : APPLICATION OF ELECTROSTATIC
EXTRUSION IN PREPARATION OF THERMOSENSITIVE
HYDROGEL MICROBEADS**

After studying thermosensitive hydrogel films with full-IPN structure, we will in this Chapter describe formation of thermosensitive hydrogels in the form of microbeads using a spray technique, electrostatic extrusion. These micro-sized hydrogels will have semi-IPN structure due to the fact that PNIPAAm will be used in the linear form, previously synthesized by free-radical polymerization in solution. Such hydrogel structures have been reported in literature but only in spherical macro form (>1 mm) and prepared by simple extrusion in the gelling solution for crosslinking of alginate [170, 171, 262]. Since we aim at development of thermosensitive hydrogel microbeads with sizes close to average textile fiber diameter (around 20 μm for cotton [263]), an accent will be put on studying the influence of several operating parameters on microbeads size and shape.

IV.1 Preparation of hydrogel microbeads by electrostatic extrusion

Prior to formation of thermosensitive semi-IPN microbeads, pure SA solution was employed for the initial studies on electrostatic extrusion with a purpose of establishing general starting conditions of the process by revealing a nature of impact of several operating and formulation parameters.

IV.1.1 Pure CA hydrogel microbeads

Aqueous SA solutions of different concentrations (1, 2 and 3 wt %) were used for electrostatic extrusion at various combination of operating parameters. Depending on the concentration of extruded SA solution, microbeads were labelled as CA-1, CA-2, and CA-3. The liquid flow rate was varied from 143 ml h^{-1} to 26.1 ml h^{-1} , used needle types were 21-gauge (21g²) and 26-gauge (26g³), while the distances from the needle tip to the surface of the gelling solution (electrodes distance) was set at 3, 5, and 8 cm. The applied voltage was in the range from 8 kV to 20 kV. The average microbead diameters and the standard deviations were determined according to 100 microbeads per sample, using optical microscopy images and applying an image analysis.

Initial electrostatic extrusion processes were performed using a 21g needle, setting the electrodes distance at 5 cm, and at maximum possible flow rate (when using 50 ml-syringe). The reason for starting with such a high flow rate of 143 ml h^{-1} , atypical for the processes of electrostatic extrusion in general [205, 265] lies in achieving high beads productivity, although it is known that high flow rate generally results in beads of higher diameters of CA beads [266]. SA solutions of various concentrations were extruded at given electrodes distance, flow rate, and voltage of 8, 11, and 14 kV. The obtained hydrogel beads are displayed in Figure IV.1. Due to their great size, images of microbeads were obtained by a digital camera and not under the optical microscope.

² 21g corresponds to inner diameter of 0.495 mm [264]

³ 26g corresponds to inner diameter of 0.241 mm [264]

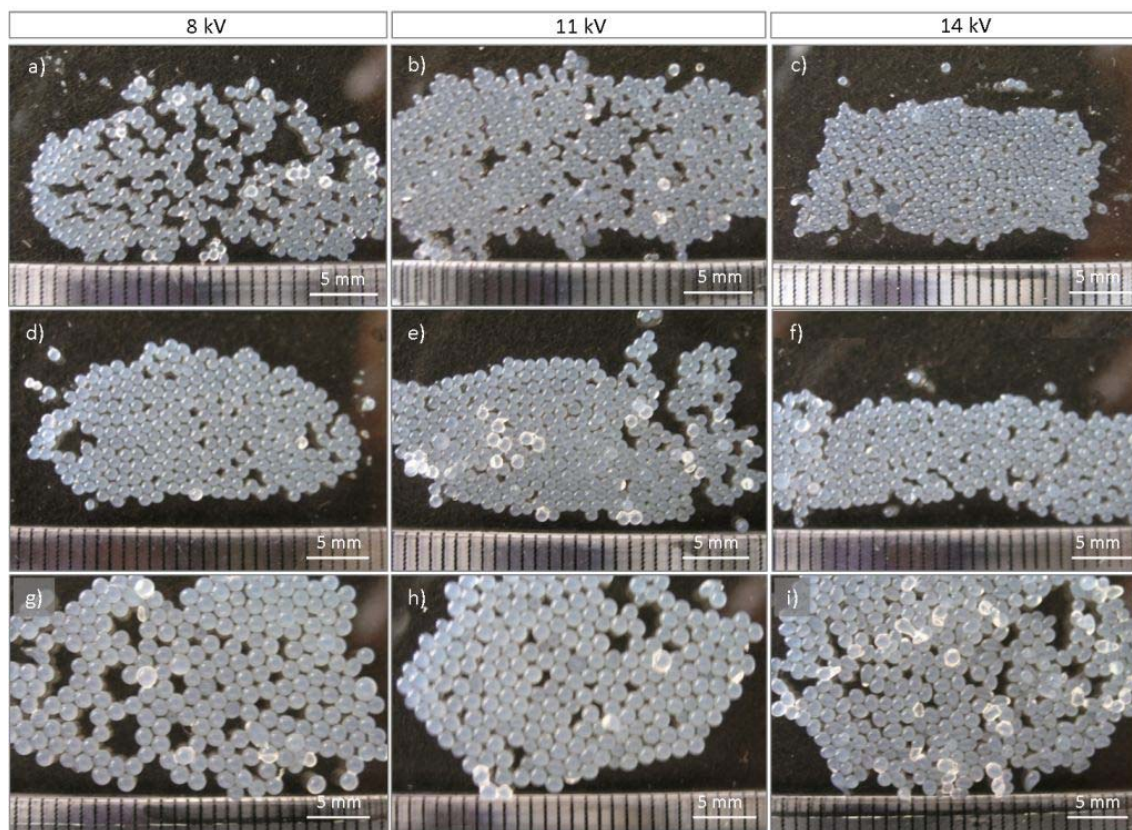


Figure IV.1. Hydrogel beads CA-1 (a-c), CA-2 (d-f), and CA-3 (g-i) and under the flow rate 143 ml h^{-1} , at the electrodes distance 5 cm, using a 21g needle and at various voltages as indicated

It can be observed that the CA beads are of regular spherical shape and of uniform size distribution. However, the size CA beads in these initial tests were far from the preferable micro sizes. Large hydrogel beads were obtained under all tested conditions, in the range from 750 up to 1350 μm . Table IV.1 contains calculated beads mean diameters that implicate the influence of the concentration of SA solution and the applied voltage. An increase in voltage did not have a considerable influence on sizes of beads based on 1 and 2 wt % SA but regarding 3 wt % SA solution, a rise from 8 to 14 kV reduced the size of the beads by about 15 %. On the other hand, the concentration of extruded solution had a pronounced impact on beads size. Under the voltage of 14 kV, CA beads produced from 1 wt % SA solution feature more than 30 % lower mean diameter than CA beads obtained from 3 wt % SA solution.

Table IV.1. Mean diameters of CA beads obtained under the flow rate 143 ml h^{-1} , at the electrode distance 5 cm, and using a 21g needle

Sample	Applied voltage, kV	Mean diameter, μm
CA-1	8	801.0 ± 31.4
	11	775.1 ± 36.5
	14	749.2 ± 70.6
CA-2	8	951.8 ± 52.5
	11	948.0 ± 38.1
	14	928.4 ± 30.3
CA-3	8	1354.7 ± 51.2
	11	1246.3 ± 57.6
	14	1138.2 ± 71.8

To achieve considerable reduction in microbeads sizes, the following extrusion runs were performed using a needle with considerably smaller inner diameter, a 26g needle. The flow rate and electrodes distance were unchanged, while voltage was maintained at 14 kV and at 20 kV. The resulting beads obtained at lower voltage were recorded by digital camera while others were recorded under the optical microscope (Figure IV.2).

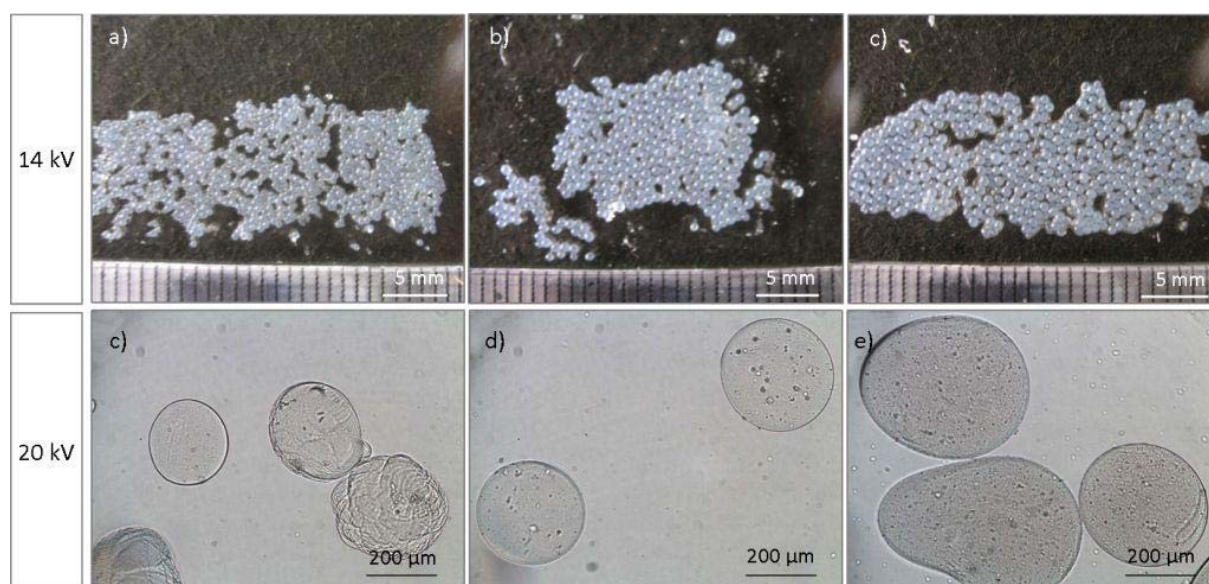


Figure IV.2. Hydrogel beads CA-1 (a,c), CA-2 (b,d), and CA-3 (c,e) and under the flow rate 143 ml h^{-1} , using a 26g needle, at the electrodes distance 5 cm, and at various voltages as indicated

The beads produced at 14 kV are of regular spherical shape and uniform size distribution, regardless of SA concentration. The reduction of beads mean diameters in comparison with beads obtained with 21g needle is clearly demonstrated by data in Table IV.2. Using a needle with two-fold smaller inner diameter resulted in decrease by almost 40 % in beads size (CA-1

and CA-3). An increase in voltage up to even 20 kV gave less regular microbeads, especially in the case of the most concentrated SA solution (Figure IV.2-f). This can be explained by high viscosity of the solution that affects the spraying mode and mechanism of droplet formation. It was reported that at lower SA concentration, i.e. low viscosity of SA solutions, elongation of the filament linking the new droplet and the meniscus at the tip of the needle was not as pronounced as in the case of high viscosity alginate [118]. This reflects to the uniformity of microbeads size. Nedovic et al. obtained irregular, elongated CA microbeads when using 3 and 4 wt % SA solution [267]. The results of the mean diameters imply significant influence of the voltage on microbeads size. Needle oscillations were observed when voltage of 20 kV was applied and this could be a reason of slightly irregular shapes of CA-3 microbeads.

Table IV.2. Mean diameters of CA microbeads obtained under the flow rate 143 ml h⁻¹, at the electrodes distance 5 cm, under voltage 14 kV, and using a 26g needle

Sample	Applied voltage, kV	Mean diameter, μm
CA-1	14	460.9 \pm 32.6
	20	274.7 \pm 90.2
CA-2	14	682.7 \pm 36.9
	20	306.0 \pm 31.1
CA-3	14	702.2 \pm 32.2
	20	471.5 \pm 80.8

The following extrusion processes were conducted using only 26g needle and the voltage was kept below 20 kV, whereas the flow rate was lowered to 26.2 ml h⁻¹. The influence of voltage was also studied in this series of extrusion runs at the unchanged electrodes distance (5 cm). Representative images of microbeads obtained at given combination of parameters are shown in Figure IV.3. Like in previous cases, the impact of SA concentration on microbeads sizes is obvious, although not significantly when comparing corresponding CA-1 and CA-2 microbeads.

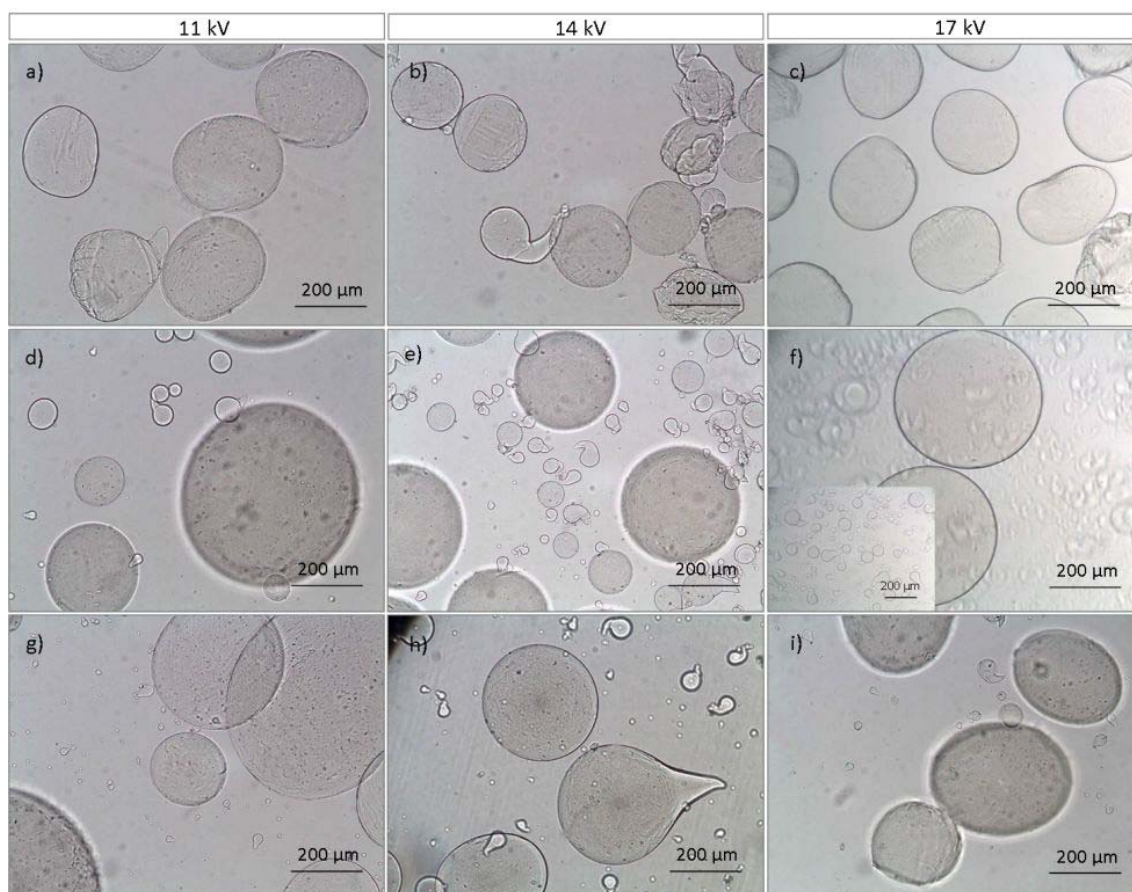


Figure IV.3. Hydrogel microbeads CA-1 (a-c), CA-2 (d-f), and CA-3 (g-i) and under the flow rate 26.2 ml h^{-1} , at the electrodes distance 5 cm, using a 26g needle and at various voltages as indicated

However, the presence of two fractions of microbeads by size was observed. Table IV.3 contains data of microbeads mean diameters and the range of captured microbeads sizes. It could be seen that the smallest satellite droplets, i.e. hydrogel microbeads reach around 10-20 μm in diameter. The appearance of the fraction of small microbeads is related to the mode of spraying, i.e. to the mechanism of the droplet formation. The non-uniform size distribution corresponds to the intensive spraying mode (sometimes discontinuous) into which dripping mode is transformed when applied voltage is increased beyond the critical value [116]. Sample and Bollini reported formation of small, so-called satellite droplets along with the main droplets at higher spraying voltages [268]. An early study on the break-up of a charged liquid jet during electrostatic extrusion showed that the instability of spherical surface at the needle tip originates from the opposing molecular and electrical forces at a curved liquid-gas interface [269]. It was proposed that stronger electrical effects over those attributable to the surface tension cause the formation of thin side filaments. The break-up of these filaments results in many small droplets, while break-up of the main jet comes from the action of gravitational and molecular forces. It could be noted that the mean diameter of microbeads obtained at the highest voltage applied (17 kV) is higher than of microbeads obtained at 14 kV. This phenomenon could be explained by too high droplet velocity for disintegration of formed droplet to occur when the voltage is close or above the critical point [118]. Hence, the adjustment of voltage should be careful so that reverse effects do not occur.

When the intensity of the electric field increases beyond the breakdown potential of the air, an arc discharge takes place. This is characterized by a heavy flow of current through the gas between the electrodes (the needle tip and a surface of CaCl₂ solution) and high dissipation of energy in the form of heat followed immediately by a sound [270]. When submitted to high electric fields, the liquid stream in an electric field becomes unstable and the extruded liquid is easily disrupted into many smaller filaments, resulting in many different microbead sizes [205]. Under given flow rate and electrodes distance, the value of critical voltage was between 11 and 13 kV, although air ionization occurred only at 30 kV.

Table IV.3. Mean diameters of CA microbeads obtained under the flow rate 26.2 ml h⁻¹, at the electrodes distance 5 cm, and using a 26g needle

Sample	Applied voltage, kV	Mean diameter, μm	Range of diameters, μm
CA-1	11	270.7±36.1	162 ÷ 317
	14	136.4±82.1	20 ÷ 239
	17	238.6±21.0	123 ÷ 270
CA-2	11	201.0±171.5	21 ÷ 550
	14	84.6±94.8	12 ÷ 343
	17	78.3±91.0	14 ÷ 397
CA-3	11	209.3±220.0	7 ÷ 620
	14	99.0±133.1	7 ÷ 432
	17	135.7±183.6	14 ÷ 500

The most important result deriving from this series of extrusion runs is a great influence of the flow rate on microbeads size, demonstrated by comparison of corresponding values in Tables IV.2 and IV.3, for the voltage of 14 kV. Lowering the flow rate from 143 to 26.2 ml h⁻¹ considerably reduces the microbeads size. Therefore, the following extrusion processes were conducted at 26.2 ml h⁻¹ and the influence of electrodes distance was analyzed (Figure IV.4). One smaller and one larger electrodes distance was chosen in comparison to previously set value (5 cm). Displayed microscopy images and data given in Table IV.4 indicate the negative impact of shorter electrodes distance on the size of the fraction of bigger microbeads as well as on the microbeads shape.

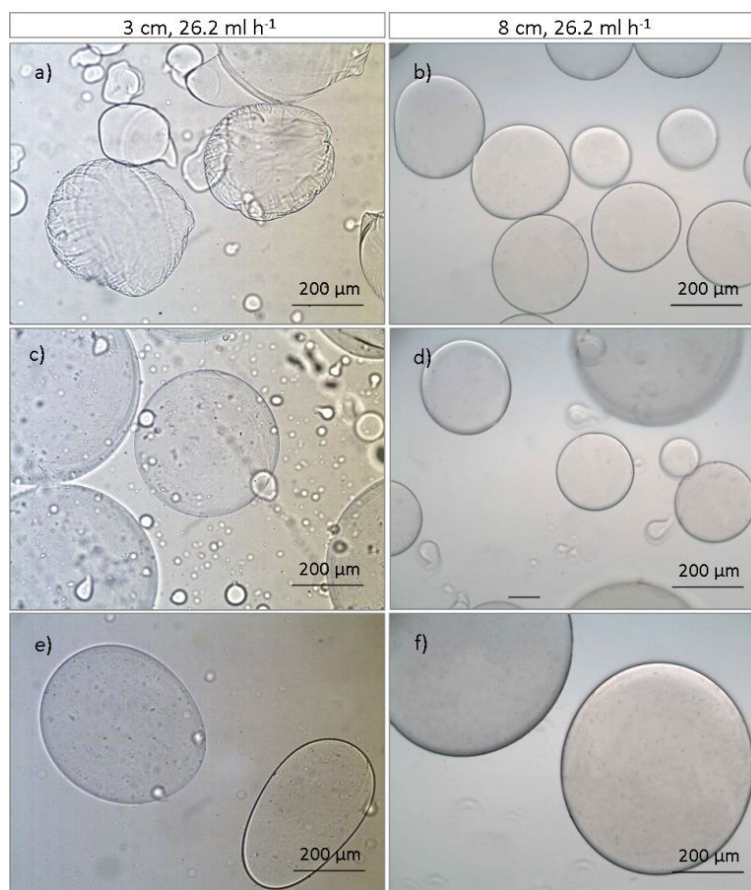


Figure IV.4. Hydrogel microbeads CA-1 (a-c), CA-2 (d-f), and CA-3 (g-i) at voltage 14 kV, flow rate 26.2 ml h^{-1} , using a 26g needle and under different electrodes distance, as indicated

The regularity of microbeads shape when electrodes distance was adjusted at 3 cm is particularly pronounced in the case of CA-1 microbeads. The shape of the microbeads is determined by the forces acting on the droplet before it enters the collecting solution. It could be assumed that too low electrodes distance allows electrical and impact-drag forces to overcome viscous-surface tension forces and that is why regular spherical shaped microbeads are not obtained [111]. The microbeads CA-2 and CA-3 obtained at smaller electrodes distance have wide size distribution due to the presence of small satellite droplets down to 10-20 μm in diameter. When the distance between the electrodes was set at 8 cm, both size and shape of microbeads were changed. The mean diameter increased but the uniformity of microbeads size and regularity of microbeads shape was considerably improved, particularly for the CA-2 microbeads. This implies the complexity of adjusting optimal combination of parameters in achieving close-to spherical shape of microbeads but also the smaller size as possible.

Table IV.4. Mean diameters of CA microbeads obtained under the voltage 14 kV, at 26 ml h^{-1} , using a 26g needle, and at various electrodes distances

Sample	Electrodes distance, cm	Mean diameter, μm
CA-1	3	-*
	8	222.7 ± 45.7
CA-2	3	41.2 ± 96.8
	8	335.2 ± 138.4
CA-3	3	43.5 ± 76.9
	8	419.4 ± 167.5

* These microbeads were difficult to analyze by image analysis software due to pronounced shape irregularity.

The influence of the concentration of the extruded solution was obvious in all cases, i.e. higher concentration results in larger hydrogel beads. However, based on our practical experience, lower solution concentration does not always imply the production of microbeads of regular spherical shape. In certain cases, 2 wt % SA solution seemed to be the most adequate in all tested conditions with regard to the regularity of the beads shape. Figure below gives examples of different beads shape and size.

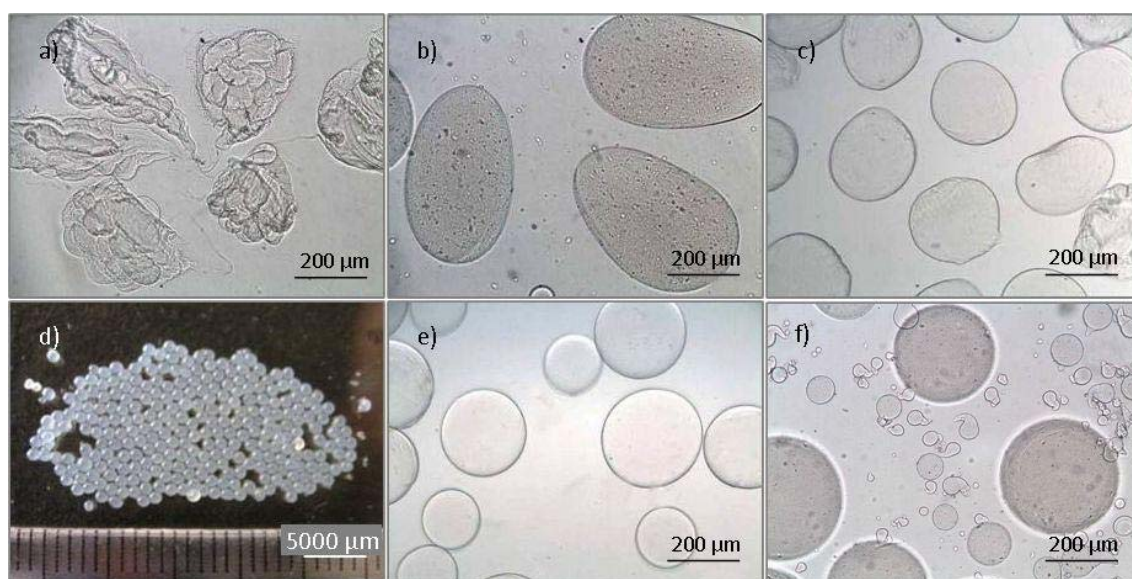


Figure IV.5. Hydrogel beads shapes and sizes obtained under various combinations of operating parameters: a) CA-1 ($26\text{g}-5\text{cm}-20\text{kV}-26.1\text{ml h}^{-1}$), b) CA-3 ($26\text{g}-5\text{cm}-20\text{kV}-143\text{ml h}^{-1}$), c) CA-1 ($26\text{g}-5\text{cm}-17\text{kV}-26.1\text{ml h}^{-1}$), d) CA-2 ($21\text{g}-\text{SA}-5\text{cm}-8\text{kV}-143\text{ml h}^{-1}$), e) CA-1 ($26\text{g}-8\text{cm}-14\text{kV}-26.1\text{ml h}^{-1}$), and f) CA-2 ($26\text{g}-5\text{cm}-14\text{kV}-26.2 \text{ ml h}^{-1}$)

The combination of various parameters qualifies the process of electrostatic extrusion as intricate and still not completely understood. Hence, the optimization of operating conditions with the aim of obtaining hydrogel microbeads of desirable properties represents a challenge and a demanding task. Formation of thermosensitive hydrogel microbeads of

semi-IPN structure imparts complexity in the given system due to the presence of neutral PNIPAAm chains.

IV.1.2 Thermosensitive semi-IPN hydrogel microbeads

Formation of thermosensitive hydrogel microbeads was performed by electrostatic extrusion of aqueous solutions containing PNIPAAm and SA, using a CaCl_2 solution as a receiving medium. Due to ability of Ca^{2+} to crosslink alginate by simple ionic exchange with Na^+ ions, formed microbeads had semi-IPN structure composed of linear PNIPAAm and CA (Figure IV.6). In this system the linear PNIPAAm chains are entrapped within the CA network as a consequence of crosslinking reaction.

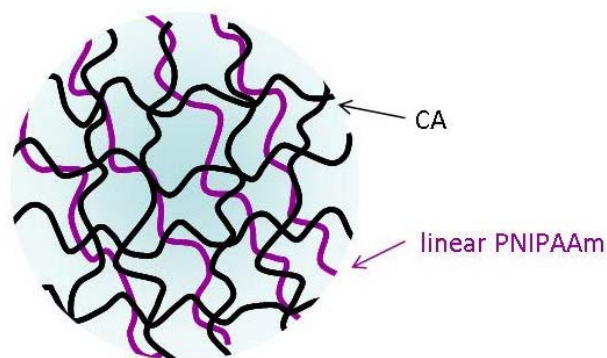


Figure IV.6. Scheme of semi-IPN structure of thermosensitive hydrogel microbeads composed of linear PNIPAAm and CA

The name codes of PNIPAAm/SA solutions were interpreted as S-X-Y, where S stands for the solution, X signifies the weight fraction of PNIPAAm in the solution, and Y stands for the weight fraction of SA in the solution. The majority of extrusion runs were conducted using two solutions: S-0.1-1 solution that contains 0.1 wt % PNIPAAm and 1 wt % SA. Name code S-0-1 represents pure 1 wt%-SA solution. The name codes of microbeads were given analogously, as semi-IPN-X-Y.

Formulation and operating parameters were varied in a set of experiments intended for setting up the optimal conditions for the production of the smallest possible thermosensitive hydrogel microbeads and of close-to-spherical shape. All extrusion processes were performed using a 27g needle, the voltage was varied from 4 to 16 kV, the electrodes distance from 4 to 16 cm, and the flow rate from 0.397 to 26.2 ml h^{-1} .

IV.1.2.1 Influence of PNIPAAm concentration in extruded solution

The initial studies on electrostatic extrusion of pure SA solution showed that the 2 wt % solution is the most satisfying regarding the microbeads shape and size. However, as a starting point for the preparation of PNIPAAm/SA solution, a 1 wt % SA solution was used because of too high viscosity of the 2 wt% solution. Indeed, even a small fraction of PNIPAAm considerably increases the viscosity of the solution, as will be shown. A too high viscosity affects the process stability. Furthermore, regular extrusion of the PNIPAAm/SA solutions based on 1 to 4 wt % PNIPAAm and 1 wt % SA was impossible since no droplets

could have been formed, regardless of the needle gauge or voltage applied. This can be explained by too low conductivity and too high viscosity of polymer solutions. Due to high concentration of neutral PNIPAAm linear chains, the diffusion of small sodium ions (Na^+) can be limited and interrupted (Figure IV.7). Poncelet et al. reported that the adsorption of the electric charge may be limited by the sterical hindrance and diffusion rate to the droplet surface [202]. This results in insufficient electric surface charge necessary for the formation of a pending droplet and more extended liquid filament is instead produced from the needle tip. Impact of high electric field on the extended filament is expected to break up in large number of smaller droplets of non-uniform size distribution. Hence, extrusion of PNIPAAm/SA solution could be less controllable and predictable when comparing to pure SA solution.

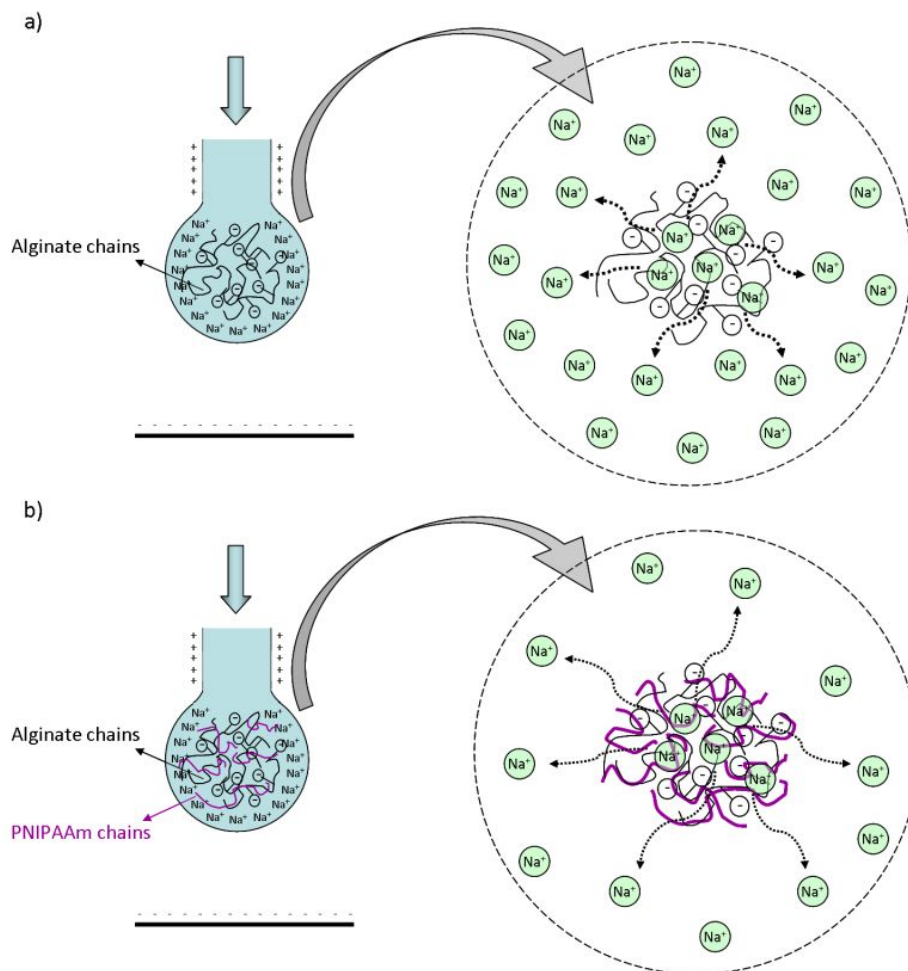


Figure IV.7. Scheme of a hanging droplet of SA solution (a) and PNIPAAm/SA solution (b) in an electric field and enlarged display of diffusion of Na^+ ions outward from the core of a droplet

Initial tests have shown that the solutions with higher concentration of PNIPAAm (above 0.5 wt %) and hence, of higher viscosities, are not desirable for the performance of the process in a controllable manner. Hence, two types of solution for the electrostatic extrusion were selected, resulting in microbeads labeled as semi-IPN-0.1-1 and semi-IPN-0.25-1. Figure IV.8 clearly displays the impact of the addition of small quantities of PNIPAAm on dynamic viscosity of aqueous solution containing 1 wt % SA. The dynamic viscosity of S-0.1-1 is in

average 16 % higher in the tested range of shear rate in comparison with the average viscosity of S-0-1. More viscous fluids have higher resistance to flow and hence are expected to give larger droplets when extruded in an electric field.

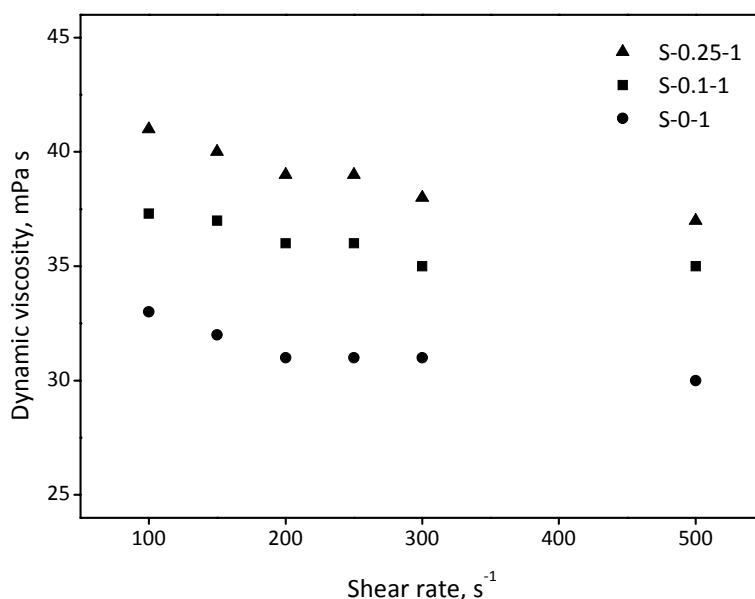


Figure IV.8. Dependence of dynamic viscosity on the shear rate for selected PNIPAAm/SA solutions intended for electrostatic extrusion

The conductivity of polymer solutions could not be neglected in predicting and analyzing the size of resulting hydrogel microbeads produced by electrostatic extrusion. Conductivity of polymer solution determines the degree of charge that could accumulate in the surface of a pending droplet on a needle tip. If conductivity of extruded liquid is high, the rate at which the charge relaxes to the liquid surface is short. This leads to the buildup of electrostatic force in which the radial component of the electrical stress is dominant, resulting in the destabilization of the liquid jet [271]. A result could be polydisperse spray with wide size distribution of droplets. The comparison of conductivity of selected polymer solutions is given in Table IV.5. Since PNIPAAm is a neutral polymer, conductivity of the solution decreases with increase in PNIPAAm fraction. In addition to viscosity, conductive effects of PNIPAAm/SA solutions will also contribute to unique behavior of these solutions in comparison to pure SA solution that was mainly studied for the production of hydrogel microbeads by electrostatic extrusion.

Table IV.5. Conductivity values of various polymer solutions at 21°C

Solution	Conductivity, mS cm ⁻¹
S-0-1	2.353±0.015
S-0.1-1	2.114±0.005
S-0.25-1	2.079±0.020

IV.1.2.2 Influence of surfactant

The properties of the solutions are important to know because of clearer analysis of the results. A balance of forces acting on a droplet from a needle tip in the system with positive needle and grounded collecting solution was discussed in Chapter II of the report (Equations II.1 and II.2). A mass of a formed droplet at the moment of its detachment from the needle tip is determined by the balance among three forces: gravitational (F_g), electrostatic (F_e) and surface tension (F_γ) [114]. According to Equation II.2, a reduction in surface tension of extruded polymer solution results in decrease of droplet diameter and hence, of hydrogel beads size. In PNIPAAm/SA solution, carriers of charge opposite to the collecting solution diffuse towards the droplet surface due to the applied electrostatic potential and thus counteract the surface tension of the droplet. Therefore, a surfactant was added to PNIPAAm/SA solution and its influence on microbeads size and shape was investigated.

Initial choice of potentially applicable two nontoxic surfactants was governed primarily by their nonionic nature (Table IV.6). This property is of importance for the crosslinking reaction of alginate when a droplet of PNIPAAm/SA solution comes in contact with CaCl_2 solution. Hence, there should be minimum interaction between the surfactant molecules and Ca^{2+} ions. Also, one of the chosen surfactants (Tween 20) was employed in the study of the formation of protein-loaded CA microbeads with diameter below $10\ \mu\text{m}$ [272].

Table IV.6. Properties of chosen surfactants [264, 273, 274]

Brand name	IUPAC name	Type	Molecular weight	HLB
Tween 20	Polyoxyethylene (20) sorbitan monolaurate	nonionic	1228	16
Brij 35	Polyoxyethylene (35) lauryl ether	nonionic	1198	16

First, S-0.1-1 solution with various concentrations of surfactants was characterized by measurement of the surface tension (Figure IV.9). The addition of 1 wt % solution of Tween 20 decreases the surface tension by approximately 12 %. The second surfactant, Brij 35, showed a much weaker effect on surface tension, regardless of the concentration. According to Figure IV.9, the surface tension of Tween 20 solutions decreases with increase of surfactant concentration. Concentration of 5 wt % is close to a critical micelle concentration above which no further decrease in surface tension could be achieved. Due to weaker impact on decrease of the surface tension of S-0.1-1, Brij 35 was not employed in the series of electrostatic extrusion runs but only Tween 20.

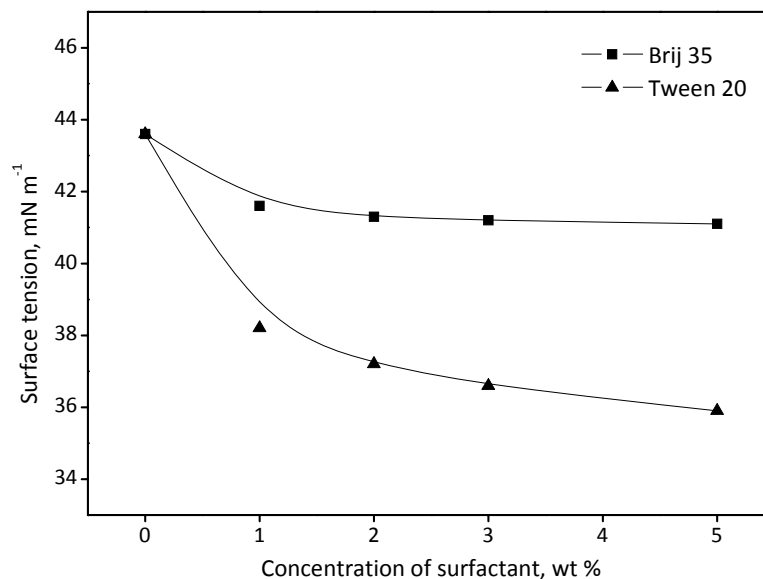


Figure IV.9. Effect of surfactants concentration on the surface tension of solution S-0.1-1

Under the same conditions, polymer solution (S-0.1-1) without and with Tween 20 were extruded. Flowing rate was set at 26.2 ml h⁻¹, electrodes distance at 8 cm, and 26g needle was used. The voltage was adjusted at 8 kV. The images of obtained microbeads are displayed at Figure IV.10. Solutions with added surfactant were labeled with letter T at the end of the name code of the microbeads, followed by a number that signifies the Tween 20 weight fraction in percentage in the solution. Analysis of microbeads diameter (using ImageJ) was based on 100 microbeads per sample. Extrusion of pure S-0.1-1 (without a surfactant) resulted in regular spherical shape of larger beads of around 274.9 μm in diameter. The addition of Tween 20 at 1 wt % did not influence the microbeads size (277.4 μm). The mean diameter of semi-IPN-0.1-1-T3 and semi-IPN-0.1-1-T5 were 297.7 μm and 297.8 μm , respectively, i.e. even high concentrations of surfactant do not influence the microbeads size at given process conditions.

In general, the addition of surfactant has no notable impact on the reduction of microbeads diameter regardless of its concentration (2, 3, and 5 wt %). The reason for this could be found in retardation of diffusion of Na⁺ ions toward the droplet surface by bulky surfactants molecules (non-ionic). Thus, charge on a droplet (q) becomes reduced comparing to solution without a surfactant and hence affects the droplet diameter increase (Equation IV.2). The effects of the surface tension reduction and surface charge decrease due to surfactant presence could be mutually circumvented, resulting in lack of surfactant impact on microbeads diameter size.

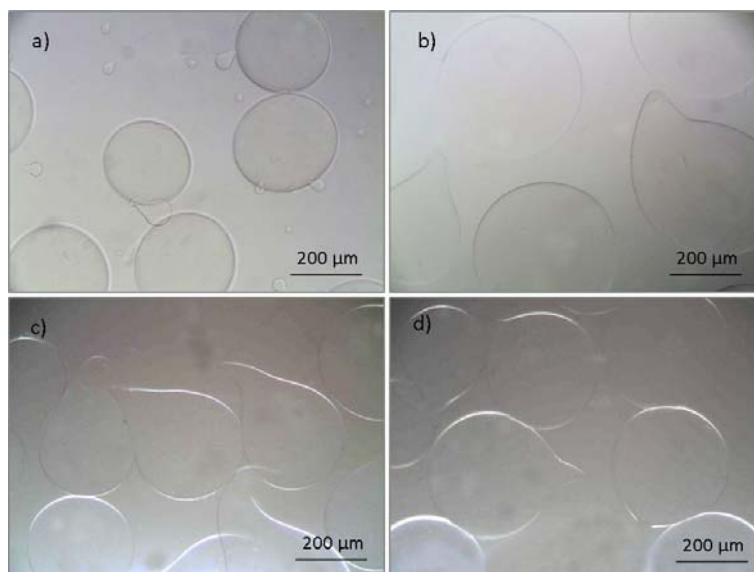


Figure IV.10. Hydrogel microbeads semi-IPN-0.1-1 without surfactant (a), semi-IPN-0.1-1-T2 (b), semi-IPN-0.1-1-T3 (c), and semi-IPN-0.1-1-T5 (d) (operating parameters: 8 kV, 8 cm, 26.2 ml h⁻¹, 26g)

Another obvious fact is that microbeads obtained from solutions with surfactant are not regular spherical but tail-shaped (Figure IV.10-b,c,d). This phenomenon could be related to the impact of higher viscosity of the solutions with surfactant but primarily due to weakened surface tension effect that governs the transition of a drop detaching from a needle tip into regular spherical drop before entering the collecting solution. The tail-shaped beads were reported by Chan et al. when pure SA solution of higher concentrations (viscosities) was extruded in the absence of an electric field [111]. Therefore, further studies on the impact of operating parameters of electrostatic extrusion were performed using only pure PNIPAAm/SA solution, without the addition of surfactants.

IV.1.2.3 Influence of the operating parameters

The electrostatic extrusion of the pure SA solution, i.e. formation of CA microbeads showed that needle gauge has distinctively notable influence on microbeads size. Hence, the needle with the smallest inner diameter (27g⁴) was used in the following series of electrostatic extrusions of SA/PNIPAAm solution (S-0.1-1) in an electric field. The influence of several operating parameters on microbeads size and shape was investigated: flow rate, voltage, and electrodes distance.

The microscopy images of microbeads were analyzed by Image Pro Plus™ software. The analysis was performed on 300 microbeads per sample (from 3 batches, 100 microbeads per batch). The regularity of microbeads shape is of significance for intended application and easier control of their behavior, particularly in drug release studies. Therefore, the roundness was determined in addition to microbeads diameters. The perfect roundness of a microbead corresponds to the value of 1. Figure IV.11 is given for acquiring clearer image of how imperfections in microbeads shape reflects in the value of roundness.

⁴ 27G corresponds to inner diameter of 0.191 mm [264]



Figure IV.11. Example of various microbeads shape and corresponding values of roundness

The starting conditions were set according to previous tests with pure SA solutions, the voltage was set at 8 kV, electrodes distance at 8 cm, and the flow rate at 26.2 ml h^{-1} . Keeping the voltage and electrodes distance constant, the value of flow rate was varied from 26.2 to 0.397 ml h^{-1} . Optical microscopy images obtained at these conditions are displayed in Figure IV.12 and corresponding values of mean roundness and mean diameter are given in Table IV.7.

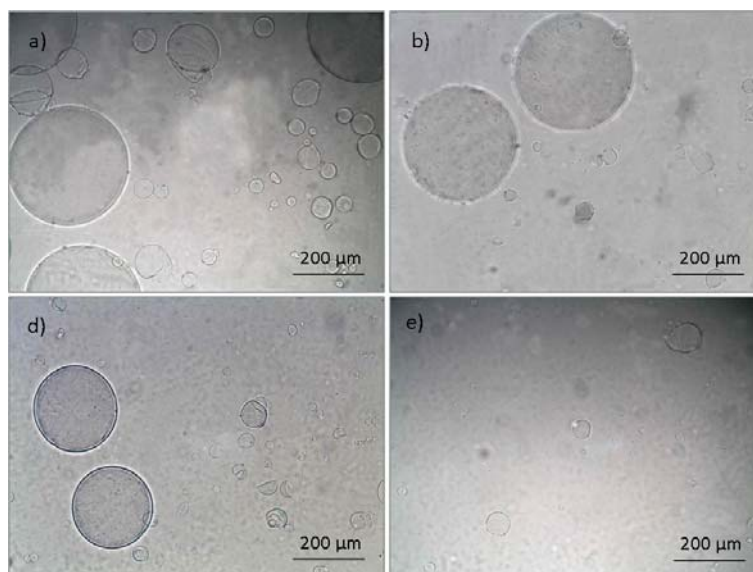


Figure IV.12. Semi-IPN-0.1-1 microbeads obtained under the voltage 8 kV, electrodes distance 8 cm, and flow rates 26.2 ml h^{-1} (a), 16.3 ml h^{-1} (b), 7.14 ml h^{-1} (c), and 0.397 ml h^{-1} (d)

It could be seen that decrease in flow rate of polymer solution considerably decreases the mean diameter of resulting hydrogel microbeads. Flow rate influences the amount of Na^+ ions moving toward the surface of the droplet. At lower flow rates more charged entities (Na^+ ions) reach the droplet surface and cause the surface tension to decrease since they will repel each other. A decrease in surface tension results in formation of smaller droplets and hence, of smaller hydrogel microbeads.

Table IV.7. Influence of the flow rate on size and shape of semi-IPN-0.1-1 microbeads (electrodes distance 8 cm, voltage 8 kV)

Flow rate, ml h ⁻¹	Description	Mean roundness	Mean diameter, μm
26.2	Bigger microbeads regular spherical, smaller mainly irregular, some tailed-shaped	1.027±0.042	78.0±97.2
16.3	Mixture of regular spherical and slightly irregular	1.054±0.096	61.7±67.6
7.14	Bigger beads regular spherical and partly tail-shaped, smaller mainly regular spherical, some half-sphere shaped	1.054±0.104	30.8±38.3
0.397	Middle size microbeads (around 100 μm) tail-shaped, smaller partially regular and partially half-sphere shaped	1.041±0.061	19.4±20.6

Large standard deviation values of mean diameters could be more clearly understood when the corresponding size distribution profiles are displayed (Figure IV.13). Microbeads of above 250 μm in diameter were detected when the flow rate was set at 26.2 and 16.3 ml h⁻¹. The narrowest size distribution and the smallest mean diameter were obtained at the lowest flow rate. This confirms the importance of the flow rate values in the process of electrostatic extrusion because of the relative roles that inertial and electrostatic forces play in the production of a liquid jet and in subsequent atomization [206].

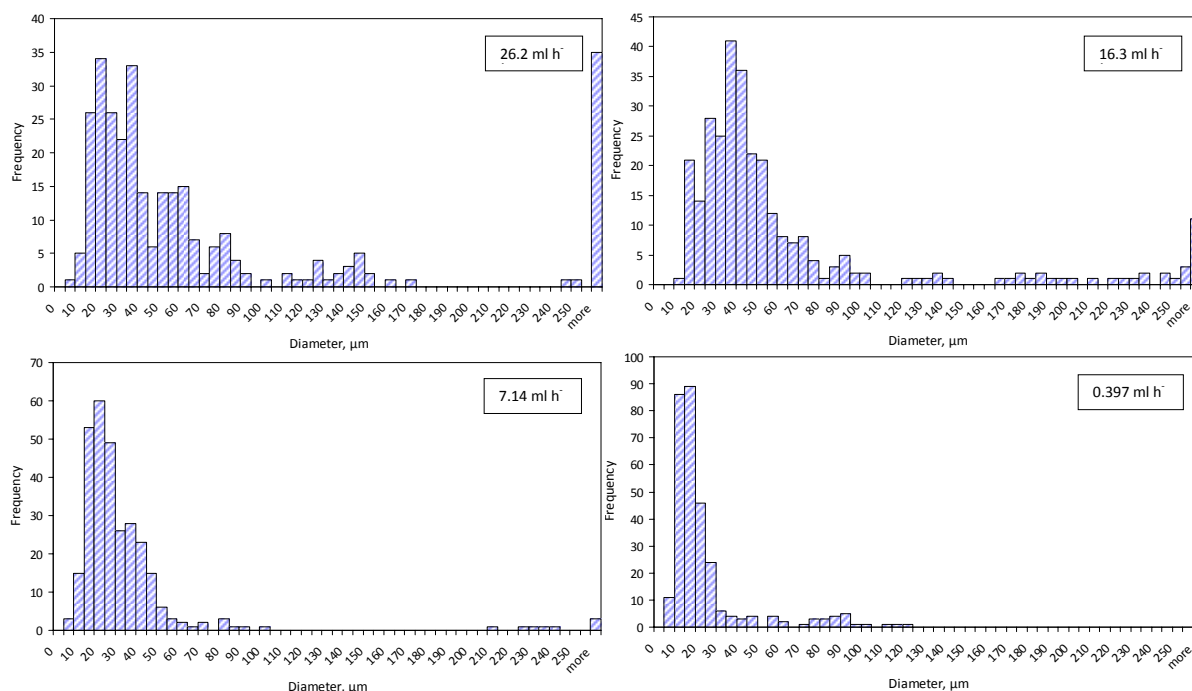


Figure IV.13. Size distribution profiles of semi-IPN-0.1-1 microbeads obtained at various flow rates, voltage 8 kV, electrodes distance 8 cm, and using a 27g needle

The values of mean roundness follow the same trend as the values of mean diameters but the roundness distribution profiles in Figure IV.14 distinctly show that the highest amount of microbeads of perfect roundness (value 1) is obtained when the flow rate of 0.397 ml h^{-1} is applied.

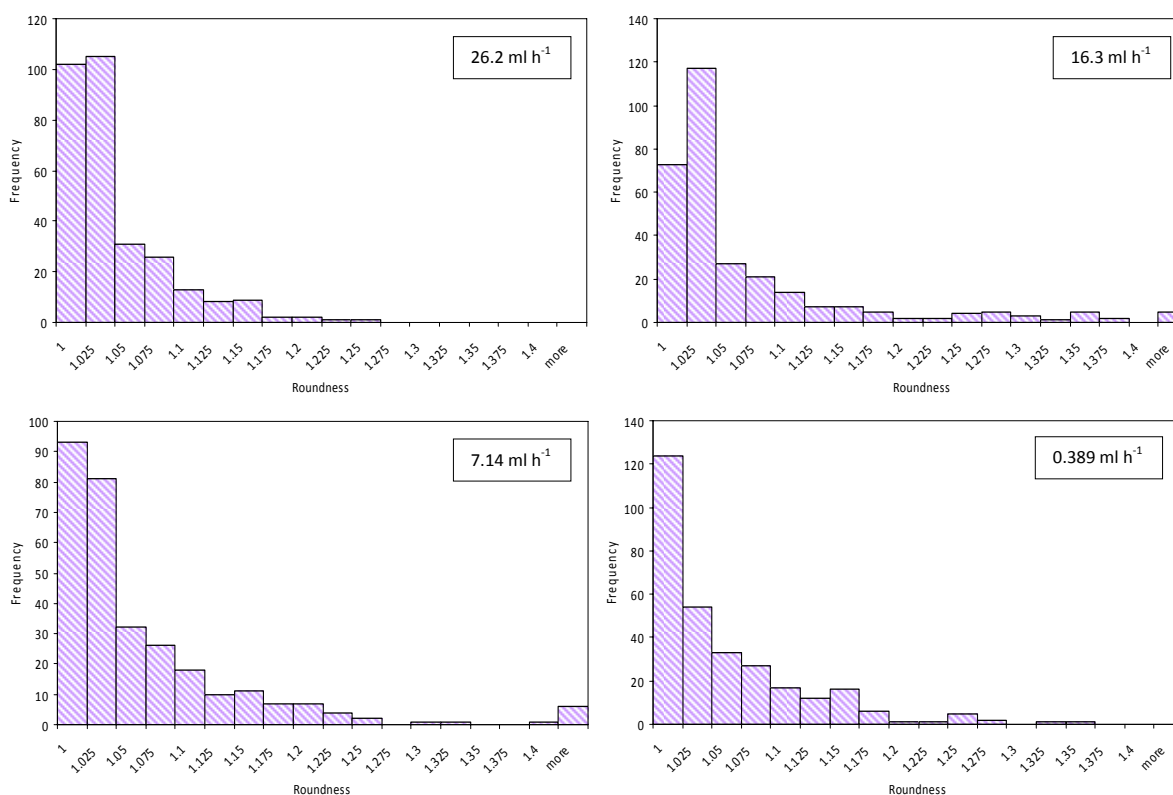


Figure IV.14. Roundness distribution profiles of semi-IPN-0.1-1 microbeads obtained at various flow rates, voltage 8 kV, electrodes distance 8 cm, and using a 27g needle

Taking into consideration the previous results, in the following extrusion runs the flow rate was kept at 0.397 ml h^{-1} , the electrodes distance at 8 cm, while voltage was increased from 8 kV to 12 and 16 kV. Increase in voltage could often result in discontinuous spraying of liquid, associated with wide droplets size distribution [116]. We assumed that controlled increase in voltage could give smaller satellite droplets. The risk of deteriorating the shape regularity of resulting microbeads was also expected due to the impact of electrical forces. For comparison, the batch of microbeads obtained at 8 kV is presented along with the newly synthesized microbeads (Figure IV.15).

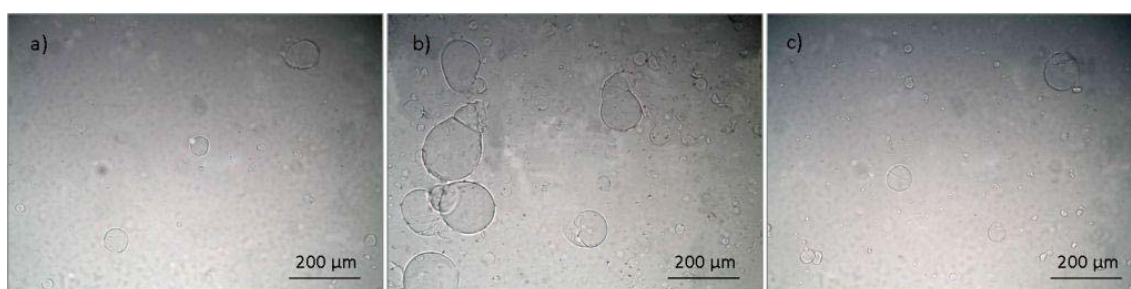


Figure IV.15. Semi-IPN-0.1-1 microbeads obtained under the flow rate 0.397 ml h^{-1} , electrodes distance 8 cm, and voltage 8 kV (a), 12 kV (b), and 16 kV (c)

Data presented in Table IV.8 indicate that increasing voltage from 8 kV to 12 kV caused reduction in mean diameter. In contrast, further increase up to 16 kV resulted in slightly bigger microbeads (than at 12 kV). Such dependence of microbeads size on applied voltage applied is already observed in the case of pure CA microbeads (Section IV.1.1). The reason for that is found in too high electric field that affects an increase in droplets velocity and hence does not favor disintegration of formed droplets [118].

Table IV.8. Influence of the voltage on size and shape of semi-IPN-0.1-1 microbeads (electrodes distance 8 cm, flow rate 0.397 ml h⁻¹)

Voltage, kV	Description	Mean roundness	Mean diameter, μm
8	Middle size microbeads ($\sim 100 \mu\text{m}$) tail-shaped, smaller partially regular and partially half-sphere shaped	1.041 \pm 0.061	19.4 \pm 20.6
12	Mixture of regular spherical and half-sphere shaped microbeads	1.018 \pm 0.049	10.9 \pm 10.1
16	Bigger microbeads ($>100 \mu\text{m}$) tail-shaped, smaller microbeads of regular shape	1.031 \pm 0.096	15.4 \pm 29.9

The increase in applied voltage reduced the amount of microbeads of diameter above 100 μm , as demonstrated by size distribution profiles in Figure IV.16.

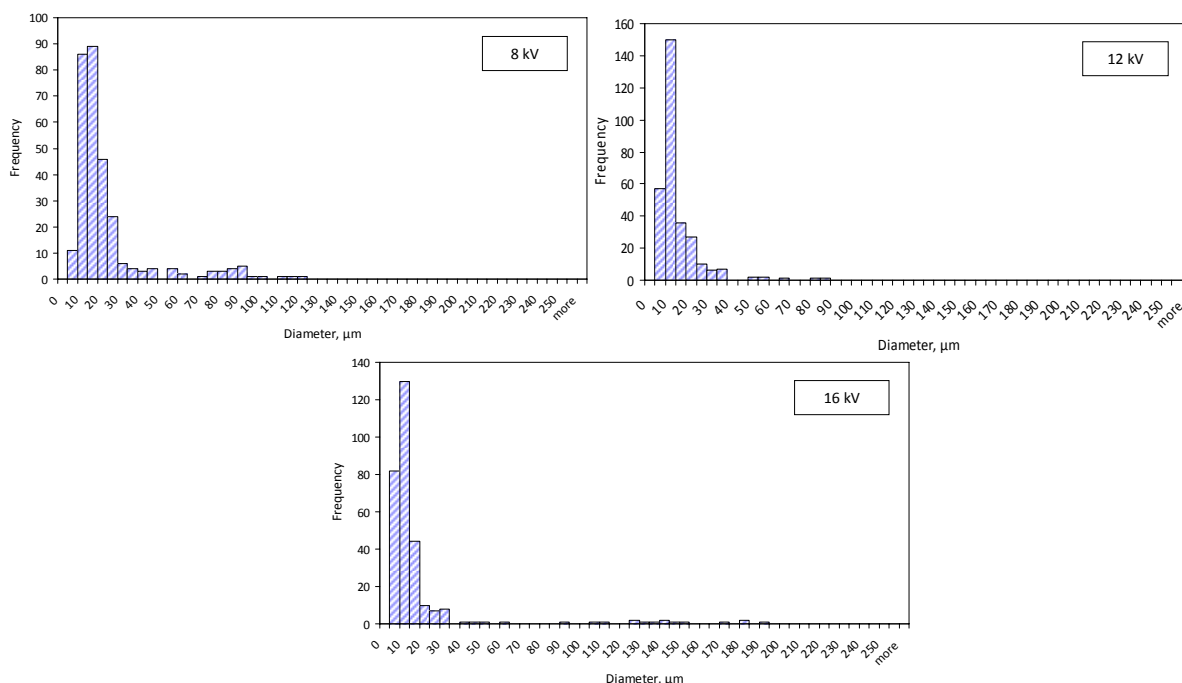


Figure IV.16. Size distribution profiles of semi-IPN-0.1-1 microbeads obtained at various voltages and at electrodes distance 8 cm, flow rate 0.397 ml h⁻¹ and using a 27g needle

Roundness distribution profiles (Figure IV.17) testify that the most regular microbeads are obtained at 12 kV. These microbeads exhibit the best ratio of mean diameter and mean

roundness. Although the microbeads produced at even higher voltage (16 kV) have also satisfying roundness, their diameter is higher.

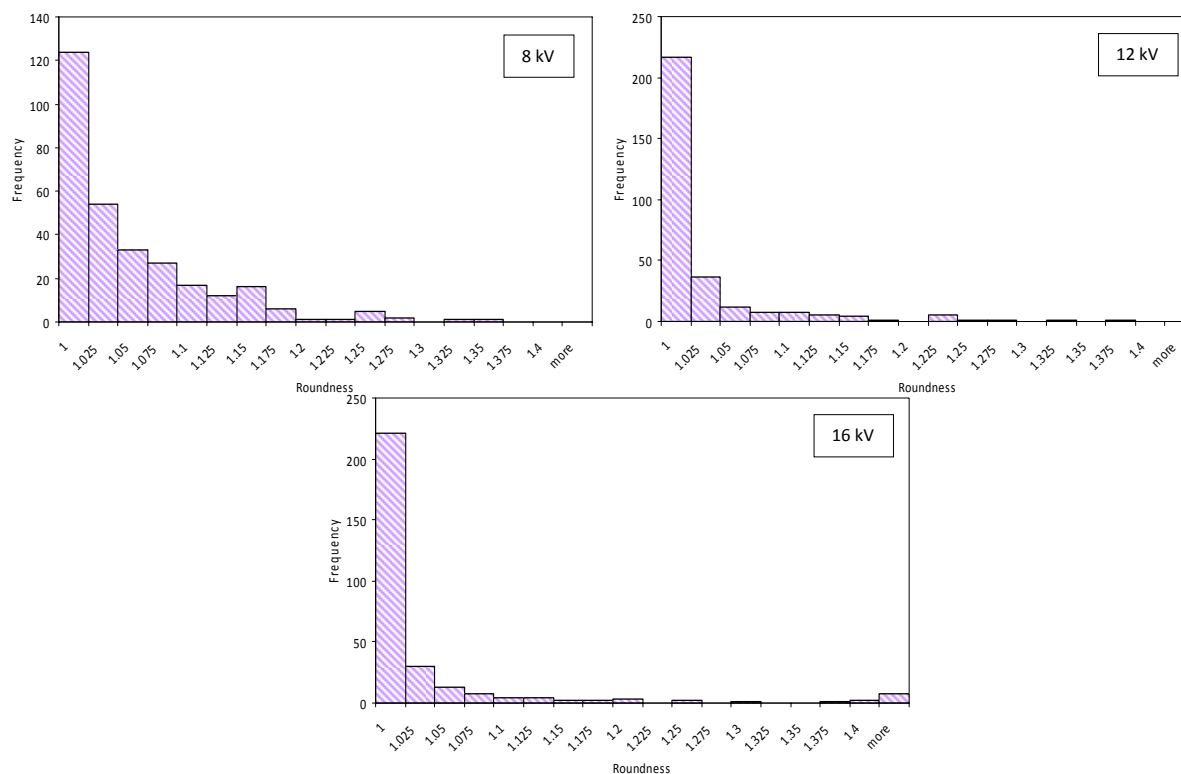


Figure IV.17. Roundness distribution profiles of semi-IPN-0.1-1 microbeads obtained at various voltages, flow rate 0.397 ml h^{-1} , electrodes distance 8 cm, and using a 27g needle

The following series of extrusion in electric field was performed to study the influence of the flow rate, this time at voltage of 12 kV (and same electrode distances). These extrusion runs were performed to investigate the economy in microbeads production. In other words, low flow rates are not preferable for industrial conditions due to low productivity and high expenses. Therefore, at constant voltage and electrodes distance, the flow rate was varied from 0.397 up to 26.2 ml h^{-1} and resulting microbeads are displayed in Figure IV.18.

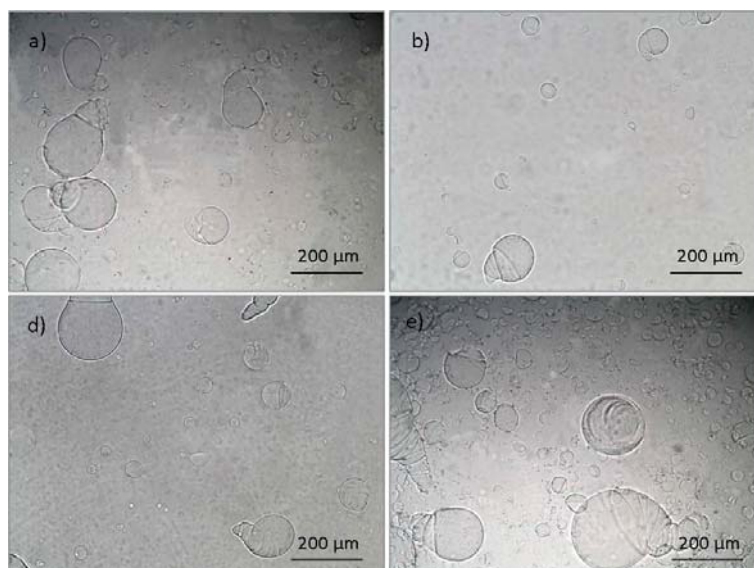


Figure IV.18. Semi-IPN-0.1-1 microbeads obtained under voltage 12 kV, electrodes distance 8 cm, and flow rate 0.397 ml h⁻¹ (a), 7.14 ml h⁻¹ (b), 16.3 ml h⁻¹ (c), and 26.2 ml h⁻¹ (d)

The increase in flow rate resulted in the increase in mean diameter that is far less pronounced than at 8 kV (Table IV.9). One promising result is the value of mean diameter of microbeads produced at 26.2 ml h⁻¹, which is around 24 μm, in comparison with 78 μm calculated for the same flow rate but at 8 kV.

Table IV.9. Influence of the flow rate on size and shape of semi-IPN-0.1-1 microbeads (voltage 12 kV, electrodes distance 8 cm)

Flow rate, ml h ⁻¹	Description	Mean roundness	Mean diameter, μm
0.397	Mixture of regular spherical and half-sphere shaped microbeads	1.018±0.049	10.9±10.1
7.14	Middle-sized microbeads slightly irregular and smaller microbeads - mixture of regular and irregular	1.042±0.087	14.7±18.2
16.3	Bigger microbeads tail-shaped, middle-sized and smaller microbeads - microbeads slightly irregular	1.089±0.126	31.3±42.0
26.2	All microbeads slightly irregular	1.069±0.097	24.3±30.3

If the corresponding size distribution profiles in Figure IV.13 (voltage 8 kV) and Figure IV.19 (voltage 12 kV) are compared, it could be observed that the voltage has more emphasized influence on the microbeads size at high flow rates. An analogous effect was reported by Tang and Gomez who studied monodisperse electrosprays of low electric conductivity liquids [275]. At 8 kV, the narrowest size distribution is again observed for the microbeads corresponding to the lowest flow rate.

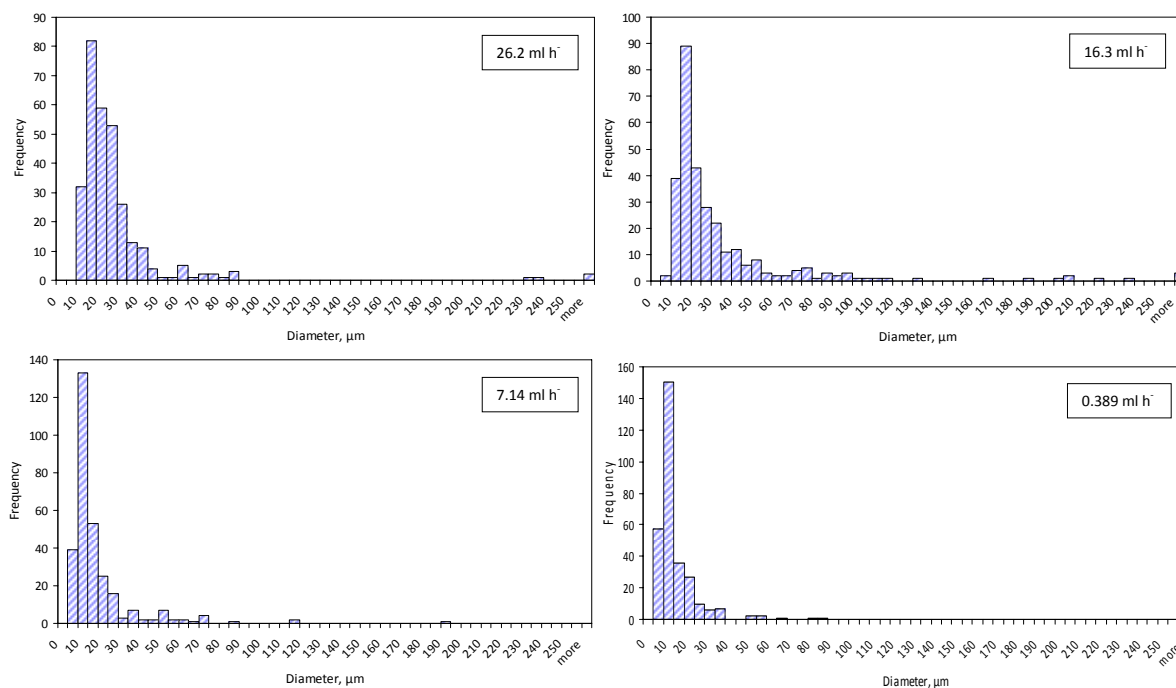


Figure IV.19. Size distribution profiles of semi-IPN-0.1-1 microbeads obtained at various flow rates and at voltage 12 kV, electrodes distance 8 cm, and using a 27g needle

The above mentioned microbeads obtained at the flow rate 26.2 ml h^{-1} could be regarded as potentially applicable on the textile surface regarding their size, but the shape regularity is not satisfying. Roundness distribution profiles clearly demonstrate the considerable impact of high flow rates on deterioration of microbeads shape (Figure IV.20).

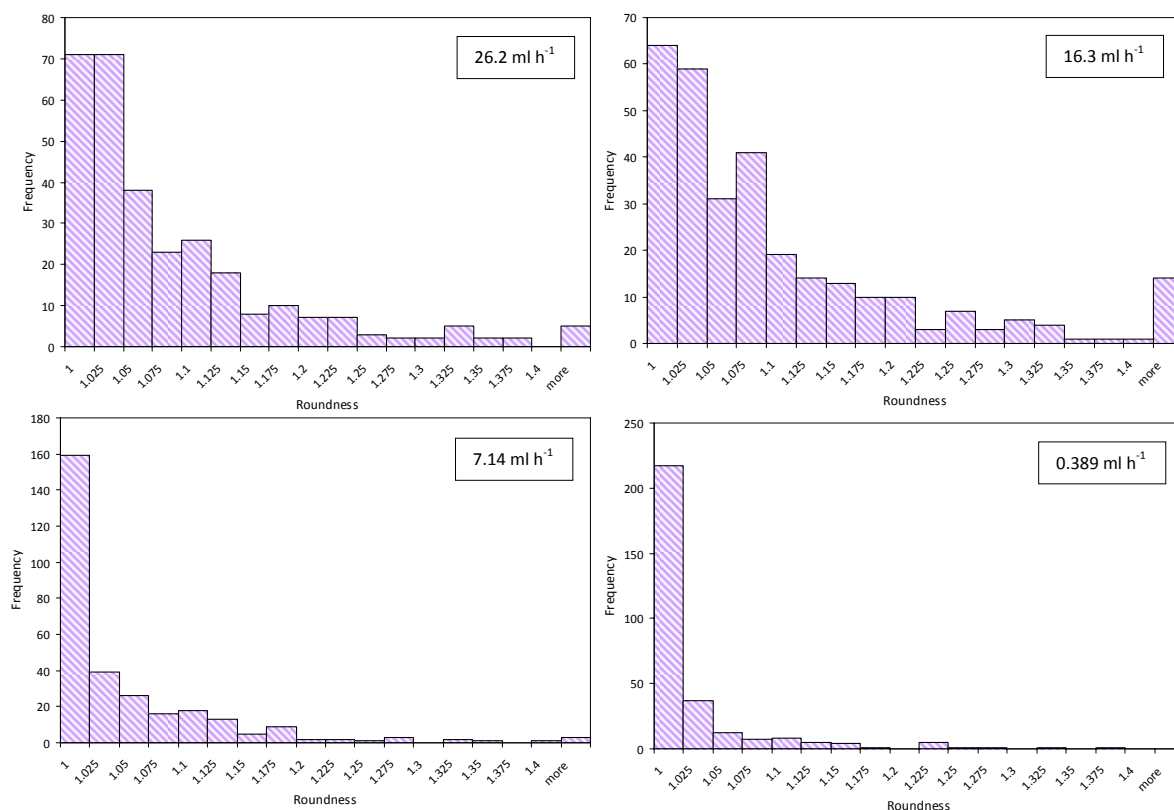


Figure IV.20. Roundness distribution profiles of semi-IPN-0.1-1 microbeads obtained at various flow rates, voltage 12 kV, electrodes distance 8 cm, and using a 27g needle

The next parameter investigated was the electrodes distance that is of considerable importance primarily for the shape of microbeads. This could be understood when taking into consideration competing forces between the surface tension-viscosity of the falling drop and the pressure of the air pushing up against the bottom of the drop [111]. Hence, at constant voltage of 12 kV and flow rate of 0.397 ml h⁻¹, two additional electrodes distances were tested, 4 cm and 16 cm. Figure IV.21 displays microscopic images of all three types of comparable hydrogel microbeads. Strong presence of microbeads of diameter above 100 μm obtained at the highest electrodes distance (16 cm) was observed.

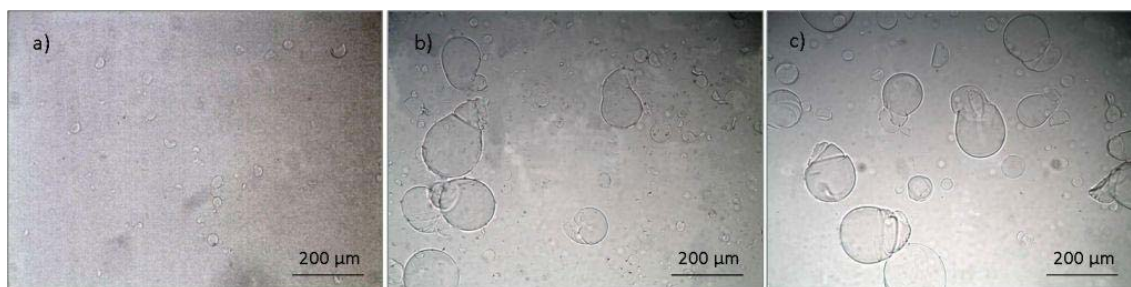


Figure IV.21. Semi-IPN-0.1-1 microbeads obtained under the voltage 12 kV, flow rate 0.397 ml h⁻¹, and electrodes distance 4 cm (a), 8 cm (b), and 16 cm (c)

The values of microbeads mean diameter (Table IV.10) show that decreasing electrodes distance from 8 cm down to 4 cm has negligible effect on microbeads size. On the other

hand, two-fold increase in electrode distance results in almost eight-fold increase in mean diameter. The weakening of the electric field has strongly reflected on microbeads size.

Table IV.10. Influence of the electrodes distance on size and shape of semi-IPN-0.1-1 microbeads (flow rate 0.397 ml h^{-1} , voltage 12 kV)

Electrodes distance, cm	Description	Mean roundness	Mean diameter, μm
4	Fraction of bigger microbeads ($>100 \mu\text{m}$) tail-shaped, smaller microbeads are mixture of regular spherical and half-sphere shaped microbeads	1.019 ± 0.060	13.3 ± 21.3
8	Mixture of regular spherical and half-sphere shaped microbeads	1.018 ± 0.049	10.9 ± 10.1
16	Fraction of bigger microbeads ($>100 \mu\text{m}$) irregular, elongated, smaller microbeads are mixture of regular spherical and half-sphere shaped microbeads	1.088 ± 0.107	79.2 ± 59.2

When electrodes distance was set at 16 cm, the presence of large fraction of microbeads of diameter ranging from 100 to 200 μm was observed (Figure IV.22). In spite of the fact that a fraction of microbeads below 20 μm was also detected, such high electrodes distance is not desirable due to too large fraction of big microbeads that should be rejected in the final application on textile material.

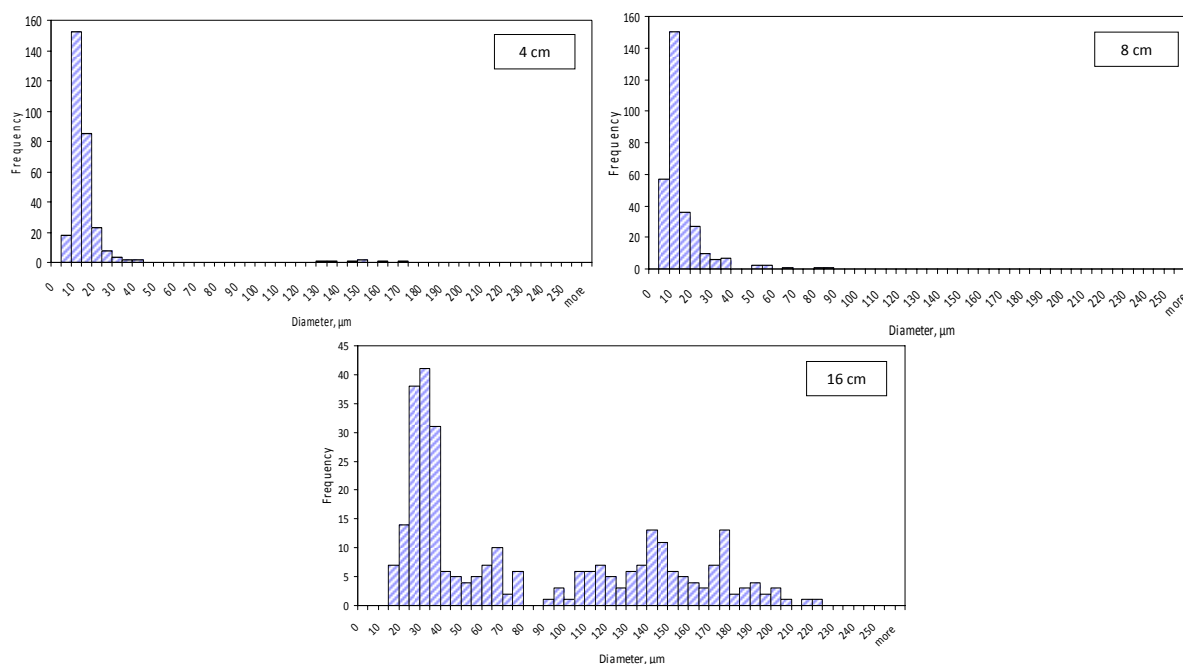


Figure IV.22. Size distribution profiles of semi-IPN-0.1-1 microbeads obtained at various electrodes distance and at voltage 12 kV , flow rate 0.397 ml h^{-1} , and using a 27g needle

Another notable characteristic of microbeads obtained at electrodes distance of 16 cm is unsatisfying mean roundness. This is mainly attributed to the fraction of big microbeads (of diameter above 100 μm). Comparison of roundness distribution profiles in Figure IV.23 offers better insight into the regularity of microbeads shape of microbeads obtained at various electrodes distances.

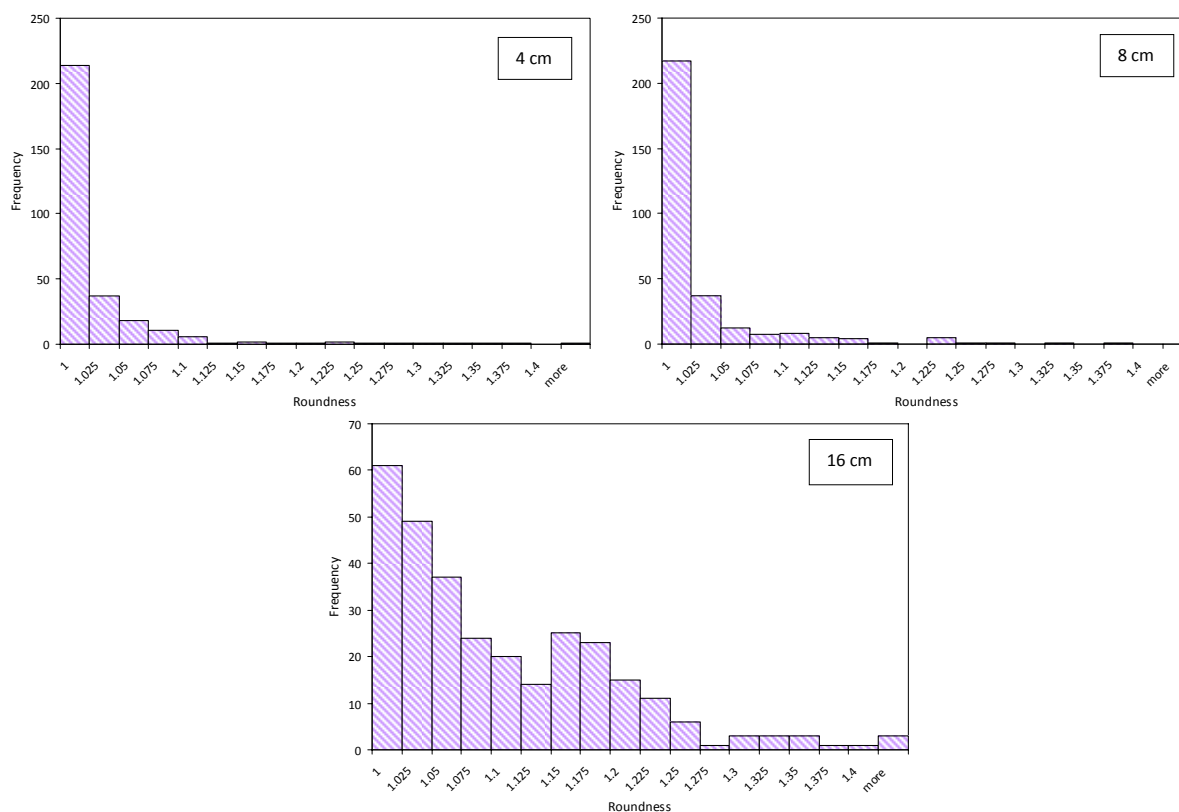


Figure IV.23. Roundness distribution profiles of semi-IPN-0.1-1 microbeads obtained at various electrodes distance and at voltage 12 kV, flow rate 0.397 ml h⁻¹, and using a 27g needle

The conducted analysis of microbeads shape and size showed that the most optimal conditions for the formation of hydrogel microbeads by electrostatic extrusion of polymer solution with 1 wt % alginate and 0.1 wt % PNIPAAm and using a 27g-needle are: 12 kV-voltage, 8 cm-electrodes distance, and 0.397 ml h⁻¹-flow rate. These microbeads have mean diameter of around 10 μm and satisfying shape. Hence, they fulfill initial requirements for the intended application on the surface of the textile material. One of the main drawbacks of hypothetical scale-up of the electrostatic extrusion under given conditions would be very low flow rate. One of the possible solutions for this issue could be construction of a multi nozzle device. Also, potentially good solution for the production of more uniform microbeads through more stable process might be use of a ring electrode [265]. This electrode should be placed around the needle, above the needle tip, especially when operating at high flow rates in a dripping mode.

IV.2 Characterization of thermosensitive semi-IPN hydrogel microbeads

Two types of semi-IPN hydrogel microbeads have been selected for more detailed characterization by FTIR, DSC, SEM and gravimetry, and were also used in the drug release studies. Those are semi-IPN-0.1-1, since solution S-0.1-1 was mainly applied in the optimization of operating parameters, and semi-IPN-0.25-1, for their higher thermosensitivity due to higher fraction of linear interpenetrant (PNIPAAm). The two types of microbeads were obtained using a 27g needle, at voltage of 8 kV, electrodes distance of 8 cm, and the flow rate of 26.2 ml h⁻¹. This combination of parameters was not the most optimal for the production of the microbeads, since the batch contained considerable fraction of small microbeads, even down to 10 μm in diameter, and mainly of very irregular shape. To avoid quite irregular microbeads and to select microbeads of more uniform size distribution desirable for the drug release studies, the microbeads were filtered using CellTrick® filter of 100 μm mesh size. The fraction of bigger beads was used in for drug release using dissolution test and was further characterized. Figure IV.24 displays both types of microbeads after filtration.

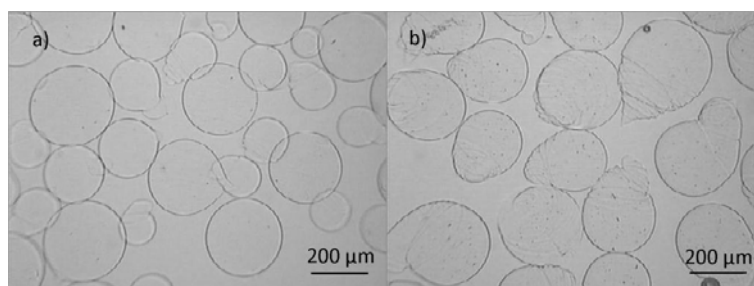


Figure IV.24. Filtered hydrogel microbeads used in drug release studies: semi-IPN-0.1-1 (a) and semi-IPN-0.25-1 (b)

Based on the analysis of 150 microbeads in each batch, we obtained the mean diameters of semi-IPN-0.1-1 and semi-IPN-0.25-1 microbeads to be 179.4 μm (±24.0 μm) and 253.2 μm (±24.8 μm), respectively. When higher concentration of PNIPAAm is present in extruded solution, charge surface density of a droplet is reduced, thus hindering diffusion of sodium ions toward the surface. As a consequence, the value of surface tension becomes higher, and thus, the droplets of greater size are formed [116]. Mean degree of roundness of semi-IPN-0.1-1 microbeads was 1.102 whereas the roundness of semi-IPN-0.25-1 was worse (degree of roundness 1.193) as a consequence of higher fraction of PNIPAAm.

IV.2.1 Chemical Structure

In the FTIR spectrum of linear PNIPAAm (Figure IV.25), characteristic absorptions of the polymer are observed, the amide I band at 1650 cm⁻¹ (C=O stretching) and amide II band at 1549 cm⁻¹ (N-H bending) of the amide group [227]. A former peak is registered in the spectra of semi-IPNs, although shifted toward the lower frequencies, partly overlapping with a broader peak arising from symmetric stretching of COO⁻ in alginate chain. The composition of the hydrogel microbeads is characterized by considerably higher amount of CA in respect

to PNIPAAm. This causes the difficulties to detect all the bands of PNIPAAm due to domination of stronger peaks of CA.

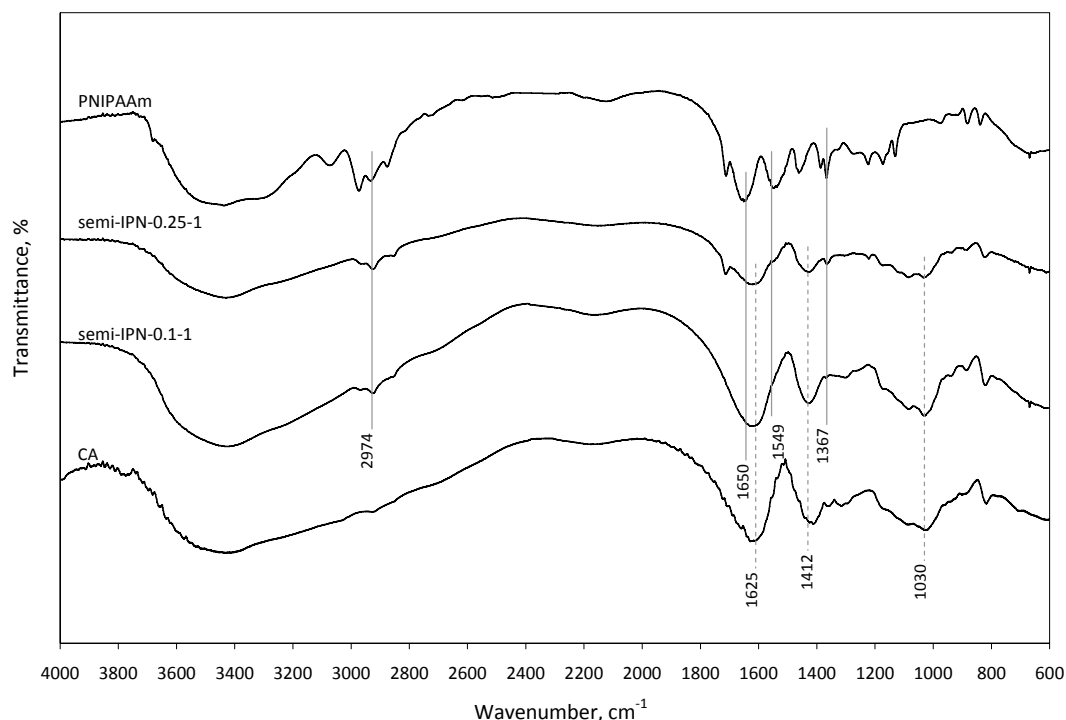


Figure IV.25. FTIR spectra (characteristic peaks of PNIPAAm chains indicated by full lines and those of CA network by dotted lines)

The bands at 1386 cm^{-1} and 1367 cm^{-1} are assigned to C-H vibrations of isopropyl group of PNIPAAm [228]. In the spectrum semi-IPN-0.25-1 the latter peak is observed, while in the sample with lower amount of PNIPAAm, these vibrations were not too strong to be detected. Another characteristic absorption band of PNIPAAm appears around 2972 cm^{-1} and is attributed to the C-H stretching vibration of $-\text{CH}-$ bridges of PNIPAAm network [276]. It is shifted toward the lower wavenumbers in the spectra of the semi-IPN microbeads ($2968/2961\text{ cm}^{-1}$). Therefore, the presence of PNIPAAm was verified in the semi-IPN microbeads. This is supported by the fact that characteristic peaks of the NIPAAm monomer are not present in the spectra of semi-IPNs (and PNIPAAm), primarily implying the bands at 1617 cm^{-1} (C=C), at 1409 cm^{-1} ($\text{CH}_2=$), as reported elsewhere [229].

The characteristic symmetric and asymmetric stretching vibrations of COO^- groups in CA network are manifested through the peaks at 1412 cm^{-1} and around 1625 cm^{-1} , respectively [19, 277]. The former peak is observed in the spectra of semi-IPNs, while the latter one is more emphasized due to overlapping with the amide I band of PNIPAAm, as previously noted. The band at 1030 cm^{-1} in these spectra is assigned to O-H bending vibrations [231], as well as to C-O stretching of alginate structural units. In the spectra of semi-IPN microbeads and CA, a broad peak between around 3600 and 3200 cm^{-1} is present due to O-H stretching vibrations in guluronate (G) and mannuronate (M) residues of alginate chain, indicating the formation of intermolecular hydrogen bonding [232]. In addition, there is contribution of N-H stretching of the repeating units of NIPAAm in the same range [276]. Hence, the presence

of both components in newly synthesized semi-IPN-0.1-1 and semi-IPN-0.25-1 hydrogel microbeads was confirmed.

IV.2.2 Thermal Characteristics

Thermal characteristics semi-IPN hydrogel microbeads with two PNIPAAm concentrations were analyzed through simple heating ramp in the range from 15 to 50°C. Onset temperatures of the phase transition (T_{onset}), volume phase transition temperatures (VPTT), and the corresponding enthalpy changes (ΔH) are summarized in Table IV.11.

Table IV.11. Thermal results of DSC analysis of semi-IPN hydrogel microbeads

(conditions: 8kV, 8 cm, 26.2 ml h⁻¹)

Sample	T_{onset} (°C)	VPTT (°C)	ΔH (J g ⁻¹)
Semi-IPN-0.1-1	30.9	31.3	0.09
Semi-IPN-0.25-1	29.7	30.2	0.14

*Standard deviation for T_{onset} and VPTT values was $\pm 0.2^\circ\text{C}$.

**Standard deviation for ΔH values was $\pm 0.02 \text{ J g}^{-1}$.

As mentioned before, the value of VPTT is influenced by the hydrophilic/hydrophobic balance within the polymer chains. Temperature increase causes the weakening and breakage of the hydrogen bonds, while favoring hydrophobic interactions [26]. It can be noted that a higher content of PNIPAAm in the final network resulted in a lower VPTT of semi-IPN-0.25-1 than of semi-IPN-0.1-1 due to a higher concentration of hydrophobic segments and facilitation of polymer aggregation. This induces higher ΔH induced in the system with higher PNIPAAm concentration. Also, sharper endothermic peak of semi-IPN-0.25-1 (Figure IV.26) is a result of faster hydrophobic interactions due to the higher PNIPAAm concentration [278].

The difference in VPTT and ΔH between semi-IPN hydrogel microbeads and full-IPN hydrogel films studied within this project and described in Chapter III (section III.3.1), is understandable when taking into consideration the form of PNIPAAm in these systems (i.e. type of their structure) as well as the concentration of this thermosensitive component. In hydrogel microbeads with semi-IPN structure, the mobility of the PNIPAAm chains is higher than of those in full-IPN films. This is because the PNIPAAm chains in microbeads are linear, while they are in a crosslinked form in the films. Moreover, in films, considerably higher polymer chain density of PNIPAAm per unit volume contributes to an increased number of hydrogen bonds. Therefore, higher energy is required for breaking those bonds and there is predomination of hydrophobic interactions and as a result, VPTT of these films (34-35°C) will be higher than of microbeads produced by electrostatic extrusion (Table IV.11). This is in direct relation with significantly lower enthalpy changes corresponding to volume phase transition of semi-IPN microbeads are than those of full-IPN films.

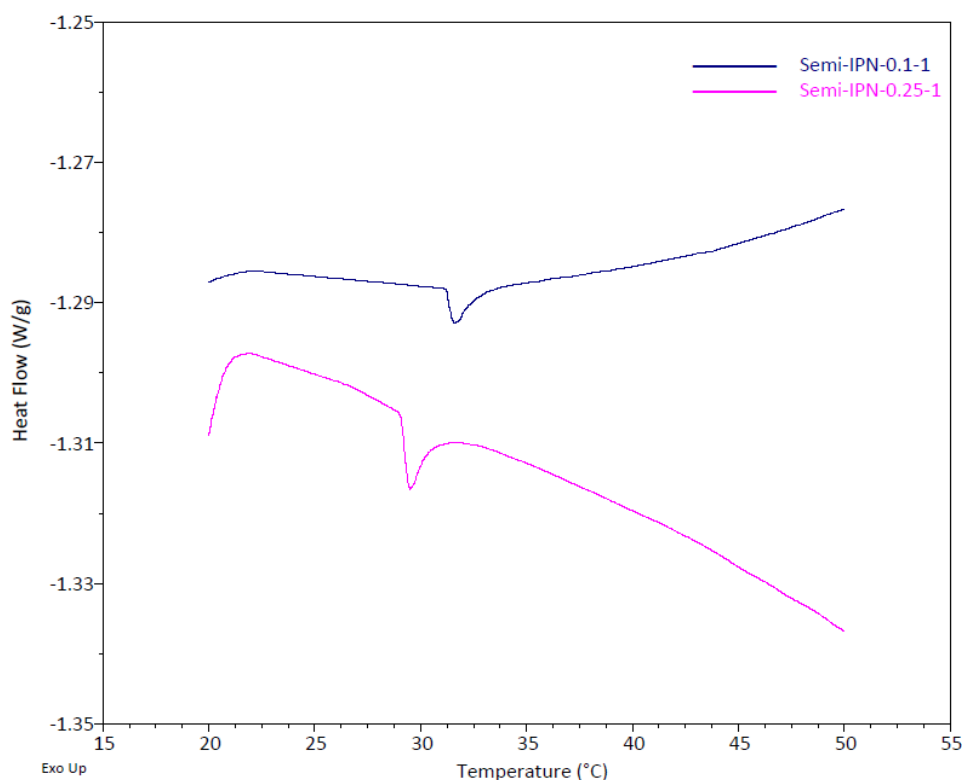


Figure IV.26. DSC thermogram of semi-IPN hydrogel microbeads obtained by electrostatic extrusion (conditions: 8kV, 8 cm, 26.2 ml h⁻¹)

IV.2.3 Swelling Behavior

Swelling behavior of semi-IPN hydrogel microbeads prepared by electrostatic extrusion was evaluated through the value of equilibrium swelling ratio (ESR) at 25°C. Characterized hydrogel microbeads were obtained using a 27g needle, under the voltage 8 kV, electrode distance 8 cm and at flow rate 26.2 ml h⁻¹. The mean values of ESR and water content (WC) corresponding standard deviations are displayed in Table IV.12.

Table IV.12. Values of equilibrium swelling degree of hydrogel microbeads at 25°C

Sample	ESR	WC, %
Semi-IPN-0.1-1	32.6±2.5	97.0±0.2
Semi-IPN-0.25-1	30.3±1.6	96.8±0.2

Results of swelling experiments show that there is no significant difference in the swelling abilities of these hydrogel microbeads and the percentage of water in their structure is very high. Shi et al. investigated similar structures, semi-IPN hydrogel beads prepared by simple dropping of PNIPAAm/SA solution into the CaCl₂ solution [170]. These thermosensitive “macrobeads” exhibited the same ESR at 25°C regardless of the weight ratio of alginate and PNIPAAm, which is confirmed in our study. However, a difference in swelling capacities is expected at temperatures above VPTT since higher PNIPAAm fraction makes the hydrogel more hydrophobic and thus decreases the ESR.

IV.2.4 Morphology

The morphological characteristics of the unfiltered semi-IPN microbeads with two fractions of PNIPAAm were analyzed by SEM and representative micrographs are displayed in Figure IV.27. The difference in shape regularity is obvious and it is confirmed that higher concentration of PNIPAAm affects roundness of the beads. The general property of pure CA microbeads is dense surface layer and porous interior [279]. Due to technical limitations, the investigation of microbeads cross-section was not possible in our study.

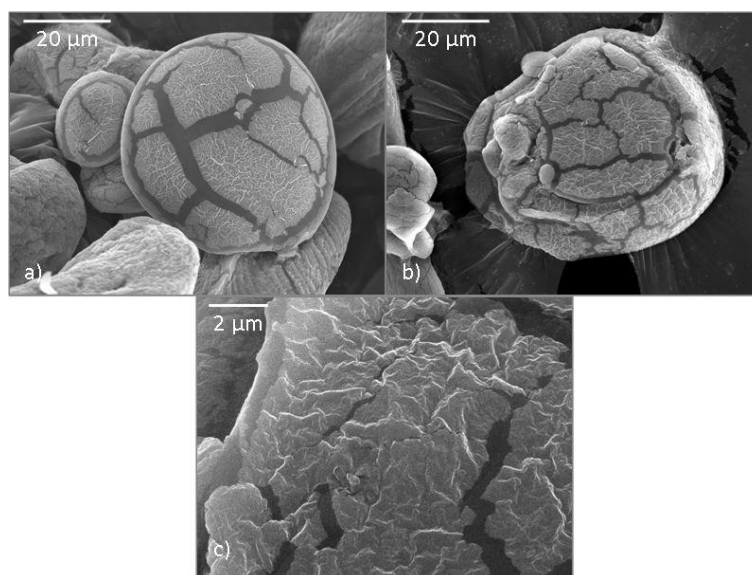


Figure IV.27. SEM micrographs of microbeads semi-IPN-0.1-1 (a) and semi-IPN-0.25-1 (b,c) obtained under conditions: 8 kV, 8 cm, 26.2 ml⁻¹ and using 27g-needle

Wrinkle-like surface of the analyzed microbeads is found to be characteristic for pure CA microbeads [280]. Lee et al. explain that the presence of such wrinkles on the surface may have been partly associated with strain-relaxation processes upon drying [281]. Clearly visible cracks on the microbeads surface (Figure IV.27-c) could be ascribed to the partial collapse of the network during freeze-drying treatment. Analyzed semi-IPN microbeads obtained by electrostatic extrusion possess morphological characteristics of pure CA because of significantly higher fraction of SA than PNIPAAm in polymer solutions used for extrusion.

IV.3 CONCLUSIONS

Electrostatic extrusion was applied to produce thermosensitive hydrogel microbeads of semi-IPN structure. It was shown that, keeping the concentration of SA in PNIPAAm/SA solution at 1 wt %, the extrusion processes are not possible for PNIPAAm concentration above 0.5 wt %. When the fraction of PNIPAAm increases from 0.1 up to 0.5 wt %, hydrogel microbeads become bigger and irregular. Solution containing 0.1 wt % PNIPAAm and 1 wt % SA was proved to be optimal for the extrusion tests and studies on influence of the operating parameters. Presence of surfactant Tween 20 in extruded solution could reduce

the surface tension of the polymer solution considerably but has no obvious influence of microbeads size. Also, deterioration of microbeads shape was observed since tail-shaped microbeads were produced.

The size of thermosensitive hydrogel microbeads diameter is affected by the value of voltage applied between the electrodes. Up to a certain value, the droplet diameter decreases with the voltage increases. When the voltage is further increased, small microbeads (below 50 μm in diameter) are formed, but bigger beads (>100 μm) are irregular, mainly tail-shaped. The formation of two fractions of microbeads sizes is observed for voltage values beyond a critical value. Thus, needle vibrations are induced, followed by unstable liquid jet and formation of many thinner liquid filaments around the central one that disperse into many small droplets (satellite droplets). To produce microbeads of uniform and spherical shape, applied voltage should thus be set below this critical value, but should be close to it so that microbeads size is efficiently reduced. The other important parameter is the flow rate whose decrease is favorable for the formation of smaller microbeads. The most optimal hydrogel microbeads regarding the size and roundness were obtained using 27g needle and under the voltage of 12 kV, electrodes distance of 8 cm and flow rate of 0.397 ml h^{-1} . Research in this field should be continued with regard to further optimization of the operating parameters as well as the properties of the extruded polymer solution.

**Chapter V : SYNTHESIS AND CHARACTERIZATION OF
THERMOSENSITIVE HYDROGEL MICROBEADS OBTAINED BY
INVERSE SUSPENSION POLYMERIZATION**

In previous chapter, we have shown the possibility of producing semi-IPN thermosensitive hydrogel microbeads of even below 20 μm in diameter by electrostatic extrusion. However, these microbeads contained only small fraction of linear PNIPAAm as thermosensitive component that drives the changes in overall hydrogel structure as response to thermal stimulus. Also, optimal conditions for the production of the smallest microbeads implied low flow rates, i.e. time-consuming process. Therefore, we opted for method of inverse suspension polymerization due to its productivity, feasibility of scale-up and the fact NIPAAm will be the principal monomer in the feed mixture. This chapter will hence encompass application of inverse suspension polymerization in preparation of thermosensitive hydrogel microbeads and their detailed characterization. Variation of formulation parameters in syntheses of pure PNIPAAm hydrogel microbeads will lead to formation of semi- and full-IPN hydrogel microbeads with SA and CA as interpenetrants, respectively. Furthermore, PNIPAAm/maleic anhydride copolymer hydrogel microbeads will be prepared due to potentially easier applicability of these microbeads on textile materials due to the presence of free carboxyl groups of maleic acid.

V.1 Synthesis

A series of thermosensitive hydrogel microbeads based on PNIPAAm were synthesized by free-radical inverse suspension polymerization according to the procedure reported by Kayaman et al. [282]. The concentration of NIPAAm was kept constant in all cases and it equaled 10 w/v % in a dispersed aqueous phase. The polymerization reactions were conducted in the presence of 2 wt % of initiator (APS) and 4.6 wt % catalyst (TEMED) at 25°C. The concentrations of APS and TEMED were calculated in ratio to NIPAAm and were unchanged in all reactions. During the optimization of synthesis conditions referring to pure PNIPAAm hydrogel microbeads, the following parameters were varied: oil-to-aqueous phase volume ratio, the concentration of emulsifier (Tween 80), and the molar ratio of monomer (NIPAAm) and crosslinker (MBAAm). When the optimal composition was established, the copolymerization with maleic acid (i.e. maleic anhydride, MA) was performed as well as the formation of semi- and full-IPN structures with linear alginate (sodium alginate, SA) and crosslinked alginate (calcium alginate, CA), respectively. The formulation parameters in conducted syntheses of hydrogel microbeads are given in Table V.1.

Modifications of PNIPAAm hydrogel microbeads by copolymerization with MA were done primarily with the purpose of their functionalization by introduction of carboxylic groups for more efficient application on previously activated textile substrate (Chapter I, section I.6.2). Furthermore, previously conducted studies on PNIPAAm hydrogels in combination with alginate (Chapter III and Chapter IV) with IPN structures gave promising results when it comes to improvement in swelling behavior, mechanical characteristics and pore structure in comparison with pure PNIPAAm hydrogels. This was the reason for preparation of semi- and full-IPN hydrogel microbeads based on PNIPAAm and alginate by inverse suspension polymerization as well.

Table V.1. Composition of feed mixtures in syntheses of hydrogel microbeads by inverse suspension polymerization

Sample	Oil/aqueous phase (vol/vol)	Emulsifier*, vol %	NIPAAm/MBAAm (mol/mol)	MA**, mol %	SA, w/v %
M-50/1(10/1)-E 0	10/1	0	50/1	0	0
M-50/1(10/1)-E 1	10/1	1	50/1	0	0
M-50/1(5/1)-E 0.5	5/1	0.5	50/1	0	0
M-25/1	5/1	1	25/1	0	0
M-50/1(5/1)-E 1 (M-50/1)	5/1	1	50/1	0	0
M-100/1	5/1	1	100/1	0	0
M-25/1-MA 2.5	5/1	1	25/1	2.5	0
M-25/1-MA 5	5/1	1	25/1	5	0
M-25/1-MA 10	5/1	1	25/1	10	0
M-25/1-SA 0.5	5/1	1	25/1	0	0.5
M-25/1-SA 1	5/1	1	25/1	0	1
M-25/1-SA 2	5/1	1	25/1	0	2
M-25/1-CA 0.5	5/1	1	25/1	0	0.5
M-25/1-CA 1	5/1	1	25/1	0	1

* In ratio to paraffin oil

** In ratio to NIPAAm

V.2 Chemical structure

FTIR spectroscopic analysis was applied for investigation of the chemical structure of the hydrogel microbeads. Figure V.1 displays spectra of representative samples including pure PNIPAAm hydrogel, PNIPAAm/MA copolymer hydrogel, semi- and full-IPN hydrogels based on alginate, as well as spectrum of pure SA (1 w/v %). Characteristic peaks of PNIPAAm are clearly visible in spectra of all analyzed hydrogel microbeads. Amide I band arising from C=O stretching of PNIPAAm and amide II band due to N-H bending of PNIPAAm are detected at 1653 cm^{-1} and 1543 cm^{-1} , respectively [227]. The bands at 1387 cm^{-1} and 1367 cm^{-1} correspond to C-H vibrations of isopropyl group of PNIPAAm [228]. A typical PNIPAAm peak is clearly seen at 2974 cm^{-1} and it is attributed to the C-H stretching vibration of -CH-bridges [227]. According to this analysis, successful polymerization of NIPAAm was confirmed.

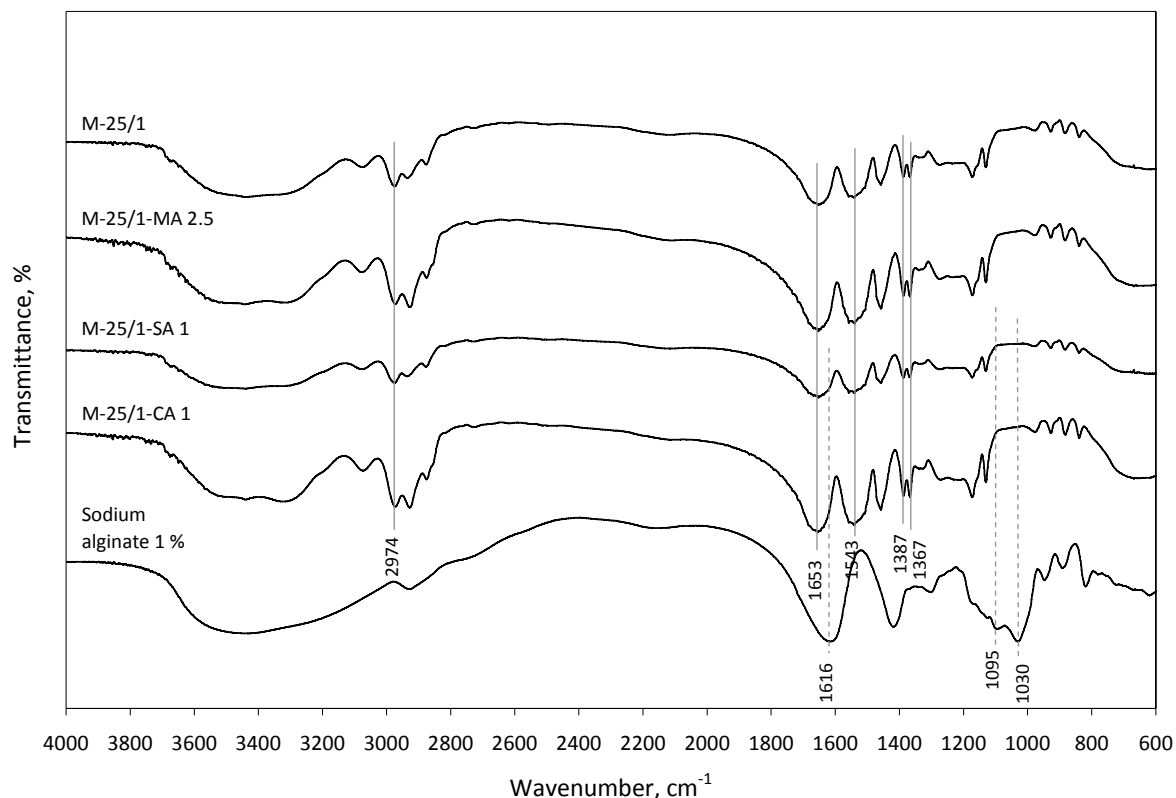


Figure V.1. FTIR spectra of hydrogel microbeads with 3 wt % MBAAm (characteristic peaks of PNIPAAm chains indicated by full lines and those of sodium alginate by dotted lines)

However, bands characteristic for alginate chains are not visible in spectra of M-25/1-SA 1 and M-25/1-CA 1. These typical peaks (seen in spectra of SA) include: peak at 1635 cm^{-1} (asymmetric stretching vibration of COO^- groups [19, 230]), peak at 1095 cm^{-1} (C-O-C stretching of the pyranose ring in mannuronate (M) and guluronate (G) residues), and peak at 1030 cm^{-1} (O-H bending and C-O stretching vibrations of alginate structural units) [231]. The reasons for the absence of these bands in the spectra of hydrogel microbeads with alginate are probably due to low quantities of alginate in these IPN hydrogel structures, below the detection limit of FTIR. Therefore, the comparison of maleic acid spectrum with that of microbeads M-25/1-MA 2.5 was redundant since amount of MA was particularly low in ratio to NIPAAm in feed mixture and was not expected to induce certain peaks in the FTIR spectrum (Table V.1).

Figure V.2 represents the reaction of copolymerization of NIPAAm and MA with simultaneous crosslinking of NIPAAm with MBAAm and the probable PNIPAAm/MA copolymer structure.

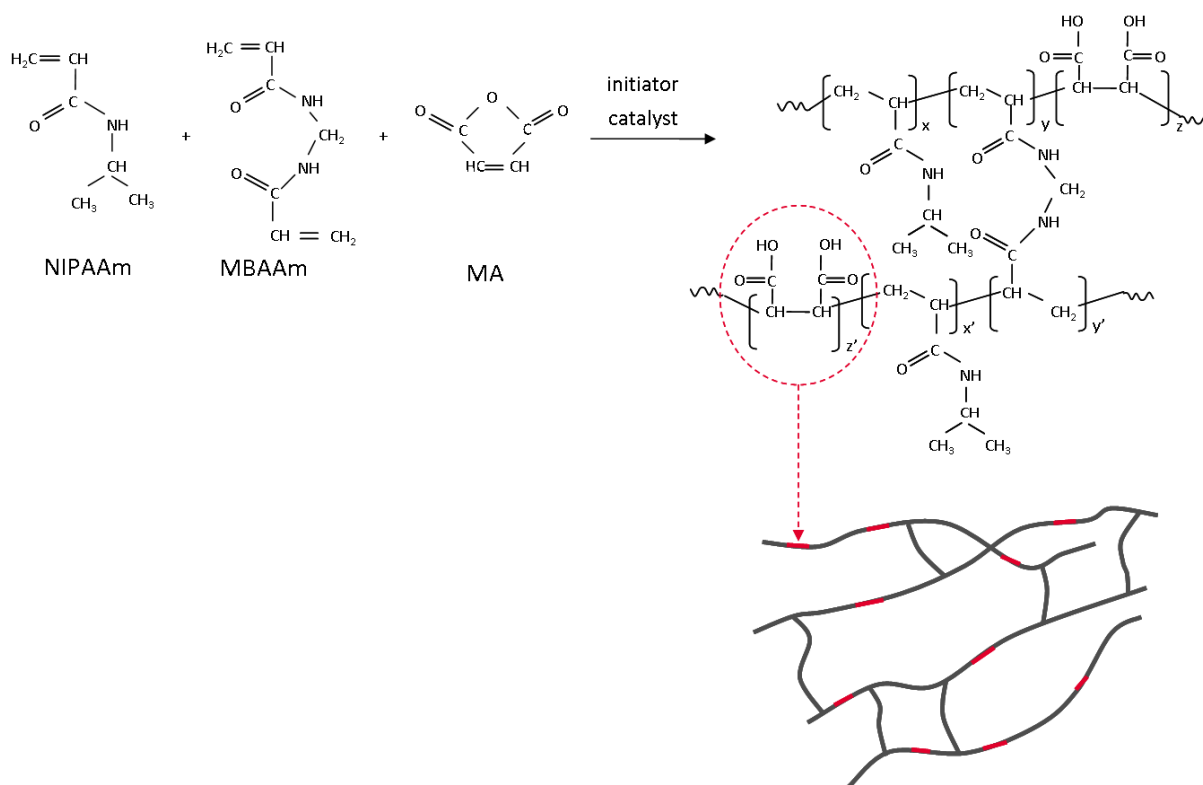


Figure V.2. Formation of PNIPAAm/MA copolymer hydrogel structure (copolymerization/crosslinking of NIPAAm adapted from [197])

The structures of semi- and full-IPN hydrogel microbeads based on PNIPAAm and alginate could be presented analogously with the structure of hydrogel films described in the Chapter III of this report (Figure V.3).

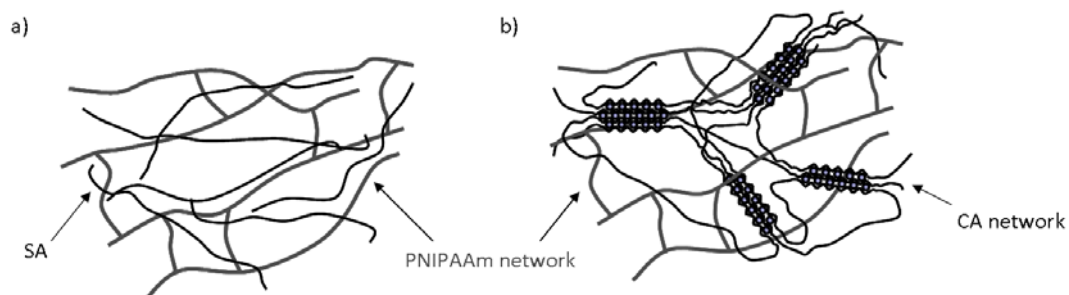


Figure V.3. Structure of semi-IPN (a) and full-IPN (b) microbeads based on PNIPAAm and alginate

V.3 Optical microscopy

A first tool in estimation of optimal formulation parameters in synthesis of pure PNIPAAm hydrogel microbeads was optical microscopy. It was used for evaluation of microbeads shape and comparison of their size. Hence, initial and approximate information on microbeads size was obtained by analysis of microscopic images using image processing software ImageJ.

Average diameters were calculated based on the analysis of 200 microbeads per batch (hydrogel sample). Obtained mean diameters of microbeads correspond to the number-length mean [283]. This approach in determination of microbeads size was applied only with the aim of mutual comparison of different microbeads types and not as valid method for determination of absolute values of mean diameters. For that purpose, laser diffraction analysis was applied and its results are given in the section V.4 of this chapter.

V.3.1 Influence of concentration of emulsifier and the oil-to-aqueous phase ratio

Table V.2 summarizes the values of oil-to-aqueous phase volume ratio, the volume fraction of emulsifier used in initial four syntheses of pure PNIPAAm hydrogel microbeads together with calculated values of mean diameters based on microscopic images. In addition to the amount of monomer (NIPAAm), initiator (APS), and catalyst (TEMED), the amount of crosslinker (MBAAm) was also kept unchanged. The molar ratio of NIPAAm to MBAAm in these reactions was 50/1.

Table V.2. Influence of the addition of emulsifier and oil-to-aqueous phase ratio on size of pure PNIPAAm hydrogel microbeads

Sample	Oil/aqueous phase (vol/vol)	Emulsifier*, vol %	Mean diameter, μm
M-50/1(10/1)-E 0	10/1	0	236.8 \pm 142.7
M-50/1(10/1)-E 1	10/1	1	46.5 \pm 25.0
M-50/1(5/1)-E 1 (M-50/1)	5/1	1	22.6 \pm 14.9
M-50/1(5/1)-E 0.5	5/1	0.5	44.3 \pm 23.8

* In ratio to paraffin oil

The first parameter whose influence on synthesis of PNIPAAm hydrogel microbeads was investigated is the presence nonionic emulsifier Tween 80. At oil-to-aqueous phase ratio of 10/1, two types of microbeads were prepared: without emulsifier and with emulsifier at concentration of 1 vol % (in ratio to oil). As it can be seen in Figure V.4, the addition of emulsifier resulted in considerably smaller microbeads in comparison with those obtained in its absence. Obtained microbeads are of regular spherical shape in both cases, although the microbeads synthesized in the presence of emulsifier had tendency toward formation of agglomerates (Figure V.4b). According to calculated mean diameters presented in Table V.2, addition of emulsifier in concentration of 1 vol % reduces drastically the microbeads diameter by over 80 %.

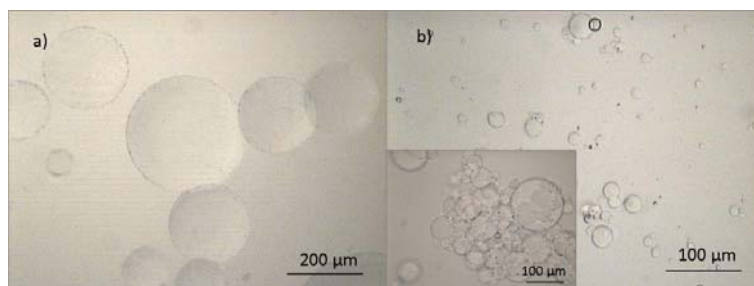


Figure V.4. Hydrogel microbeads M-50/1(10/1)-E 0 synthesized in the absence of emulsifier (a) and microbeads M-50/1(10/1)-E 1 synthesized in the presence of 1 vol % emulsifier (b)

The investigation of the influence of oil-to-aqueous phase volume ratio in the presence of 1 vol % emulsifier showed that this ratio had no significant influence on the microbeads shape, i.e. microbeads kept the same regular spherical shape when this ratio was 5/1 (Figure V.5a). Concerning the size, these microbeads had even smaller mean diameter than M-50/1(10/1)-E 1, around 20 μm . Therefore, following syntheses were conducted under smaller oil-to-aqueous phase volume ratio. This was done out of economic as well as practical reasons related to easier purification of microbeads, i.e. the removal of oil phase.

The following synthesis of PNIPAAm hydrogel microbeads was performed using 0.5 vol % emulsifier (M-50/1(5/1)-E 0.5). We have assumed that satisfying microbeads size and shape could be obtained even at lower concentration of emulsifier. Also, we wanted to facilitate the process of microbeads removal from oil phase and their purification using smaller quantity of emulsifier. However, it was shown that this decrease in emulsifier concentration caused emphasized formation of agglomerates and less regular shape of microbeads, as displayed in Figure V.5-b. In addition, their size was increased. Therefore, further polymerization reactions were performed using 1 vol % emulsifier.

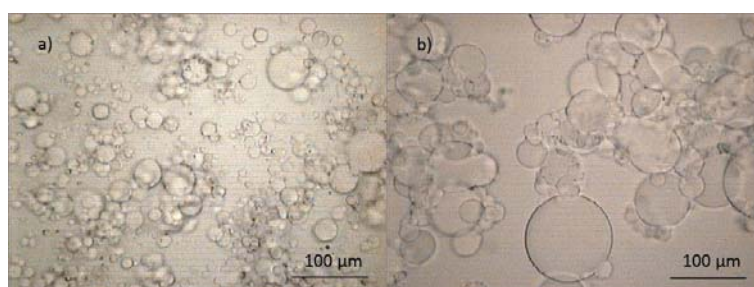


Figure V.5. Hydrogel microbeads M-50/1(5/1)-E 1(1 vol % emulsifier) (a) and microbeads M-50/1(5/1)-E 0.5 (0.5 vol % emulsifier) (b)

V.3.2 The influence of PNIPAAm crosslinking degree

After establishing the optimal oil-to-aqueous phase volume ratio (5/1) and the concentration of emulsifier (1 vol %), the amount of crosslinker was varied. The crosslinking degree of PNIPAAm network was optimized by analyzing microbeads synthesized under three different molar ratios of monomer (NIPAAm) and crosslinker (MBAAm): 25/1, 50/1, and 100/1. Table V.3 contains values of mean diameters obtained from microscopic images of microbeads with different crosslinking degree.

Table V.3. Influence of PNIPAAm crosslinking degree on size of pure PNIPAAm hydrogel microbeads

Sample	NIPAAm/MBAAm (mol/mol)	Mean diameter, μm
M-25/1	25/1	32.1 \pm 19.9
M-50/1(5/1)-E 1 (M-50/1)	50/1	22.6 \pm 14.9
M-100/1	100/1	27.4 \pm 19.6

According to the results of image analysis, there is no enormous discrepancy in mean diameters of microbeads and they do not correspond to the expected trend (higher the crosslinking degree, smaller the mean diameter). This could be ascribed to fact that the microbeads composing the agglomerates or clusters could have not been analyzed. Figure V.6 displays all three types of microbeads with different crosslinking degree of PNIPAAm.

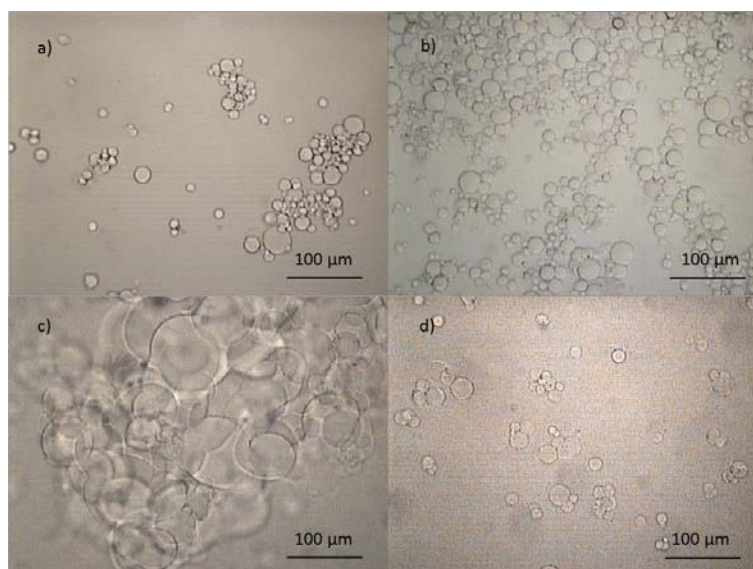


Figure V.6. Hydrogel microbeads M-25/1 (a), M-50/1 (b), and M-100/1 (c and d) (oil-to-aqueous phase volume ratio 5/1, 1 vol % emulsifier)

Microbeads with higher crosslinking degree (M-25/1 and M-50/1) were more uniform and of regular spherical shape (Figure V.6-a,b). There were no notable differences between these two microbeads type (M-25/1 and M-50/1). In contrast, the microbeads synthesized with the lowest amount of crosslinker (M-100/1) are characterized by increased presence of agglomerates composed of irregular beads as well as the presence of regular spherical beads, but in lower percentage (Figure V.6-c,d). The affinity of these microbeads towards the agglomeration could derive from weak mechanical stability caused by looser PNIPAAm network. Therefore, the following steps of microbeads modifications by copolymerization with MA as well as formation of IPN structures with alginate were conducted at the highest amount of crosslinker MBAAm, i.e. at molar ratio NIPAAm/MBAAm of 25/1.

V.3.3 The influence of the presence of MA

At constant amounts of monomer, initiator, catalyst, crosslinker, emulsifier, and oil-to-aqueous phase volume ratio, the amount of comonomer maleic anhydride (MA) was varied. Table V.4 summarizes the values of microbeads mean diameters of the obtained microbeads using image analysis.

Table V.4. Influence of the presence of MA on size of PNIPAAm/MA copolymer hydrogel microbeads

Sample	MA, mol %	Mean diameter, μm
M-25/1-MA 2.5	2.5	16.6 \pm 12.8
M-25/1-MA 5	5	22.7 \pm 16.7
M-25/1-MA 10	10	20.0 \pm 12.4

The mean diameters of PNIPAAm/MA copolymer hydrogel microbeads were found to be around 20 μm . Microscopic images of these hydrogel microbeads displayed in Figure V.7 shows that there is no change in shape, i.e. all microbeads are of regular spherical shape. However, increase in concentration of MA induces enhanced presence of agglomerates. This is displayed in example of M-25/1-MA 10 in Figure V.7-d.

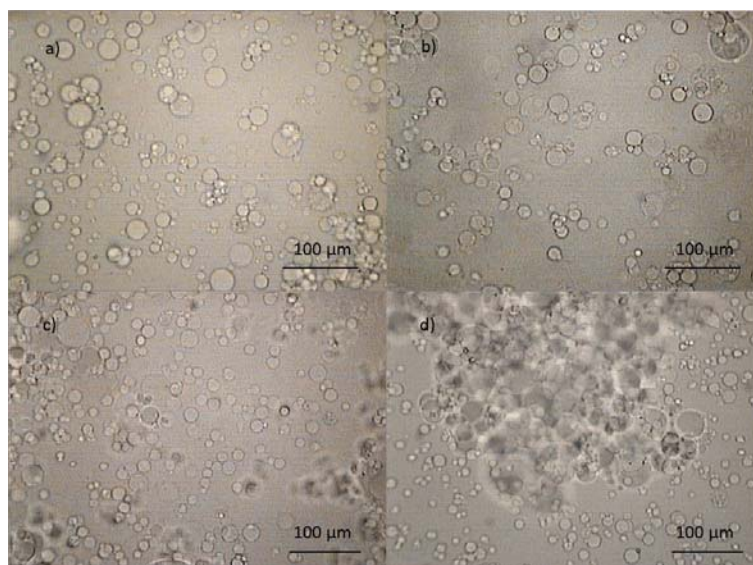


Figure V.7. Hydrogel microbeads M-25/1-MA 2.5 (a), M-25/1-MA 5 (b), and M-25/1-MA 10 (c-d) (oil-to-aqueous phase volume ratio 5/1, 1 vol % emulsifier)

Synthesis of M-25/1-MA 10 microbeads was of significantly lower yield and the product was of different consistency in comparison with other PNIPAAm/MA copolymer microbeads. This was primarily due to clearly visible irregular pieces of hydrogels that could have been observed and which revealed to enormously big agglomerates of tightly packed microbeads. The agglomerates were impossible to be included into the calculation microbeads size, which explains relatively small mean diameter of these microbeads given in Table V.4 (this also refers to the sample M-100/1 and calculated mean diameter in Table V.3).

V.3.4 Influence of presence of linear and crosslinked alginate

Another series of hydrogel microbeads based on PNIPAAm were synthesized in the presence of SA. Beside the semi-IPN microbeads, the hydrogels microbeads with full-IPN structure were prepared by crosslinking of alginate by calcium ions. This step was applied after complete purification of semi-IPN microbeads by incubation in calcium chloride solution. The values of mean diameters calculated using the microscopic images are displayed in Table V.5.

Table V.5. Influence of the presence of alginate on size of semi- and full-IPN PNIPAAm-based hydrogel microbeads

Sample	SA, w/v %	Mean diameter, μm
M-25/1-SA 0.5	0.5	24.1 \pm 12.0
M-25/1-SA 1	1	23.5 \pm 14.2
M-25/1-SA 2	2	-
M-25/1-CA 0.5	0.5	24.7 \pm 12.7
M-25/1-CA 1	1	29.0 \pm 13.0

Furthermore, slight irregularities of shape are observed at semi- and full-IPN microbeads prepared at 0.5 and 1 w/v % alginate (Figure V.9). Image analysis of these microbeads resulted in rather low mean diameters in comparison to valid values obtained by laser diffraction measurements (Table V.6). The main reason for this is the distinctive presence of aggregates, such as those shown in the inset of the Figure V.9-a. This phenomenon is further discussed in the section V.4.4 of this chapter within the discussion of the results of laser diffraction analysis.

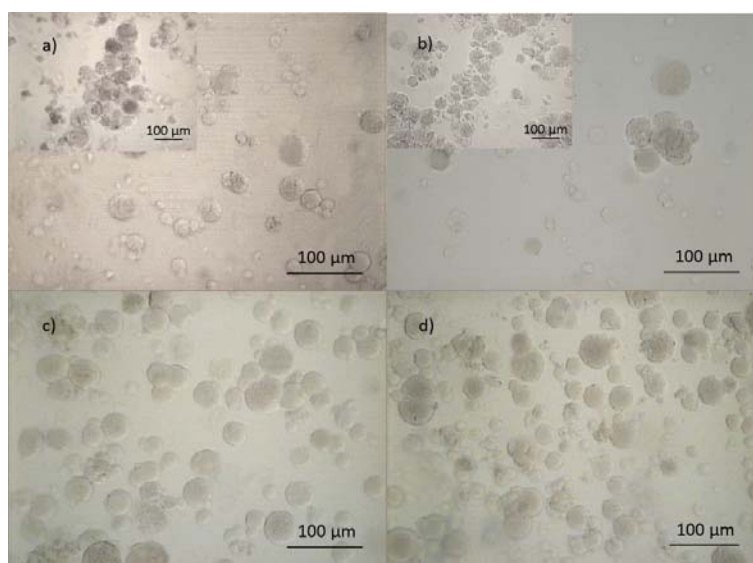


Figure V.8. Hydrogel microbeads M-25/1-SA 0.5 (a), M-25/1-SA 1 (b), M-25/1-CA 0.5 (c), and M-25/1-CA 1 (d)

In contrast to pure PNIPAAm and PNIPAAm/MA copolymer hydrogel microbeads that have smooth surface, the topology of microbeads with alginate is explained by high concentration of the alginate chains that affect lower PNIPAAm crosslinking efficiency. It is more clearly seen from the Figure V.10 that the hydrogel microbeads based on PNIPAAm and alginate have rather rough surface, very different from those of previously analyzed microbeads types.

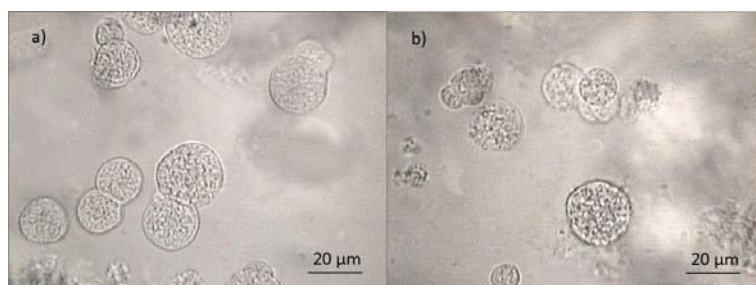


Figure V.9. Hydrogel microbeads M-25/1-SA 1 (a) and M-25/1-CA 1 (b)

The least spherical and non-uniform shapes were obtained in the case of the highest concentration of alginate in semi-IPN structures (Figure V.10). Hence, corresponding full-IPN microbeads were not prepared and further characterized. The reason for the absence of formation of regular spherical microbeads could lie in high viscosity of the dispersed phase due to the presence of sodium alginate, making it difficult to disrupt into regular droplets by a stirrer.

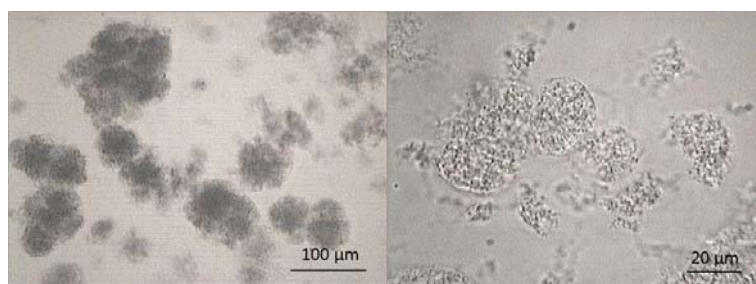


Figure V.10. Hydrogel microbeads M-25/1-SA 2

V.4 Size and size distribution

Hydrogel microbeads were further characterized by laser diffraction technique for determining representative values of mean diameter and the adequate size distribution profiles. Table V.6 summarizes results obtained by MasterSizer 2000 referring to diameters $d_{(0.1)}$, $d_{(0.5)}$, $d_{(0.9)}$, volume-weighted mean diameter (D), and microbead size dispersal coefficient (δ). Diameter $d_{(0.1)}$ defines the diameter value under which 10 % of analyzed microbeads were found, 50 % of analyzed microbeads has diameter smaller than $d_{(0.5)}$, while 90% of analyzed beads has diameter smaller than $d_{(0.9)}$. We have taken the volume-weighted mean diameter as a representative mean value for analyzing the influence of different formulation parameters on size of hydrogel microbeads. It could be seen that volume-weighted mean diameter ranges from around 20 to 108 μm (excluding the sample prepared

without the addition of emulsifier), which is in accordance with typical values of microbeads diameter characteristic for inverse suspension polymerization reactions, ranging from 1 to 200 μm [284]. The value of δ is a measure of polydispersity and is calculated according to the following formula:

$$\delta = \frac{d_{(0.9)} - d_{(0.1)}}{d_{(0.5)}} \quad (V.1)$$

The lower the value of δ , the narrower will be the size distribution of microbeads is. Hence, all microbeads obtained could not be regarded as monodisperse according to a criterion for emulsions $\delta \geq 0.4$ [285]. Microbeads size distribution profiles given in the following sections reveal size distribution by volume (%).

Table V.6. Values of hydrogel microbeads diameters based on laser diffraction measurements

Sample	$d_{(0.1)}$	$d_{(0.5)}$	$d_{(0.9)}$	D, μm	δ
M-50/1(10/1)-E 0	365.8	531.6	768.1	552.2	0.8
M-50/1(10/1)-E 1	11.9	27.4	70.0	35.9	2.1
M-50/1(5/1)-E 0.5	11.4	22.0	47.0	26.3	1.6
M-25/1	10.3	18.3	33.6	20.7	1.3
M-50/1(5/1)-E 1 (M-50/1)	9.3	20.2	44.0	23.9	1.7
M-100/1	11.8	27.6	58.3	31.8	1.7
M-25/1-MA 2.5	10.3	18.7	34.2	20.7	1.3
M-25/1-MA 5	12.3	24.0	51.6	28.8	1.6
M-25/1-MA 10	10.7	22.9	61.7	33.7	2.2
M-25/1-SA 0.5	11.9	47.4	114.1	56.1	2.2
M-25/1-SA 1	12.1	56.4	134.7	66.2	2.2
M-25/1-SA 2	21.3	89.3	221.6	108.0	2.2
M-25/1-CA 0.5	11.7	48.2	147.9	67.8	2.8
M-25/1-CA 1	13.0	66.3	154.9	76.8	2.1

V.4.1 Influence of concentration of emulsifier and the oil-to-aqueous phase ratio

The influence of emulsifier on size and size distribution of pure PNIPAAm hydrogel microbeads is demonstrated in Figure V.12. Under the same synthesis conditions where the oil-to-aqueous phase volume ratio was 10/1, and molar ratio of monomer to crosslinker 50/1, mean diameter of microbeads obtained in the absence of emulsifier (M-50/1(10/1)-E 0) was 522.2 μm , while those obtained after emulsifier addition in concentration 1 vol % (M-50/1(10/1)-E 1) was 35.9 μm . Addition of emulsifier reduced the microbeads size by 93 %

but affected increase in microbeads polydispersity [$\delta(M-50/1 (10/1)-E 1) > \delta(M-50/1 (10/1)-E 0)$], as shown in Figure V.11.

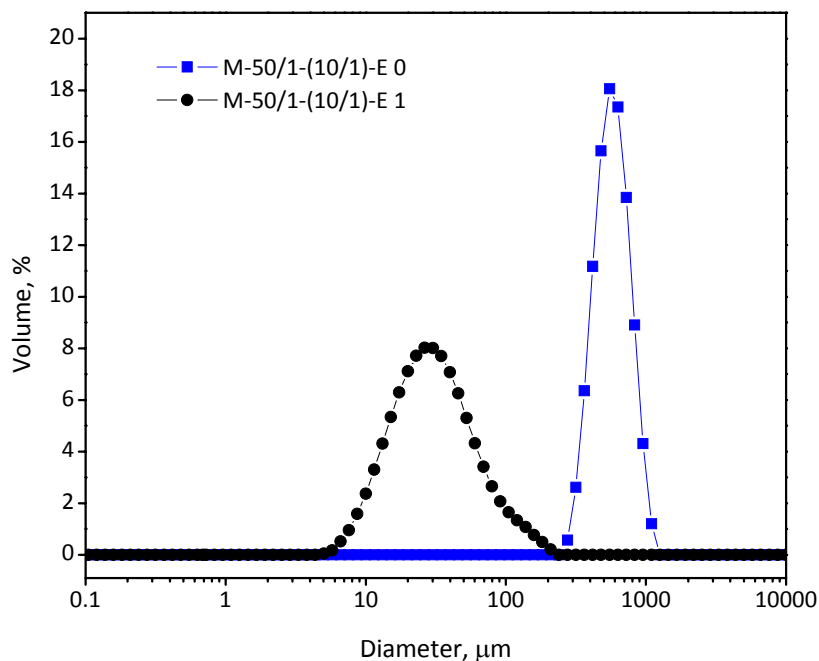


Figure V.11. Influence of emulsifier addition on size and size distribution of hydrogel microbeads (oil-to-aqueous phase volume ratio 10/1)

The oil-to-aqueous phase volume ratio in the presence of 1 vol % emulsifier was another parameter whose impact on microbeads size was studied (Figure V.12). The results of laser diffraction measurements show that smaller fraction of oil phase caused reduction in microbeads size (from 35.9 μm to 23.9 μm), which corresponds to the observations under optical microscope and image analysis results. It is obvious that smaller oil-to-aqueous phase volume ratio resulted in slightly reduced microbeads polydispersity. These results are not in big contradiction with the empirical relationships since microbeads diameter is complex function of physicochemical properties of the system.

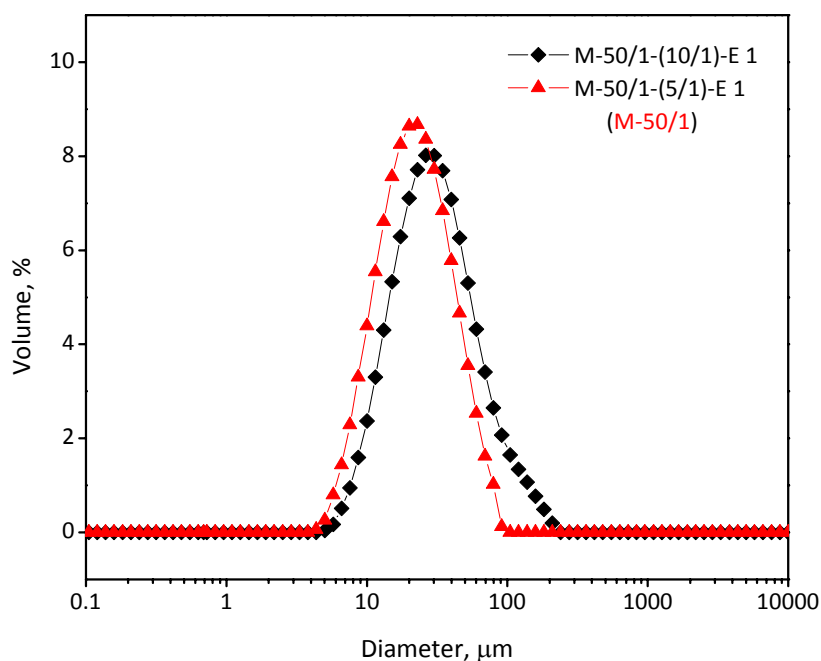


Figure V.12. Influence of *o/w* ratio on size and size distribution of hydrogel microbeads

Laser diffraction measurements showed that microbeads synthesized at 0.5 vol % emulsifier feature smaller mean diameter than analogous microbeads synthesized with 1 vol % emulsifier (Table V.6) and their size distribution is narrower (Figure V.13). However, it should be pointed out that according to images from optical microscope, the microbeads M-50/1 (10/1)-E 1 are of more regular spherical shape. Lower concentration of emulsifier caused more emphasized agglomeration, indicating less stable suspension. Hence, 1 vol % emulsifier in oil phase is the optimal concentration for obtaining hydrogel microbeads in the given system and this parameter was kept constant in the following syntheses.

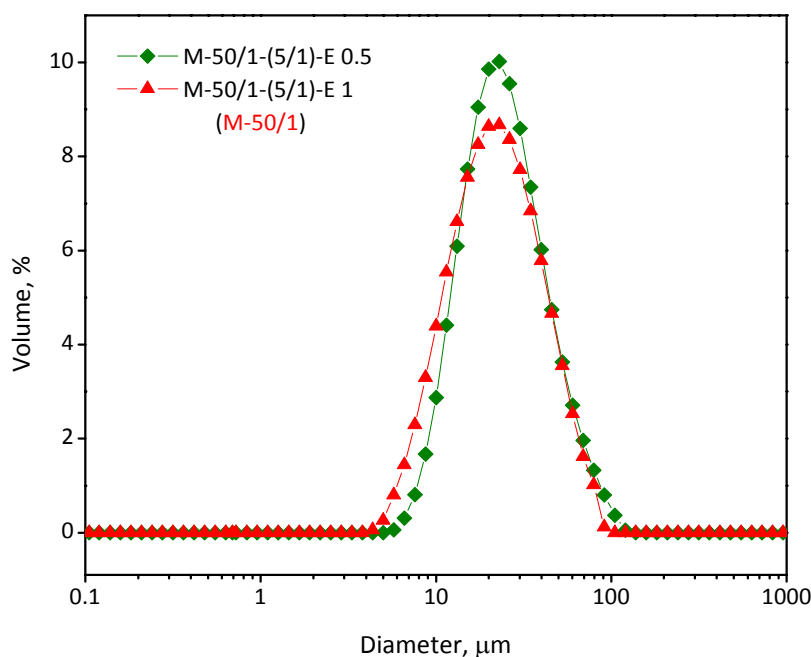


Figure V.13. Influence of emulsifier concentration size and size distribution of hydrogel microbeads (oil-to-aqueous phase volume ratio 5/1)

V.4.2 The influence of PNIPAAm crosslinking degree

The increase in molar ratio of monomer to crosslinker, i.e. formation of looser crosslinked polymer network, causes increase in microbeads mean diameters from 20.7 to 31.8 μm for M-25/1 and M-100/1, respectively. This is expected since the copolymerization/crosslinking reaction stops earlier when crosslinker content in the feed mixture increases [286]. In addition, the size distribution width is enhanced, as displayed in Figure V.14. The value of δ was the lowest for microbeads with the highest crosslinking degree (1.3) due to reduced presence of agglomerates and higher regularity of microbeads in comparison with those of lower crosslinking degree. This is demonstrated by images from the optical microscope given in the subsection V.3.2 of this chapter. General decrease in microbeads size with increase in crosslinker concentration is explained by the formation of more compact and dense polymer network.

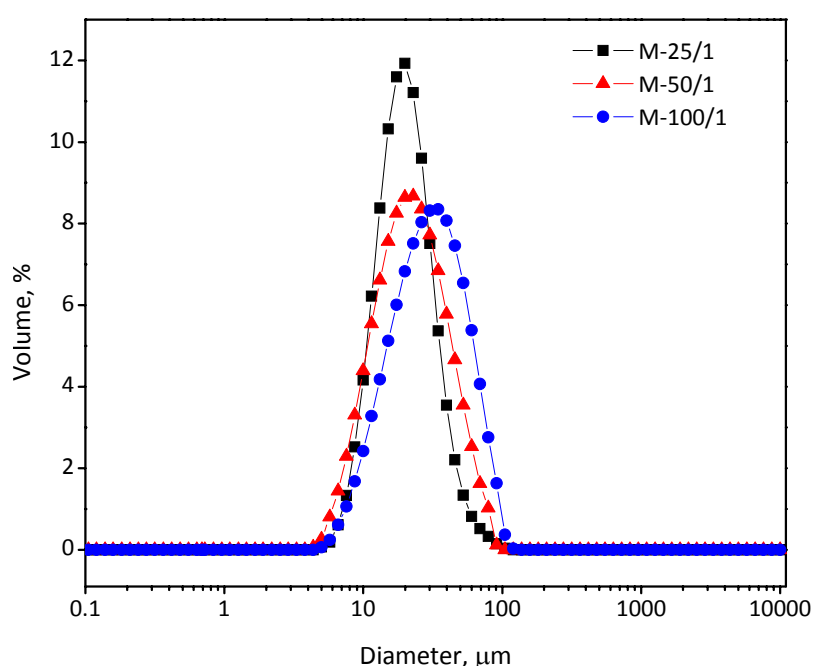


Figure V.14. Influence of crosslinking degree of PNIPAAm on size and size distribution of hydrogel microbeads

V.4.3 The influence of the presence of MA

When taking into consideration the modification of PNIPAAm network by addition of MA as a hydrophilic comonomer, it was concluded that there is no change in size and size distribution of microbeads when the lowest fraction of MA (2.5 mol %) was used. However, with increase in the fraction of MA (5 and 10 mol %), diameter of microbeads rises along with their size distribution width (Figure V.15). Mean diameters of PNIPAAm/MA copolymer hydrogel microbeads were in the range from 20.7 to 33.7 μm . It could be observed that distribution curve of microbeads prepared at the highest fraction of MA has emphasized shoulder at higher values of diameters. This implicates increased presence of fractions of higher diameters or the presence of agglomerates, as already confirmed by optical microscopy (Figure V.7). It should be noted that all microbeads types were exposed to 3 min

long ultrasonic treatment prior laser diffraction measurements. However, the observed shoulder in the distribution profile of the sample M-25/1-MA 10 (Figure V.15) implicates the strong adhesion of the microbeads into compact agglomerates that are difficult to disrupt. Introducing higher amounts of MA in the system and consequently higher amount of hydrophilic carboxylic groups probably attributed to damage of the emulsifier layer at the interface oil/aqueous phase. As a result, enhanced agglomeration of microbeads was characteristic for the sample M-25/1-MA 10. This led to bimodal microbeads size distribution and hence high size dispersal coefficient (>2) (Table V.6).

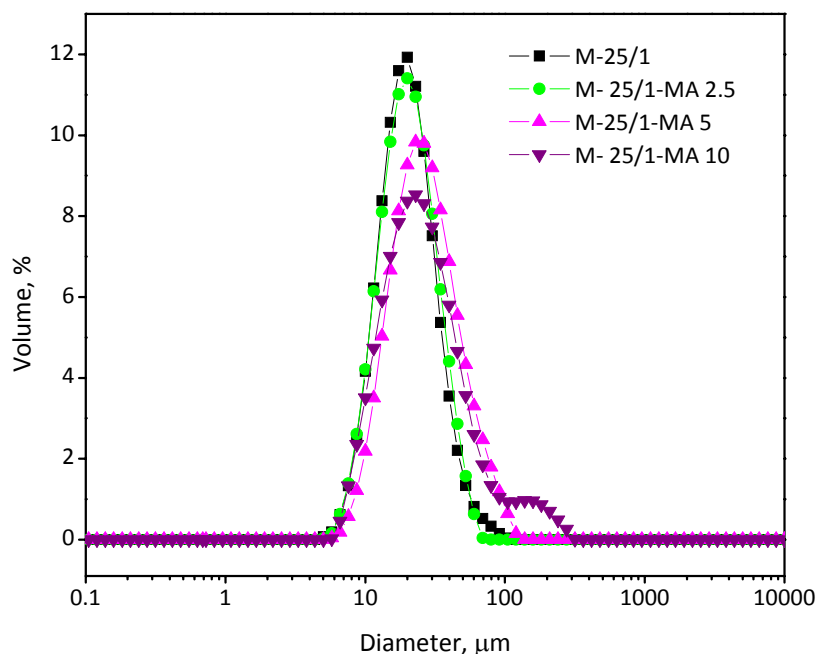


Figure V.15. Influence of MA on size and size distribution of hydrogel microbeads

V.4.4 Influence of the presence of linear and crosslinked alginate

Size distribution curves of semi-IPN hydrogel microbeads based on PNIPAAm and SA with different fractions of alginate (M-25/1-SA x , $x=0.5,1,2$) are shown in Figure V.16. The size distribution width of these samples is considerably increased in comparison with previously analyzed size distribution profiles. In addition, there is three- to five-fold increase in mean diameter with respect to the pure PNIPAAm microbeads (M-25/1). The viscosity of the initial aqueous phase should be taken into account when considering such high increase in microbeads diameter, since the fractions of SA in this phase were 0.5, 1 and 2 w/v %. Therefore, under unchanged force of disruption (rate of stirring), the aqueous droplets in oil phase could be only bigger than in the case of less viscous dispersed (droplet) phase [198, 287]. According to the laser diffraction analysis, mean diameter of semi-IPN hydrogel microbeads with SA increases from 56.1 to 108.0 μm when the fraction of SA in the feed solution increases four times (from 0.5 to 2 wt %). Furthermore, rise in SA fraction causes changes in distribution mode. Size distribution of the microbeads M-25/1-SA 0.5 inclines to bimodal with increase of alginate fraction (for the samples M-25/1-SA 1 and M-25/1-SA 2). The explanation of this phenomenon could be found in the destabilization of emulsifier layer at the interface oil/aqueous phase interface due to the high concentration of carboxylate

groups in alginate chains. Also, the impact of viscosity on uniformity of microbeads sizes could not be neglected. It is indeed known that increased viscosity of the dispersed phase induces increase in mean diameter of the resulting microbeads [288].

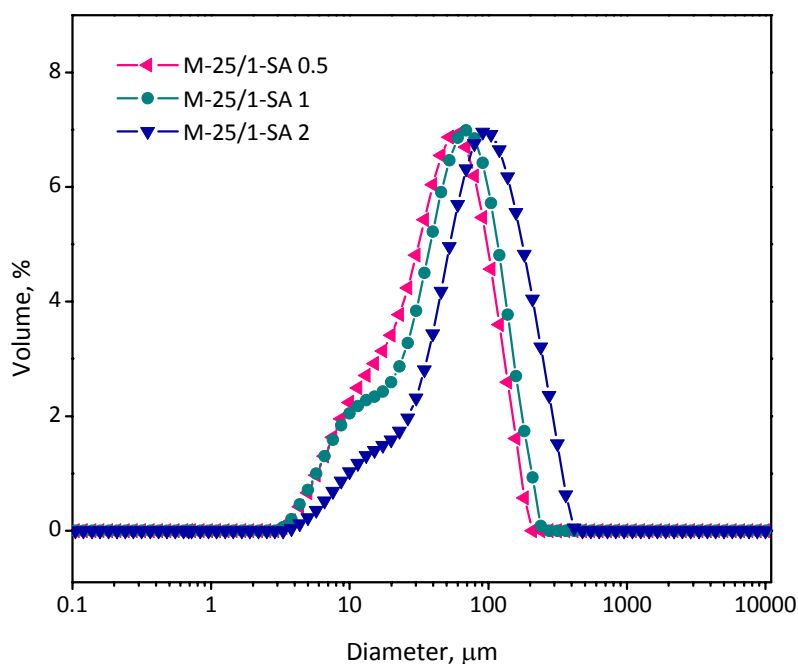


Figure V.16. Influence of SA on size and size distribution on semi-IPN hydrogels microbeads

When hydrogel microbeads with semi-IPN structure of crosslinked PNIPAAm and linear alginate are placed in calcium chloride solution, crosslinking of alginate occurred and microbeads with full-IPN structure were obtained (Figure V.17). As previously stated for semi-IPN microbeads, the increase in alginate fraction, i.e. increase in viscosity of aqueous phase results in microbeads of larger diameters. Hence, microbeads M-25/1-CA 1 are bigger than M-25/1-CA 0.5. The sizes of full-IPN microbeads have slightly increased (Table V.6) in comparison with semi-IPN microbeads. It was expected that the crosslinking of alginate with calcium ions resulted in slightly smaller microbeads due to the shrinking phenomenon characteristic for the formation of pure CA microbeads [289, 290]. However, the “backbone” of our system is PNIPAAm network that prevents the shrinking phenomenon. Higher diameters of corresponding full-IPN than semi-IPN microbeads could be caused by the presence of previously discussed semi-IPN microbeads agglomerates. They could be responsible for the crosslinking of alginate chains in the surface layers of neighboring microbeads. Newly formed aggregates are even more difficult to be disrupted by ultrasonic treatment. Also, the accommodation of Ca^{2+} ions into the PNIPAAm network with linear alginate chains by exchange with Na^+ ions could contribute the overall expansion of the resulting matrix.

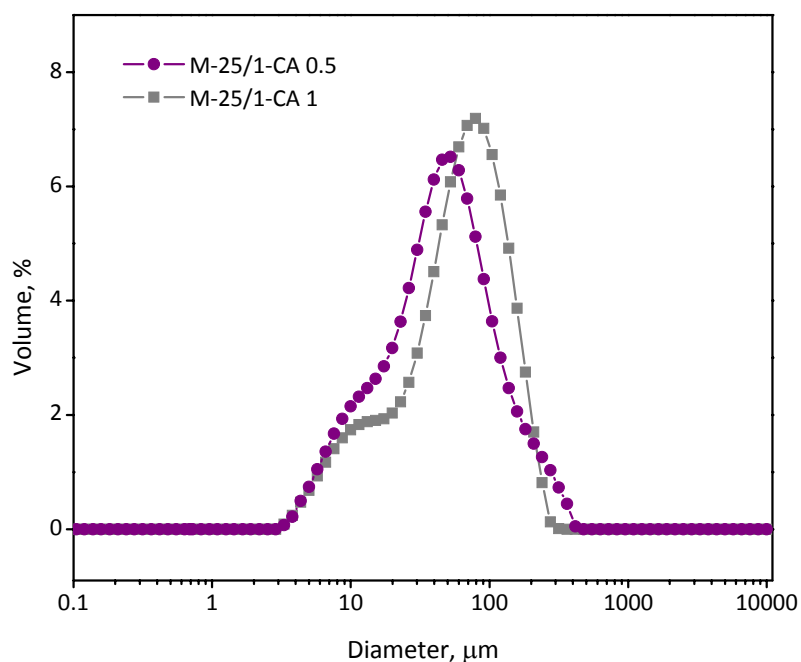


Figure V.17. Influence of CA on size and size distribution on full-IPN hydrogels microbeads

V.5 Thermal characteristics

Thermal characteristics of the selected thermosensitive hydrogel microbeads were analyzed through heating-cooling-heating cycle in the range from 15 to 50°C. Onset temperatures of the phase transition (T_{onset}), volume phase transition temperatures (VPTT), and the corresponding enthalpy changes (ΔH) are summarized in Table V.7.

Table V.7. Thermal results of DSC heating-cooling-heating cycle of hydrogel microbeads

Sample	Heating I			Cooling			Heating II		
	T_{onset}^* (°C)	VPTT* (°C)	ΔH^{**} (J g ⁻¹)	T_{onset} (°C)	VPTT (°C)	ΔH (J g ⁻¹)	T_{onset} (°C)	VPTT (°C)	ΔH (J g ⁻¹)
M-25/1	32.7	33.5	1.21	32.3	31.4	1.20	32.5	33.5	1.20
M-50/1	32.1	32.8	1.23	32.3	31.5	1.30	32.2	32.2	1.26
M-100/1	32.6	33.3	1.23	32.1	31.3	1.23	32.6	33.0	1.18
M-25/1-MA 2.5	32.4	34.3	0.86	34.6	32.8	0.86	32.6	34.4	0.83
M-25/1-MA 5	-	-	-	-	-	-	-	-	-
M-25/1-SA 0.5	32.5	33.1	1.13	32.8	31.9	1.14	32.6	33.2	1.21
M-25/1-SA 1	32.1	32.7	0.97	32.5	32.0	1.00	32.2	32.7	1.02
M-25/1-CA 0.5	32.0	32.9	1.17	32.5	31.9	1.18	32.3	32.9	1.14
M-25/1-CA 1	31.7	32.6	0.32	32.3	31.7	0.35	31.8	32.5	0.37

*Standard deviation for T_{onset} and VPTT values was $\pm 0.2^\circ\text{C}$.

** Standard deviation for ΔH values was $\pm 0.19 \text{ J g}^{-1}$.

The obtained results demonstrate that VPTTs of pure PNIPAAm microbeads (M-25/1, M-50/1, and M-100/1) are close and imply that the crosslinking degree of PNIPAAm has no considerable influence on VPTT of the hydrogels [59]. This is also shown in the case of thermosensitive hydrogel films and presented in Chapter III of the report (section III.3.1). Furthermore, the enthalpy changes corresponding to the volume phase transitions in all three cycles are almost identical for the mentioned hydrogels. This means that main contribution to ΔH values come from the breakage (during heating steps) or formation (during cooling step) of hydrogen bonds between water molecules and isopropyl groups of PNIPAAm [239]. Since the amount of NIPAAm in all feed mixtures in the preparation of pure PNIPAAm hydrogel microbeads was the same, the amount of isopropyl groups in the resulting polymer networks is assumed to be the same. This implicates the same number of hydrogen bonds established between water molecules and isopropyl groups and hence, the same energetic effect during heating/cooling over a critical temperature, i.e. VPTT. The analogous results are acquired when thermosensitive hydrogel films were analyzed.

Furthermore, reversibility of the volume phase transition of all analyzed thermosensitive hydrogel microbeads is clearly demonstrated by the complete thermograms in Figures V.18-V.21 that represent each type of hydrogel microbeads: pure PNIPAAm (M-50/1), PNIPAAm/MA copolymer (M-25/1-MA 2.5), semi-IPN PNIPAAm/SA (M-25/1-SA 0.5), and full-IPN PNIPAAm/CA (M-25/1-CA 0.5). The endothermic peaks of the first and the third thermal step overlap in all cases, indicating that after the cooling step hydrogel samples come into fully swollen state with re-established hydrogen bonds with water molecules. This is in direct relation with the close ΔH values of the three steps in the performed thermal cycles. Low ΔH values obtained for the sample ΔH values could not be explained.

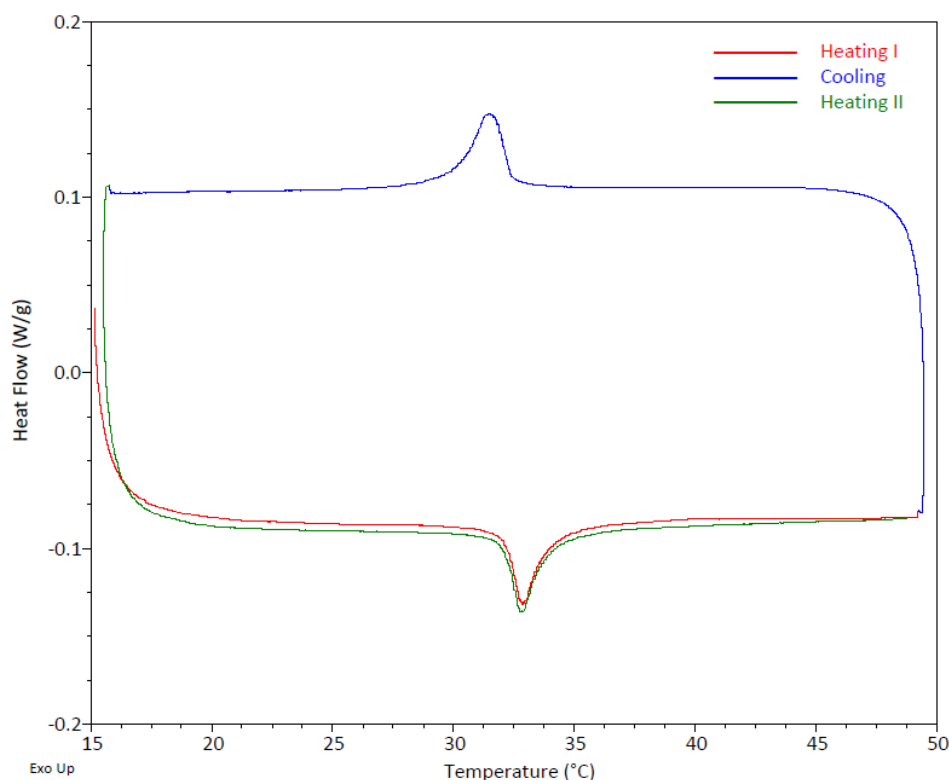


Figure V.18. DSC thermogram of hydrogel microbeads M-50/1

DSC thermogram of PNIPAAm/MA copolymer hydrogel microbeads with the lowest amount of MA (M-25/1-MA 2.5) is displayed in Figure V.19. VPTT of this hydrogel type is shifted towards higher values (around 1°C) in comparison with the pure PNIPAAm hydrogel microbeads (Table V.7). This is in accordance with the studies showing that hydrophilicity of comonomers in PNIPAAm-based hydrogels causes the increase in VPTT [291]. This could be explained by the ability of maleic acid to break PNIPAAm chain sequences thus impairing the hydrophilic/hydrophobic balance in PNIPAAm chains, as was the case with PNIPAAm copolymer hydrogels with acrylic acid [292, 293]. Hence, hydrophobic interactions among isopropyl groups are weakened leading to greater energy necessary for their domination and the resulting collapse of PNIPAAm chains. Taşdelen et al., who studied PNIPAAm/MA copolymer hydrogels synthesized by γ -radiation technique, also reported that the presence of MA causes increase in VPTT with respect to the pure PNIPAAm hydrogel [191]. Furthermore, Figure V.19 demonstrates that endothermic peaks of M-25/1-MA 2.5 are broader than those of pure PNIPAAm hydrogels (see Figure V.18). These broader peaks could be explained by the statistical distribution of comonomer units that affects structuring of water molecules around polymer chains, i.e. weakens hydrophobic aggregation of PNIPAAm chains [194, 291]. Broader phase transition of PNIPAAm/MA copolymer bulk hydrogels were reported by Taşdelen et al. [191]. Also, sample M-25/1-MA 2.5 feature lower enthalpy changes with respect to pure PNIPAAm hydrogel microbeads during the volume phase transition (Table V.7). The presence of hydrophilic comonomer contributes to better hydration of polymer chains implying smaller number of hydrogen bonds disrupted during the phase transition and consequently lower heat of reaction.

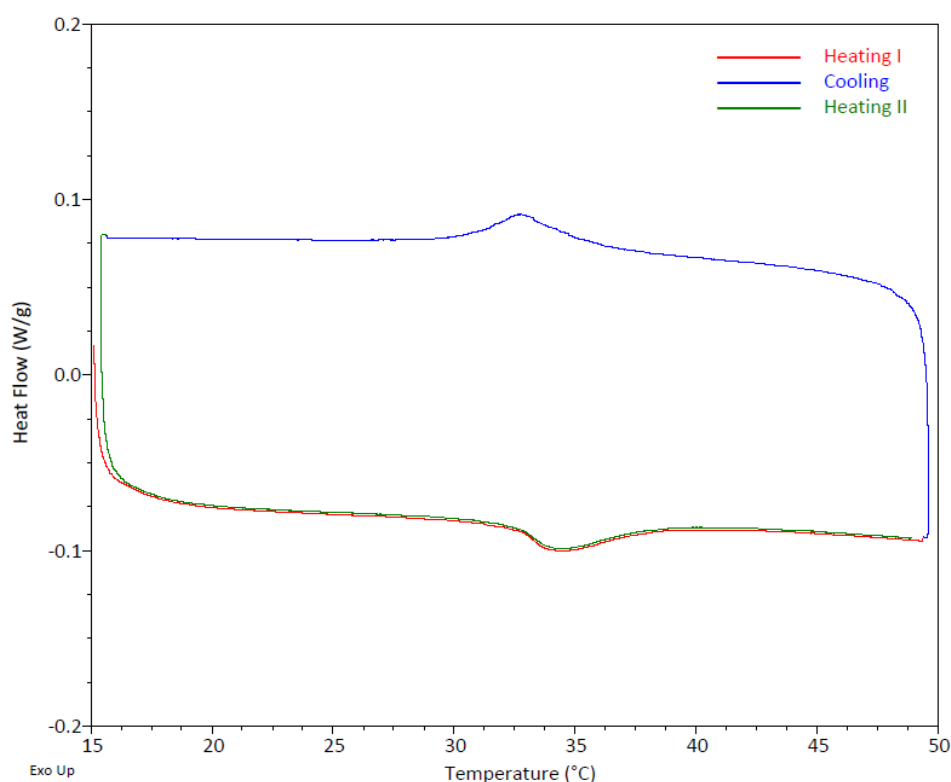


Figure V.19. DSC thermogram of hydrogel microbeads M-25/1-MA 2.5

The DSC analysis of PNIPAAm/MA copolymer hydrogel microbeads with higher amount of MA (M-25/1-MA 5) has not resulted in expected peaks in thermogram that implicates

deteriorated thermosensitivity of these hydrogel microbeads. Obviously, incorporation of MA comonomer (5 mol % MA in ratio to NIPAAm) caused considerable disturbance of continuous sequence of PNIPAAm chains, i.e. isopropyl groups than govern the volume phase transition (shrinking) of hydrogel [293]. This led to over weakened hydrophobic interactions among isopropyl groups and hence feeble or eliminated thermosensitivity of hydrogel, which is already reported for a certain concentrations of acrylic acid (AAc) in PNIPAAm/AAc copolymer hydrogel [293]. Therefore, copolymer hydrogel microbeads based on the highest amount of MA (10 mol %) were not analyzed by DSC.

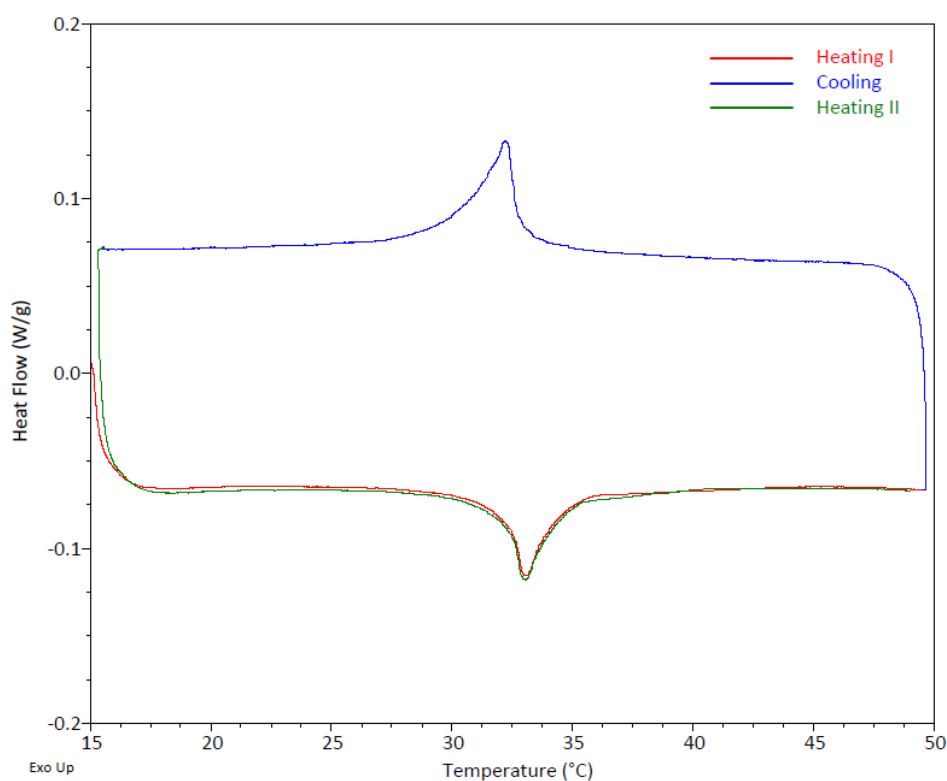


Figure V.20. DSC thermogram of hydrogel microbeads M-25/1-SA 0.5

According to the analysis of hydrogel microbeads based on PNIPAAm and alginate with both semi-IPN and full-IPN structures, VPTT is not affected by the alginate presence, neither as linear (SA) or crosslinked component (CA). This is characteristic for IPN hydrogels in which each individual component maintains its own properties since no chemical bonds between them exists. Hence, thermosensitive property of PNIPAAm is not affected by the presence of alginate chains. This is also demonstrated through their sharp and narrow endothermic and exothermic peaks (Figures V.20 and V.21).

Regardless of the type of hydrogel microbeads, DSC analysis showed that exothermic peaks detected in the cooling step (Table V.7) are shifted toward slightly lower values in comparison with endothermic peaks obtained in the heating steps. This phenomenon is known as hysteresis, also demonstrated by DSC analysis of thermosensitive hydrogel films (Chapter III). As already noted, this delay in the cooling step following the heating step is explained by the formation of some additional hydrogen bonds between the $>C=O$ and $H-N<$ groups of PNIPAAm chains only in the collapsed state [238].

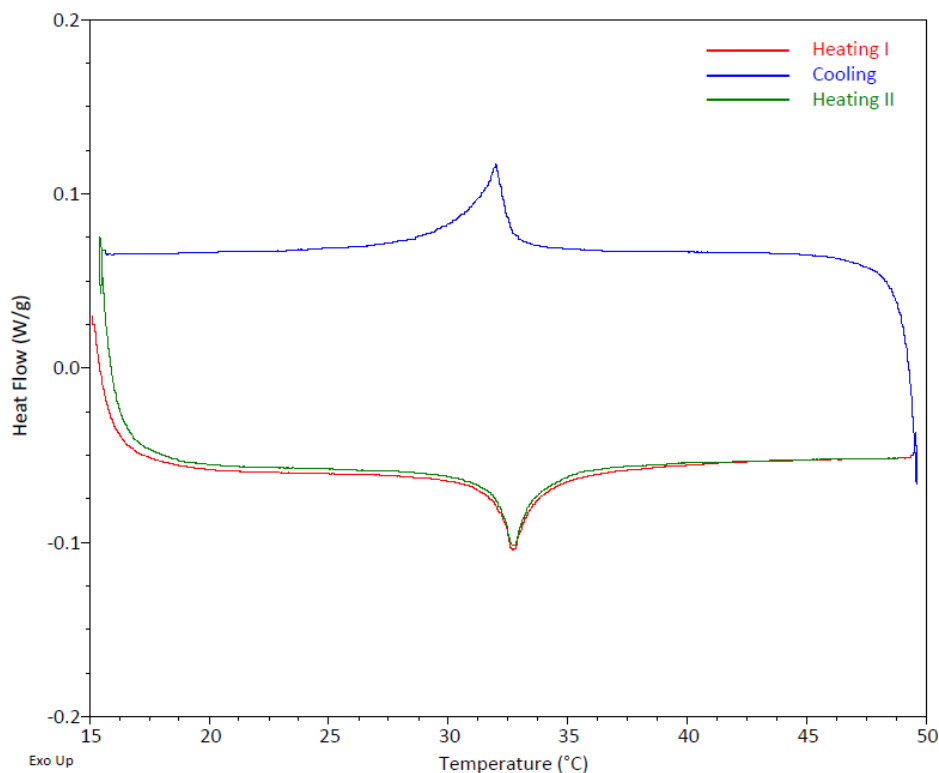


Figure V.21. DSC thermogram of hydrogel microbeads M-25/1-CA 0.5

Finally, if the DSC thermograms of hydrogel films are compared with those of hydrogel microbeads, the information on the difference in the rate of response to temperature changes could be gained. In other words, obviously sharper and narrower endothermic and exothermic peaks detected for hydrogel microbeads denote their faster response rate with respect to hydrogel films [294]. This result is in direct relation with the hydrogels dimensions since it is known that hydrogel swelling rate is inversely proportional to the square of the gel dimension [295].

V.6 Swelling behavior

V.6.1 Equilibrium swelling ratio

Equilibrium swelling ratio (ESR) of hydrogel microbeads at 25°C was determined gravimetrically. The mean values of ESR and equilibrium water content (EWC) of all hydrogel microbeads and corresponding standard deviations are presented in Table V.8.

Table V.8. Values of equilibrium swelling degree and equilibrium water content of hydrogel microbeads at 25 °C

Sample	ESR	EWC, %
M-50/1(10/1)-E 0	13.0±0.6	92.9±0.3
M-50/1(10/1)-E 1	23.1±1.0	95.8±0.2
M-50/1(5/1)-E 0.5	13.9±0.7	93.2±0.3
M-25/1	15.0±0.8	93.6±0.9
M-50/1(5/1)-E 1 (M-50/1)	14.8±0.6	93.5±0.1
M-100/1	27.5±1.9	96.5±0.2
M-25/1-MA 2.5	18.7±0.5	94.6±0.5
M-25/1-MA 5	32.1±1.9	97.2±0.3
M-25/1-MA 10	44.9±1.3	97.7±0.2
M-25/1-SA 0.5	16.3±0.5	94.2±0.2
M-25/1-SA 1	24.3±1.4	96.0±0.2
M-25/1-CA 0.5	33.5±2.6	97.1±0.2
M-25/1-CA 1	29.3±1.5	96.7±0.2

In a series of microbeads with various crosslinking degrees, i.e. molar ratios NIPAAm/MBAAm varying from 25/1 to 100/1, the ESR values were in the range from 15 to 23. For clearer presentation, these values are given graphically in Figure V.22.

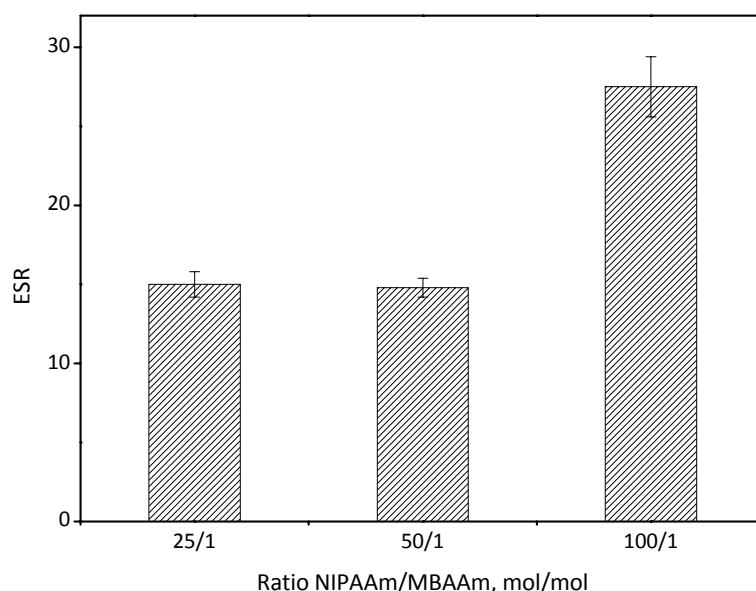


Figure V.22. Influence of crosslinking degree of PNIPAAm on ESR of pure PNIPAAm hydrogel microbeads

When taking these results as a whole, the trend of ESR increase with decrease in crosslinking degree is noticeable, as expected and also found in similar studies [296]. More crosslinked structure feature weaker water absorption abilities. However, the ESR of M-25/1 and M-50/1 are almost identical. The influence of denser network of M-25/1 in comparison with M-50/1 could be annulled by the influence of slightly higher mean diameter of M-50/1 on the ESR values (Table V.6). These competitive phenomena resulted in close values of their ESRs. The general trend confirms the influence of crosslinking degree on lowering the swelling capacities of hydrogel microbeads due to the formation of more dense and tighter polymer network that limits the water absorption. This dependence is valid for both microbeads as well as bulk hydrogels [286, 297].

PNIPAAm hydrogel microbeads modified with MA showed improved swelling abilities in comparison with analogous pure PNIPAAm microbeads (M-25/1). As clearly seen in Figure V.23, there is a regular rising trend of ESR caused by increased fraction of hydrophilic component MA. Addition of MA in fraction of 10 mol % in ratio to NIPAAm in feed mixture resulted in even three-fold increase in value of ESR. There are several parameters responsible for this dependence on the fraction of MA and ESR of microbeads. First, the incorporation of hydrophilic moieties in PNIPAAm network, i.e. the electrostatic interactions among carboxylate groups of MA units, as already reported for PNIPAAm/MA copolymer bulk hydrogel [191]. These electrostatic interactions (repulsions) induce increase of the osmotic pressure in the hydrogel that results in increased swelling [298]. Furthermore, addition of MA results in reduced overall crosslinking density of the network and hence in increased swelling abilities.

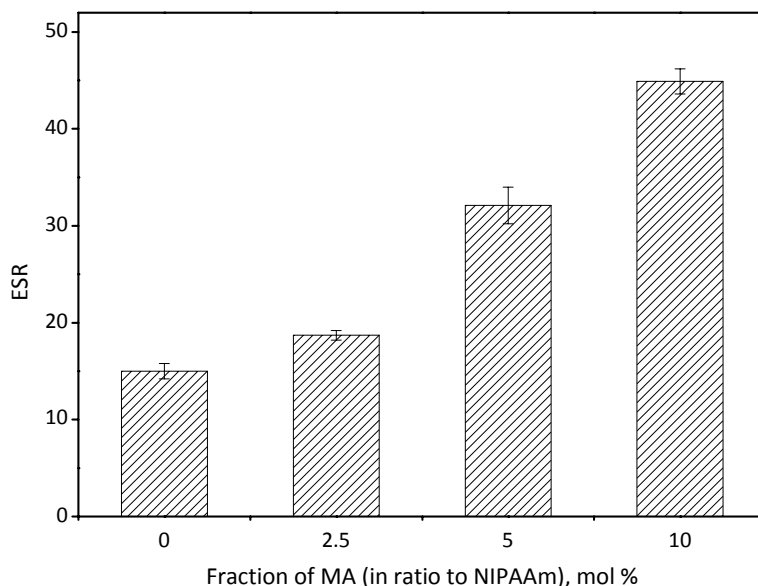


Figure V.23. Influence of MA on ESR of hydrogel microbeads

The influence of alginate on ESR was investigated in the case of both semi- and full-IPN hydrogels microbeads based on 0.5 and 1 w/v % of alginate (Figure V.24). The ESR of M-25/1-SA 1 is higher than that of M-25/1-SA 0.5 due to the increased presence of carboxylate groups. These results are explained by the formation of expanded network structure during polymerization process due to electrostatic repulsions among carboxylate groups of alginate chains[136]. Furthermore, the content of PNIPAAm in dry mass of hydrogel is considerably

reduced⁵ in semi- and full-IPN hydrogel microbeads in comparison with pure PNIPAAm sample M-25/1, meaning that hydrophobicity is lowered and consequently contributes to their higher swelling ratio. Also, an increase in alginate content in semi-IPN hydrogel microbeads results in an increase in ESR whereas opposite effect is observed for full-IPN hydrogel microbeads. The effect of ESR decrease in full-IPN systems is explained by additional crosslinking of alginate chains due to complexation of carboxylate groups by calcium ions. The trends obtained were also reported for swelling behavior of similar semi- and full-IPN bulk hydrogels [299]. Finally, stronger swelling abilities of full-IPN with respect to semi-IPN hydrogel microbeads with the same amounts of alginate can be explained by their greater size, i.e. formation of aggregates that are capable of holding a certain amount of water in “interstitial” space among the individual microbeads.

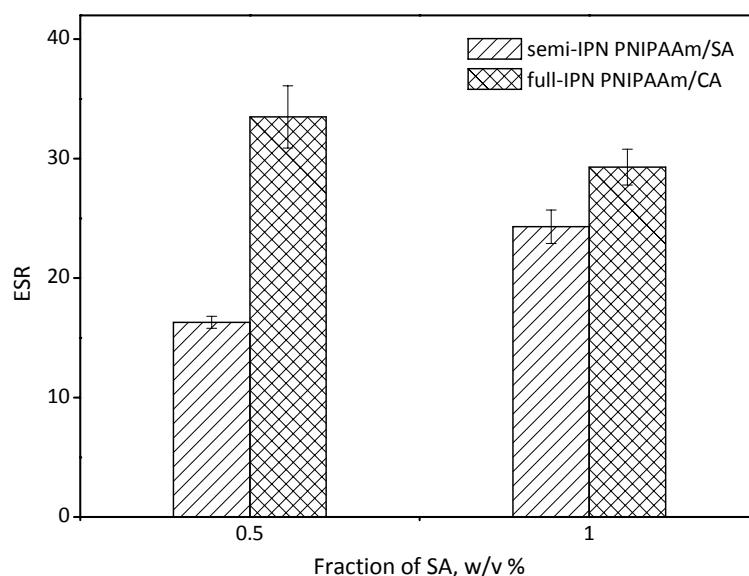


Figure V.24. Influence of SA on ESR of hydrogel microbeads

V.6.2 Response of dried microbeads to water presence

The rate of response of dried hydrogel microbeads when coming in contact with water was investigated by optical microscope at room temperature (23°C). A drop of microbeads suspension was dried on a glass slide for 2 h at 50°C. Afterwards, the slide was positioned on a microscopic stage and finally a drop of water was carefully placed on the dried microbeads fixed on a glass slide. From that moment on, snapshots were taken at short time intervals. Figure V.25 presents M-25/1 hydrogel microbeads in dried state and after 30 s, 2 min, and 10 min from the contact with water, i.e. start of swelling. These microscopic images show that dried microbeads have very fast response in contact with water since they swell almost instantly. Already after 30 s the microbeads are of regular shape and swelled. Based on the given images, it can be concluded that there are no significant differences in the swelling degree (microbeads size) after 30s and 10 min from the start of swelling.

⁵ Note that values alginate concentration in the feed mixtures (0.5 and 1 w/v %) are relative to the whole mixture whereas values MA concentrations are (2.5, 5 and 10 mol %) are relative to NIPAAm content.

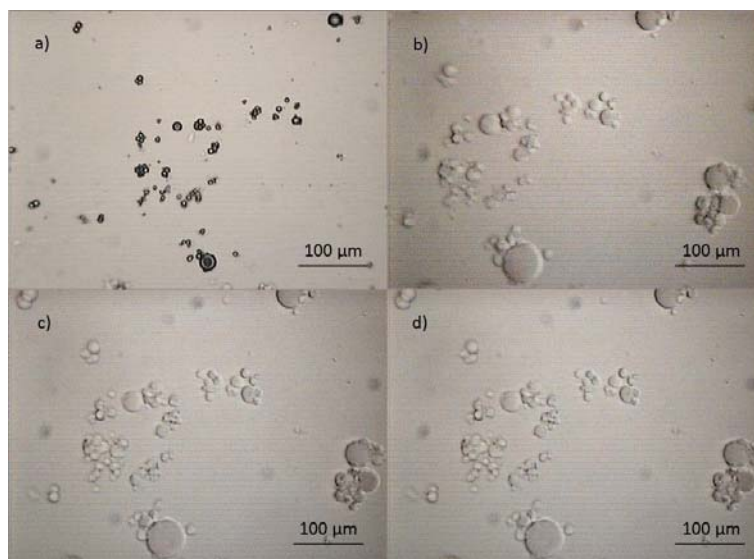


Figure V.25. Response of dried microbeads M-25/1 (a) to water presence after 30 s (b), 2 min (c), and 10 min (d)

The PNIPAAm/MA copolymer hydrogels had also fast response to water presence, i.e. higher swelling rate, as shown in Figure V.26. It can be estimated that seconds are enough for the hydrogel microbeads to swell from dried state, which is one of their beneficial property in comparison with macro forms of hydrogels studied within this thesis and described in Chapter III. Those hydrogels in the form of disks took several hours to swell close to equilibrium (Figure III.9 of the Chapter III). Suárez et al. investigated pure PNIPAAm microbeads using inverse suspension polymerization method for synthesis. Their microbeads were of diameters between 8 and 60 μm and have swelling time of around 1 s [300].

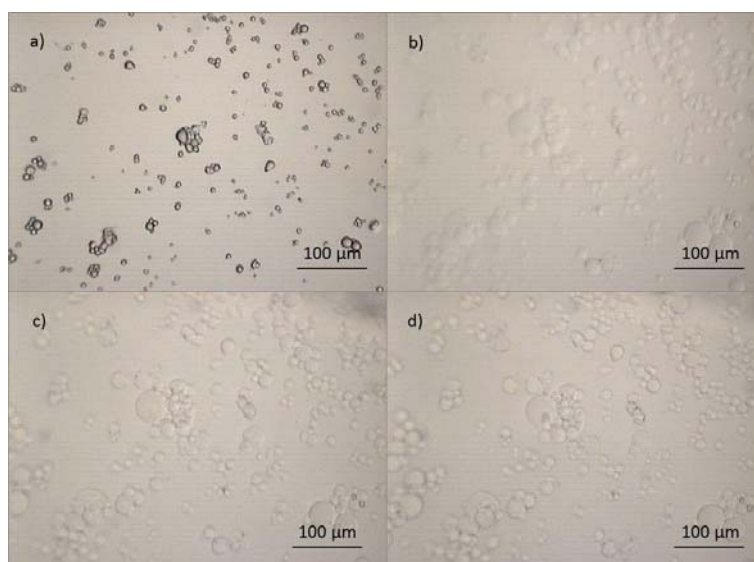


Figure V.26. Response of dried microbeads M-25/1-MA 2.5 (a) to water presence after 30 s (b), 2 min (c), and 10 min (d)

Initially, the aim was to track microbeads swelling throughout 1 h or more. However, this was not possible since water evaporated quickly in air. Figure V.27 displays microbeads MS-25/1-MA 2.5 after being left in contact with drop of water for 1 h, when the major part of

water already evaporated. Afterwards, in less than 30 s, due to additional heating by microscopic light source, the microbeads became almost dried again. This indicates high drying rate of microbeads, in addition to their fast swelling.

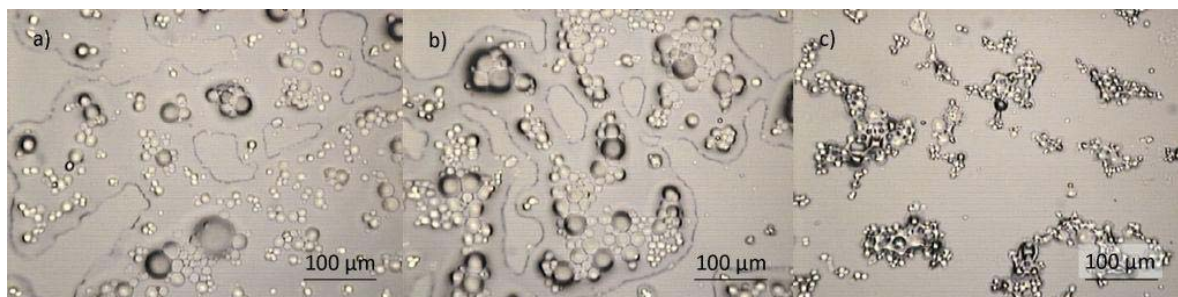


Figure V.27. Change in dimensions of microbeads M-25/1-MA 2.5 while getting dried in air under microscopic light source: at the moment of turning on a lamp on (a), after 8 s (b), and 16 s (c)

Semi- and full-IPN microbeads with alginate showed equally fast response to the presence of water, as pure PNIPAAm microbeads (see Appendix).

V.7 Morphology

Morphology of freeze-dried microbeads was analyzed using SEM. Obtained micrographs are presented in Figures V.28-V30. The image analysis software was applied for determination of mean pore size of microbeads (200 per sample) (Table V.9). Data for the sample M-25/1-MA 10 are not shown in this table since freeze-drying of this sample was incomplete and due to the presence of water in the gels structure the SEM analysis was not successful. It was observed that the size of freeze-dried microbeads were almost the same as prior to treatment in the swollen state, observed under the optical microscope, indicating successful freeze-drying treatment.

SEM micrographs of the freeze-dried microbeads showed that synthesized thermosensitive hydrogel microbeads feature highly porous structure with interconnected pores. This is in particular favorable regarding the drug loading/release applications. Interconnected (open) pores are also evidence of the successful removal of paraffin oil from the reaction mixture, i.e. complete washing steps. For instance, Topuz and Okay explained the existence of closed pores in macroporous hydrogel beads based on the monomers acrylamide and 2-acrylamido-2-methylpropane sulfonic acid sodium salt as a result of trapped paraffin oil within the monomer droplets during the inverse suspension polymerization [301].

Table V.9. Values of mean pore size of freeze-dried microbeads determined from the SEM micrographs 25°C

Sample	Mean pore size, μm	Mean diameter, μm
M-50/1(10/1)-E 0	7.93 ± 3.12	$372.2 \pm 201.0^*$
M-50/1(10/1)-E 1	4.41 ± 1.66	49.2 ± 23.5
M-50/1(5/1)-E 0.5	5.83 ± 1.16	38.2 ± 18.2
M-25/1	4.39 ± 0.98	28.9 ± 13.0
M-50/1(5/1)-E 1 (M-50/1)	4.09 ± 0.86	27.6 ± 12.9
M-100/1	3.91 ± 1.54	40.3 ± 15.4
M-25/1-MA 2.5	4.10 ± 1.02	24.7 ± 12.6
M-25/1-MA 5	5.43 ± 3.04	$34.0 \pm 21.1^{**}$
M-25/1-MA 10	-	-
M-25/1-SA 0.5	4.99 ± 1.29	-
M-25/1-SA 1	3.66 ± 1.05	-
M-25/1-CA 0.5	4.42 ± 1.49	-
M-25/1-CA 1	3.44 ± 1.57	-

* based on 17 analyzed microbeads

** based on 64 analyzed microbeads

Results of SEM analysis confirmed already proven influence of emulsifier content on size of pure PNIPAAm microbeads, i.e. microbeads synthesized in the presence of emulsifier are much smaller than those synthesized in the absence of emulsifier (Figure V.28-a,b).

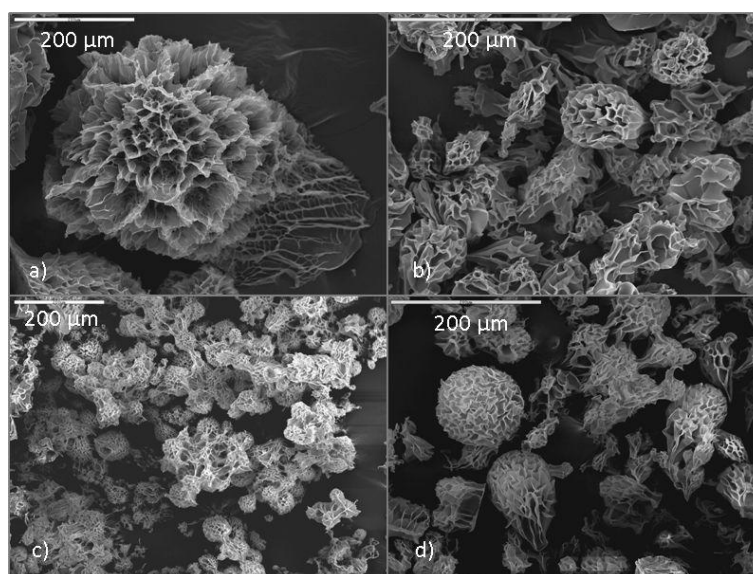


Figure V.28. SEM micrographs of microbeads with various amounts of emulsifier and volume ratio of oil to aqueous phase: M-50/1(10/1)-E 0 (a), M-50/1(10/1)-E 1 (b), M-50/1(5/1)-E 1 (c), and M-50/1(5/1)-E 0.5 (d)

It is clearly seen from Figure V.28-a that the microbeads prepared without emulsifier (M-50/1(10/1)-E 0) have flower-like porous structure. Such structure was reported by Cheng et al. who studied pure PNIPAAm microbeads prepared by inverse emulsion polymerization [302]. Honey-comb like structure of other types of hydrogel microbeads allowed calculation of their mean pore sizes by image analysis. Obtained values of mean pore sizes of analyzed microspheres are in range from 4.2 to 7.9 μm and have proportional dependence on microbeads diameters determined by laser diffraction (Table V.6). Furthermore, SEM analysis confirmed the impact of oil-to-aqueous phase value ratio in synthesis of microbeads on their ultimate size (Figure V.28-b and Figure V.28-c). Likewise, analysis by optical microscopy showed that microbeads M-50/1(10/1)-E 0.5 obtained at lower amount of emulsifier (0.5 vol % emulsifier), have larger diameters and are more polydisperse (Figure V.28-d) than analogous microbeads obtained under higher amount of emulsifier (Figure V.28-c).

Figure V.29 represents the influence of crosslinking degree of PNIPAAm on pure PNIPAAm microbeads morphology and size. It can be seen that the least crosslinked microbeads (M-100/1) have a pronounced tendency towards assembling into agglomerates. Image analysis showed that mean pore size values only slightly increase with increase in the crosslinking degree of PNIPAAm. The insignificant impact of the crosslinker concentration (beyond certain value) on the pore size of pure PNIPAAm microbeads could be found in the study of Park and Hoffman who characterized microbeads prepared by inverse suspension polymerization and having diameters in the range from 200 μm to 400 μm [167].

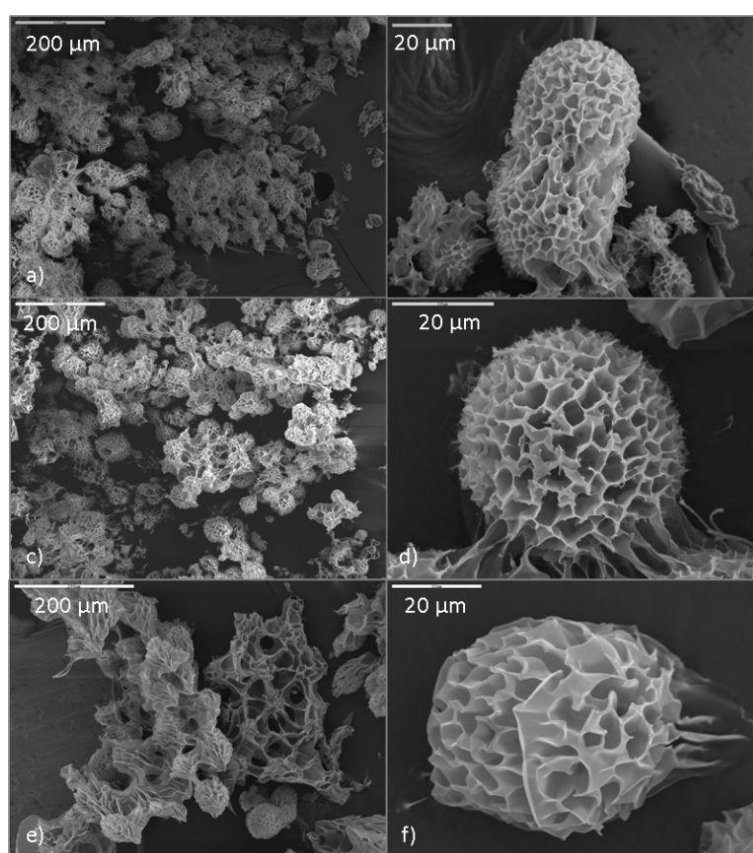


Figure V.29. SEM micrographs of microbeads with various crosslinking degrees: M-25/1 (a,b), M-50/1 (c,d), and M-100/1 (e,f)

Analysis of micrographs of PNIPAAm/MA copolymer microbeads have confirmed the results of laser diffraction measurements indicating larger mean diameter of microbeads based on 5 mol % in comparison with those based on 2.5 mol % MA. Figure V.30 clearly shows that PNIPAAm/MA copolymer microbeads maintain the porous, honeycomb-like structure, with similar mean pore sizes as of pure PNIPAAm microbeads. Introduction of hydrophilic functionality in the PNIPAAm network has not impaired desired porosity of the resulting microbeads, beneficial for efficient matrices in drug release studies.

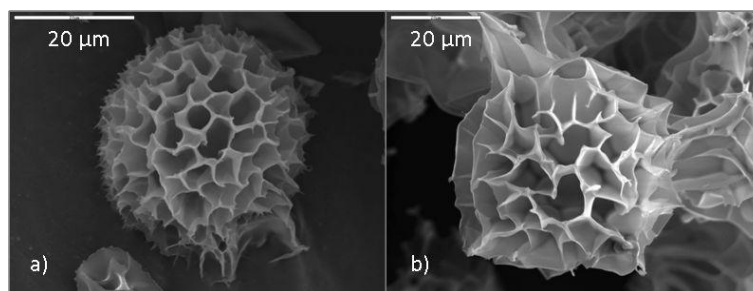


Figure V.30. SEM micrographs of microbeads M-25/1-MA 2.5 (a) and M-25/1-MA 5 (b)

Morphology of microbeads with semi-IPN structure of crosslinked PNIPAAm and SA is displayed in Figure V.31. Clearly, the pore structure of microbeads is affected by the concentration of alginate. The pore sizes are decreasing with the increase in alginate fraction (Table V.9). The most regular pore structure is characteristic for the microbeads M-25/1-SA 1.

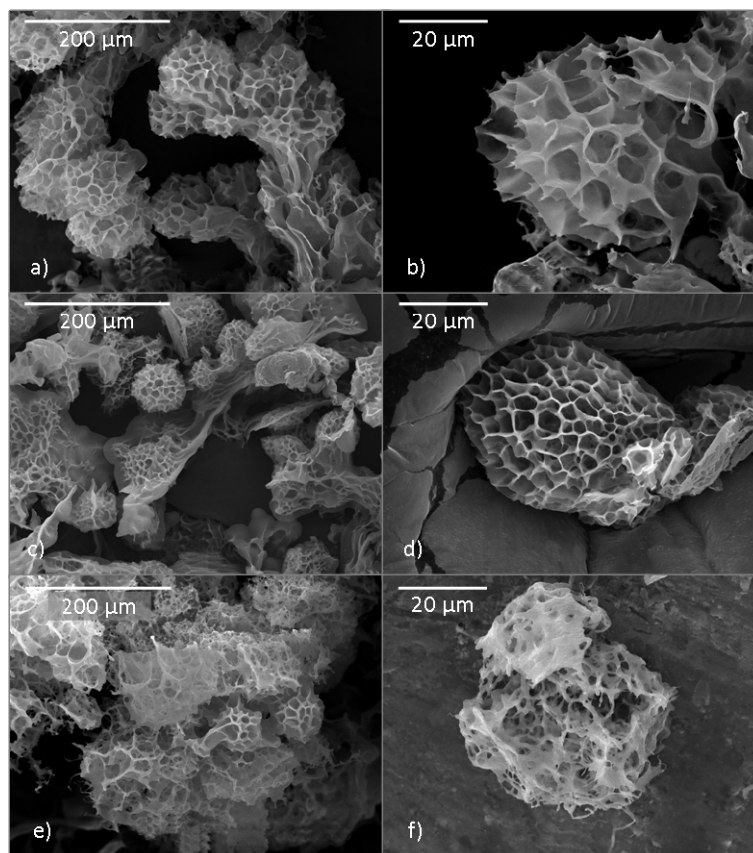


Figure V.31. SEM micrographs of microbeads M-25/1-SA 0.5 (a,b), M-25/1-SA 1 (c,d), and M-25/1-SA 2 (e,f)

Optical microscopy showed that semi-IPN hydrogel microbeads with the highest fraction of alginate feature irregular shape and this was confirmed by SEM micrographs in Figure V.31-e,f. The most regular, honeycomb-like structure was observed for the microbeads based on 1 w/v % alginate.

The full-IPN microbeads composed of crosslinked PNIPAAm and CA are also characterized by the porous, honeycomb-like structure (Figure V.32). It was calculated that the mean pore size value of M-25/1-CA 0.5 are smaller than that of M-25/1-CA 1. Also, the mean pore size of these microbeads is smaller than of corresponding semi-IPNs (Table V.9). The regularity of pore structure is maintained with respect to semi-IPN microbeads.

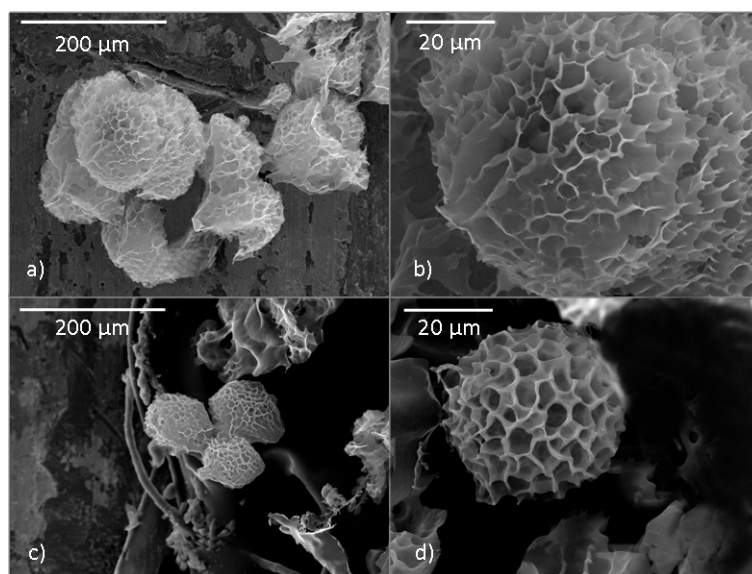


Figure V.32. SEM micrographs of microbeads M-25/1-CA 0.5 (a,b) and M-25/1-CA 1 (c,d)

Prepared hydrogel microbeads of all types (pure PNIPAAm, PNIPAAm/MA copolymer, semi-IPN PNIPAAm/SA, full-IPN PNIPAAm/CA) could be classified under macroporous structures that are favorable for drug loading/release applications [255].

The presence of considerable number of “tailed” microbeads in almost all micrographs is the consequence of vacuum drying pretreatment of microbeads that was part of freeze-drying procedure. The reason for “tails” formation could be also found in freezing process that causes the water within the top of a microbead to flow downward while being gradually frozen [302] and are reported for similar freeze-dried PNIPAAm microbeads [62]. Finally, similar values of microbeads size obtained by analysis of SEM micrographs (Table V.9) and by analysis of images from optical microscope (Table V.2 to Table V.5) indicate that freeze-drying was successful.

V.8 CONCLUSIONS

A series of thermosensitive hydrogel microbeads based on crosslinked PNIPAAm were synthesized by inverse suspension polymerization. In addition to variation of the oil-to-aqueous phase volume ratio, concentration of emulsifier, and the crosslinking degree, PNIPAAm microbeads were functionalized by using MA for the formation of copolymer hydrogels. Furthermore, semi- and full-IPN hydrogel microbeads were prepared with linear and crosslinked alginate, respectively. The optimization of formulation parameters showed that decrease in volume ratio of oil-to-aqueous phase volume ratio, presence of emulsifier, and lower fraction of crosslinker cause a decrease in mean diameter. It was shown that the most regular and the smallest pure PNIPAAm hydrogel microbeads of 20 μm in diameter could be obtained at 5/1 oil-to-aqueous phase volume ratio, at 1 vol % of emulsifier (in oil phase), and at 25/1 NIPAAm/MBAAm molar ratio. Increase in the fraction of MA in PNIPAAm/MA copolymer hydrogel microbeads enhanced formation of agglomerates, caused an increase in microbeads size, and weakened microbeads thermosensitivity. The VPTT of pure PNIPAAm hydrogels was around 33°C whereas VPTT of PNIPAAm/MA copolymer hydrogel with the lowest concentration of MA is shifted towards higher values (around 34°C). VPTT of PNIPAAm in semi- and full-IPN hydrogels is not affected by the presence of alginate chains. Pure PNIPAAm microbeads of less crosslinked network feature higher ESR than those of more crosslinked network. PNIPAAm/MA copolymer hydrogel microbeads exhibit higher ESR than pure PNIPAAm microbeads with the same NIPAAm/MBAAm ratio. The joint feature of all synthesized microbeads in the presence of emulsifier is porous, honeycomb-like structure with the pore size of around 4 μm . Large open pores indicate existence of interconnected channels making favorable structure for drug release applications.

Regular spherical thermosensitive hydrogel microbeads obtained by inverse suspension polymerization could be considered as potential matrices in drug release studies. The intended application of these microbeads includes design of a textile-based system for transdermal release of a drug in a controlled manner, via temperature changes. Hence, optimization of synthesis conditions should be considered in the future steps with the aim of obtaining even smaller microbeads (below 20 μm) based on PNIPAAm and alginate for easier application on a textile material. This could be achieved by the adjustment in the stirring rate and reaction temperature.

**Chapter VI : CONTROLLED DRUG RELEASE FROM
THERMOSENSITIVE HYDROGEL MICROBEADS**

The applicability of selected thermosensitive hydrogel microbeads in controlled release of procaine HCl will be investigated in this Chapter. The first part of studies will refer to two types of thermosensitive hydrogel microbeads obtained by electrostatic extrusion, semi-IPN-0.1-1 and semi-IPN-0.25-1. These microbeads are chosen to estimate the impact of the fraction of PNIPAAm on overall hydrogel thermosensitivity and the drug release profiles at different temperatures. In the second part of the Chapter, the drug release from the thermosensitive hydrogel microbeads obtained by inverse suspension polymerization will be studied. Pure PNIPAAm (M-25/1) and full-IPN PNIPAAm/CA hydrogel microbeads (M-25/1-CA 1) will be used for the drug loading and release to estimate the impact of CA on the drug release profiles at temperature below and above VPTT of the hydrogel microbeads.

Two methods of drug release will be applied. The first one is a dissolution test method usually used for formulations intended for oral application and it will be employed for the microbeads prepared using electrostatic extrusion. For the second microbead type, a Franz diffusion cell will be used as a valid standard for testing of pharmaceutical formulations intended for transdermal applications.

VI.1 Thermosensitive hydrogel microbeads obtained by electrostatic extrusion

The drug release experiments were performed using two types of hydrogel microbeads: semi-IPN-0.1-1 and semi-IPN-0.25-1 that were described and characterized in Chapter IV, section IV.2. These microbeads differ in the fraction of PNIPAAm (0.1 and 0.25 wt %). The drug used was procaine HCl. Drug release experiments were conducted at two temperatures, above (40°C) and below (23°C) VPTT of the microbeads, according to the procedure described in Chapter II, section II.5.1.2.

VI.1.1 Drug loading

Initially, two calibration curves were determined using UV spectrophotometer, for solutions of procaine HCl in distilled water and in 1 mol dm⁻³ sodium citrate. Sodium citrate solution was used for destruction of drug-loaded microbeads in order to determine the overall amount of drug in the hydrogel matrix. Calibration curves in Figure VI.1-a,b show that the citrate salt had negligible influence on the absorbance of the drug in comparison with water.

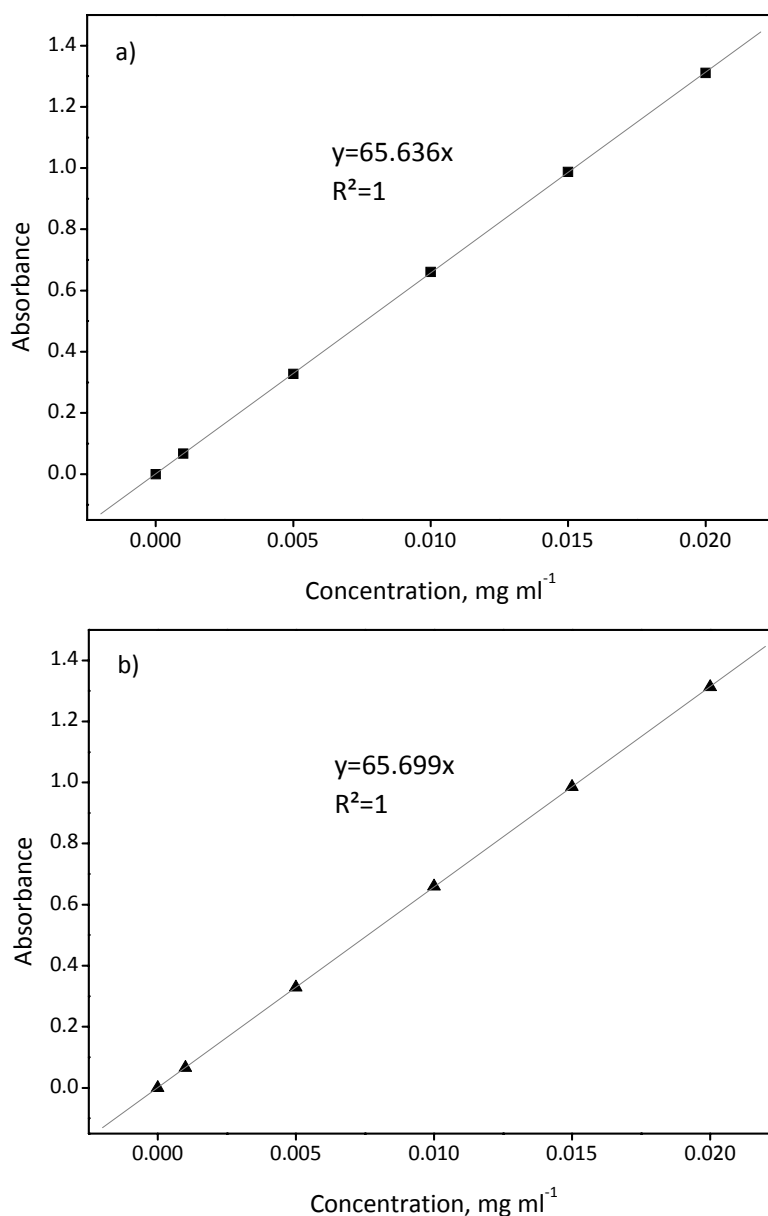


Figure VI.1. Calibration curves of procaine HCl solution in water (a) and sodium citrate (b)

Analysis of the efficiency of drug loading in the two semi-IPN hydrogels showed the impact of PNIPAAm concentration. Higher amount of procaine HCl entrapped in the microbeads with lower amount of PNIPAAm in semi-IPN-0.25-1. If the drug loading or total drug uptake is expressed as the weight of the loaded drug per dry weight of polymer matrix (xerogel), we obtained 0.86 mg mg^{-1} for semi-IPN-0.1-1 microbeads and 0.54 mg mg^{-1} for semi-IPN-0.25-1. A lower concentration of PNIPAAm in semi-IPN-0.1-1 results in looser resulting network, making it less compact and more favorable for the drug sorption/entrapment. Another explanation could be found in the pH value of the loading solution of procaine HCl that equaled to 6.9. This implies the presence of the positively charged form of the drug in the solution, since its pKa value is found to be 8.9-9.3 [303, 304]. Calcium alginate network contains polymer chains composed of guluronate and mannuronate residues, bearing carboxylate groups. Their negative charge contributes to the enhancement of the drug sorption efficiency from the loading solution into the hydrogel matrix (pKa for mannuronic and guluronic acid monomers are reported as 3.38 and 3.65, respectively [106]). The amount

of the drug loaded is thus dependent on the amount of linear component (PNIPAAm) in semi-IPNs, as confirmed by the lower total drug uptake by the hydrogel microbeads with a lower PNIPAAm content.

VI.1.2 Drug release using dissolution test

Release from the semi-IPN hydrogel microbeads obtained by electrostatic extrusion was studied by dissolution test, as described in Chapter II. The obtained drug release profiles are displayed in Figure VI.2. In all cases, the largest fraction was released during the first 30 minutes. The initial burst release of procaine HCl is attributed to the presence of surface immobilized, loosely attached drug molecules.

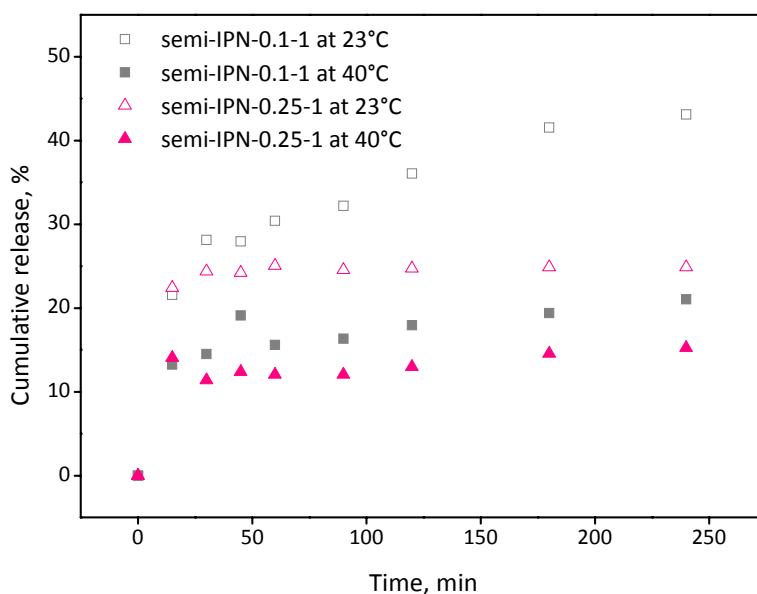


Figure VI.2. Release profile of procaine HCl from semi-IPN-0.1-1 and semi-IPN-0.25-1 at 23°C and 40°C

Results show that the beads with higher amount of PNIPAAm (semi-IPN-0.25-1) released lower amount of drug, partly because of a lower amount of polymer chain per unit volume of the network. At the end of the investigated period at 23°C, the difference in cumulative release was almost 20 % between the two types of microbeads. This difference is due to higher amount of drug initially loaded into semi-IPN-0.1-1 microbeads and hence, higher concentration gradient leading to a more pronounced drug release. Also, the semi-IPN-0.1-1 microbeads were smaller (section IV.2, Chapter IV) and hence featured higher specific surface area, i.e. an increased polymer-water interface that favors drug diffusion.

A dependence of drug release rate on temperature of releasing medium is clearly observed. Above VPTT, the microbeads are in shrunken form and show lower drug release compared to beads below VPTT. This is probably due to the collapse of PNIPAAm chains during volume phase transition that causes the entrapment of the drug within the matrix, stopping the drug diffusion process. In addition, possible reasons for this reduced release are enhanced ionic interactions between positively charged form of the drug and negative carboxylate groups in alginate chain, which become more exposed at 40°C, owing to this collapse of PNIPAAm chains.

It should be pointed out that majority of mathematical models developed to describe the drug release profiles are valid for only for early-time data points [305]. Our release profiles show that there were insufficient data points below 60 % release to provide accurate values of applicable models' parameters.

VI.2 Thermosensitive hydrogel microbeads obtained by inverse suspension polymerization

Drug release studies from selected hydrogel microbeads obtained by inverse suspension polymerization were performed using Franz diffusion cell with jacketed donor and receptor chamber. The drug release profiles obtained at two temperatures of donor chamber (25°C and 37°C) were compared to analyze the impact of microbeads thermosensitivity on the drug release pattern.

VI.2.1 Drug loading

Total uptake of procaine HCl was expressed as the weight ratio of loaded drug and the dry gel, i.e. polymer matrix. This value depends on the interaction of a drug with polymer matrix, the compact structure of the hydrogel, swelling ratio, the surface area of the individual microbeads (microbeads size), etc. Three types of the microbeads were chosen for loading tests: pure PNIPAAm hydrogel microbeads (M-25/1 and M-100/1), PNIPAAm/MA copolymer hydrogel microbeads (M-25/1-MA 2.5), and full-IPN PNIPAAm/CA hydrogel microbeads (M-25/1-CA 0.5 and M-25/1-CA 1). Obtained values of total drug uptake are presented in Figure VI.3.

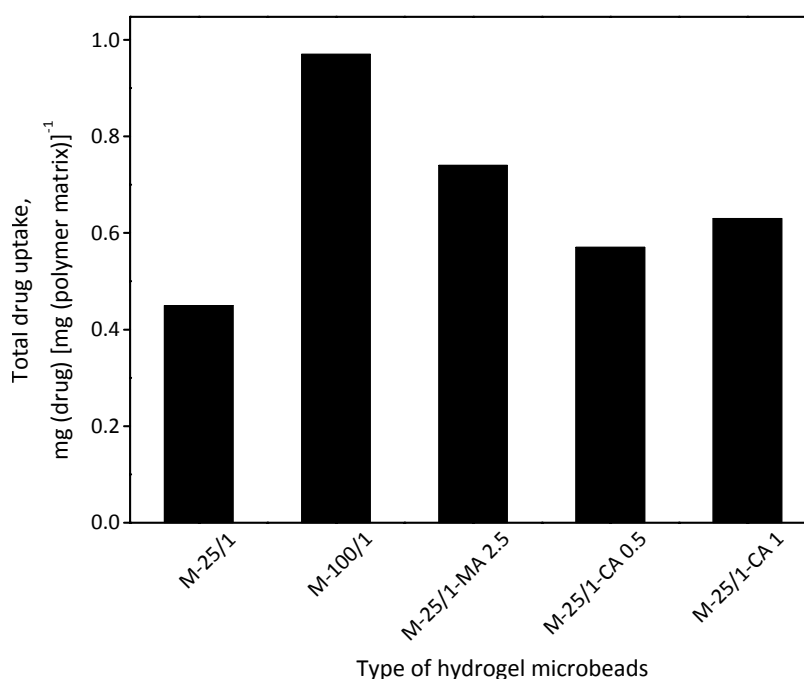


Figure VI.3. Total drug uptake by thermosensitive hydrogel microbeads obtained by inverse suspension polymerization

The lowest amount of drug was loaded into the pure PNIPAAm hydrogel microbeads with the highest crosslinking degree, M-25/1. On the other hand, the highest total drug uptake was obtained for the microbeads M-100/1 that are characterized by the loosest PNIPAAm network. The formation of IPN microbeads with alginate resulted in improved drug uptake with respect to M-25/1, and it slightly depends on the fraction of hydrophilic interpenetrant, CA.

Table VI.1 gives the comparison of the total drug uptake and the microbeads mean diameter obtained by laser diffraction measurements. It is known that smaller size of microbeads contributes to higher amount of drug uptake due to higher surface area of microbeads. However, this was not the case in our study since the selected microbeads types featured different structures. Therefore, the composition of hydrogel network could be regarded as a more influential parameter on the amount of drug loaded into the microbeads with respect to their mean diameter.

Table VI.1. Values of total drug uptake of selected hydrogel microbeads, volume-weighted mean diameter, and ESR values

Sample	Total drug uptake, mg(drug)/mg(polymer matrix)	D, μm	ESR (25°C)
M-25/1	0.45	20.7	15.0
M-100/1	0.97	31.8	27.5
M-25/1-MA 2.5	0.74	20.7	18.7
M-25/1-CA 0.5	0.57	67.8	33.5
M-25/1-CA 1	0.63	76.8	29.3

The swelling capacity of hydrogel microbeads could also affect the amount of drug uptake when the loading process is performed via sorption of drug solution by dry microbeads. The values of ESR were previously determined at 25°C (section V.6.1 of the Chapter V), which corresponds to temperature of the drug loading process. The impact of ESR values on total drug uptake could be compared for the microbeads M-25/1 and M-100/1 because they have the same composition (pure PNIPAAm network). The ESR values given in Table VI.1 indicate that almost two-fold higher ESR of M-100/1 results in double increase in total drug uptake. Difference in mean diameter is obviously too low to have substantial impact on the drug loading into these microbeads. The PNIPAAm/MA copolymer hydrogel microbeads (M-25/1-MA 2.5) could be compared to M-25/1, concerning the PNIPAAm crosslinking degree (25/1) and mean diameter. The difference in total drug uptake between these two microbeads types (0.74 mg mg⁻¹ and 0.45 mg mg⁻¹, respectively) is primarily caused by the presence/absence of hydrophilic comonomer. The pH value of 10 mg ml⁻¹ solution of procaine HCl, used for loading, was 6.6. The first and second dissociation constants of maleic acid are pK_{a1}=1.85 and pK_{a2}=6.06 respectively [306]. Hence, ionized form of hydrophilic comonomer in the matrix of M-25/1-MA 2.5 provided additional interactions with ionized form of procaine HCl molecules. Thus, the amount of loaded drug in PNIPAAm/MA copolymer hydrogel microbeads was higher than in the M-25/1 microbeads.

Full-IPN PNIPAAm/CA hydrogel microbeads (M-25/1-CA 0.5 and M-25/1-CA 1) are characterized by higher total drug uptake than corresponding pure PNIPAAm hydrogel microbeads (M-25/1). The reason for this is partly related to considerably higher ESR values of full-IPN microbeads than of M-25/1, and partly to their IPN structure with CA alginate as hydrophilic interpenetrant. In addition, the pH of loading solution was well above the pK_a for mannuronic and guluronic acid residues of alginate chains (3.38 and 3.65, respectively [106]). However, the total drug uptake of full-IPN microbeads was lower than of PNIPAAm/MA copolymer microbeads, although the amount of carboxylate groups in full-IPN microbeads was considerably higher than in copolymer microbeads, according to much higher amount of SA than MA in the preparation mixture (Table II.10 of the Chapter II). In addition to considerably higher size of full-IPN microbeads that affects lower drug uptake, their tight structure with smaller mesh size contributes lower loading capacity in comparison with M-25/1-MA 2.5. Finally, the higher the alginate content is, the higher total drug uptake will be.

VI.2.2 Drug release using Franz diffusion cell

Two microbead types were chosen for the drug release study using Franz diffusion cell: the pure PNIPAAm hydrogel microbeads with the highest crosslinking density and full-IPN PNIPAAm/CA hydrogel microbeads with higher amount of alginate. The microbeads M-25/1 showed temperature-positive drug release behavior, i.e. enhanced release rate at higher temperatures (Figure VI.4-a,b). This dependence of drug release pattern on temperature is in direct relation with difference in the arrangement of PNIPAAm chains at temperatures below and above VPTT of the hydrogel microbeads. In pure PNIPAAm network, strong collapse of polymer chains at higher temperature results in squeezing-out effect and hence higher drug release [170]. Furthermore, enhanced drug release at 37°C is partly a consequence of different strength of interactions between the drug molecules and the polymer chains at 37 and 25°C. At temperatures above VPTT of the hydrogel, hydrophobic interactions among PNIPAAm chains are dominant and affect weakening of the interactions of hydrophilic drug molecules with the hydrophilic segments of PNIPAAm chains. When exhibiting volume phase transition, the isopropyl groups of PNIPAAm are oriented toward the aqueous environment [307]. Thus, the amide groups are hidden and the interactions with the drug molecules are weakened. The situation is different at temperatures below VPTT of the hydrogel when the hydrophilic interaction among the procaine HCl and hydrophilic segments of PNIPAAm chains are strengthened. When predicting an on-off drug release from these pure PNIPAAm hydrogel microbeads by subsequent alteration of temperature, drug pulse at higher temperatures could be expected governed by a squeezing-out effect after the chain collapse.

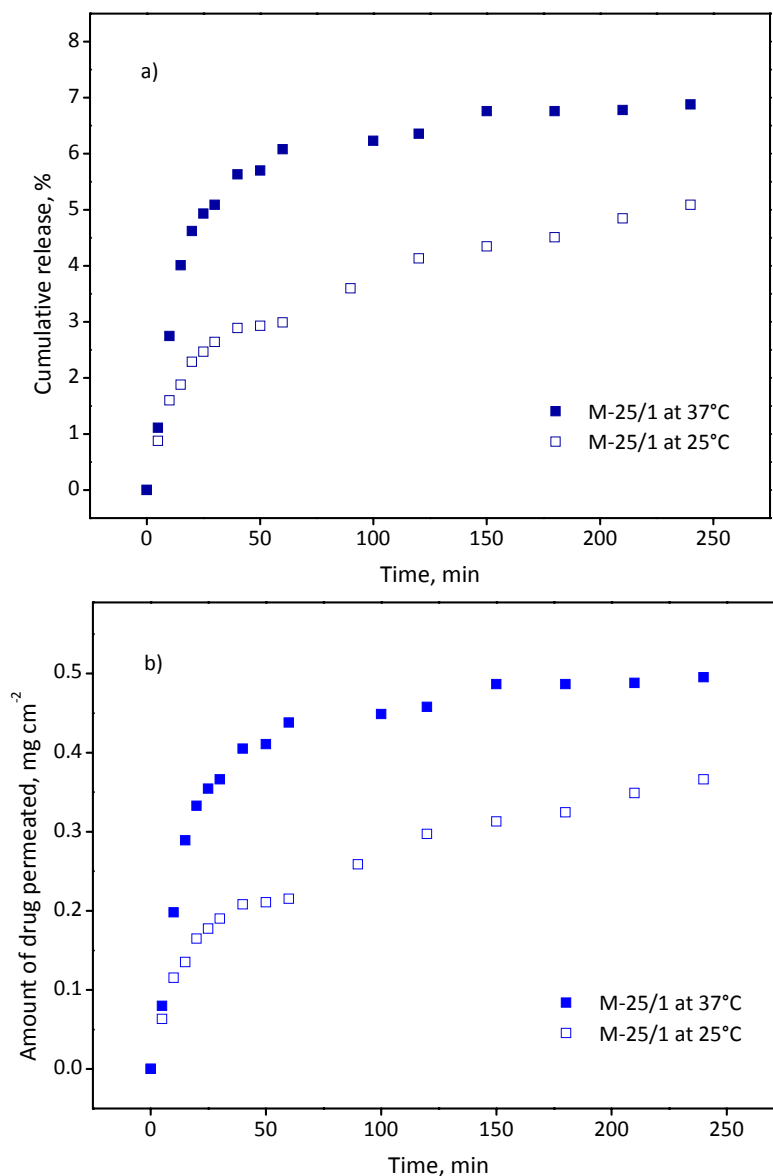


Figure VI.4. Release profiles of procaine HCl from the microbeads M-25-1 at 25°C and 37°C: cumulative release vs. time (a) and amount of drug permeated vs. time (b)

Drug-loaded hydrogel microbeads of full-IPN structure, M-25/1-CA 1 were employed in the second series of drug release studies. This microbeads type did not show such distinctive behavior between release at 25°C and at 37°C as pure PNIPAAm hydrogel microbeads did (Figure VI.5-a,b). The release profile of procaine HCl at both temperatures exhibits two stages, before and after the first hour of measurements. Rate of drug release was moderately higher at 37°C in the initial period whereas the opposite was observed in the second, third, and fourth hour of release. When analyzing the mechanism of drug release, dependence of drug diffusivity on temperature should be taken into consideration. According to Arrhenius relationship, diffusivity of drug molecule increases with increase in temperature [308]. Slightly faster release of drug at 37°C than at 25°C in first 60 min could be ascribed to temperature differences that affect faster diffusion of drug molecules distributed on the surface of the microbeads. Supposing the main part of drug diffused from the microbeads surfaces, the following stage of release profile originates from the drug entrapped within the polymer matrices. From that point onward, the structure of hydrogel

probably becomes the predominant factor of the drug release process. The hydrophobic interactions within polymer matrix of full-IPN structure are not pronounced enough to impact the interactions of drug with polymer chains as was the case with pure PNIPAAm hydrogel microbeads. Hence, contribution of smaller hydrogel mesh size at 37°C becomes the leading factor in rate of drug release. The result is slightly higher drug release at temperature below VPTT of the microbeads.

Generally similar release rate at given temperatures could also indicate slower/weak domination of hydrophobic interactions at 37°C than at 25°C. In other words, differences in PNIPAAm chains conformations at these two temperatures are moderate primarily due to the presence of CA as non-thermosensitive interpenetrant in the full-IPN structure. Although VPTT of the microbeads M-25/1-CA 1 is around 32°C (Table V.7, Chapter V), weakened thermosensitivity of polymer matrix results in insufficiently strong collapse of PNIPAAm network that could more strongly affect the drug transport.

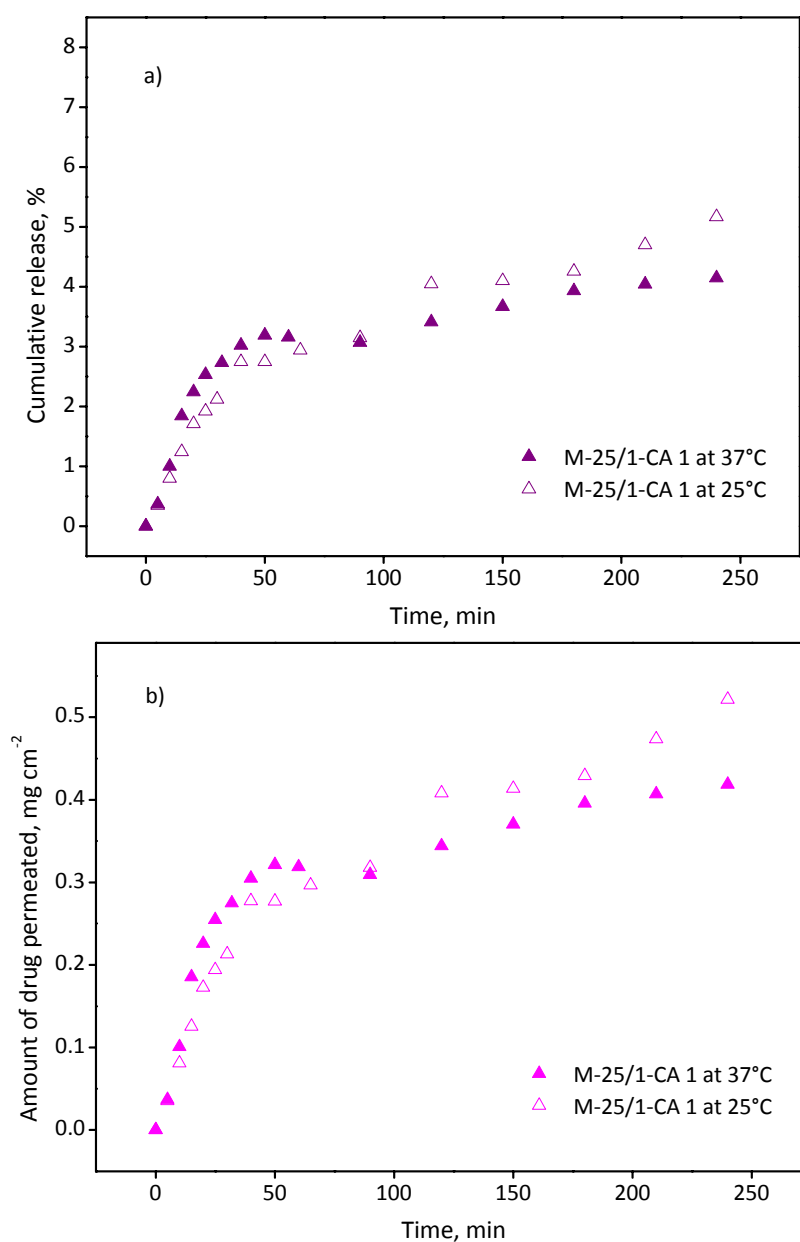


Figure VI.5. Release profiles of procaine HCl from the microbeads M-25-1/CA 1 at 25°C and 37°C: cumulative release vs. time (a) and amount of drug permeated vs. time (b)

When considering small size of procaine HCl molecule ($M_w=272.77$), low percentage of cumulative release from both types of microbeads is obtained after the 4h-experiment with Franz diffusion cell (Figure VI.4 and Figure VI.5). Such weak release of the procaine HCl is probably the consequence of strong interactions between drug molecules and polymer matrix. It is assumed that the ionized (cationic) form of the drug is present in our system, according to literature data [159]. Although the PNIPAAm chains are expected to be nonionic, an anionic residue ($-SO_4^-$) of the initiator (APS) probably remains at the chain ends [51]. This implicates possibility of establishment of attractive interactions between the drug and ionized side groups of the hydrogel. In the case of full-IPN microbeads, there is possible additional contribution of carboxylate groups of alginate that could interact with the drug molecules (apart from the cooperative binding with calcium ions). It is obvious that the presence of alginate chains induces the difference in drug release profiles when comparing to the pure PNIPAAm microbeads at temperatures below and above their VPTT of the hydrogels. Lower cumulative release of drug from the microbeads M-25/1-CA 1 than from M-25/1 could be partly ascribed to the stronger adsorption properties of the former structure toward the procaine HCl molecules. In addition, almost four times higher mean diameter of M-25/1-CA 1 than of M-25/1 (Table V.6) signifies increased diffusional path length for drug molecules and hence slower drug release.

VI.2.3 Drug release mechanism

The early-time release data could be fitted to an empirical relationship to determine whether a particular device is diffusion-controlled or not. An empirical power equation developed by Peppas [309] was applied for analysis of procaine HCl release mechanism from the hydrogel microbeads (Equations VI.1 and VI.2).

$$\frac{M_t}{M_\infty} = kt^n \quad (VI.1)$$

$$\log \frac{M_t}{M_\infty} = n \log t + \log k \quad (VI.2)$$

Where M_t and M_∞ are the absolute cumulative amount of drug released at time t and at infinite time (initially loaded), k is a structural/geometric or rate constant for a particular system and n is a release exponent representing the release mechanism. The parameters k and n were calculated from the initial 60 % of cumulative release curve [159]. Figure VI.6 displays linear fits for the early-time release data according to Peppas model.

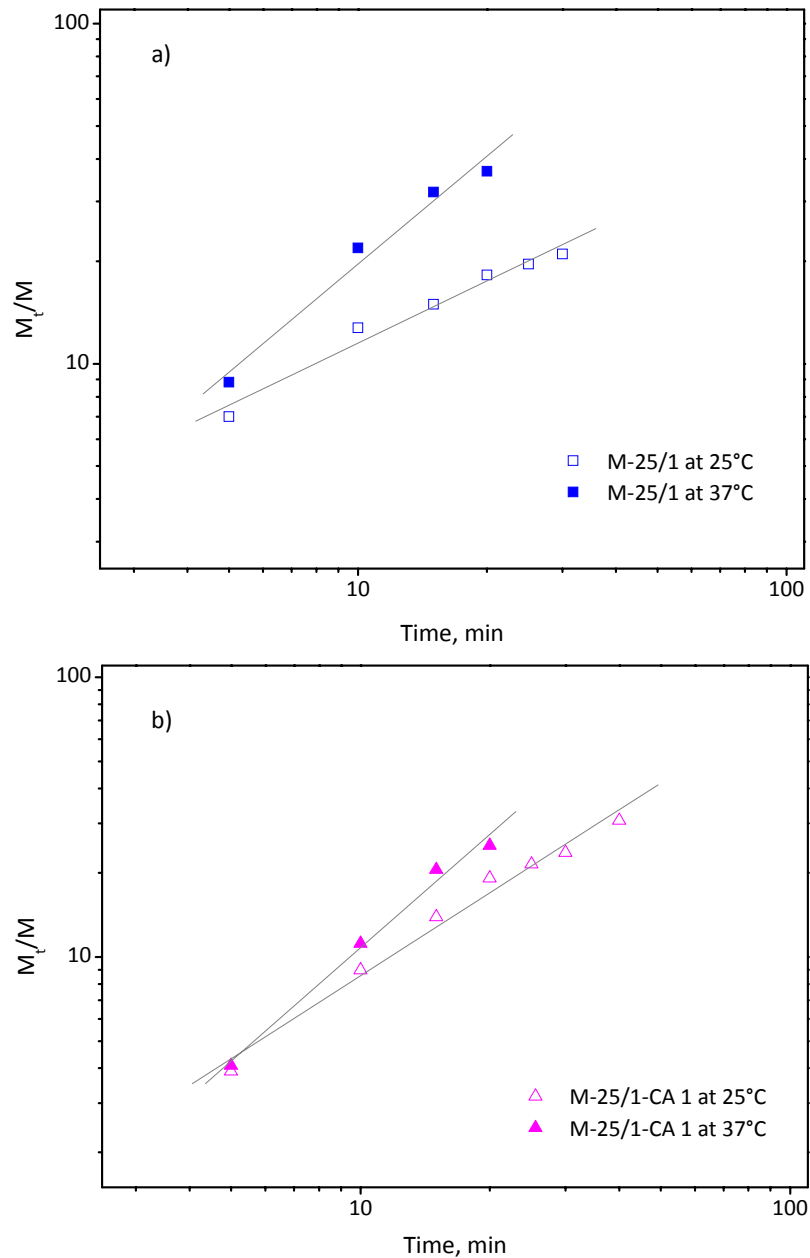


Figure VI.6. Plots of $\log (M_t/M_\infty)$ against $\log t$ for the microbeads M-25/1 (a) and M-25/1-CA 1 (b) at 25°C and 37°C

Table VI.2 summarizes calculated release exponent values of Peppas model for the procaine HCl release from both microbeads types at 25°C and 37°C. Values of correlation exponent ($R^2=0.986-0.995$) show that fit of experimental data using the applied model is satisfying. When the matrix geometry is a sphere, diffusion-controlled drug release corresponds to $n=0.43$ and it is called Fickian diffusion, whereas for $n=0.85$ case-II transport, release is governed by the polymer matrix relaxation and characterized by independence of drug release rate on drug concentration [84, 310]. When the value of release exponent is between 0.43 and 0.85, the mechanism of transport is non-Fickian or anomalous. This means that drug diffusion and the polymer relaxation are comparable, i.e. drug release is both, diffusion- and swelling-controlled. Super case II mechanism is present when $n>0.85$ and is related to the polymer relaxation during hydrogel swelling and suggests the drug release by more than one mechanism [311].

Table VI.2. Release exponent (n) and correlation coefficient (R^2) for drug release from the microbeads M-25/1 and M-25/1-CA 1 at 25°C and 37°C

Sample	Temperature, °C	n	R^2	Mechanism
M-25/1	25	0.61	0.986	Anomalous
	37	1.05	0.988	Super case II
M-25/1-CA 1	25	0.99	0.992	Super case II
	37	1.35	0.995	Super case II

Obtained data show the absence of pure diffusion-controlled mechanism. Release of procaine HCl from M-25/1 microbeads at 25°C could be classified under non-Fickian or anomalous transport since $0.43 < n < 0.85$. Other analyzed cases belong to super case II transport, that is, a type of swelling-controlled system. The rate of drug diffusion is dependent on the concentration and time but also on the rate of swelling and relaxation of the polymer chains, i.e. the rate of solvent uptake [312]. The value of n for full-IPN microbeads is higher than for the pure PNIPAAm microbeads, indicating that in more compacted hydrogels, chains relaxation facilitates the drug transport. This was observed for BSA release from various bulk PNIPAAm/CA full-IPN hydrogels [169]. Therefore, procaine HCl release could be modified by changing the hydrogels structure and swelling behavior, which is the leading idea in designing efficient and controllable drug release vehicles.

VI.3 CONCLUSIONS

Release studies of procaine HCl from the thermosensitive microbeads prepared by electrostatic extrusion resulted in retarded release at 40°C compared to 23 °C. This could be caused by stronger entrapment of the drug in the deswelled matrix, as a consequence of the collapse of PNIPAAm chains. Higher the amount of PNIPAAm linear chains in these semi-IPN microbeads, lower the drug loading efficiency will be but also the cumulative amount of drug release due to lower intensity of interactions between drug molecules and hydrogel matrix. Drug release from thermosensitive microbeads using Franz diffusion cell showed that release of procaine HCl could be tuned by modifying the PNIPAAm network. Incorporation of CA in PNIPAAm network resulted in slightly temperature-negative drug release pattern in comparison with temperature-positive drug release from the pure PNIPAAm hydrogel microbeads. Fitting of release data was successfully achieved by application of Peppas model. The mechanism of drug release is in all cases dependent on microbeads swelling behavior and not solely on diffusion. Increasing the temperature above VPTT of the hydrogel microbeads contributes to stronger dependence of drug transport on polymer relaxation process. Low cumulative release of drug should direct further research in revealing the nature of drug-hydrogel interactions that could help to understand and predict the drug release pattern. Initial results of drug release studies implicate potential applicability of the analyzed thermosensitive hydrogel microbeads in development of transdermal delivery systems controlled by temperature changes.

GENERAL CONCLUSIONS

GENERAL CONCLUSIONS

The topic of this thesis encompassed development and characterization of macro and micro forms of thermosensitive hydrogels intended for the future applications in controlled delivery of drugs via transdermal route. As already known, a crucial parameter in controlling the swelling behavior of the developed hydrogels, and hence the rate of drug release, is temperature. Hence, temperature of the volume phase transition should be near the temperature of the human skin surface. In addition, among the high-priority prerequisites in design of a material for this biomedical use are biocompatibility, good mechanical properties, and fast response to temperature changes. Therefore, synthetic polymer poly(*N*-isopropylacrylamide) (PNIPAAm) and natural polysaccharide alginate were chosen as main components for preparation of the hydrogels with desired properties. It was shown that synergistic properties of these components could be successfully achieved by formation of the interpenetrating polymer networks (IPNs). Such hybrid materials were developed in the form of films and microbeads taking into consideration their future application on a heating textile material, i.e. formation of hydrogel/textile systems in the form of intelligent patch.

Thermosensitive hydrogel microbeads are far less studied physical forms regarding their application on textile materials than thermosensitive hydrogel films. However, in the field of controlled drug release, micro forms of hydrogels feature mutual benefits over the macro forms. Thermosensitive hydrogel microbeads have faster response to temperature changes and better swelling properties. This is in direct relation with their high drug loading capacities. Their size can be easily controlled by adjusting synthesis conditions, directly impacting drug diffusional pathway during the release. However, application of hydrogel microbeads on textile materials is more demanding and complex task than of hydrogel films. Taking into consideration their advantages and shortcomings, work presented in this thesis referred to both physical forms of thermosensitive hydrogels, with accent on thermosensitive hydrogel microbeads and their applicability in the controlled drug release. Table C-1 represents the comparison of general characteristics of developed macro and micro forms of thermosensitive hydrogels of various structures.

Characterization of full-IPN hydrogel films composed of crosslinked PNIPAAm and crosslinked alginate (calcium alginate, CA) demonstrated their advantages over pure PNIPAAm hydrogels films. Adjusting the alginate content at 1 wt % in full-IPN hydrogels resulted into better swelling capacity than pure PNIPAAm hydrogels at temperatures below their VPTT. They also exhibit the most rapid response to temperature increase from 25°C up to 40°C in comparison with other studied hydrogels. The full-IPN hydrogels based on 1 wt % of alginate feature more porous network comparing to pure PNIPAAm hydrogels at 23°C. In comparison with pure PNIPAAm, these hydrogels feature better mechanical properties, greater pore sizes and improved swelling behavior, i.e. response to temperature changes. The presented results qualify thermosensitive full-IPN hydrogels based on PNIPAAm and CA as potential matrices intended for a controlled release of drugs. Performed syntheses and characterizations of hydrogels are good base for additional study on their combination with heating textiles as a part of drug delivery system for transdermal applications.

Formation of thermosensitive hydrogel microbeads was conducted in two manners and of different network structures:

- a) semi-IPN with linear PNIPAAm and crosslinked alginate,
- b) semi-IPN with crosslinked PNIPAAm and linear alginate, and
- c) full-IPN with crosslinked both, PNIPAAm and alginate.

Electrostatic extrusion was employed for the formation of thermosensitive hydrogel microbeads with the semi-IPN structure containing linear PNIPAAm and crosslinked alginate (CA). This spray technique was demonstrated to be a complex function of operating parameters when aiming at formation of the semi-IPN microbeads below 20 μm in diameter and of regular spherical shape. Droplet diameter is affected by applied voltage between the electrodes. Up to a certain value of voltage, the droplet diameter decreases with voltage increase. When the voltage is further increased, small microbeads (below 50 μm in diameter) are formed along with bigger microbeads (>100 μm) of irregular shape. The formation of two fractions of microbeads sizes is a result of the increase in voltage beyond a certain (critical) value. In order to produce microbeads of uniform and spherical shape, applied voltage should be set below but close to the critical region of voltage values. The other important parameter is the flow rate whose decrease is favorable for formation of smaller microbeads. When aqueous polymer solution with 0.1 wt % PNIPAAm and 1 wt % SA are used for the extrusion in an electric field, the most optimal hydrogel microbeads regarding the size and roundness were obtained using 27g-needle and under the voltage of 12 kV, electrode spacing of 8 cm and flow rate of 0.397 ml h^{-1} . Their mean diameter reached even 10.9 μm .

Another method applied in synthesis of series of thermosensitive hydrogel microbeads based on crosslinked PNIPAAm was inverse suspension polymerization. In addition to preparation of semi- and full-IPN hydrogel microbeads with linear and crosslinked alginate, respectively, the copolymer hydrogel microbeads of PNIPAAm and maleic anhydride (MA) were also developed, supposing the contribution of MA for easier application of microbeads on a textile material in future research. The optimization of formulation parameters showed that increase in volume ratio of oil to aqueous phase, absence of emulsifier, and lower fraction of crosslinker cause a decrease in mean diameter of the pure PNIPAAm hydrogel microbeads. The smallest microbeads obtained were pure PNIPAAm hydrogel microbeads with the highest crosslinking degree and their mean diameter equaled 20.1 μm . However, addition of alginate affects considerable increase in microbeads size (three to four-fold increase) while the presence of MA in chosen concentrations has only slight contribution. VPTT of PNIPAAm in semi- and full-IPN hydrogel microbeads is not affected by the presence of alginate chains and equals around 33°C. VPTT of PNIPAAm/MA copolymer hydrogel microbeads with the lowest concentration of MA is shifted toward higher values (around 1°C) in comparison with pure PNIPAAm hydrogel whereas higher concentrations of MA weaken thermosensitivity of resulting copolymer hydrogels. The joint morphological feature of all synthesized microbeads is honeycomb-like structure and existence of interconnected channels that are favorable for the drug release applications. Hence, optimization of synthesis conditions should be considered with the principle of obtaining smaller microbeads based on PNIPAAm and alginate for easier application on a textile material. This could be achieved by adjusting reaction conditions such as the stirring rate and reaction temperature.

Table C-1. Comparison of general characteristics of various physical forms and structures of developed thermosensitive hydrogels

	Films - polymerization in solution	Microbeads - Electrostatic extrusion -	Microbeads - inverse suspension polymerization
Structure	Full-IPN crosslinked PNIPAAm + CA	Semi-IPN linear PNIPAAm + CA	Semi-IPN crosslinked PNIPAAm + SA Full-IPN crosslinked PNIPAAm + CA
Swelling characteristics - ESR at 25°C -	14-25	30-33	16-29
Pore size	10-87 μm	-	3-5 μm
Thermal characteristics - VPTT -	$\approx 35^\circ\text{C}$	$\approx 30^\circ\text{C}$	$\approx 33^\circ\text{C}$

Drug release studies from the selected thermosensitive hydrogel microbeads obtained by inverse suspension polymerization were conducted using a Franz diffusion cell. It was shown that loading and release of procaine HCl could be tuned by modifying the PNIPAAm network. Incorporation of CA in PNIPAAm network resulted in slightly temperature-negative drug release pattern in comparison with temperature-positive drug release from the pure PNIPAAm hydrogel microbeads. Fitting of release data was successfully achieved by application of Peppas power law equation. The mechanism of drug release in all cases is governed by polymer chains relaxation process and not solely on diffusion. Increasing the temperature above VPTT of the hydrogel microbeads contributes to stronger dependence of drug transport on swelling behavior. Low cumulative release of drug should direct further research in revealing the nature of drug-hydrogel interactions that could help to understand and predict the drug release pattern. The results of drug release studies implicate potential applicability of the analyzed thermosensitive hydrogel microbeads in applications such as transdermal delivery systems controlled by temperature changes.

The continuation of the research encompassed by this thesis should be realized in several directions. First of all, optimization of conditions of inverse suspension polymerization in formation of hydrogel microbeads with semi- and full-IPN structure, based on PNIPAAm and alginate, should be continued. Operating parameters whose values could considerably impact diameter reduction of such hydrogel microbeads are stirring rate and preparation temperature. Higher stirring rate and higher temperature are expected to result in smaller microbeads. Also, lowering fraction of sodium alginate in initial reaction mixture could contribute to formation of smaller microbeads, close to the average fiber diameter. Furthermore, detailed study on drug release properties of thermosensitive hydrogel microbeads should be continued using Franz diffusion cell. Nature of interactions between drug and hydrogel matrix should be further elucidated. Also, consideration of testing another model drug could be taken into account.

Finally, there are various approaches in the design of the heating textile/thermosensitive hydrogel system, as a leading idea of conducted research. One of the possible procedures in the formation of thermosensitive hydrogel layer on the surface of the textile material is pad drying of polymer solution and subsequent crosslinking of this polymer layer on the textile to form hydrogel (Figure C-1).

Attachment of thermosensitive hydrogel microbeads on textile material seems to be a more demanding and challenging task. Up to our knowledge, there are no reports on these systems up to now. One of the possible ways in achieving such systems is to use of an adequate binder that will serve as a link between the hydrogel and the textile (Figure C-1). In addition, activation of the surface of textile material using plasma or corona treatment could result in considerably improved binding abilities and efficient application of hydrogel microbeads.

Another approach in attaching hydrogel microbeads to the textile surface is via grafting reaction (Figure C-1). Procedure of grafting of hydrogel microbeads is complex but seems to be more adequate for intended application of hydrogel/textile system as transdermal drug delivery vehicle. In comparison with use of a binder for attaching microbeads to textile material, grafting method provides better “access” of the drug loaded in the microbeads to diffuse to the skin surface. Also, contact of a binder with skin is not desirable due to possible irritation.

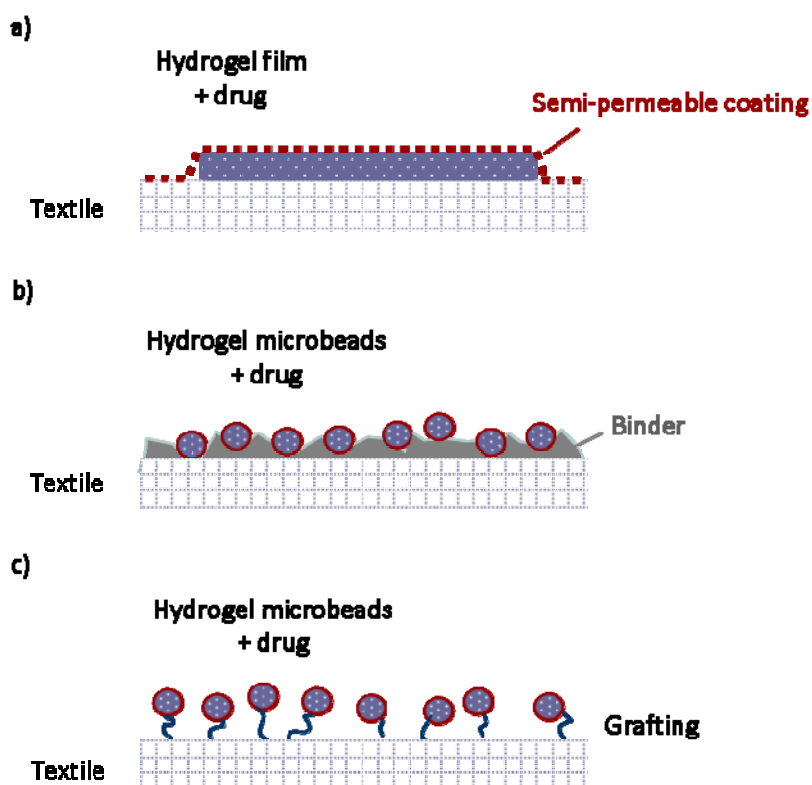


Figure C-1. Possible systems of thermosensitive hydrogels and textile material

Therefore, results of this doctoral thesis could serve as a good base for future research in several fields and open doors to significant achievements and innovations regarding intelligent textiles for biomedical applications.

REFERENCES

- [1] Wichterle, O.; Lim, D., *Nature*, (1960) **185**, 117.
- [2] Kopecek, J., *Biomaterials*, (2007) **28**, 5185.
- [3] El-Rehim, H. A. A., *Journal of Applied Polymer Science*, (2006) **101**, 3572.
- [4] Hoffman, A. S., *Advanced Drug Delivery Reviews*, (2002) **43**, 3.
- [5] Chen, K.-S.; Tsai, J.-C.; Chou, C.-W.; Yang, M.-R.; Yang, J.-M., *Materials Science and Engineering: C*, (2002) **20**, 203.
- [6] Xie, J. B.; Hsieh, Y. L., *Journal of Applied Polymer Science*, (2003) **89**, 999.
- [7] Kulkarni, A.; Tourrette, A.; Warmoeskerken, M. M. C. G.; Jovic, D., *Carbohydrate Polymers*, (2010) **82**, 1306.
- [8] Tourrette, A.; De Geyter, N.; Jovic, D.; Morent, R.; Warmoeskerken, M. M. C. G.; Leys, C., *Colloids and Surfaces A: Physicochemical and Engineering Aspects*, (2009) **352**, 126.
- [9] Djonlagic, J.; Petrovic, Z. S., *Journal of Polymer Science Part B: Polymer Physics*, (2004) **42**, 3987
- [10] Zhang, X. Z.; Wu, D. Q.; Chu, C. C., *Biomaterials*, (2004) **25**, 3793.
- [11] Muniz, E. C.; Geuskens, G., *Journal of Materials Science: Materials in Medicine*, (2001) **12**, 879.
- [12] Zhang, H.-f.; Zhang, L.-l.; Chen, S.-b.; Zhao, Y.-j.; Zhu, Y.-L.; Wang, J.-t., *Carbohydrate Polymers*, (2010) **79**, 131.
- [13] Moura, M. R.; Aouada, F. A.; Guilherme, M. R.; Radovanovic, E.; Rubira, A. F.; Muniz, E. C., *Polymer Testing*, (2006) **25**, 961.
- [14] Zhao, Q.; Sun, J.; Ling, Q.; Zhou, Q., *Langmuir*, (2009) **25**, 3249.
- [15] Sayil, C.; Okay, O., *Polymer*, (2001) **42**, 7639.
- [16] Fu, G.; Soboyejo, W. O., *Materials Science and Engineering C*, (2010) **30**, 8.
- [17] Varghese, J. M.; Ismail, Y. A.; Lee, C. K.; Shin, K. M.; Shin, M. K.; Kim, S. I.; So, I.; Kim, S. J., *Sensors and Actuators B: Chemical*, (2008) **135**, 336.
- [18] Ciofani, G.; Raffa, V.; Menciassi, A.; Micera, S.; Dario, P., *Biomedical Microdevices*, (2007) **9**, 395.
- [19] Kim, M. H.; Kim, J.-C.; Lee, H. Y.; Kim, J. D.; Yang, J. H., *Colloids and Surfaces B: Biointerfaces*, (2005) **46**, 57.
- [20] Wang, A.; Tao, C.; Cui, Y.; Duan, L.; Yang, Y.; Li, J., *Journal of Colloid and Interface Science*, (2009) **332**, 271.
- [21] Nobuhiko Yui, R. J. M., Kinam Park Ed. *Reflexive Polymers and Hydrogels: : understanding and designing fast responsive polymeric systems*, CRC Press LLC: Boca Raton, Florida, (2004).
- [22] Peppas, N. A., Hydrogels, In *Biomaterials Science: An Introduction to Materials in Medicine*, Ratner, B. D.; Hoffman, A. S.; Schoen, F. J.; Lemons, J. E. Eds.; Elsevier Academic Press: San Diego, California, (1996); 100.

- [23] Janusz M. Rosiak, F. Y., *Nuclear Instruments and Methods in Physics Research B*, (1999) **151**, 56.
- [24] Gerlach, G.; Arndt, K.-F. Eds., *Hydrogels Sensors and Actuators*, Springer-Verlag: Berlin, (2009).
- [25] Ratner, B. D.; Hoffman, A. S., *Synthetic Hydrogels for Biomedical Applications*, In *Hydrogels for Medical and Related Applications*, Andrade, J. Ed. American Chemical Society: Washington, DC, (1976); 1.
- [26] Satish, C. S.; Satish, K. P.; Shivakumar, H. G., *Indian Journal of Pharmaceutical Sciences*, (2006) **68**, 133.
- [27] Galaev, I.; Mattiasson, B. Eds., *Smart polymers: Applications in Biotechnology and Biomedicine*, CRC Press LLC: Boca Raton, Florida, (2008).
- [28] Ratner, B. D.; Hoffman, A. S.; Schoen, F. J.; Lemons, J. E. Eds., *Biomaterials Science: An Introduction to Materials in Medicine*, Elsevier Academic Press: San Diego, California, (1996).
- [29] Hennink, W. E.; Nostrum, C. F., *Advanced Drug Delivery Reviews*, (2002) **54**, 13.
- [30] Porter, T. L.; Stewart, R.; Reed, J.; Morton, K., *Sensors*, (2007) **7**, 1980.
- [31] Flory, P. J.; Rehner, B. D., *Journal of Chemical Physics*, (1943) **11**, 521.
- [32] Flory, P. J., *Proceedings of the Royal Society of London: Series A*, (1976) **351**, 351.
- [33] Flory, P. J., *Principles of Polymer Chemistry*, Cornell University Press: Ithaca, New York, (1953).
- [34] Peppas, N. A.; Leobandung, W., *Journal of Biomaterials Science, Polymer Edition*, (2004) **15**, 125.
- [35] Barbucci, R. Ed. *Hydrogels: Biological Properties and Applications*, Springer-Verlag Italia: Milan, (2009).
- [36] Gupta, P.; Vermani, K.; Garg, S., *Drug Discovery Today*, (2002) **7**,
- [37] Dušek, K.; Patterson, D., *Journal of Polymer Science Part A-2*, (1968) **6**, 1209.
- [38] Tanaka, T., *Physical Review Letters*, (1978) **40**, 820.
- [39] Yong Qiu, K. P., *Advanced Drug Delivery Reviews*, (2001) **53**, 321.
- [40] Klouda, L.; Mikos, A. G., *European Journal of Pharmaceutics and Biopharmaceutics*, (2008) **68**, 34.
- [41] Peppas, N. A.; Hilt, J. Z.; Khademhosseini, A.; Langer, R., *Advanced Materials*, (2006) **18**, 1345.
- [42] Kulkarni, R. V.; Sa, B., *Journal of Bioactive and Compatible Polymers*, (2009) **24**, 368.
- [43] Hsu, C. S.; Block, L. H., *Pharmaceutical Research*, (1996) **13**, 1865.
- [44] Kim, S. J.; Kim, H. I.; Park, S. J.; Kim, I. Y.; Lee, S. H.; Lee, T. S.; Kim, S. I., *Smart Materials and Structures*, (2005) **14**, 511.
- [45] Kaewpirom, S.; Boonsang, S., *European Polymer Journal*, (2006) **42**, 1609.
- [46] Tanaka, T.; Fillmore, J. D.; Sun, S.-T.; Nishio, I.; Swislo, G.; Shah, A., *Physical Review Letters*, (1980) **45**, 1636.
- [47] Messing, R.; Schmidt, A. M., *Polymer Chemistry*, (2011) **2**, 18.

- [48] Yoshida, R.; Okano, T., Stimuli-Responsive Hydrogels and Their Application to Functional Materials, In *Biomedical Applications of Hydrogels Handbook*, Park, K.; Okano, T. Eds.; Springer: New York, (2010).
- [49] Katayama, S.; Ohata, A., *Macromolecules*, (1985) **18**, 2781.
- [50] Okano, T.; Bae, Y. H.; Jacobs, H.; Kim, S. W., *Journal of Controlled Release*, (1990) **11**, 255.
- [51] Panayiotou, M., Doctoral Dissertation, *École Polytechnique Fédérale de Lausanne Lausanne*, (2005).
- [52] Taylor, L. D.; Cerankowski, L. D., *Journal of Polymer Science: Polymer Chemistry Edition*, (1975) **13**, 2551.
- [53] Boutris, C.; Chatzi, E. G.; Kiparissides, C., *Polymer*, (1997) **38**, 2567
- [54] Heskins, M.; Guillet, J. E., *Journal of Macromolecular Science*, (1968) **2**, 1441.
- [55] Dušek, K. Ed. *Responsive Gels: Volume Transitions II*, Springer-Verlag: Berlin, (1993).
- [56] Zhang, J.; Pelton, R.; Yulin Deng, Y., *Langmuir*, (1995) **11**, 2301.
- [57] Fujishige, S.; Kubota, K.; Ando, I., *Journal of Physical Chemistry*, (1989) **93**, 3311.
- [58] Xue W.; Hamley, I. W., *Polymer*, (2002) **43**, 3069.
- [59] Otake, K.; Inomata, H.; Konno, M.; Saito, S., *Macromolecules*, (1990) **23**, 283.
- [60] Schild, H. G.; Tirrell, D. A., *Journal of Physical Chemistry*, (1990) **94**, 4352.
- [61] Inomata, H.; Goto, S.; Saito, S., *Macromolecules*, (1990) **23**, 4887.
- [62] Lin, S.-Y.; Chen, K.-S.; Liang, R.-C., *Polymer*, (1999) **40**, 6307.
- [63] Kumara, A.; Srivastava, A.; Galaev, I.; Mattiasson, B., *Progress in Polymer Science*, (2007) **32**, 1205.
- [64] Hydrogels and Smart Polymers, In *Plastics Technology Handbook*, Chanda, M.; Roy, S. K. Eds.; Taylor & Francis Group, LLC: (2007); 117.
- [65] Yamada, N.; Okano, T.; Sakai, H.; Karikusa, F.; Sawasaki, Y.; Sakurai, Y., *Die Makromolekulare Chemie, Rapid Communications*, (1990) **11**, 571.
- [66] Katayama, Y.; Sonoda, T.; Maeda, M., *Macromolecules*, (2001) **34**, 8569.
- [67] Matsukata, M.; Aoki, T.; Sanui, K.; Ogata, N.; Kikuchi, A.; Sakurai, Y.; Okano, T., *Bioconjugate Chemistry*, (1996) **7**, 96.
- [68] Rzaev, Z. M. O.; Dincer, S.; Piskin, E., *Progress in Polymer Science*, (2007) **32**, 534.
- [69] Cai, W. S.; Gupta, R. B., *Industrial & Engineering Chemistry Research*, (2001) **40**, 3406.
- [70] Hoogenboom, R.; Thijs, H. M. L.; Jochems, M. J. H. C.; van Lankvelt, B. M.; Fijten, M. W. M.; Schubert, U. S., *Chemical Communications*, (2008) **44**, 5758.
- [71] Meunier, F.; Elaissari, A., Poly(N-isopropylacrylamide)-Based Particles: Preparation and Colloidal Characterization, In *Colloidal polymers: Synthesis and characterization*, Elaissari, A. Ed. Marcel Dekker, Inc.: New York, (2003); 111.
- [72] Lee, D. S.; He, C., In-Situ Gelling Stimuli-Sensitive PEG-Based Amphiphilic Copolymer Hydrogels, In *Biomedical Applications of Hydrogels Handbook*, Park, K.; Okano, T. Eds.; Springer: New York, (2010); 123.
- [73] Kawaguchi, H., Stimuli-Sensitive Microhydrogels, In *Biomedical Applications of Hydrogels Handbook*, Park, K.; Okano, T. Eds.; Springer: New York, (2010); 107.

- [74] Horne, R. A.; Almeida, J. P.; Day, A. F.; Yu, N. T., *Journal of Colloid and Interface Science*, (1971) **35**, 77.
- [75] Wu, C., *Polymer*, (1998) **39**, 4609.
- [76] Wang, K. L.; Burban, J. H.; Cussler, E. L., Hydrogels as Separation Agents, In *Responsive Gels. Volume Transitions II*, Dušek, K. Ed. Springer-Verlag: Berlin, (1993); 67.
- [77] DeRosa, M. E.; DeRosa, R. L.; Noni, L. M.; Hendrick, E. S., *Journal of Applied Polymer Science*, (2007) **105**, 2083.
- [78] Fujimoto, K.; Nakajima, Y.; Kashiwabara, M.; Kawaguchi, H., *Polymer International*, (1993) **30**, 237.
- [79] Pelton, R., *Journal of Colloid and Interface Science*, (2010) **348**, 673.
- [80] Zhang, X.-Z.; Zhuo, R.-X., *Materials Letters*, (2002) **52**, 5.
- [81] Tauer, K.; Daniel G.; Schulze, S.; Völkel, A.; Dimova, R., *Colloid and Polymer Science*, (2009) **287**, 299.
- [82] Marchetti, M.; Prager, S.; Cussler, E. L., *Macromolecules*, (1990) **23**, 3445.
- [83] Arndt, K.-F.; Richter, A.; Monch, I., Synthesis of Stimuli-Sensitive Hydrogels in the μm and sub- μm Range by Radiation Techniques and their Application, In *Hydrogels: Biological Properties and Applications*, Barbucci, R. Ed. Springer-Verlag: Milan, (2009); 121.
- [84] Lin, C. C.; Metters, A. T., *Advanced Drug Delivery Reviews*, (2006) **58**, 1379.
- [85] Soppimath, K. S.; Aminabhavi, T. M.; Dave, A. M.; Kumbar, S. G.; Rudzinski, W. E., *Drug Development and Industrial Pharmacy*, (2002) **28**, 957.
- [86] Anal, A. K., *Recent Patents on Endocrine, Metabolic & Immune Drug Discovery*, (2007) **1**, 83.
- [87] Gutowska, A.; Bae, Y. H.; Jacobs, H.; Feijen, J.; Kim, S. W., *Macromolecules*, (1994) **27**, 4167.
- [88] Zhang, J.-T.; Huang, S.-W.; Cheng, S.-X.; Zhuo, R.-X., *Journal of Polymer Science Part A: Polymer Chemistry*, (2004) **42**, 1249.
- [89] Choudhary, S.; Reck, J. M.; Bhatia, S. R., Hydrophobically Modified Alginate for Drug Delivery Systems, In *IEEE 35th Annual Northeast Bioengineering Conference, NEBEC 2009*, Institute of Electrical and Electronics Engineers, Inc.: Boston, MA, USA, (2009).
- [90] Coviello, T.; Matricardi, P.; Marianecchi, C.; Alhaique, F., *Journal of Controlled Release*, (2007) **119**, 5.
- [91] Nussinovitch, A., *Polymer Macro- and Micro-Gel Beads: Fundamentals and Applications*, Springer: New York, (2010).
- [92] Dimitriu, S. Ed. *Polysaccharides: Structural Diversity and Functional Versatility*, Marcel Dekker, Inc.: (2005).
- [93] Draget, K. I.; Moe, S. T.; Skjåk-Bræk, G.; Smidsrød, O., Alginates, In *Food Polysaccharides and Their Applications*, Stephen, A. M.; Phillips, G. O.; Williams, P. A. Eds.; CRC Press, Taylor & Francis Group: Boca Raton, FL, (2006); 245.
- [94] Liew, C. V.; Chan, L. W.; Ching, A. L.; Heng, P. W. S., *International Journal of Pharmaceutics*, (2006) **309**, 25.

- [95] Prakash, O.; Talat, M.; Hasan, S. H.; Pandey, R. K., *Bioresource Technology*, (2008) **99**, 4524.
- [96] McHugh, D. J., Production, Properties and Uses of Alginates, In *Production and Utilization of Products from Commercial Seaweeds*, McHugh, D. J. Ed. Food and Agriculture Organization of the United Nations: Rome, (1987); 58.
- [97] Grant, G. T.; Morris, E. R.; Rees, D. A., *Febs Letters*, (1973) **32**, 195.
- [98] Franklin, M. J.; Chitnis, C. E.; Gacesa, P.; Sonesson, A.; White, D. C.; Ohman, D. E., *Journal of Bacteriology*, (1994) **176**, 1821.
- [99] Kvam, B. J.; Grasdalen, H.; Smidsrød, O.; Anthonsen, T., *Acta Chemica Scandinavica*, (1986) **40b**, 735.
- [100] Moe, S. T.; Draget, K. I.; Skjak-Braek, G.; Smidsrod, O., Alginates, In *Food Polysaccharide and Application*, Marcel Dekker: New York, (1995); 245.
- [101] Smidsrød, O.; Haug, A., *Acta Chemica Scandinavica*, (1972) **26**, 79.
- [102] Matsumoto, T.; Kawal, M.; Masuda, T., *Biorheology*, (1992) **29**, 411.
- [103] Draget, K. I.; Skjåk-Bræk, G.; Smidsrød, O., *International Journal of Biological Macromolecules*, (1997) **21**, 47.
- [104] Gomez d'Ayala, G.; Malinconico, M.; Laurenzio, P., *Molecules*, (2008) **13**, 2069.
- [105] Gombotz, W. R.; Wee, S., *Advanced Drug Delivery Reviews*, (1998) **31**, 267.
- [106] Saether, H. V.; Holme, H. K.; Maurstad, G.; Smidsrød, O.; Stokke, B. T., *Carbohydrate Polymers*, (2008) **74**, 813.
- [107] Soni, M. L.; Kumar, M.; Namedo, K. P., *International Journal of Drug Delivery*, (2010) **2**, 64.
- [108] Wang, J.-Y.; Jin, Y.; Xie, R.; Liu, J.-Y.; Ju, X.-J.; Meng, T.; Chu, L.-Y., *Journal of Colloid and Interface Science*, (2011) **353**, 61.
- [109] Blandino, A.; Macías, M.; Cantero, D., *Journal of Bioscience and Bioengineering*, (1999) **88**, 686.
- [110] Velings, N. L.; Mestdagh, M. M., *Polymer Gels and Networks*, (1995) **3**, 311.
- [111] Chan, E.-S.; Lee, B.-B.; Ravindra, P.; Poncelet, P., *Journal of Colloid and Interface Science*, (2009) **338**, 63.
- [112] Chai, Y.; Mei, L.-H.; Wu, G.-L.; Lin, D.-Q.; Yao, S.-J., *Biotechnology and Bioengineering*, (2004) **87**, 228.
- [113] Bugarski, B.; Li, Q.; Goosen, M. F. A.; Poncelet, D.; Neufeld, R. J.; Vunjak, G., *AIChE Journal*, (1993) **40**, 1026
- [114] Poncelet, D.; Babak, V. G.; Neufeld, R. J.; Goosen, M. F. A.; Bugarski, B., *Advances in Colloid and Interface Science*, (1999) **79**, 213.
- [115] Al-Hajry, H. A.; Al-Maskry, S. A.; Al-Kharousi, L. M.; El-Mardi, O.; Shayya, W. H.; Goosen, M. F. A., *Biotechnology Progress*, (1999) **15**, 768.
- [116] Nedovic, V. A.; Obradovic, B.; Leskosek-Cukalovic, I.; Trifunovic, O. P., R.; Bugarski, B., *Process Biochemistry*, (2001) **37**, 17.
- [117] Knezevic, Z.; Bobic, S.; Milutinovic, A.; Obradovic, B.; Mojovic, L.; Bugarski, B., *Process Biochemistry*, (2002) **38**, 313.

- [118] Bugarski, B. M.; Obradovic, B.; Nedovic, V. A.; Goosen, M. F. A., Electrostatic Droplet Generation Technique for Cell Immobilization, In *Finely Dispersed Particles: Micro-, Nano-, and Atto-Engineering*, Hsu, A. M. S. a. J.-P. Ed. CRC Press: (2006).
- [119] Manojlovic, V.; Djonlagic, J.; Obradovic, B.; Nedovic, V.; Bugarski, B., *Journal of Chemical Technology and Biotechnology*, (2006) **81**, 505.
- [120] Manojlovic, V.; Rajic, N.; Djonlagic, J.; Obradovic, B.; Nedovic, V.; Bugarski, B., *Sensors*, (2008) **8**, 1488.
- [121] Dashevsky, A., *International Journal of Pharmaceutics*, (1998) **161**, 1.
- [122] Tan, W.-H.; Takeuchi, S., *Advanced Materials*, (2007) **19**, 2696.
- [123] Qin, Y., *Journal of Applied Polymer Science*, (2006) **100**, 2516.
- [124] Xu, F.; Burg, K. J. L., *Cytotechnology*, (2007) **54**, 135.
- [125] Sperling, L. H., *Introduction to Physical Polymer Science*, John Wiley & Sons, Inc.: Hoboken, New Jersey, (2006).
- [126] IUPAC, Interpenetrating Polymer Network, In *IUPAC Compendium of Chemical Terminology*, IUPAC: (1996); 2305.
- [127] Bajpai, A. K.; Shukla, S. K.; Bhanu, S.; Kankane, S., *Progress in Polymer Science*, (2008) **33**, 1088.
- [128] Hoare, T. R.; Kohane, D. S., *Polymer*, (2008) **49**, 1993.
- [129] Chivukula, P.; Dušek, K.; Wang, D.; Dušková-Smrčková, M.; Kopečková, P.; Kopeček, J., *Biomaterials*, (2006) **27**, 1140.
- [130] Prabakaran, M.; Mano, J. F., *Macromolecular Bioscience*, (2006) **6**, 991.
- [131] Guilherme, M. R.; Silva, R.; Rubira, A. F.; Geuskens, G.; Muniz, E. C., *Reactive and Functional Polymers*, (2004) **61**, 233.
- [132] Guilherme, M. R.; Silva, R.; Girotto, E. M.; Rubira, A. F.; Muniz, E. C., *Polymer*, (2003) **44**, 4213.
- [133] Guilherme, M. R.; Toledo, E. A.; Rubira, A. F.; Muniz, E. C., *Journal of Membrane Science*, (2002) **210**, 129.
- [134] Guilherme, M. R.; Moura, M.; Radovanovic, E.; Geuskens, G.; Adley, F. R.; Edvani, C. M., *Polymer*, (2005) **46**, 2668.
- [135] Moura, M. R.; Guilherme, M. R.; Campese, G. M.; Radovanovic, E.; Rubira, A. F.; Muniz, E. C., *European Polymer Journal*, (2005) **41**, 2845.
- [136] Zhang, G.-Q.; Zha, L.-S.; Zhou, M.-H.; Ma, J.-H.; Liang, B.-R., *Colloid and Polymer Science*, (2005) **283**, 431.
- [137] Hernández, R.; Mijangos, C., *Macromolecular Rapid Communications*, (2009) **30**, 176.
- [138] Dumitriu, R. P.; Mitchell, G. R.; Vasile, C., *Polymer International*, (2011) **60**, 222.
- [139] Kim, J. H.; Lee, S. B.; Kim, S. J.; Lee, Y. M., *Polymer*, (2002) **43**, 7549.
- [140] Brannon-Peppas, L., *Medical Plastics and Biomaterials*, (1997) **4**, 34.
- [141] Acharya, G.; Park, K., *Advanced Drug Delivery Reviews*, (2006) **58**, 387.
- [142] Heller, J., Drug Delivery Systems, In *Biomaterials science: An Introduction to Materials in Medicine*, Ratner, B. D.; Hoffman, A. S.; Schoen, F. J.; Lemons, J. E. Eds.; Academic Press: (1996).
- [143] Chaterji, S.; Kwon, K.; Park, P., *Progress in Polymer Science*, (2007) **32**, 1083.

-
- [144] Kikuchi, A.; Okano, T., *Advanced Drug Delivery Reviews*, (2002) **54**, 53.
- [145] Peppas, N. A.; Bures, P.; Leobandung, W.; Ichikawa, H., *European Journal of Pharmaceutics and Biopharmaceutics*, (2000) **50**, 27.
- [146] Geever, L. M.; Cooney, C. C.; Lyons, J. G.; Kennedy, J. E.; Nugent, M. J. D.; Devery, S.; Higginbotham, C. L., *European Journal of Pharmaceutics and Biopharmaceutics*, (2008) **69**, 1147.
- [147] Guy, R. H.; Hadgraft, J. Eds., *Transdermal Drug Delivery*, Marcel Dekker: (2003).
- [148] Keleb, E.; Sharma, R. K.; B mossa, E.; Z aljahwi, A., *International Journal of Advances in Pharmaceutical Sciences*, (2010) **1**, 201.
- [149] Doh, H. J.; Cho, W. J.; Yong, C. S.; Choi, H. G.; Kim, J. S.; Lee, C. H.; Kim, D. D., *Journal of Pharmaceutical Sciences*, (2003) **92**, 1008.
- [150] Koo, J. Y. M.; Lee, C. S.; Lebwohl, M. G. Eds., *Mild-to-moderate Psoriasis*, Informa Healthcare USA, Inc.: New York, (2009).
- [151] Sun, Y.-M.; Huang, J.-J.; Lin, F.-C.; Lai, J.-Y., *Biomaterials*, (1997) **18**, 527.
- [152] Gayet, J. C.; Fortier, G., *Journal of Controlled Release*, (1996) **38**, 177.
- [153] Hubbell, J. A., *Journal of Controlled Release*, (1996) **39**, 305.
- [154] Chen, L.-L. H.; Chien, Y. W., *Journal of Controlled Release*, (1996) **40**, 187.
- [155] Lee, T.-W.; Kim, J.-C.; Hwang, S.-J., *European Journal of Pharmaceutics and Biopharmaceutics*, (2003) **56**, 407.
- [156] Tan, J. P. K.; Tan, M. B. H.; Tam, M. K. C., *Local and Regional Anesthesia*, (2010) **3**, 93.
- [157] Moraes, C.; Matos, A.; Lima, R.; Rosa, A.; Paula, E.; Fraceto, L., *Journal of Biological Physics*, (2007) **33**, 455.
- [158] Moraes, C. M.; Lima, R.; Rosa, A. H.; Paula, E.; Fraceto, L. F., *Macromolecular Symposia*, (2009) **281**, 106.
- [159] Schaffazick, S. R.; Pohlmann, A. R.; Mezzalira, G.; Guterres, S. S., *Journal of Brazilian Chemical Society*, (2006) **17**, 562.
- [160] Li, N.; Duan, J.; Chen, G., *Analytical Sciences*, (2003) **19**, 1587.
- [161] <http://www.chemblink.com/products/51-05-8.htm> (October 2011).
- [162] Tan, J. P. K.; Goh, C. H.; Tam, K. C., *European Journal Of Pharmaceutical Sciences: Official Journal Of The European Federation For Pharmaceutical Sciences*, (2007) **32**, 340.
- [163] Tan, J. P. K.; Wang, Q.; Tam, K. C., *Journal of Controlled Release*, (2008) **128**, 248.
- [164] Coughlan, D. C.; Quilty, F. P.; Corrigan, O. I., *Journal of Controlled Release*, (2004) **98**, 97.
- [165] Wu, J.-Y.; Liu, S.-Q.; Heng, P. W.-S.; Yang, Y.-Y., *Journal of Controlled Release*, (2005) **102**, 361.
- [166] Gu, J.; Xia, F.; Wu, Y.; Qu, X.; Yang, Z.; Jiang, L., *Journal Of Controlled Release: Official Journal Of The Controlled Release Society*, (2007) **117**, 396.
- [167] Park, T. G.; Hoffman, A. S., *Biotechnology Progress*, (1994) **10**, 82.
- [168] Tasdelen, B.; Kayaman-Apohan, N.; Mİslıllı, Z.; Guven, O.; Baysal, B. M., *Journal of Applied Polymer Science*, (2005) **97**, 1115.
-

- [169] Moura, M. R.; Aouada, F. A.; Favaro, S. L.; Radovanovic, E.; Rubira, A. F.; Muniz, E. C., *Materials Science and Engineering C*, (2009) **29**, 2319.
- [170] Shi, J.; Alves, N. M.; Mano, J. F., *Macromolecular Bioscience*, (2006) **6**, 358.
- [171] Shi, J.; Liu, L.; Sun, X.; Cao, S.; Mano, J. F., *Macromolecular Bioscience*, (2008) **8**, 260.
- [172] Khorram, M.; Vasheghani-Farahani, E.; Dinarvand, R., *Journal of Controlled Release*, (2006) **116**, e31.
- [173] Horrocks, A. R.; Anand, S. C. Eds., *Handbook of Technical Textiles*, Woodhead Publishing Ltd and CRC Press LLC: (2000).
- [174] Hipler, U.-C.; Elsner, P. Eds., *Biofunctional Textiles and the Skin*, Karger: Basel, (2006).
- [175] Wienforth, F.; Landrock, A.; Schindler, C.; Siegert, J.; Kirch, W., *Journal of Clinical Pharmacology*, (2007) **47**, 653.
- [176] Liu, B.; Hu, J., *Fibres and Textiles in Eastern Europe*, (2005) **13**, 45.
- [177] Boczkowska, A.; Leonowicz, M., *Fibres and Textiles in Eastern Europe*, (2006) **14**, 13.
- [178] Jovic, D., *Research Journal of Textile and Apparel*, (2008) **12**, 58.
- [179] Shishoo, R. Ed. *Plasma Technologies for Textiles*, Woodhead Publishing: Cambridge, (2007).
- [180] Garg, S.; Hurren, C.; Kaynak, A., *Synthetic Metals*, (2007) **157**, 41.
- [181] Oltargevskaya, N. D.; Krichevsky, G. E., Textile finishing for the production of new generation of medical textiles, In *Medical Textiles and Biomaterials*, Anand, S. C.; Miraftab, M.; Rajendran, S.; Kennedy, J. F. Eds.; Woodhead Publishing Ltd.: Cambridge, (2005); 482.
- [182] Serra, M., *Smart Materials Bulletin*, (2002) **2002**, 7.
- [183] Petruyte, S., *Danish Medical Bulletin*, (2008) **55**, 71.
- [184] Liu J.; Zhai, M.; Ha, H., *Radiation Physics and Chemistry*, (1999) **55**, 55.
- [185] Gupta, B.; Mishra, S.; Saxena, S., *Radiation Physics and Chemistry*, (2008) **77**, 553.
- [186] Kondo, T.; Koyama, M.; Kubota, H.; Katakai, R., *Journal of Applied Polymer Science*, (1998) **67**, 2057.
- [187] Wen, O. H.; Kuroda, S.; Kubota, H., *European Polymer Journal*, (2001) **37**, 807.
- [188] Hu, J.-L.; Liu, B.-H.; Liu, W.-G., *Textile Research Journal*, (2006) **76**, 853.
- [189] Chen, K.-S.; Tsai, J.-C., Chou, C.-W.; Yang, M.-R.; Yang, J.-M., *Materials Science and Engineering: C*, (2002) **20**, 203.
- [190] Li, R.; Ye, L.; Mai, Y.-W., *Composites Part A: Applied Science and Manufacturing*, (1997) **28**, 73.
- [191] Taşdelen, B.; Kayaman-Apohan, N.; Güven, O.; Baysal, B. M., *Radiation Physics and Chemistry*, (2004) **69**, 303.
- [192] Kesim, H.; Rzaev, Z. M. O.; Dinçer, S.; Pişkin, E., *Polymer*, (2003) **44**, 2897.
- [193] Erbil, C.; Aras, S.; Uyanik, N., *Journal of Polymer Science Part A: Polymer Chemistry*, (1999) **37**, 1847.
- [194] Çaykara, T., *Journal of applied polymer science*, (2004) **92**, 763.
- [195] Liu, R.; Fraylich, M.; Saunders, B. R., *Colloid and Polymer Science*, (2009) **287**, 627.
- [196] Lijing, G.; Opheim, B.; Coretsopoulos, C. N.; Scranton, A. B., *Chemical Engineering Communications*, (2006) **193**, 620.

- [197] Zhang, X.-Z.; Wu, D.-Q.; Chu, C.-C., *Journal of Polymer Science: Part B: Polymer Physics*, (2003) **41**, 582.
- [198] Arshady, R., *Colloid and Polymer Science*, (1992) **270**, 717.
- [199] Van Herk, A. M.; Monteiro, M., Heterogeneous Systems, In *Handbook of Radical Polymerization*, Matyjaszewski, K.; Davis, T. P. Eds.; John Wiley & Sons, Inc.: Hoboken, (2002); 301.
- [200] Annaka, M.; Matsuura, T.; Kasai, M.; Nakahira, T.; Hara, Y.; Okano, T., *Biomacromolecules*, (2003) **4**, 395.
- [201] <http://www.btinternet.com/~martin.chaplin/hyalg.html> (October 2011).
- [202] Poncelet, D.; Neufeld, R. J.; Goosen, M. F. A.; Bugarski, B.; Babak, V. G., *AIChE Journal*, (1999) **45**, 2018.
- [203] Manojlovic, V.; Djonlagic, J.; Obradovic, B.; Nedovic, V.; Bugarski, B., *International Journal of Nanomedicine*, (2006) **1**, 163.
- [204] Rayleigh, J. W. S., *Philosophical Magazine*, (1882) **14**, 184.
- [205] Amsden, B. G.; Goosen, M. F. A., *Journal of Controlled Release*, (1997) **43**, 183.
- [206] Hayati, I.; Bailey, A. I.; Tadros, T. F., *Journal of Colloid and Interface Science*, (1987) **117**, 205.
- [207] Gabbott, P. Ed. *Principles and Applications of Thermal Analysis*, Blackwell Publishing Ltd.: Oxford, (2008).
- [208] Feil, H.; Bae, Y. H.; Feijen, J.; Kim, S. W., *Macromolecules*, (1993) **26**, 2496.
- [209] Price, D. M., Thermomechanical, Dynamic Mechanical and Dielectric Methods, In *Principles of Thermal Analysis & Calorimetry*, Haines, P. J. Ed. The Royal Society of Chemistry: (2002).
- [210] http://www.netzsch-thermal-analysis.com/fr/produits/dma_dmta/, In.
- [211] Meyvis, T. K. L.; Stubbe, B. G.; Van Steenberghe, M. J.; Hennink, W. E.; Smedt, S. C.; Demeester, J., *International Journal of Pharmaceutics* **244** (2002) 163-168, (2002) **244**, 163.
- [212] Hou, Y.; Matthews, A. R.; Smitherman, A. M.; Bulick, A. S.; Hahn, M. S.; Hou, H.; Han, A.; Grunlan, M. A., *Biomaterials*, (2008) **29**, 3175.
- [213] Spectra/Por closures, Spectrum Laboratories Inc., <http://www.spectrumlabs.com/dialysis/RegClose.html> (October 2011).
- [214] <http://www.emcourses.com/sputter.htm> (October 2011).
- [215] Mastersizer 2000 Brochure, Malvern Instruments Ltd., (2005); available at: <http://www.malvern.com/ms2000> (October 2011).
- [216] http://www.malvern.com/LabEng/technology/laser_diffraction/analyzing_light_scattering.htm (October 2011).
- [217] Aouada, F. A.; Moura, M. R.; Fernandes, P. R. G.; Rubira, A. F.; Muniz, E. C., *European Polymer Journal*, (2005) **41**, 2134.
- [218] Seydack, M., Particle-Based Assays: Applications and Unresolved Issues, In *Standardization and Quality Assurance in Fluorescence Measurements II* Resch-Genger, U. Ed. Springer: Berlin, (2008); 449.

- [219] Rheomat RM 180 Sales Brochure, Maple Instruments Ltd., (2001); available at: <http://www.mapleinstruments.com/literature/Rheomat%20RM%20180%20Sales%20Brochure.pdf> (October 2011).
- [220] Flow Type Franz Cell, PermeGear, <http://www.permegear.com/franzflow.htm>, October 2011.
- [221] Levin, S.; Gad, S. C., *High Performance Liquid Chromatography (HPLC) in the Pharmaceutical Analysis*, John Wiley & Sons, Inc.: Hoboken, (2010).
- [222] Weston, A.; Brown, P. R., *HPLC and CE: Principles and Practice*, Academic Press: San Diego, (1997).
- [223] Meyer, V. R., *Practical High-Performance Liquid Chromatography*, John Wiley & Sons, Ltd.: Chichester, (2010).
- [224] Gehrke, S. H.; Palasis, M.; Akhtar, M. K., *Polymer International*, (1992) **29**, 29.
- [225] Kuckling, D.; Arndt, K.-F.; Richter, S., Synthesis of Hydrogels, In *Hydrogels Sensors and Actuators*, Gerlach, G.; Arndt, K.-F. Eds.; Springer-Verlag: Berlin, (2009); 26.
- [226] Sayil, Ç.; Okay, O., *Polymer Bulletin*, (2000) **45**, 175.
- [227] Mohan, Y. M.; Premkumar, T.; Joseph, D. K.; Geckeler, K. E., *Reactive and Functional Polymers*, (2007) **67**, 844.
- [228] Liu, W.; Zhang, B.; Lu, W. W.; Li, X.; Zhu, D.; Yao, K. D.; Wang, Q.; Zhao, C.; Wang, C., *Biomaterials*, (2004) **25**, 3005.
- [229] Tan, J. P. K.; Tam, K. C., *Journal of Controlled Release*, (2007) **118**, 87.
- [230] Tam, S. K.; Dusseault, J.; Polizu, S.; Menard, M.; Halle, J.-P.; Yahia, L. H., *Biomaterials*, (2005) **26**, 6950.
- [231] Sakugawa, K.; Ikeda, A.; Takemura, A.; Ono, H., *Journal of Applied Polymer Science*, (2004) **93**, 1372.
- [232] Puttipipatkachorn, S.; Pongjanyakul, T.; Priprem, A., *International Journal of Pharmaceutics*, (2005) **293**, 51.
- [233] Hirokawa, Y.; Tanaka, T., *Journal of Chemical Physics*, (1984) **81**, 6379.
- [234] Moura, M. R.; Rubira, A. F.; Muniz, E. C., *Polímeros: Ciência e Tecnologia*, (2008) **18**, 132.
- [235] Erbil, C.; Kazancoglu, E.; Uyanlk, N., *European Polymer Journal*, (2004) **40**, 1145.
- [236] Szilágyi, A.; Zrínyi, M., *Polymer*, (2005) **46**, 10011.
- [237] Varghese, S.; Lele, A. K.; Srinivas, D.; Mashelkar, R. A., *Journal of Physical Chemistry B*, (1990) **103**, 9530.
- [238] Cheng, H.; Shen, L.; Wu, C., *Macromolecules*, (2006) **39**,
- [239] Schild, H., *Progress in Polymer Science*, (1992) **17**, 163.
- [240] Chen, H.; Hsieh, Y.-L., *Journal of Polymer Science: Part A: Polymer Chemistry*, (2004) **42**, 3293.
- [241] Sousa, R. G.; Magalhaes, W. F.; Freitas, R. F. S., *Polymer Degradation and Stability*, (1998) **61**, 275.
- [242] Ortega, A.; Bucio, E.; Burillo, G., *Polymer Bulletin*, (2008) **60**, 515.
- [243] Meléndez-Ortiz, H. I.; Bucio, E.; Burillo, G., *Radiation Physics and Chemistry*, (2009) **78**, 1.

- [244] Zhang, X. Z.; Zhuo, R. X., *Journal of Colloid and Interface Science*, (2000) **223**, 311.
- [245] Kaneko, Y.; Yoshida, R.; Sakai, K.; Sakurai, Y.; Okano, T., *Journal of Membrane Science*, (1995) **101**, 13.
- [246] Bae, Y. H.; Okano, T.; Hsu, R.; Kim, S. W., *Makromolekulare Chemie Rapid Communication*, (1987) **8**, 481.
- [247] Bae, Y. H.; Okano, T.; Kim, S. W., *Journal of Controlled Release*, (1989) **9**, 271.
- [248] Sato, S.; Kim, S. W., *International Journal of Pharmaceutics*, (1984) **22**, 229.
- [249] Yoshida, R.; Kaneko, Y.; Sakai, K.; Okano, T.; Sakurai, Y.; Bae, Y. H.; Kim, S. W., *Journal of Controlled Release*, (1994) **32**, 97.
- [250] Caykara, T.; Kiper, S.; Demirel, G., *European Polymer Journal*, (2006) **42**, 348.
- [251] Myung, D.; Waters, D.; Wiseman, M.; Duhamel, P.-E.; Noolandi, J.; Ta, N. T.; Frank, C. W., *Polymers for Advanced Technologies*, (2008) **19**, 647.
- [252] Hong, P.-D.; Chen, J.-H., *Polymer*, (1998) **39**, 5809.
- [253] Matyjaszewski, K.; Davis, T. P. Eds., *Handbook of Radical Polymerization*, John Wiley & Sons, Inc.: Hoboken, (2002).
- [254] Okay, O., Macroporous Hydrogels from Smart Polymers, In *Smart Polymers: Applications in Biotechnology and Biomedicine*, Galaev, I.; Mattiasson, B. Eds.; CRC Press: Boca Raton, Florida, (2008); 273.
- [255] Mattiasson, B.; Kumar, A.; Galaev, I. Y. Eds., *Macroporous Polymers: Production Properties and Biotechnological/Biomedical Applications*, CRC Press: Boca Raton, FL, (2010).
- [256] Okay, O., Production of Macroporous Polymeric Materials by Phase Separation Polymerization, In *Macroporous Polymers: Production Properties and Biotechnological/Biomedical Applications*, Mattiasson, B.; Kumar, A.; Galaev, I. Y. Eds.; CRC Press: Boca Raton, FL, (2010); 3.
- [257] Zhang, H.-f.; Zhong, H.; Zhang, L.-l.; Chen, S.-b.; Zhao, Y.-j.; Zhu, Y.-l., *Carbohydrate Polymers*, (2009) **77**, 785.
- [258] Gil, E. S.; Hudson, S. M., *Biomacromolecules*, (2007) **8**,
- [259] Okay, O., General Properties of Hydrogels, In *Hydrogels Sensors and Actuators*, Gerlach, G.; Arndt, K.-F. Eds.; Springer-Verlag: Berlin, (2009); 1.
- [260] Zhang, J.-T.; Thunga, M.; Petersen, S.; Bhat, R.; Liu, Y.; Weidisch, R.; Fahr, A.; Jandt, K. D., *Advanced Engineering Materials*, (2009) **11**, B12.
- [261] Kloxin, A. M.; Kloxin, C. J.; Bowman, C. N.; Anseth, K. S., *Advanced Materials*, (2010) **22**, 3484.
- [262] Sun, X.; Shi, J.; Zhang, Z.; Cao, S., *Journal of Applied Polymer Science*, (2011) **122**, 729.
- [263] Karande, V. S.; Bharimalla, A. K.; Hadge, G. B.; Mhaske, S. T.; Vigneshwaran, N., *Fibers and Polymers*, (2011) **12**, 399.
- [264] Syringe needle gauge chart, Sigma-Aldrich, <http://www.sigmaaldrich.com/chemistry/stockroom-reagents/learning-center/technical-library/needle-gauge-chart.html> (October 2011).
- [265] Xie, J.; Wang, C.-H., *Journal of Colloid and Interface Science*, (2007) **312**, 247.
- [266] Klok, T. I.; Melvik, J. E., *Journal of Microencapsulation*, (2002) **19**, 415.

- [267] Nedovic, V.; Manojlovic, V.; Pruesse, U.; Bugarski, B.; Djonlagic, J.; Vorlop, K., *CI&CEQ*, (2006) **12**, 53.
- [268] Sample, S. B.; Bollini, R., *Journal of Colloid and Interface Science*, (1972) **41**, 185.
- [269] Magarvey, R. H.; Outhouse, L. E., *Journal of Fluid Mechanics*, (1962) **13**, 151.
- [270] Panicker, P. K., Doctoral Dissertation, *The University of Texas at Arlington* (2003).
- [271] Huneiti, Z. A.; Balachandran, W.; Machowski, W. W., *Industry Applications, IEEE Transactions on*, (1998) **34**, 279.
- [272] Weiming, W. X., L.; Weiting, Y. X., M., *Chinese Science Bulletin*, (2006) **51**, 279–286.
- [273] http://www.sigmaaldrich.com/catalog/ProductDetail.do?lang=en&N4=858366|ALDRICH&N5=SEARCH_CONCAT_PNO|BRAND_KEY&F=SPEC (October 2011)
- [274] Surfactants classified by HLB numbers, Sigma-Aldrich, <http://www.sigmaaldrich.com/materials-science/material-science-products.html?TablePage=22686648> (October 2011).
- [275] Tang, K.; Gomez, A., *Journal of Colloid and Interface Science*, (1996) **184**, 500.
- [276] Mohan, Y. M.; Premkumar, T.; Joseph, D. K.; Geckeler, K. E., *Reactive and Functional Polymers*, (2007) **67**, 844.
- [277] Susan K. Tam, S. K.; Dusseault, D.; Polizu, S.; Ménard, M.; Hallé, J.-P.; Yahia, L'H., *Biomaterials*, (2005) **26**, 6950.
- [278] Constantin, M.; Cristea, M.; Ascenzi, P.; Fundueanu, G., *eXPRESS Polymer Letters*, (2011) **5**, 839.
- [279] George, M.; Abraham, T. E., *International Journal of Pharmaceutics*, (2007) **335**, 123.
- [280] Shi, X.; Du, Y.; Sun, L.; Zhang, B.; Dou, A., *Journal of Applied Polymer Science*, (2006) **100**, 4614.
- [281] Lee, O.-S.; Ha, B.-J.; Park, S.-N.; Lee, Y.-S., *Macromolecular Chemistry and Physics*, (1997) **198**, 2971.
- [282] Kayaman, N.; Kazan, D.; Erarslan, A.; Okay, O.; Baysal, B. M., *Journal of Applied Polymer Science*, (1998) **67**, 805.
- [283] Rawle, A., Basic Principles of Particle Size Analysis, application note MRK034, Malvern Instruments Ltd., (1993), available at: http://golik.co.il/Data/BasicPrinciplesofParticlesize_1126925513.pdf (October 2011).
- [284] Landfester, K.; Hentze, H.-P., Heterophase Polymerization in Inverse Systems, In *Reactions and Synthesis in Surfactant Systems*, Texter, J. Ed. Marcel Dekker, Inc.: New York, (2001); 471.
- [285] Chu, L.-Y.; Park, S.-H.; Yamaguchi, T.; Nakao, S.-I., *Langmuir*, (2002) **18**, 1856.
- [286] Mayoux, C.; Dandurand, J.; Ricard, A.; Lacabanne, C., *Journal of Applied Polymer Science*, (2000) **77**, 2621.
- [287] Luciani, C. V.; Choi, K. Y.; Xiao, Z., *Chemical Engineering and Technology*, (2010) **33**, 1833.
- [288] Hashim, S.; Brooks, B. W., *Chemical Engineering Science*, (2002) **57**, 3703.
- [289] Kuo, C. K.; Ma, P. X., *Journal of Biomedical Materials Research Part A*, (2007) **84A**, 899.
- [290] Zhang, W.; Kim, J. H.; Franco, C. M. M.; Middelberg, A. P. J., *Applied Microbiology and Biotechnology*, (2000) **54**, 28.

-
- [291] Kuckling, D.; Adler, H.-J. P.; Arndt, K.-F.; Ling, L.; Habicher, W. D., *Macromolecular Chemistry and Physics*, (2000) **201**, 273.
- [292] Ebara, M.; Aoyagi, T.; Sakai, K.; Okano, T., *Macromolecules*, (2000) **33**, 8312.
- [293] Xu, X.-D.; Zhang, X.-Z.; Cheng, S.-X.; Zhuo, R.-X.; Kennedy, J. F., *Carbohydrate Polymers*, (2007) **68**, 416.
- [294] Zhang, X.-Z.; Zhuo, R.-X., *Langmuir*, (2001) **17**, 12.
- [295] Kaneko, Y.; Sakai, K.; Kikuchi, A.; Sakurai, Y.; Okano, T., *Macromolecular Symposia*, (1996) **109**, 41.
- [296] Dowding, P. J.; Vincent, B.; Williams, E., *Journal of Colloid and Interface Science*, (2000) **221**, 268.
- [297] Özeroglu, C.; Birdal, A., *eXPRESS Polymer Letters*, (2009) **3**, 168.
- [298] Liu, H.; Zhen, M.; Wu, R., *Macromolecular Chemistry and Physics*, (2007) **208**, 874.
- [299] Lee, S. B.; Park, E. K.; Lim, Y. M.; Cho, S. K.; Kim, S. Y.; Lee, Y. M.; Nho, Y. C., *Journal of Applied Polymer Science*, (2006) **100**, 4439.
- [300] Suárez, I. J.; Fernández-Nieves, A.; Márquez, M., *Journal of Chemical Physics B*, (2006) **110**, 25729.
- [301] Topuz, F.; Okay, O., *Reactive and Functional Polymers*, (2009) **69**, 273.
- [302] Cheng, C.-J.; Chu, L.-Y.; Zhang, J.; Wang, H.-D.; Wei, G., *Colloid and Polymer Science*, (2008) **286**, 571.
- [303] Arias, C.; Lopez-Cabarcos, E.; Rueda, C., *Il Farmaco*, (2001) **56**, 533.
- [304] Merino, C.; Junquera, E.; Jimenez-Barbero, J.; Aicart, E., *Langmuir*, (2000) **16**, 1557.
- [305] Serra, L.; Doménech, J.; Peppas, N. A., *Biomaterials*, (2006) **27**, 5440.
- [306] Akkaş, P.; Sarı, M.; Şen, M.; Güven, O., *Radiation Physics and Chemistry*, (1999) **55**, 717.
- [307] Silva, R. M. P.; Mano, J. F.; Reis, R. L., *Trends in Biotechnology*, (2007) **25**, 577.
- [308] Hsu, Y.-Y.; Gresser, J. D.; Stewart, R. R.; Trantolo, D. J.; Lyons, C. M.; Simons, G. A.; Gangadharam, P. R. J.; Wise, D. L., *Journal of Pharmaceutical Sciences*, (1996) **85**, 706.
- [309] Peppas, N. A., *Pharmaceutica Acta Helveticae*, (1985) **60**, 110.
- [310] Siepmann, J.; Peppas, N. A., *Advanced Drug Delivery Reviews*, (2001) **48**, 139.
- [311] Wang, Q.; Zhang, J.; Wang, A., *Carbohydrate Polymers*, (2009) **78**, 731.
- [312] Sezer, A. D.; Akbuğa, J., *International Journal of Pharmaceutics*, (1995) **121**, 113.

APPENDIX

Chapter III

III.2 Chemical structure

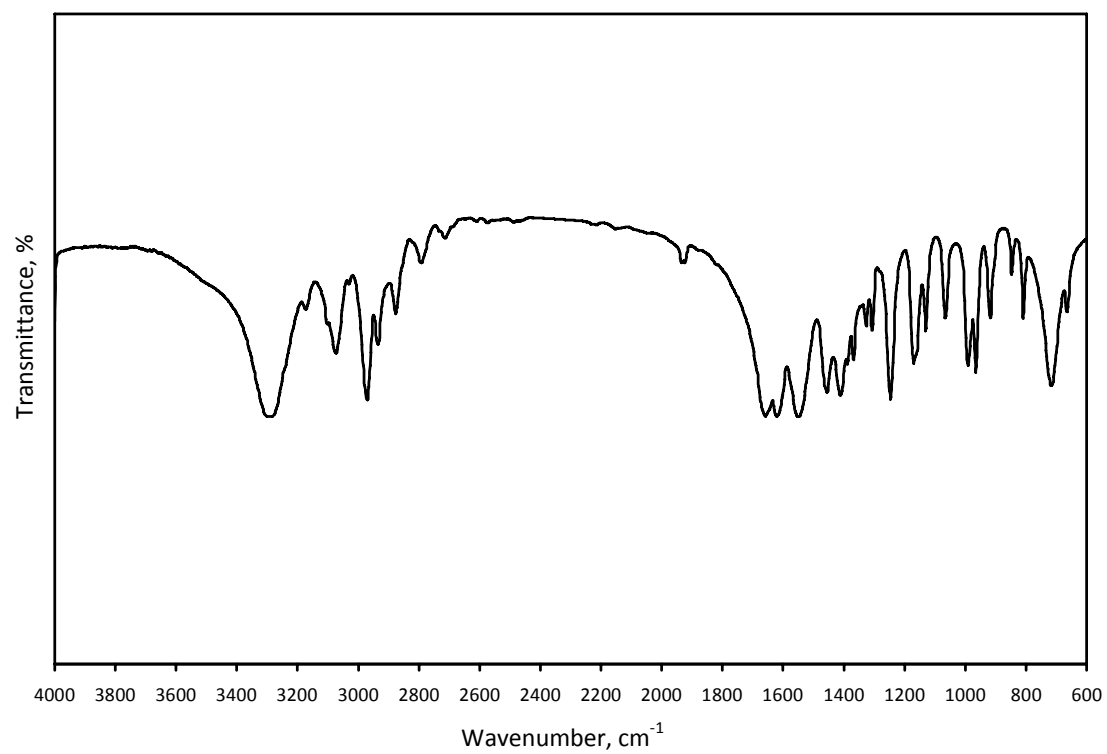


Figure A-1. FTIR spectra of monomer NIPAAm

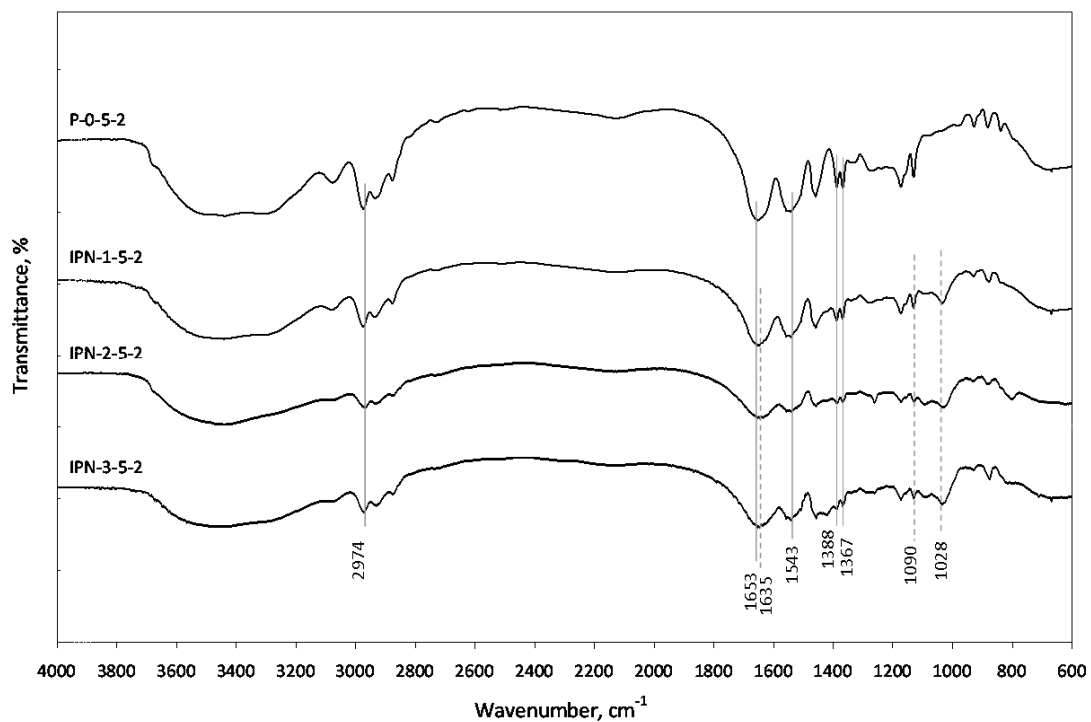


Figure A-2. FTIR spectra of hydrogels with 2 wt % MBAAm (characteristic peaks of PNIPAAm chains indicated by full lines and those of CA network by dotted lines)

III.3 Thermal characteristics

III.3.1 Volume phase transition temperature

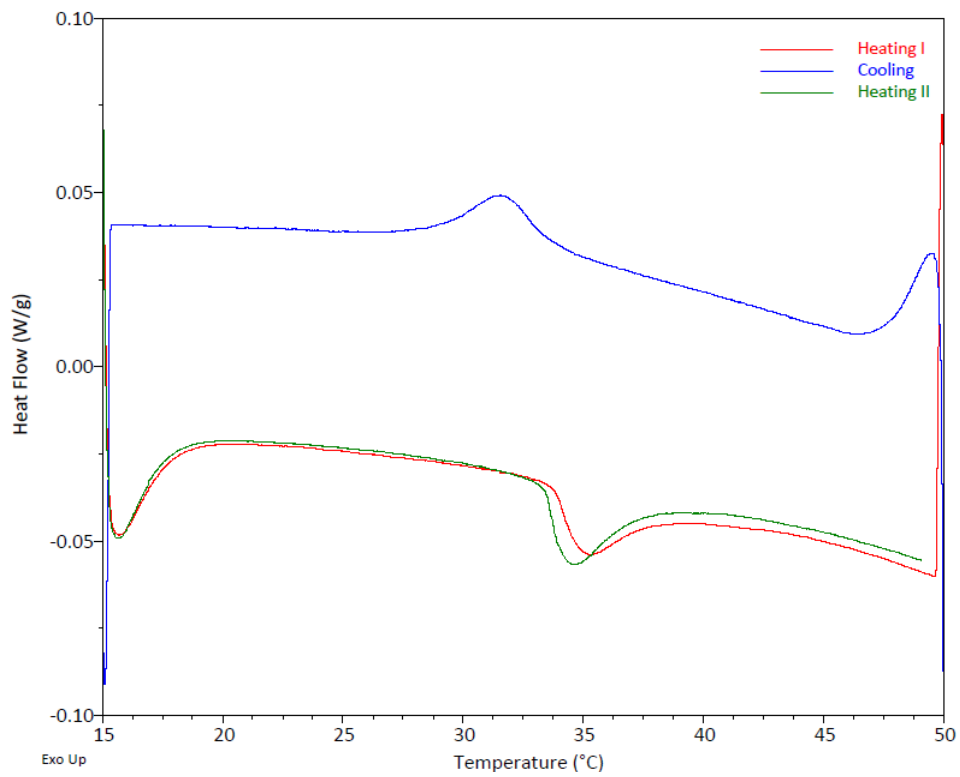


Figure A-3. DSC thermogram for determination of VPTT of IPN-1-5-2

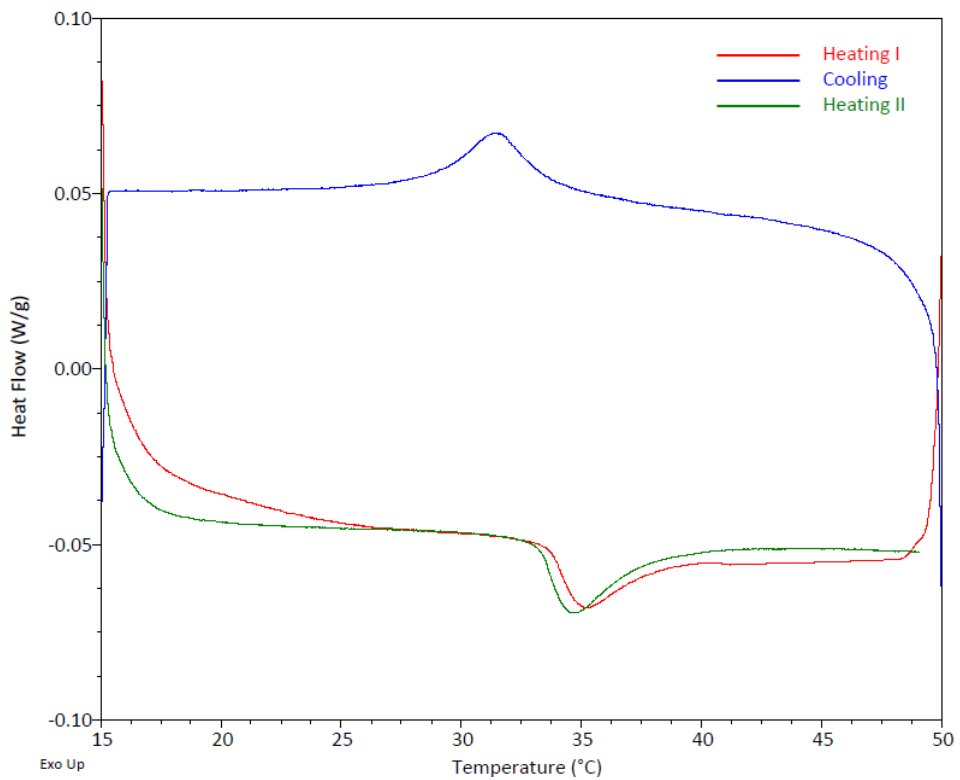


Figure A-4. DSC thermogram for determination of VPTT of IPN-2-5-2

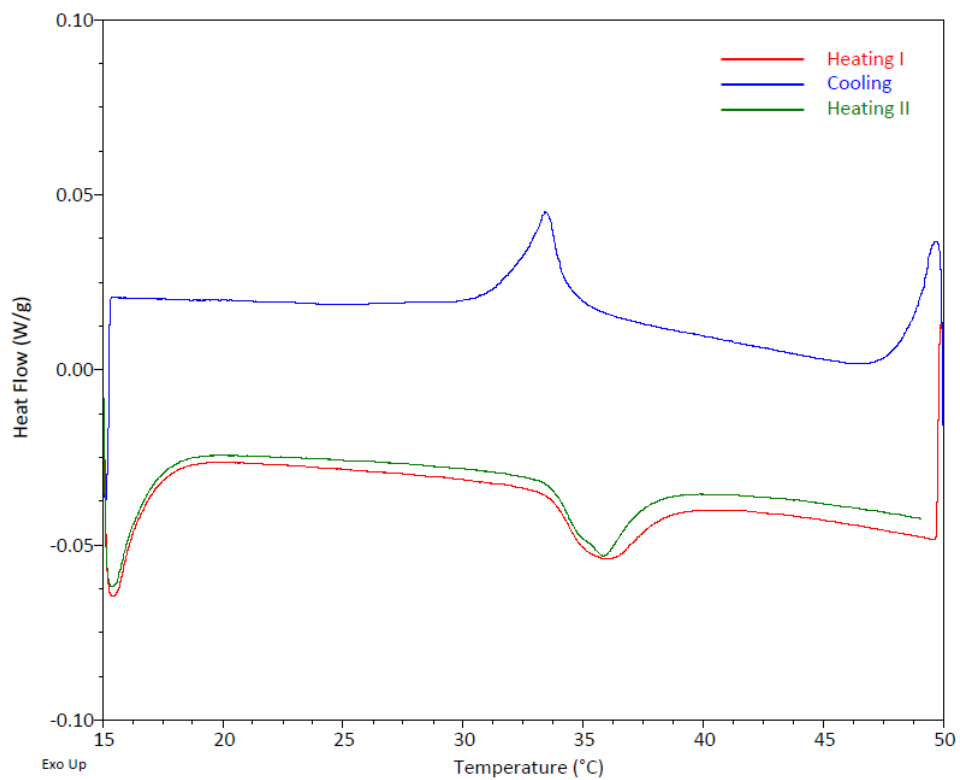


Figure A-5. DSC thermogram for determination of VPTT of P-0-5-3

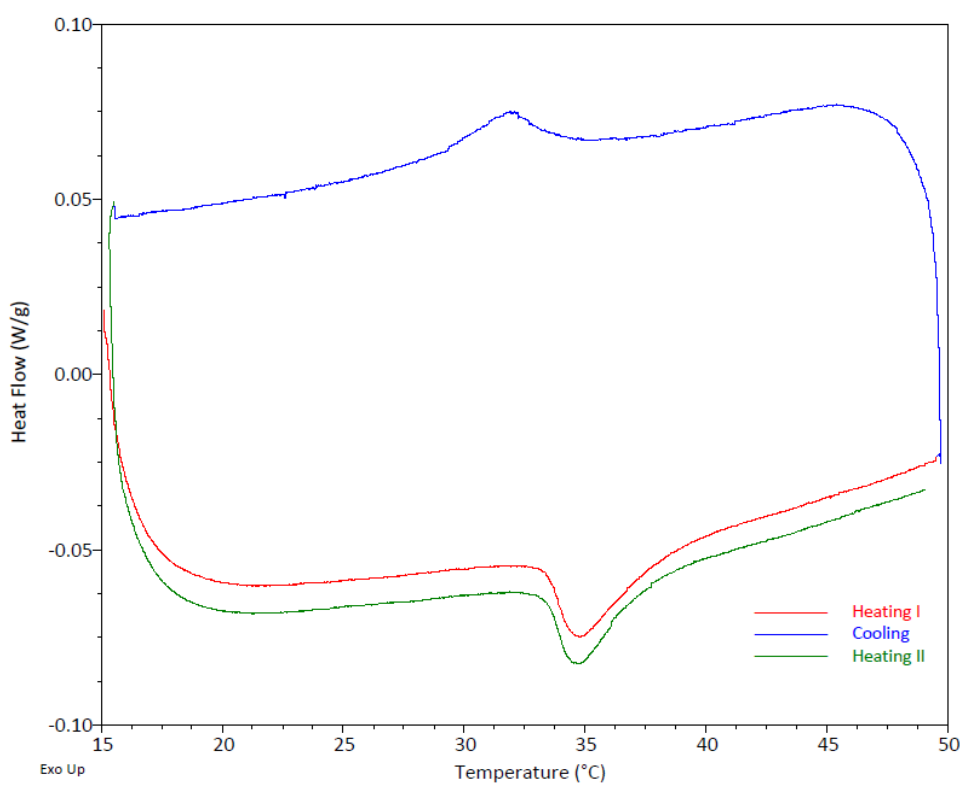


Figure A-6. DSC thermogram for determination of VPTT of IPN-1-5-3

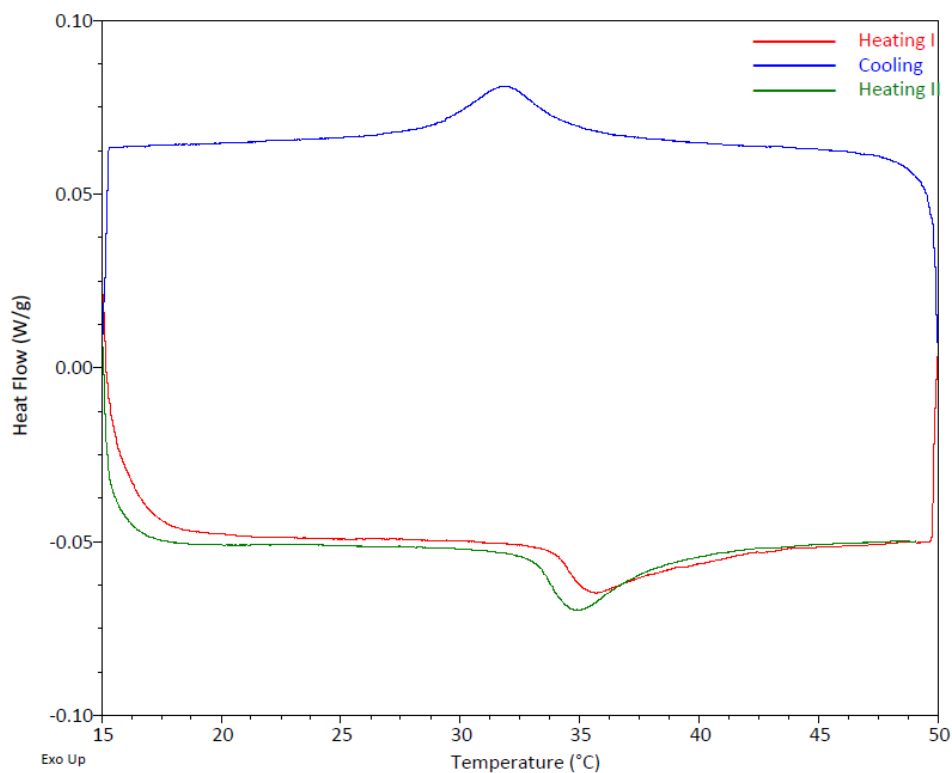


Figure A-7. DSC thermogram for determination of VPTT of IPN-2-5-3

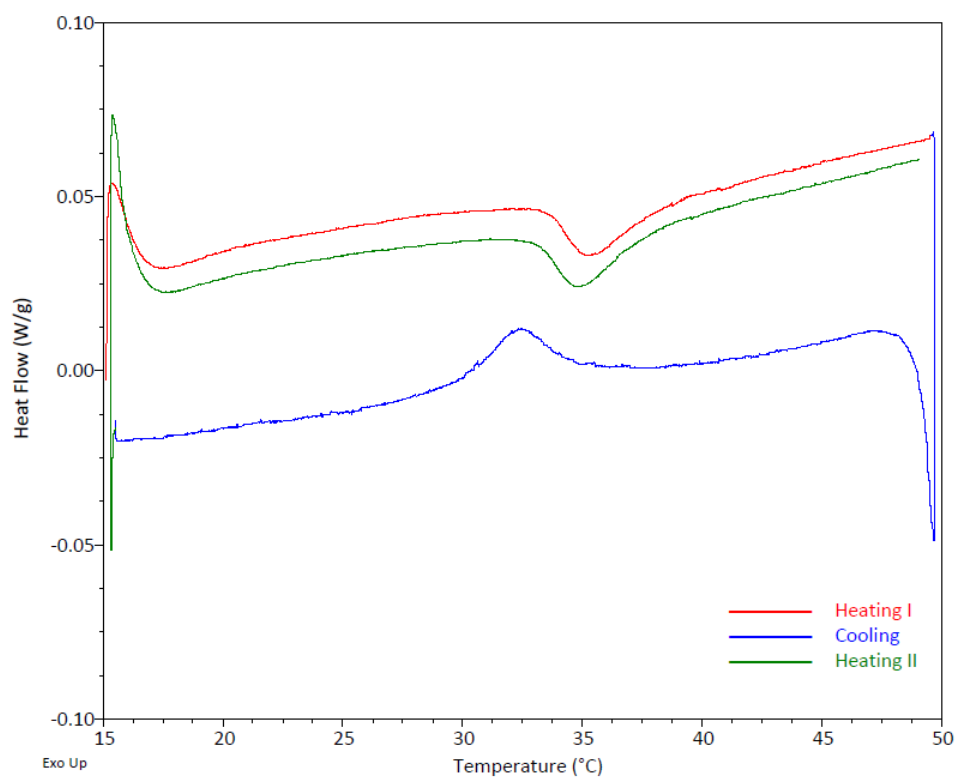


Figure A-8. DSC thermogram for determination of VPTT of IPN-3-5-3

Chapter V

V.2 Chemical structure

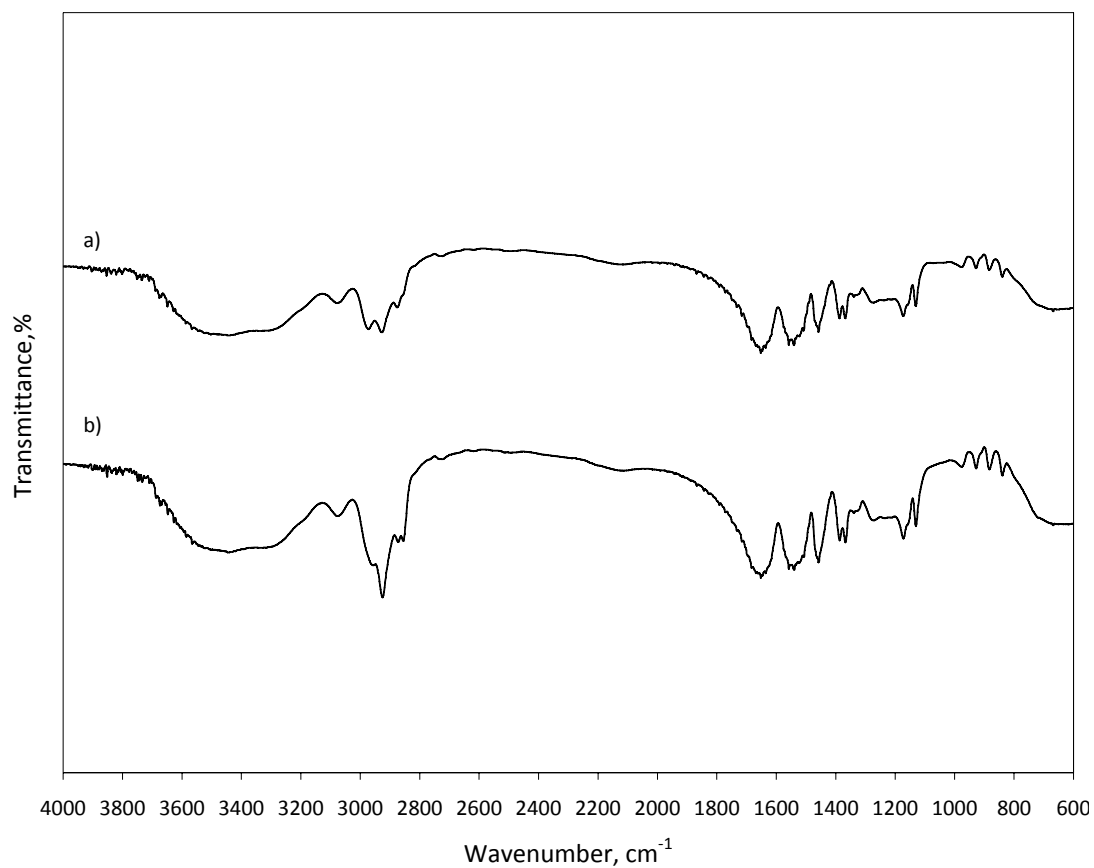


Figure A-9. FTIR spectra of pure PNIPAAm hydrogel microbeads M-100/1 (a) and M-50/1 (b)

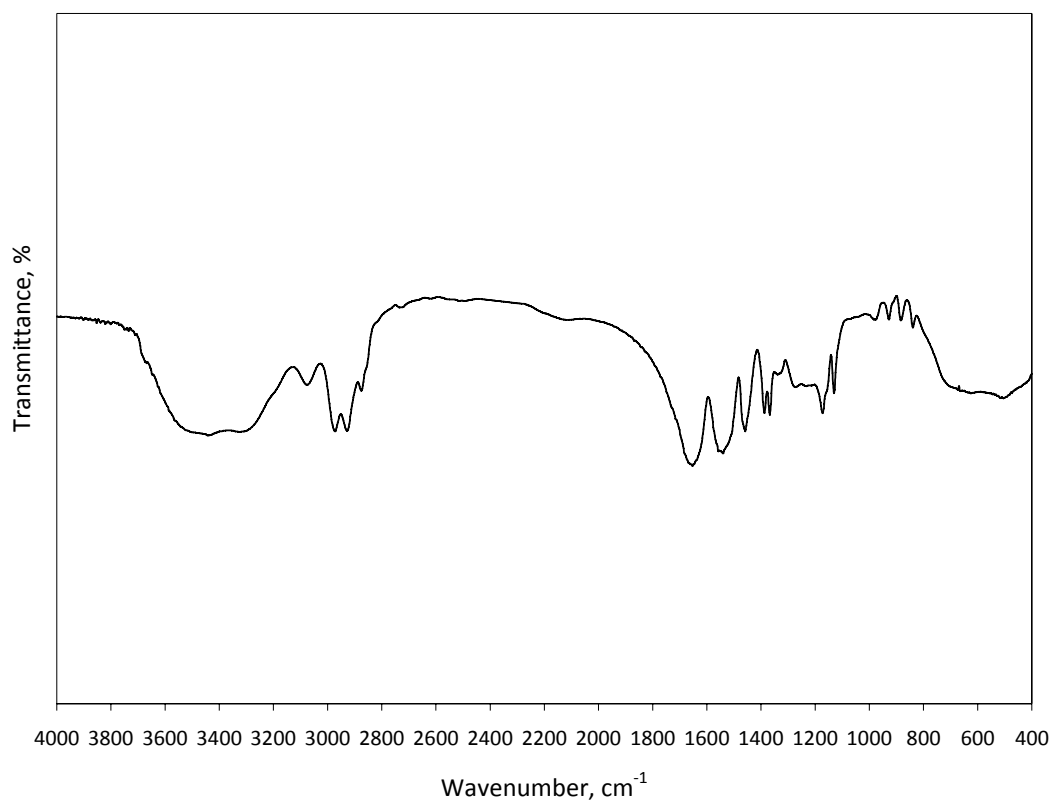


Figure A-10. FTIR spectra of PNIPAAm/MA copolymer hydrogel microbeads (M-25/1-MA 5)

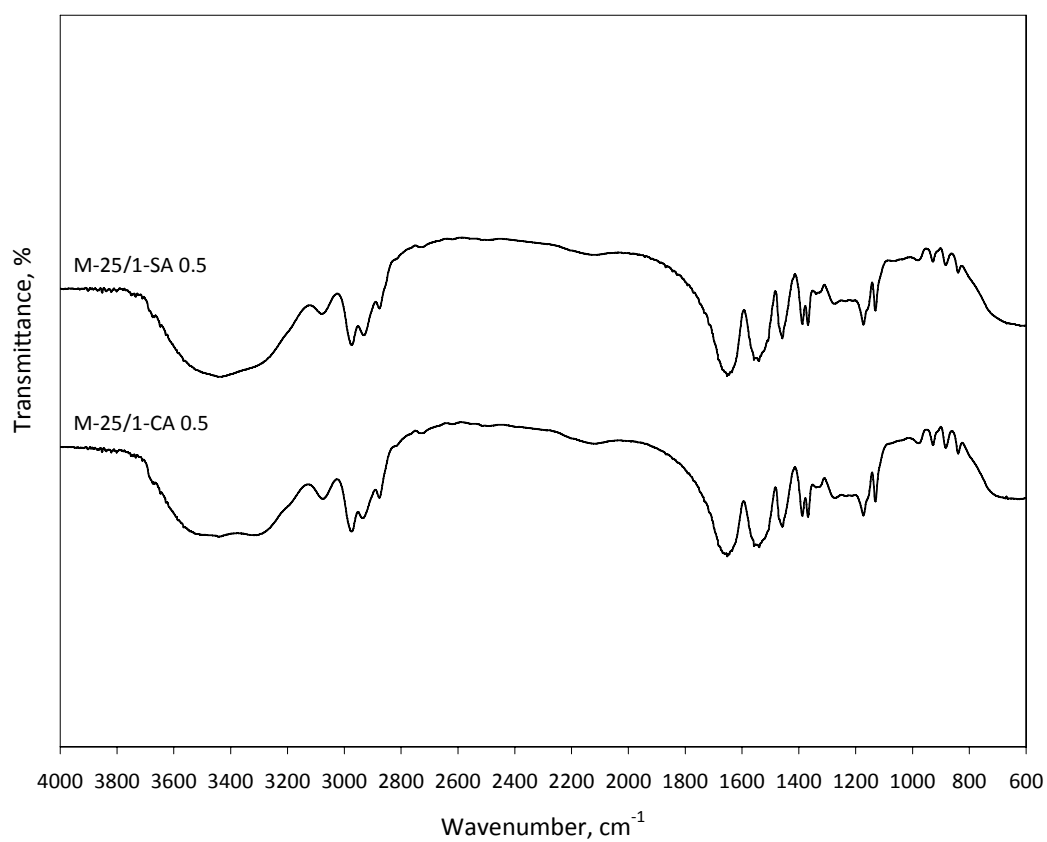


Figure A-11. FTIR spectra of semi- and full-IPN hydrogel microbeads based on 0.5 w/v % alginate

V.5 Thermal characteristics

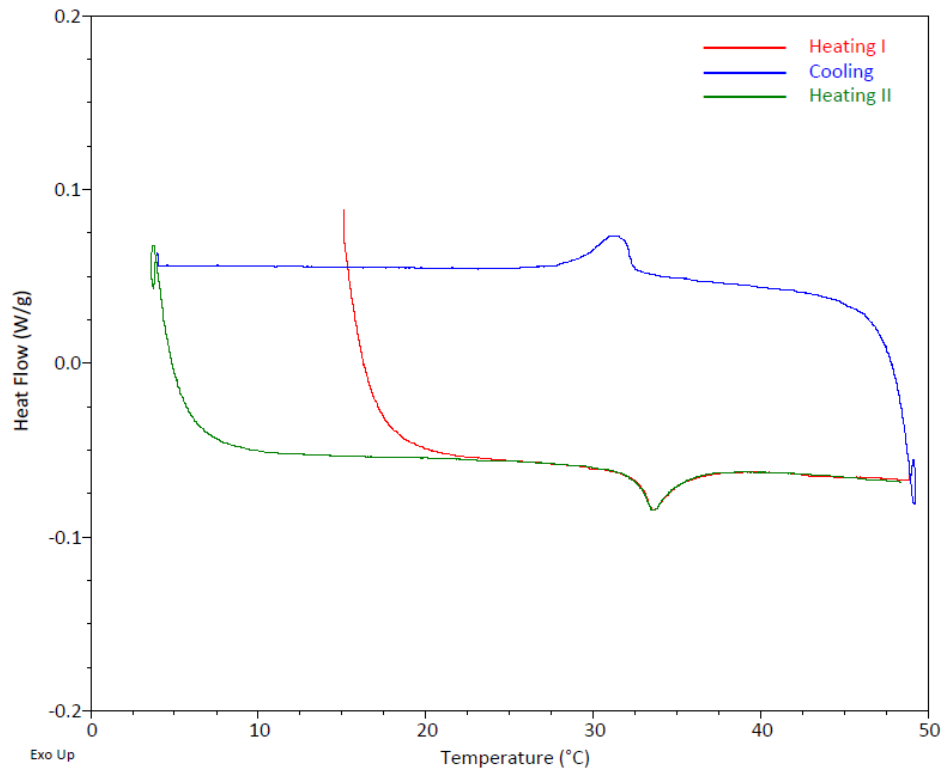


Figure A-12. DSC thermogram of hydrogel microbeads M-25/1

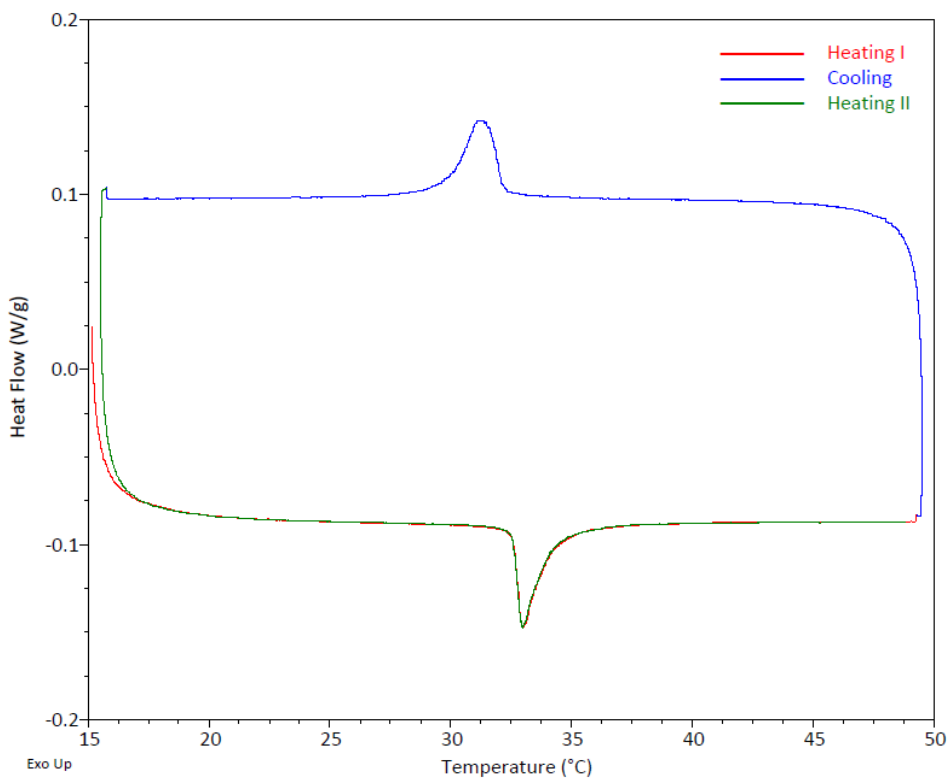


Figure A-13. DSC thermogram of hydrogel microbeads M-100/1

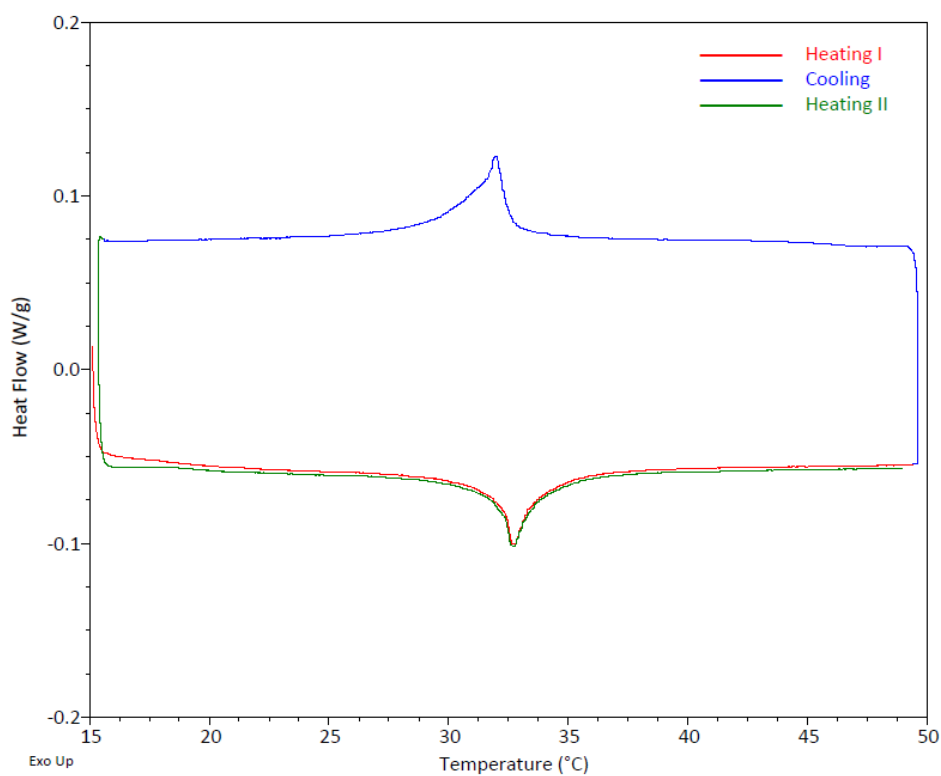


Figure A-14. DSC thermogram of hydrogel microbeads M-25/1-SA 1.0

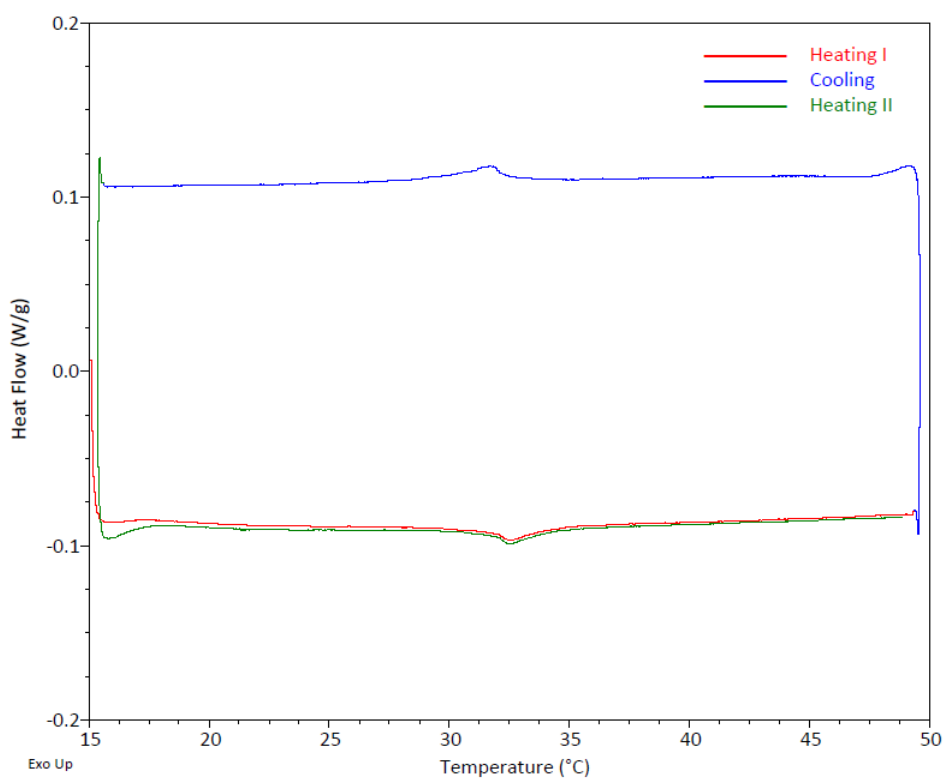


Figure A-15. DSC thermogram of hydrogel microbeads M-25/1-CA 1.0

V.6. Swelling behavior

V.6.2 Response of dried microbeads to water presence

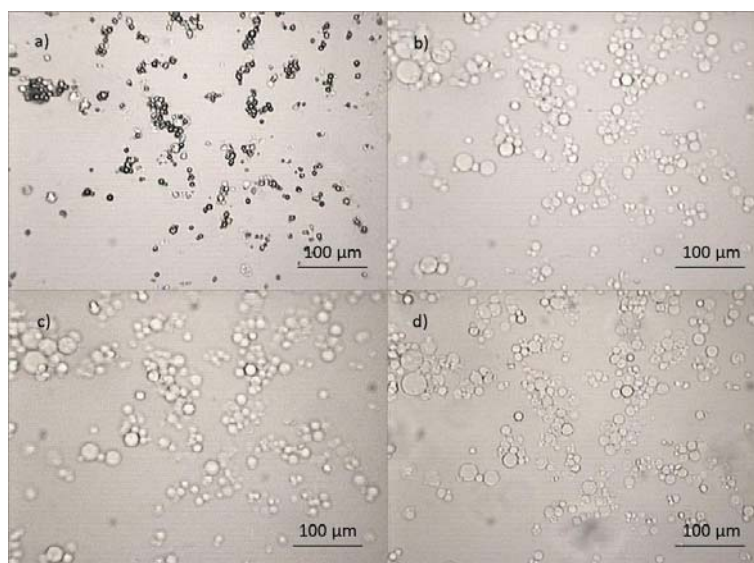


Figure A-16. Response of dried microbeads M-25/1-MA 5 (a) to water presence after 30 s (b), 2 min (c), and 10 min (d)

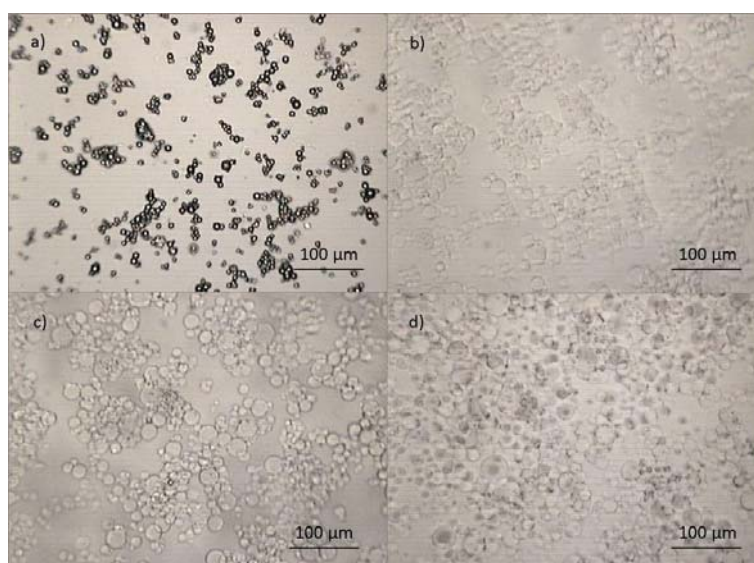


Figure A-17. Response of dried microbeads M-50/1 (a) to water presence after 30 s (b), 2 min (c), and 10 min (d)

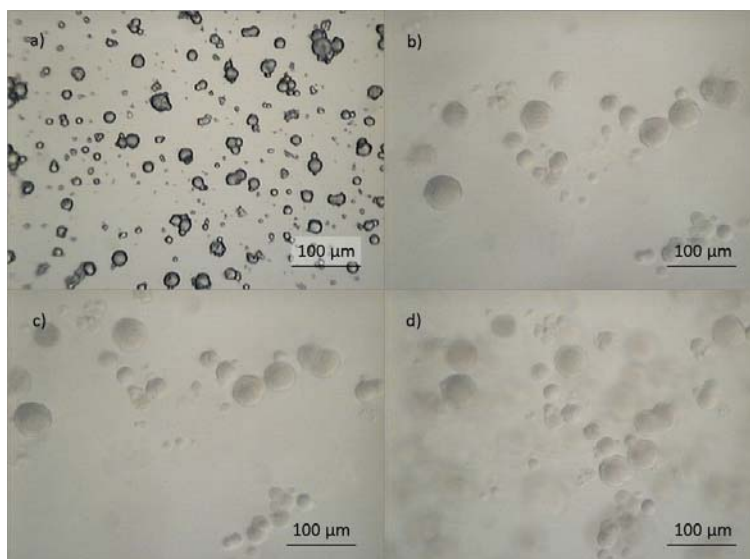


Figure A-18. Response of dried microbeads M-25/1-SA 1 (a) to water presence after 30 s (b), 2 min (c), and 10 min (d)

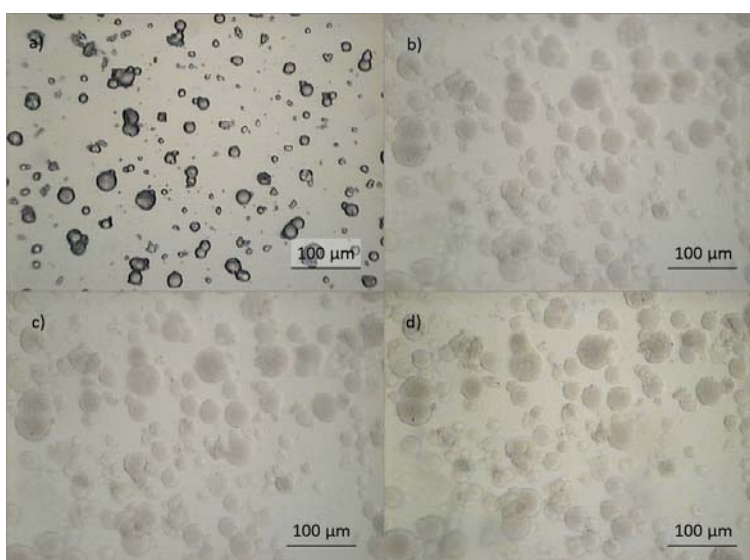


Figure A-19. Response of dried microbeads M-25/1-CA 1 (a) to water presence after 30 s (b), 2 min (c), and 10 min (d)

LIST OF PUBLICATIONS

Journal publication

1. S. Petrusic, M. Lewandowski, S. Giraud, P. Jovancic, B. Bugarski, S. Ostojic, V. Koncar, Development and Characterization of Thermosensitive Hydrogels Based on Poly(*N*-isopropylacrylamide) and Calcium Alginate, *Journal of Applied Polymer Science* (DOI 10.1002/app.35122).

Full Papers in Conference Proceedings (oral presentations)

1. S. Petrusic, M. Lewandowski, V. Koncar, S. Giraud, P. Jovancic, B. Bugarski, Thermo-Sensitive Hydrogels Based on Poly(*N*-isopropylacrylamide) for Drug Release System, *AUTEX 2009 World Textile Conference*, 26-28 May, Izmir, Turkey, Proceedings (CD-ROM), 162-168 (2009) (ISBN 978-975-483-787-2).
2. S. Petrusic, M. Lewandowski, V. Koncar, S. Giraud, P. Jovancic, B. Bugarski, Synthesis and Characterization of Thermo-Sensitive Hydrogels Based on Poly(*N*-isopropylacrylamide), *2nd International Scientific Conference "Textiles of the Future" – Futurotextiel 2008*, 13-15 November, Kortrijk, Belgium, Proceedings (CD-ROM), 6 pages (2008).

Abstracts in Conference Book of Abstracts (oral presentations)

1. S. Petrusic, M. Lewandowski, V. Koncar, S. Giraud, P. Jovancic, B. Bugarski, Study of Thermo-Sensitive Hydrogels Based on Poly(*N*-isopropylacrylamide) for Textile Drug Delivery Application, *European Congress and Exhibition on Advanced Material and Processes - EUROMAT 2009*, 7-10 september Glasgow, Scotland (2009).
2. S. Petrusic, B. Bursac, S. Grujic, P. Jovancic, J. Đonlagic, Thermosensitive hydrogel microbeads based on poly(*N*-isopropylacrylamide) aimed at controlled drug release, *49th Meeting of Serbian Chemical Society*, 13-14 May, Kragujevac, Book of abstracts, 114 (2011) (ISBN 978-86-7132-045-0).

Macro and micro forms of thermosensitive hydrogels intended for controlled drug release applications

ABSTRACT: The objective of this thesis is to develop adequate forms of thermosensitive hydrogels intended for a textile-based controlled transdermal drug release application. This work deals with thermosensitive hydrogels based on poly(*N*-isopropylacrylamide) (PNIPAAm). This polymer was combined in both linear and crosslinked form with alginate to form hydrogels with interpenetrating polymer network structure. Thus, the properties of conventional pure PNIPAAm hydrogel have been improved. Hydrogels of crosslinked PNIPAAm and calcium alginate (CA) were initially synthesized in the form of films. The presence of CA contributes to the improvement of mechanical properties without affecting the volume phase transition temperature (VPTT) of PNIPAAm. The technique of electrostatic extrusion was applied for the preparation of hydrogel microbeads. Operating parameters were varied to understand and optimize the conditions of the production of microbeads below 20 μm in diameter and of regular spherical shape. Inverse suspension polymerization was afterwards used for the preparation of microbeads of regular spherical shape and diameter in the range from 20 to 80 μm . They had porous, honeycomb-like structure. A Franz diffusion cell was employed to investigate the release of procaine hydrochloride from selected hydrogel microbeads. The incorporation of CA in PNIPAAm network resulted in slightly temperature-negative drug release pattern in comparison with temperature-positive drug release from the pure PNIPAAm hydrogel microbeads. The mechanism of the drug release at temperatures above and below the VPTT of microbeads depended on hydrogel swelling behavior and not solely on diffusion.

Keywords: thermosensitive hydrogels, poly(*N*-isopropylacrylamide), alginate, interpenetrating polymer network, hydrogel films, hydrogel microbeads, electrostatic extrusion, controlled drug release, Franz diffusion cell

Etude de macro et micro formes d'hydrogels thermosensibles destinés à la libération contrôlée de médicament

RÉSUMÉ: L'objectif de cette thèse est de mettre au point des formes adéquates d'hydrogels thermosensibles destinées à une application textile transdermique de libération contrôlée de médicament. Les travaux concernent les hydrogels thermosensibles à base de poly(*N*-isopropylacrylamide) (PNIPAAm). Ce polymère a été combiné sous une forme linéaire et/ou réticulée avec l'alginate, pour former des hydrogels ayant une structure de réseaux de polymères interpénétrés. On améliore ainsi les propriétés du PNIPAAm pur. Des hydrogels de PNIPAAm et d'alginate de calcium (CA) ont d'abord été synthétisés sous forme de films. La présence de CA contribue à l'amélioration des propriétés mécaniques, sans modifier la température de transition de phase du PNIPAAm. Nous avons ensuite appliqué la technique d'extrusion électrostatique pour préparer des microsphères d'hydrogel. Les paramètres du procédé ont été variés afin de comprendre et d'optimiser les conditions de fabrication de microsphères ayant un diamètre inférieur à 20 μm et une forme sphérique régulière. Nous avons utilisé la polymérisation en suspension inverse pour synthétiser des microsphères qui sont de forme plutôt régulière et sphérique, avec un diamètre variant de 20 à 80 μm . Leur structure était poreuse, en forme de nid d'abeille. La libération de l'hydrochlorure de procaine des microsphères d'hydrogel a été étudiée avec une cellule de diffusion de Franz. L'incorporation de CA dans le réseau de PNIPAAm engendre une libération de type légèrement négatif, tandis que le PNIPAAm pur présente un type positif. La libération de procaine dépend non seulement du phénomène de diffusion mais aussi du comportement de l'hydrogel au gonflement.

Mots clés: hydrogels thermosensibles, poly(*N*-isopropylacrylamide), alginate, réseau polymère interpénétrant, film d'hydrogel, microcapsules d'hydrogel, extrusion électrostatique, libération contrôlée de médicament, cellule de diffusion de Franz

Home laboratories

Laboratoire Génie et Matériaux Textiles
(GEMTEX)
Ecole Nationale Supérieure des Arts et
Industries Textiles (ENSAIT)
2 allée Louise et Victor Champier - BP 30329
59056 Roubaix
France
Tel: +33.(0)320.256.456

Faculty of Technology and Metallurgy
University of Belgrade
4 Karnegijeva
11000 Belgrade
Serbia
Tel: +381.(0)113.370.460
